Towards detecting connectivity in EEG: A comparative study of effective and functional connectivity measures on simulated data

by

Hanieh Bakhshayesh

Thesis
Submitted to Flinders University
for the degree of

Doctor of Philosophy

College of Science and Engineering

19/07/2019

Abstract

In neuroscience, there is considerable current interest in investigating the connections between different parts of the brain. EEG is one modality for examining brain function, with advantages such as high temporal resolution and low cost. Many measures of connectivity have been proposed, but which is the best measure to use? In this thesis, we address the following question: which measure is best able to detect connections between signals, in the challenging situation of non-stationary and noisy data from nonlinear systems, like EEG?

The problem with using EEG is that we don't known when a measure is giving the "right" answer. Hence we choose to apply connectivity measures to simulated data that is similar to EEG rather than EEG itself, so we always know the "right" answer.

We compare almost all of the most widely used or most promising measures, in total 26 functional connectivity measures and 20 effective connectivity measures. The performance of functional connectivity measures is tested on simulated data from two systems: two coupled Hénon maps; and two channels of simulated EEG. The performance of effective connectivity measures is tested on simulated data from three systems: three coupled Hénon maps; a multivariate autoregressive (MVAR) model with and without EEG as an exogenous input; and simulated EEG. To determine whether connectivity is detected, surrogate data were generated and analysed, and a threshold determined from the surrogate ensemble.

No measure performed best in all tested situations. In the comparison of the functional connectivity measures, correlation and coherence performed best on stationary data with many samples, in both high and low noise. S-estimator, correntropy coefficient, mean-phase

coherence (Hilbert), mutual information (kernel), nonlinear interdependence (S) and nonlinear interdependence (N) performed most reliably on non-stationary data with small to medium window sizes, in both high and low noise. Of these, correlation and S-estimator have execution times that scale slower with the number of channels and the number of samples. In the comparison of effective connectivity measures, the measures that model the data as MVAR perform well when the data are drawn from that model. Frequency domain measures perform well when the data have a clearly defined band of interest. When neither of these are true, information theoretic measures perform well, as does Copula Granger causality.

Table of contents

List of figures

List of tables

Declaration

I certify that this thesis does not incorporate without acknowledgment any material previously submitted for a degree or diploma in any university; and that to the best of my knowledge and belief it does not contain any material previously published or written by another person except where due reference is made in the text.

Signed

Date   30/11/2018

Acknowledgements

List of abbreviations

AIC: Akaike information criterion

BIC: Bayesian information criterion

BM: Bookmaker (informedness)

ECG: Electrocardiogram

EEG: Electroencephalography

EMG: Electromyogram

EOG: Electro-oculogram

EVS: Event synchronisation

fMRI: Functional magnetic resonance imaging

FNR: False negative rate

FPR: False positive rates

GC: Granger causality

IAAFT: Iteratively refined amplitude adjusted Fourier transform

IQR: Interquartile range

IS: Identical systems

MEG: Magnetoencephalography

MVAR: Multivariate autoregressive

NIRS: Near-infrared spectroscopy

NS1: Nonidentical systems 1

NS2: Nonidentical systems 2

PDF: Probability density function

TFD: Time-frequency distribution

TNR: True positive rates

TPR: True positive rates

VAR: Vector Autoregressive

Table of measures name

Functional connectivity measures

Abbreviated form	Full name
Correlation	Correlation coefficient
Coherence	Coherence
Correntropy	Correntropy coefficient
Coh-entropy	Coh-entropy coefficient
Wave-entropy	Wave-entropy
PC	Partial coherence
EVS	Event synchronisation
Hilbert phase	Mean phase coherence (Hilbert)
wavlet pahse	Mean phase coherence (wavelet)
event phase	Mean phase coherence (event)
$PCV_{unwrapped}$	Phase coherence value unwrapped
$PCV_{wrapped}$	Phase coherence value wrapped
$\tilde{\lambda}$	Conditional probability based phase synchrony
$I_{histogram}$	Mutual information (histograms)
$I_{adaptive\ histogram}$	Mutual information (adaptive histograms)
I_{kernel}	Mutual information (kernels)
I_{ω}	Mutual information (time-frequency plane)
KNN	Nearest-neighbour mutual information
histogram KL	Kullback Leibler divergence (histogram)
Rényi	Rényi Divergence
Jensen-Shannon	Jensen-Shannon divergence
Jensen-Rényi	Jensen-Rényi divergence
MLMI	Maximum likelihood mutual information
H^{k}	Nonlinear Interdependence (H^{k})
S^{K}	Nonlinear Interdependence (S^{k})
N^{K}	Nonlinear Interdependence (N^{k})
Ω	Omega Complexity
S_{est}	S-estimator

Table of measures name

Effective connectivity measures

Abbreviated form	Full name
CGC	Conditional Granger causality
FCGC	Conditional frequency domain Granger causality
PGC	Partial Granger causality
QGC	Copula Granger causality
MVGC	Multivariate Granger causality
SMVGC	Multivariate frequency domain Granger causality
DC	Directed coherence
DTF	Directed transfer function
PDC	Partial directed coherence
GPDC	Generalised partial directed coherence
DDTF	Direct directed transfer function
EDC	Extended directed coherence
EPDC	Extended partial directed coherence
TE	Transfer entropy
PTE	Partial transfer entropy
PMI	Partial mutual information
STE	Symbolic transfer entropy
SPTE	Symbolic partial transfer entropy
KL	Kullback-Leibler divergence
DPLV	Directional phase locking value

CHAPTER 1   INTRODUCTION

The identification of hidden dependencies among simultaneously observed time series from a complex dynamical system is an essential and challenging task in many scientific fields [1], and is of particular significance for brain dynamics. Representing patterns of interactions between different brain areas could be a major step to understanding the functional aspects of normal and pathological brain processes, such as the determination of the source of neuronal activity in epilepsy [2]. There has been wide-ranging research aimed at detecting underlying relationships (which may be nonlinear and/or nonstationary) in multi-output dynamic systems, to give useful insight into their spatio-temporal organisation [3]. Two significant approaches to defining dynamical links within a distributed system, such as the brain, are functional and effective connectivity. Effective connectivity refers to the influence that one neural system has over another [4]. Functional connectivity refers to the link between different brain regions that do similar things at similar times [5]. There has been recent explosive growth in the number of measures developed for studying brain functional and effective connectivity. They aim to characterise brain connectivity patterns using brain signals such:

- Functional magnetic resonance imaging (fMRI): mapping brain activity by detecting changes related to blood flow, using the electromagnetic properties of oxygenated blood;

- Magnetoencephalography (MEG): mapping brain activity by measuring the magnetic fields produced by the electrical currents which naturally occur in the brain;

- Near-infrared spectroscopy (NIRS): mapping brain activity by measuring blood flow changes, using infrared light to measures oxygenation levels; and

- Electroencephalography (EEG): mapping brain activity by recording brain electrical activity through electrodes placed on the scalp.

EEG has several clear advantages for studying the brain. Firstly, changes in the brain's electrical activity happen very quickly, and so a very high time resolution system is required to accurately capture these electrical events. EEG technology can precisely detect brain activity with high time resolution, e.g. milliseconds or less. Secondly, EEG electrodes are simply attached on the scalp. It is therefore a non-invasive procedure which allows relatively easy access to the human brain. Thirdly, in comparison to most other modalities, EEG equipment is relatively inexpensive and simple to use. Fourthly, EEG measures neuronal brain activity directly, not blood flow that is reacting to brain activity, ie it is a direct measurement not an indirect measurement. Hence our focus in this thesis is on the modality of EEG.

The evaluation of connectivity measures on EEG presents several challenges. Human brains are complex dynamic nonlinear systems, and so EEG signals generated by the brain are typically nonlinear and nonstationary. Another big challenge in using EEG is the very small signal-to-noise ratio of the recordings, due to contamination of brain signals by a wide variety of noise sources. Although some techniques have been developed for reducing some sources of noise, there will always be sources of noise affecting our signals. Therefore, it is extremely important that a connectivity measure for EEG should be robust to noise, as well as be able to detect both nonlinear and nonstationary relationships between signals.

When there are more than two signals, which will always be the case for EEG, another significant challenge arises: the possibility of detecting "connections" that are not truly there. For example, the coupling scheme in Figure 1-1 (left) may give the same pattern of connectivity as the scheme in Figure 1-1 (right). Another example is where one signal drives a second signal, and the second signal drives a third. Effective connectivity may incorrectly detect a causal influence from the first signal to the third signal. Ideally, we seek measures that are able to disambiguate these situations.

Figure 1-1:   Two distinct connectivity pattern among three signals. A pairwise effective connectivity analysis may not distinguish these two patterns.

Some publications use real EEG for the comparison of measures [6]. The difficulty with using EEG is that we don't know when a measure is giving the "right" answer. We claim that there is merit in comparing measures on simulated data where the true connections are known, rather than on real EEG data where our understanding is imperfect.

Hence in this thesis, we focus on simulated systems that mimic EEG in some way, where we have some knowledge or control of the level of nonlinearity, nonstationary and noise, and where we know the true connectivity patterns.

Some measures use linear approaches and measures the linear interaction among signals in the time domain or in the frequency domain. Linear measures have generally been assumed to only capture linear relationships, and these measures have rarely been tested on nonlinear relationships. Some linear measures first fit a linear model to the time series and then evaluate connectivity between the times series. For example, an MVAR model is used for many measures based on the concepts of Granger causality or coherence. An alternative nonlinear approach that has the advantage of being model-free is based on information theory. These measures estimate information shared or transferred between time series. Other measures are based on the phase relationship between time series, and hence are nonlinear. Another approach reconstructs the phase space of the signals, then measures the connectivity between the temporal evolution of the two trajectories described by the time series. And finally, there are measures based on the relative timings of predefined types of events extracted from the time series. Note that this thesis is focused on the comparison of measures, not on defining new

measures. Therefore, all measures are briefly outlined following the literature, and references are provided for more information. Some changes have been made where any inconsistency in notation may cause any confusion or misunderstanding.

There are several publications that compare many measures that include both functional (ie non-directed) measures and effective (i.e. directed) measures [6-8]. Some of the measures they include are effective connectivity measures, i.e. directed by definition. Others are based on functional connectivity measures, but are adapted to provide directional information as well. We argue that there are significant difficulties with comparing directed and nondirected measures. For example, we can generate data from a simulated system with directed connections, and compare the connections detected by a directed measure to the truth. But for a non-directed measure, we have only a single connection between two signals, so we either compare to both the directed connections or to the combination of them. In the first case, the non-directed measure can never detect the truth unless the connection is bidirectional, and in the second case the non-directed measure has half the comparisons of the directed measure. Hence neither comparison is clearly fair, and so in this thesis we compare functional connectivity measures and effective connectivity measures separately.

In addition, the literature generally takes a simplistic view that linear measures won't perform well on nonlinear datasets, but provides little evidence supporting this. It is therefore not sufficient to characterise the strength of the "linear component" in a nonlinear dataset, as a linear measure may not be totally insensitive to the "nonlinear component", and different measures may be differentially sensitive. Hence we have chosen to test all measures on all datasets and let the results speak.

Previous studies of coupled identical and nonidentical systems mostly have focused on a few measures [3, 9-14]. Many of the comparative studies of connectivity measures have focused

on bivariate tests e.g. [15], while some studies have considered the effectiveness of only model-based measures, e.g. [2, 16] or information theoretic measures, e.g. [17-19]. Hence we claim that there is no thorough comparison of many measures on simulated data, and so we adopt this approach in this thesis.

Another significant issue is that different measures do not calculate values on the same scale. A higher value of connectivity in one measure may indicate no connection between two signals, whereas a lower value in a different measure may indicate a connection between the signals. Because they are not measuring on the same scale, significant variation in the raw values can be seen across measures. Hence to reliably compare different measures we need a statistical approach to identify when a connectivity value is significantly different from its background level.

To test the statistical significance of a connectivity value and determine whether connectivity is detected, we generate surrogates to give data with the same statistical properties as the simulated data but without the dependencies between signals. A collection of surrogate data can be analysed with the connectivity measure to obtain a distribution of connectivity values corresponding to signals without connectivity, and a threshold determined from the surrogate ensemble. If the connectivity measure calculated on the original data exceeds this threshold, then it is regarded as statistically significant.

While the use of surrogates is not new, the literature only has studies using surrogates with a very limited number of measures. Hence the combination of surrogates with many measures in this thesis is a novel contribution.

In summary, the overall goal of the analyses is to provide a detailed comparison of many connectivity measures on simulated data, Measures from multiple families of measures, some linear and some non-linear, will be considered, and functional and effective connectivity measures will be compared separately. A careful statistical approach to evaluate the

significance of connectivity calculations will be used, to remove subjectivity from the comparisons.

This thesis is organised as follows. In Chapter 2, we review the literature on EEG and brain connectivity, describe the various families of both functional and effective connectivity measures, and review the use of surrogates for identifying significant connections. In Chapter 3, we apply the functional connectivity measures to simulated data generated from a pair of unidirectionally coupled Hénon maps, looking at the effects of increasing coupling strength, nonstationary coupling, and the influence of noise. In this chapter, we also apply the measures to simulated EEG signals. In Chapter 4, we apply effective connectivity measures first to a well-understood nonlinear system (three coupled Hénon maps), then an MVAR model with and without exogenous inputs, and finally we apply all measures to simulated EEG. In Chapter 5, we address the question of the selection of the parameters of connectivity measures, such as model order and time lag. Additionally, we consider the effect of data length. Finally, in Chapter 6, we summarise the results, discuss them, and present our conclusions.

CHAPTER 2   LITERATURE REVIEW

In this section we will give an introduction to EEG signals, and the different forms of brain connectivity. We then review the literature on connectivity measures, and the use of surrogates for detecting significant connections.

2.1 EEG and brain connectivity

2.1.1 Electroencephalography (EEG)

The post-synaptic ionic current flows within neurons produce an electrical field, which can be measured on the surface of head. Electrical activity of the brain is measured on the scalp is called electroencephalography (EEG).

The amplitude of the EEG is of the order of 100 μV. Clinically EEG typically considers frequencies from 0 to 30 Hz, but in research frequencies up to 100 Hz and beyond are now considered important.

In order to taking measurements on the head, small electrodes are placed on the scalp in standard locations with standard labels[1]. The voltage difference between an electrode and the reference electrode is called an EEG channel and uses the label of the electrode.
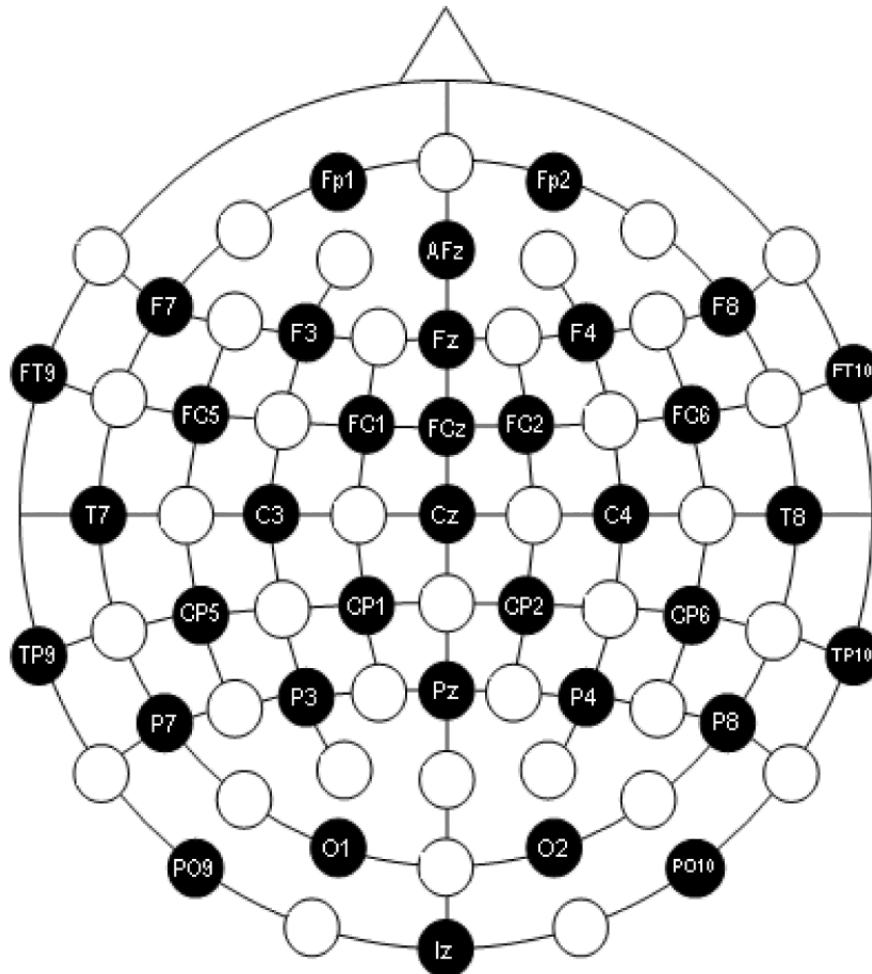
Figure 2-1:   10-20 system with large equidistant 34-channel arrangement [21]

Because the signals recorded at these channels are due to the synapsing of billions of neurons interacting in complex and varying ways, the signals are necessarily nonlinear and nonstationary.

---

[1] The 10-20 system is a standard that labels and describes the location of scalp electrodes for typical clinical EEG use. "The "10" and "20" refer to the fact that the actual distances between adjacent electrodes are either 10% or 20% of the total front–back or right–left distance across the skull" [20] Y. Li, J. Huang, H. Zhou, and N. Zhong, "Human Emotion Recognition with Electroencephalographic Multidimensional Features by Hybrid Deep Neural Networks," *Applied Sciences,* vol. 7, p. 1060, 2017.

EEG recording also is highly vulnerable to a wide variety of forms and sources of noises. Some noises are external, i.e. come from the environment, such as electromagnetic interference from AC power, lighting and electronic equipment. Other noises are internal, i.e. are generated by various physiological sources. The most common physiological noises are cardiac signals (electrocardiogram, ECG), muscle artefacts (electromyogram, EMG) and ocular artefacts (electro-oculogram, EOG). While several methods have been designed and developed to reduce and remove these noises (both at the time of recording as well as during processing), some noise will always remain. Thus, in addition to EEG signals being nonlinear and nonstationary, they are also noisy.

Recording the EEG is like recording audio using many microphones in a stadium. You can't tell what any individual is doing but you can get an idea of what a group is doing, if they are synchronised and there are sufficiently many. In EEG, location and orientation of neurons is also important [22].

"This image has been removed due to copyright restrictions."

Figure 2-2 : Audio analogy of EEG: recording EEG is like recording audio using many microphones in a stadium.

2.1.2 Brain connectivity

The identification of dependencies among simultaneously observed time series from a complex dynamical system is an essential and challenging task in many scientific fields [1], and is of particular significance for brain dynamics. Representing patterns of interactions between different brain areas could be a major step to understanding the brain. These connectivity patterns may let us assess the differences in normal and pathological brain processes, such as located the source of focal epileptic activity [23]. It may also indicate how different areas of the brain communicate. This may lead to understanding how information is transmitted within the brain, or how the different nervous system units interact to give rise to perception or

behaviour Brain connectivity patterns can be formed by the structural links i.e. synapses or fiber pathways (anatomical connectivity), synchronous dependencies (functional connectivity) and causal interactions (effective connectivity) between individual neurons, neuronal populations or anatomically separated brain regions.

2.1.2.1 Anatomical connectivity

Anatomical connectivity refers to the presence and structural integrity between neighbouring neurons through synaptic contacts or fiber tracks connecting neuron pools in spatially distant brain areas i.e. white matter tracts connecting [24].

2.1.2.2 Functional connectivity

Functional connectivity refers to the link between different brain regions that do similar things at similar times. More precisely, it can be defined as "temporal correlations between spatially remote neurophysiological events" [25]. Functional connectivity is symmetric, and so evaluates the strength of the interaction without considering its direction.

2.1.2.3 Effective connectivity

Effective connectivity refers to the influence that one neural system has over another [4]. Effective connectivity is asymmetric, evaluating the strength of interaction in a particular direction, independent of the interaction in the other direction. Aertsen and Preissl in [26] proposed that ''effective connectivity should be understood as the experiment- and time-dependent, simplest possible circuit diagram that would replicate the observed timing relationships between the recorded neurons.''

"This image has been removed due to copyright restrictions."

Figure 2-3: Types of brain connectivity. Structural connectivity (fiber pathways), functional connectivity (correlations), and effective connectivity (information flow) among four brain regions in macaque cortex [27].

2.2   Connectivity measures

Connectivity measures or estimators are mathematical formulations which have been developed to evaluate connectivity between time series. These estimators are either functional or effective connectivity measures. Functional connectivity measures evaluate similarities between time series, identifying non-directional relationships between time series. In contrast, effective connectivity measures evaluate the influence that one time series has over another, i.e. identifying directional relationships between time series.

One of the most interesting uses of connectivity measures is in neuroscience, for example EEG, the modality that is the focus of this thesis. In section 2.1.1 we saw that EEG is a noisy, non-stationary signal with many interfering sources. Therefore a good connectivity measure for EEG should be insensitive to noise, including non-brain signals, as well as being able to detect linear, nonlinear and nonstationary relationships between signals.

2.2.1   Functional connectivity measures (synchronisation measures)

Synchronisation is a basic phenomenon which occurs in nearly all sciences. This phenomenon was first reported in the 17th century by Christiaan Huygens on his observation of the synchronisation of two pendulum clocks [28]. "In the classical sense, synchronisation means adjustment of frequencies of periodic self-sustained oscillators due to weak interaction"[29]. The concept of synchronisation has been generalised to the case of chaotic oscillatory systems with irregular behaviour. The study of synchronisation between signals from such systems has been a topic of increasing interest, and has found applications in areas such as laser dynamics, solid state physics, electronics, biology, medicine, communication and even economics.

Synchronisation can manifest itself in different ways, hence a large variety of measures have been proposed to quantify synchronisation between signals. The classical measures use linear approaches to provide information about interacting systems in terms of their time delay

(correlation); in particular correlation coefficient [30] and coherence[30] are clearly the measures most used so far. Linear measures have generally been assumed to only capture linear relationships, and so these measures are rarely used to detect nonlinear relationships in synthetic data [3, 14].

In contrast to classical methods, new measures typically are nonlinear. Some measures are nonlinear extensions of linear measures, most commonly correlation. The correntropy coefficient is an extension of the correlation coefficient which is sensitive to a higher-order statistical and/or nonlinear relationship between the signals [12]. The coh-entropy coefficient can be approximately interpreted as an adaption of correntropy coefficient to the frequency domain, or as a non-linear extension of the coherence function [6]. It has been demonstrated that the wavelet transform is an effective and handy tool for EEG analysis [31]. Hence correntropy coefficient has also been extended to the time-frequency domain by substituting the wavelet transforms for the signals in the definition of correntropy coefficient yielding wave entropy [31, 32].

Event synchronisation (EVS) is based on the relative timings of predefined events extracted from signals. These events can be any repetitive feature, e.g. spikes in single-neuron recordings, epileptiform spikes in EEG, zero-crossings, local extrema. To perform event synchronisation, one needs to process the input signals $x(n)$ and $y(n)$ to indicator signals $e_x(n)$ and $e_y(n)$, whose values are zero everywhere except when an event occurs, where the value of the indicator signal is one. The event could be the occurrence of a local maximum (a peak), or local minimum (a trough), or zero crossing (positive-going or negative-going, or both) [33, 34].

In some cases, the phases of two signals are related even when their amplitudes are independent. Phase synchrony measures were specifically formulated to estimate any phase relationship between signals independent of their amplitude. To calculate phase synchrony, one

first needs to extract the instantaneous phase of signals. The two methods commonly used in the literature use the Hilbert transform [35] and the wavelet transform [36], yielding mean phase coherence (Hilbert) and mean phase coherence (wavelet). Alternatively, phase can be extracted from a signal using the previously outlined events approach [34], yielding mean phase coherence (event). Phase coherence value (*PCV*) is another approach to define phase synchronisation, based on the Shannon entropy of the distribution of phase difference [37-39]. As the signals' phases can be unwrapped or wrapped (removing or retaining phase jumps of 2□), we obtain two PCV measures: phase coherence value unwrapped and phase coherence value wrapped. It is also possible to define phase synchronisation using conditional probability [38, 39], yielding conditional probability based phase synchrony ($\tilde{\lambda}$).

The information-theoretic measures analyse information flow between two systems or between constituent subsystems of a complex system. These methods do not explicitly model the underlying interaction, and hence do not make any assumption about the underlying system [40, 41]. There are two groups of information-theoretic approaches for measuring interdependencies between signals: similarity measures, based on mutual information; and dissimilarity measures, that quantify the information divergence between two signals. Mutual information quantifies the amount of shared information between two random variables [42]. Mutual information is traditionally calculated from estimates of the joint, marginal and/or conditional probability density functions of one or more signals. The density estimation can be done simply using a histogram. In this paper, we test two measures: mutual information (histograms) ($I_{histogram}$) uses uniform bin widths, and mutual information (adaptive histograms) ($I_{adaptive\,histogram}$) uses non-uniform bin widths. Density estimation can be also done with more advanced techniques, such as kernel density estimation [43]. Histograms are inherently discontinuous, and if the distribution is known to be smooth it may be beneficial to estimate it using kernels, where the smoothness is inherent in the model, yielding mutual

information (kernel) (I_{kernel}). Alternatively, maximum likelihood mutual information (*MLMI*) [44] does not estimate several densities individually, but instead estimates the required ratio of densities directly, thereby avoiding the potential for magnifying estimation errors when dividing. Finally, we also estimate mutual information directly from samples using an estimator based on a sample's k-nearest-neighbours: nearest-neighbour mutual information (*KNN*) [45]. Another alternative in estimating an information theoretic measure is to substitute the probability density function with a time-frequency distribution (TFD). With an appropriate choice of kernel function, the TFD can have the desirable properties of preserving energy and the marginal distributions. If a spectrogram is used, then the TFD is also non-negative, which is necessary for calculating information theoretic measures [41, 46]. Here we use mutual information (time-frequency) (I_{ω}).

The second group of information theoretic measures estimate a dissimilarity between the two signals, where minimum dissimilarity corresponds to maximum similarity. Hence, following [47], we have normalised and inverted these measures so that zero corresponds to no synchrony and one corresponds to maximum synchrony. Kullback-Leibler divergence (*KL*) [48] and Jensen-Shannon divergence [41] are extensions of entropy that measure the distance between two distributions. Rényi divergence [6, 49] and Jensen-Rényi divergence [41] are non-linear variations on the same idea.

The final approach reconstructs the phase space of the signals, then measures the synchronisation between the temporal evolution of the two trajectories described by the signals [50, 51]. This yields four measures: nonlinear interdependence (H^k), nonlinear interdependence (S^k), nonlinear interdependence (N^k), and S-estimator.

In this section, we describe every functional connectivity (synchronisation) measure used in the thesis, arranged in groups of measures that are conceptually related.

2.2.1.1 Correlation coefficient and related measures

Correlation, coherence and related measures have been widely used in the literature to estimate synchronisation in the time and frequency domains.

2.2.1.1.1 Correlation coefficient

The correlation coefficient is one of the most well-known linear synchrony measures. It quantifies the linear correlation between two discrete-time signals $x(n)$ and $y(n)$ and is defined as [30]:

$$r = \frac{1}{N} \sum_{n=1}^{N} \frac{(x(n) - \bar{x})(y(n) - \bar{y})}{\sigma_x \sigma_y} \qquad \text{2-1}$$

where N is the length the signals, $\bar{x}$ and σ_x are the mean and standard deviation of the signal $x(n)$; and similarly for $y(n)$. If the two signals $x(n)$ and $y(n)$ are not linearly correlated (no synchrony), r will be close to zero. When signals are identical (maximal synchrony), then $r = 1$.

2.2.1.1.2 Coherence

Linear correlations can also be computed in the frequency domain by means of the cross spectrum:

$$C_{xy}(f) = E[X(f)Y^*(f)] \qquad \text{2-2}$$

where $E[.]$ is the expectation operator, $X(f)$ is the (discrete) Fourier transform of $x(n)$, the asterisk indicates complex conjugation, and f is frequency. In practice, a finite number of samples will give a noisy estimate of (cross- and auto-) spectra. To reduce the noise, signals are segmented into equal length pieces, and the spectra of each segment is averaged (Welch's method [52]

The coherence function $c(f)$ is the square of the cross spectrum, normalised by the auto-spectra of the two signals [30]:

$$c(f) = \frac{\left|\langle C_{xy}(f)\rangle\right|^2}{\left|\langle C_{xx}(f)\rangle\right|\left|\langle C_{yy}(f)\rangle\right|} \qquad 2\text{-}3$$

where $\langle.\rangle$ stands for average over the segments. This measure is particularly useful when the correlation between signals is limited to a particular frequency band [53].

Where the angled brackets indicate an average over segments. This measure is particularly useful when correlation between signals is limited to some particular frequency band [53].

2.2.1.1.3 Correntropy coefficient

The correntropy coefficient is an extension of the correlation coefficient which is sensitive to a higher-order statistical and/or nonlinear relationship between the signals. Just as correlation is a normalisation of covariance, the correntropy coefficient r_E for signals $x(n)$ and $y(n)$ is a normalisation of a generalisation of covariance known as centred cross-correntropy coefficient $U(x, y)$ [12]:

$$U(x,y) = \frac{1}{N}\sum_{i=1}^{N} k\big(x(i), y(i)\big) - \frac{1}{N^2}\sum_{i,j} k\big(x(i), y(j)\big) \qquad 2\text{-}4$$

where N is the number of samples, and $k(\cdot)$ is a symmetric positive-definite kernel function e.g. Gaussian, sigmoidal, or polynomial kernel [54]. The correntropy coefficient is therefore:

$$r_E = \frac{U(x, y)}{\sqrt{U(x, x)}\sqrt{U(y, y)}} \qquad 2\text{-}5$$

The kernel has a significant effect on the result, and so must be chosen carefully. In this paper we use the Gaussian kernel: $k(x, y) = \dfrac{e^{-(x-y)^2/2\sigma^2}}{\sqrt{2\pi\sigma}}$. For this kernel, the choice of kernel width

σ is critical. The recommended approach is Silverman's rule of thumb [55]: $\sigma = 0.9AN^{-1/5}$, where A is the smaller value of the standard deviation of the data and the data interquartile range scaled by 1.34, and N is the number of data samples.

2.2.1.1.4 **Coh-entropy coefficient**

The coh-entropy coefficient can be approximately interpreted as an adaption of correntropy coefficient to the frequency domain, or as a non-linear extension of the coherence function. Coh-entropy C_E is given by [6]:

$$C_E(f) = \frac{\langle k\big(X(f), Y(f)\big)\rangle}{k(0)}$$

2-6

where $\langle \cdot \rangle$ stands for average over the segments, $X(f)$ and $Y(f)$ are the Fourier transforms of segments of the signals $x(n)$ and $y(n)$ respectively, and $k(\cdot)$ is a kernel function. Following the literature, e.g.[12], in this paper we use a Gaussian kernel with Silverman's rule. As our calculations of coh-entropy coefficient normalises both signals $X(f)$ and $Y(f)$ by mean and standard deviation before evaluating C_E, Silverman's rule determines the width to be $\sigma = 0.4$.

2.2.1.1.5 **Wav-entropy coefficient**

It has been demonstrated that the wavelet transform is an effective and handy tool for EEG analysis [31]. Hence correntropy coefficient has also been extended to the time-frequency domain by substituting the wavelet transforms $W_x^{\psi}(s,\tau)$ and $W_y^{\psi}(s,\tau)$ for the signals $x(t)$ and $y(t)$ respectively in the definition of correntropy coefficient, yielding the wav-entropy coefficient $W_E(f)$. The (continuous) wavelet transform of $x(t)$ is given by [31, 32]:

$$W_x^{\psi}(s,\tau) = A_{\psi} \int \psi^*\left(\frac{t-\tau}{s}\right) x(t)dt$$

2-7

where $\psi^*(t)$ indicates the complex conjugation of the mother wavelet $\psi(t)$, τ is the wavelet translation parameter, and s is the wavelet scaling factor. Values of scale s can be mapped to frequency, viz $f = 1/s$. In this study , we use the complex Morlet wavelet, as given in [32]:

$$\psi(t) = \frac{e^{-t^2/2\sigma_t^2} e^{2\pi i f_0 t}}{\sqrt{2\pi\sigma_t^2}} \qquad 2\text{-}8$$

where σ_t represents the bandwidth parameter and f_0 the central frequency of the wavelet. Following [32], we set the wavenumber $\omega_0 = 2\pi f_0 \sigma_t = 6$.

2.2.1.1.6 Partial coherence

Traditionally the partial coherence between a pair of signals is calculated using a multivariate autoregressive model (MVAR). The MVAR model of a set of n signals $x_1(t), x_2(t), \dots, x_n(t)$ is given by [56]:

$$\begin{bmatrix} x_1(t) \\ \vdots \\ x_n(t) \end{bmatrix} = \sum_{l=1}^{P} A_l \begin{bmatrix} x_1(t-l) \\ \vdots \\ x_n(t-l) \end{bmatrix} + \begin{bmatrix} e_1(t) \\ \vdots \\ e_n(t) \end{bmatrix} \qquad 2\text{-}9$$

where P is the model order, the model coefficients A_i are $n \times n$ matrices, and each $e_i(t)$ is a zero-mean Gaussian random process. According to this model, each signal is assumed to linearly dependent on its own p past values and the p past values of the other signals, plus an innovation or noise input. Transforming to the frequency domain gives $X(f)[I - A(f)] = E(f)$, where $A(f) = \sum_{l=1}^{P} A_l e^{2\pi i f l}$, and hence the covariance matrix $S(f)$ of the model signals is $S(f) = H(f)VH(f)^H$, where $H(f) = [I - A(f)]^{-1}$ and V is the prediction error covariance matrix [56]. Note that in principal Fourier analysis or other spectral estimation approaches can be used to calculate spectral density matrix, and so the calculation of partial coherence does not necessarily involve an MVAR model.

Then the partial coherence between $x_i(t)$ and $x_j(t)$ is defined using $M_{ij}(f)$, the $(i,j)^{\text{th}}$ minor of $S(f)$, as [56, 57]:

$$C_{ij}(f) = \frac{M_{ij}(f)}{\sqrt{M_{ii}(f)}\sqrt{M_{jj}(f)}} \qquad \text{2-10}$$

The partial coherence $C_{ij}(f)$ estimates the coherence of a pair signals $x_i(t)$ and $x_j(t)$ at each frequency f with the influence of other signals statistically eliminated.

2.2.1.2 Event synchronisation

Event synchronisation is based on the relative timings of predefined events extracted from signals. These events can be any repetitive feature, e.g. spikes in single-neuron recordings, epileptiform spikes in EEG, zero-crossings, local extrema. To perform event synchronisation, one needs to process the input signals $x(n)$ and $y(n)$ to indicator signals $e_x(n)$ and $e_y(n)$, whose values are zero everywhere except when an event occurs, where the value of the indicator signal is one. The event could be the occurrence of a local maximum (a peak), or local minimum (a trough), or zero crossing (positive-going or negative-going, or both).

Local maxima and minima [34]: The signal $x(n)$ has local maxima and local minima if $x(n) > x(n \pm 1)$ and $x(n) < x(n \pm 1)$ respectively. These can be identified from the signal $S_x(n)$ defined as:

$$S_x(n) = \text{sgn}(x(n) - x(n-1)) + \text{sgn}(x(n) - x(n+1))$$

where sgn $(\cdot)$ denotes the signum function. $S_x(n) = -2$ for local minima, $S_x(n) = 2$ for local maxima, and zero otherwise. We can form an indicator signal for a local maximum as:

$$e_x^{\max}(n) = 1 + \text{sgn}(S_x(n) - 2) \qquad \text{2-11}$$

and similarly an indicator signal for a local minimum is:

$$e_x^{\min}(n) = 1 - \text{sgn}(S_x(n) + 2) \qquad \text{2-12}$$

Zero crossings: The signal $x(n)$ has a positive-going zero crossing if $x(n) < 0$ and $x(n+1) > 0$. These can be identified from the signal $Z_x(n)$ defined as:

$$Z_x(n) = \text{sgn}(x(n)) - \text{sgn}(x(n-1))$$

$Z_x(n) = +2$ for positive-going zero crossings, $Z_x(n) = -2$ for negative-going zero crossings, and ± 1 or zero otherwise. Hence an indicator signal for positive-going zero crossings is:

$$e_x^{+z}(n) = 1 + \text{sgn}(Z_x(n) - 2) \tag{2-13}$$

And similarly for a negative-going zero crossings:

$$e_x^{-z}(n) = 1 - \text{sgn}(Z_x(n) + 2) \tag{2-14}$$

or for any zero-crossing:

$$e_x^{z}(n) = 2 + \text{sgn}(Z_x(n) - 2) - \text{sgn}(Z_x(n) + 2) \tag{2-15}$$

Measuring event synchronisation [33, 34]: Given two indicator signals $e_x(n)$ and $e_y(n)$, we measure event synchronisation by counting how often an event in one signal is preceded by an event in the other signal within a specified time τ. The count can be computed as:

$$C^\tau(x|y) = \sum_{k=1}^{N}\sum_{d=1}^{\tau} e(k)e(k-d)$$

Event synchronisation is then calculated from this count and it symmetric counterpart $C^\tau(y|x)$:

$$EVS = \frac{C^\tau(x|y) + C^\tau(y|x)}{2\sqrt{E_x E_y}} \tag{2-16}$$

where E_x and E_y are the total number of events in the signals $x(n)$ and $y(n)$, ie

$$E_x = \sum_{k=1}^{N} e_x(k)$$

In this study, these events used will be local maxima, local minima, and zero crossings

20

2.2.1.3 Phase synchrony

In some cases, the phase of two signals are related even when their amplitudes are independent. Phase synchrony measures were specifically formulated to estimate any phase relationship between signals independent of their amplitude. To calculate phase synchrony, one first needs to extract the instantaneous phase of signals. The two methods commonly used in the literature use the Hilbert transform [35] or the wavelet transform [36]. The Hilbert transform can be written as a convolution:

$$\breve{x}(t) = \frac{1}{\pi t} * x(t) \qquad \qquad \textit{2-17}$$

It calculates the imaginary component of the analytic signal $x_a(t)$:

$$x_a(t) = x(t) + i\breve{x}(t) \qquad \qquad \textit{2-18}$$

Finally, $\varphi_x^H(t)$, the instantaneous phase of the signal, is given by:

$$\varphi_x^H(t) = \arg(x(t) + i\breve{x}(t)) = \arctan\left(\frac{\breve{x}(t)}{x(t)}\right) \qquad \qquad \textit{2-19}$$

For narrowband signals, this formulation using the Hilbert transform can work well. For broadband signals, like EEG, it is recommended that a bandpass filter is used to select the frequency band of interest before calculating the Hilbert transform [58]. Another well-known phase extraction approach uses the wavelet phase transform of signal. In this case, the phase is extracted from the convolution of the signal with a wavelet function $\psi(t)$ [59]:

$$X(t) = \int_{-\infty}^{\infty} \psi(\tau) x(t - \tau) d\tau \qquad \qquad \textit{2-20}$$

and the phase calculated as before: $\varphi_x^W(t) = \arg(X(t))$. Both of these quantities depend on the chosen wavelet, which is traditionally a complex Morlet wavelet, used here with wavenumber $\omega_0 = 2\pi f_0 \sigma_t = 6$ as before. Unlike the Hilbert transform, the wavelet transform is effectively a bandpass filter, so it works for both narrowband and broadband signals [60].

Alternatively, phase can be extracted from a signal using the previously defined events approach. Suppose t_k are a sequence of times where a certain event appears once per cycle, then the phase can be defined as: $\varphi(t_j) = 2\pi(j - 1)$. Effectively, the phase is defined at the times of the events' occurrences and interpolated linearly in between. The phase estimate is then a uniform sampling of this waveform, at the same sampling rate as the original signal [34].

2.2.1.3.1 Mean phase coherence

Let $\varphi_x(t)$ and $\varphi_y(t)$ be the extracted phase from signals $x(t)$ and $y(t)$ respectively, via one of the techniques described above. Then, the (n, m) phase difference of the signals, where n and m are integers, can be defined as [28, 38]:

$$\Delta\varphi(t) = n\varphi_x(t) - m\varphi_y(t) \qquad\qquad 2\text{-}21$$

If the (n, m) phase difference of the signals remains bounded, then the signals are said to be $n{:}m$ synchronised. In the most cases, only $m = n = 1$ is considered [52]. The mean phase coherence, also known as phase synchronisation index, R is given by [28, 52, 61, 62]:

$$R = \langle e^{-i\Delta\varphi(t)} \rangle = \sqrt{\langle\cos(\Delta\varphi(t))\rangle^2 + \langle\sin(\Delta\varphi(t))\rangle^2} \qquad\qquad 2\text{-}22$$

where the angle brackets represent an average over time. The mean phase coherence will be zero if the phases are not synchronised and will be one for a constant phase difference.

2.2.1.3.2 Phase coherence value

It is also possible to define phase synchronisation from the Shannon entropy of the distribution of phase difference. The phase coherence value PCV is defined as [37-39]:

$$PCV = \frac{S_{\max} - S}{S_{\max}} \qquad\qquad 2\text{-}23$$

where $S = -\sum_{k=1}^{N} \rho_k \ln\rho_k$ and $S_{max} = \ln(N)$ is the maximal entropy, where N is the number of bins in the histogram of the phase difference, and ρ_k is the relative frequency of phase

differences in the kth bin. The standard approach to estimating the number of bins is N=....,
where M is the number of samples is $N = exp[0.626 + 0.4ln(M - 1)]$, where M is the
number of samples [63]. PCV ranges from $PCV = 0$, corresponding to a uniform distribution
of phase differences (no synchronisation), to $PCV = 1$, corresponding to a Dirac-like
distribution of phase differences (constant phase difference or maximal synchronisation).

2.2.1.3.3 Conditional probability based phase synchrony

Suppose that two phases $\varphi_x(t_k)$ and $\varphi_y(t_k)$ are extracted from signals $x(t)$ and $y(t)$, and the
phases are quantised into M bins on the ranges $[0, n2\pi]$ and $[0, m2\pi]$ respectively. The phase
synchrony index based on conditional probability is defined as [38, 39]:

$$\tilde{\lambda} = \frac{1}{M} \sum_{l=1}^{M} |r_l| \qquad \text{2-24}$$

$$r_l = \frac{1}{M_l} \sum_{k \in K_l} e^{i\varphi_x(t_k)} \qquad \text{2-25}$$

where K_l is the set of all time indices such that $\varphi_y(t)$ belongs to bin l, and M_l is the number of
indices in the set. In other words, r_l is the average of the unit vectors of the phase of $x(t)$ for
those times when the unit vectors of $y(t)$ point in approximately the same direction. It will
have a magnitude of one when the phase relationship is consistent, and a small magnitude when
the phase relationship is random. $\tilde{\lambda}$ is the average across the bins, and hence approaches 1 when
the phase relationship is consistent, and tends to zero when the phase relationship is random.

2.2.1.4 Information-theoretic measures

The information-theoretic measures analyse information flow between two systems or between
constituent subsystems of a complex system. These methods do not explicitly model the
underlying interaction, and hence do not make any assumption about the underlying system
[40, 41].

In this section, we provide a detailed overview of two groups of information-theoretic approaches for measuring interdependencies between signals: similarity measures, based on mutual information; and dissimilarity measures, that quantify the information divergence between two signals. As these measures estimate a dissimilarity, their minimum corresponds to maximum similarity. Hence, following [47], we have normalised and inverted these measures so that zero corresponds to no synchrony and one corresponds to maximum synchrony.

We first introduce the concept of entropy which measures the uncertainty of a discrete random variable. Let X and Y be random variables with probability density functions $\rho(x) = P_r\{X = x\}$ and $\rho(y) = P_r\{Y = y\}$, then the Shannon entropy $H(X)$ measures the average amount of information gained from and observation of X. It is defined as:

$$H(X) = -\sum_x \rho(x)\log(\rho(x)) \qquad \text{2-26}$$

Similarly, the joint entropy $H(X,Y)$ is:

$$H(X,Y) = -\sum_x \sum_y \rho(x,y)\log(\rho(x,y)) \qquad \text{2-27}$$

where $\rho(x,y) = P_r\{X = x, Y = y\}$ is the joint probability of these values occurring together.

Finally, the conditional entropy $H(X|Y)$ of X given Y is defined using the conditional probability $\rho(x|y) = P_r\{X = x | Y = y\}$ as:

$$H(X|Y) = -\sum_x \sum_y \rho(x,y)\log\big(\rho(x|y)\big) \qquad \text{2-28}$$

The joint entropy can be expressed in terms of the conditional entropy and the Shannon entropy as $H(X,Y) = H(X|Y) + H(Y)$. Mutual information $I(X;Y)$ quantifies the amount of shared information between X and Y [42]:

$$I(X;Y) = \sum_x \sum_y \rho(x,y)\log\left(\frac{\rho(x,y)}{\rho(x)\rho(y)}\right) \qquad \text{2-29}$$

Mutual information can be equivalently expressed as

$$I(X;Y) = H(X) - H(X|Y) = H(Y) - H(Y|X) = H(X) + H(Y) - H(X,Y)$$
$$= H(X,Y) - H(X|Y) - H(Y|X) \qquad \text{2-30}$$

Mutual information is not normalised, so to use it as a measure of synchronisation we need to normalise it. Several normalisations have been proposed, including NMI_L by Lancichinetti et al in [64]:

$$NMI_L = 1 - \frac{1}{2}\left(\frac{H(X|Y)}{H(X)} + \frac{H(Y|X)}{H(Y)}\right) \qquad \text{2-31}$$

and the normalised mutual information NMI_{FJ} by Fred and Jain in [65]:

$$NMI_{FJ} = \frac{2I(X;Y)}{H(X) + H(Y)} \qquad \text{2-32}$$

In this paper we use NMI_{FJ}.

Mutual information is traditionally calculated from estimates of the joint, marginal and/or conditional probability density functions of one or more signals. The density estimation can be done simply using a histogram, or with a more advanced technique such as kernel density estimation [43]. Maximum likelihood mutual information does not estimate several densities individually, but instead estimates the required ratio of densities directly, thereby avoiding the potential for magnifying estimation errors when dividing. We also examine new approaches to estimate mutual information directly from samples using k-nearest-neighbour (kNN) based estimators [45].

Another alternative is to substitute the probability density function with a time-frequency distribution (TFD). With an appropriate choice of kernel function, the TFD can have the

desirable properties of preserving energy and the marginal distributions. If a spectrogram is used, then the TFD is also non-negative, which is necessary for calculating information theoretic measures [41, 46].

2.2.1.4.1 Mutual information using histograms

The histogram is the oldest and the most straightforward approach for estimating probability density functions. This method involves in partitioning the samples into n bins b_i of finite size. Then probability density function (PDF) can be estimated by counting the number of samples falling into each bin b_i, and dividing each by the total number of samples. Assume we have random variable X, and the number of samples falling into the ith bin of X is B_i, then the histogram approximation of the density is:

$$\rho(x) = \frac{B_i}{N}, x \in b_i$$

2-33

where $N = \sum_{i=1}^{n} B_i$ is the total number of samples.

Optimal bin size selection is crucial in achieving sufficient samples in each bin to obtain a reliable estimate of the PDF. There are various theoretical rules for determining bin sizes, which can be uniform or non-uniform. In this thesis, we use the Freedman-Diaconis rule [66] to obtain a suitable width for uniformly-sized bins, and adaptive partitioning [67] for optimising the sizes of the bins when using non-uniform bins, referred to as mutual information (histograms) and mutual information (adaptive histograms) respectively.

2.2.1.4.2 Mutual information using kernels

Histograms are inherently discontinuous, and if the distribution is known to be smooth it may be beneficial to estimate it using kernels, where the smoothness is inherent in the model. Kernel estimators place a scaled kernel function (a non-negative real-valued integrable symmetric function) at each of N data points to smooth out the contribution of each observed data point

over a local neighbourhood [55]. If we denote the kernel function as $k(u)$ where $\int_{-\infty}^{\infty} k(u)\,du = 1$, the estimated density at any point x is:

$$\rho(x) = \frac{1}{Nh}\sum^{N} k\left(\frac{x - x_i}{h}\right)$$

<div align="right">2-34</div>

where h is the bandwidth, a parameter that determines the smoothness of the estimated pdf. There are many possible kernel functions. In this study, we again use the Gaussian kernel function $k(u) = e^{-u^2/2}/\sqrt{2\pi}$. The choice of the bandwidth is critical to good estimation. Again, a common method to choose the optimal bandwidth is Silverman's rule of thumb [55].

2.2.1.4.3 **Maximum likelihood mutual information (MLMI)**

The methods discussed so far all estimate the probability densities directly. Instead, MLMI directly models the density ratio:

$$\omega(x, y) = \frac{\rho(x, y)}{\rho(x)\rho(y)}$$

<div align="right">2-35</div>

From an estimate of this ratio $\hat{\omega}(x, y)$ and N samples of X and Y, MI can be approximated by [44]:

$$I(X; Y) = \sum^{N} \log(\omega(x_i, y_i))$$

<div align="right">2-36</div>

2.2.1.4.4 **Nearest-neighbour mutual information**

The Kraskov, Stögbauer, and Grassberger mutual information estimator [45] is a widely used measure based on entropy estimates from k nearest-neighbour distances (KNN). Distances are measured in three ways, distances between samples in X, distances between samples in Y, and the maximum of these two distances for corresponding samples, commonly referred to as a distance in Z. For a time, point indicated by the subscript i, we can determine the distance $d_Z(i)$ in Z between the sample Z_i and Z_k, its kth nearest neighbour. We then determine $n_x(i)$ as the

number of points X_j whose distance from X_i is strictly less than $d_Z(i)$, and similarly for $n_x(i)$.

Then the nearest neighbour mutual information is given by:

$$I(X;Y) = \psi(k) - \langle \psi(n_x + 1) + \psi(n_y + 1) \rangle + \psi(N) \qquad 2\text{-}37$$

where $\langle \cdot \rangle$ denotes averaging over all $i \in [1, \cdots, N]$ and $\psi(x)$ is the digamma function $\psi(x) = d\ln(\Gamma(x))/dx$, ie the logarithmic derivative of the gamma function $\Gamma(x)$ [45, 68].

2.2.1.4.5 Mutual information on the time-frequency plane

Mutual information can be calculated from TFDs as [46]:

$$I(C_x, C_y) = \sum_{n,f} C_{x,y}(n,f)\log\left(\frac{C_{xy}(n,f)}{C_x(n,f)C_y(n,f)}\right) \qquad 2\text{-}38$$

where $C_x(n,f)$ and $C_{xy}(n,f)$ are the normalised auto- and cross- time-frequency distributions respectively, and can be calculated from the spectrogram $S_x(n,f)$ as:

$$C_x(n,f) = \frac{|S_x(n,f)|^2}{\sum_{n,f}|S_x(n,f)|^2} \qquad 2\text{-}39$$

$$C_{xy}(n,f) = \frac{|S_x(n,f)S_y^*(n,f)|}{\sum_{n,f}|S_x(n,f)S_y^*(n,f)|} \qquad 2\text{-}40$$

In this paper, we calculate the spectrogram using the short-term Fourier transform with a Hamming window.

2.2.1.4.6 Kullback-Leibler divergence

For densities P and Q, the Kullback-Leibler divergence is given by [48]:

$$K(P|Q) = \sum_i P_i\log\left(\frac{P_i}{Q_i}\right) \qquad 2\text{-}41$$

Rather than use pdfs, here we use the TFDs [6, 47]:

$$K(C_x, C_y) = \sum_{n,f} C_x(n,f)\log\left(\frac{C_x(n,f)}{C_y(n,f)}\right) \qquad 2\text{-}42$$

The Kullback-Leibler divergence is an asymmetric measure, but it can be symmetrised by taking the average of $K(C_x, C_y)$ and $K(C_y, C_x)$ [69].

$$K(C_x; C_y) = \frac{K(C_x, C_y) + K(C_y, C_x)}{2} \qquad \text{2-43}$$

2.2.1.4.7 Rényi divergence

The Rényi divergence of order α is defined as [6, 49]:

$$D_\alpha(C_x, C_y) = \frac{1}{\alpha - 1} \log \left(\sum_{n,f} [C_x(n,f)]^\alpha [C_y(n,f)]^{(1-\alpha)} \right) \qquad \text{2-44}$$

It is a generalisation of the Kullback–Leibler divergence, and as $\alpha \to 1$ it equals the Kullback-Leibler divergence [70]. This measure is asymmetric measure except for $\alpha = 0.5$, which is the value used in this paper.

2.2.1.4.8 Jensen-Shannon divergence

Jensen-Shannon divergence is a way of deriving distance measures from entropy. The Jensen-Shannon divergence of two time-frequency distributions $C_x(n,f)$ and $C_y(n,f)$ is given by [41]:

$$J(C_x, C_y) = H\left(\frac{C_x + C_y}{2}\right) - \frac{H(C_x) + H(C_y)}{2} \qquad \text{2-45}$$

where H denotes the Shannon entropy given by:

$$H(C_x) = \sum_{n,f} C_x(n,f) \log C_x(n,f) \qquad \text{2-46}$$

2.2.1.4.9 Jensen-Rényi divergence

Jensen-Rényi divergence is modification of the Jensen-Shannon divergence from an arithmetic to a geometric mean [41]:

$$J(C_x, C_y) = H_\alpha\left(\sqrt{C_x C_y}\right) - \frac{H_\alpha(C_x) + H_\alpha(C_y)}{2} \qquad \text{2-47}$$

where H_α denotes the Rényi entropy given by:

$$H_\alpha(C_x) = \frac{1}{\alpha - 1} \log \sum_{n,f} (C(n,f))^\alpha \qquad \text{2-48}$$

2.2.1.5 Synchronisation based on state space

Synchronisation can be measured by calculating the interdependence between the signals in state space. Therefore, the first step is to project the signals into state space, a procedure known as state space reconstruction. The method of delays is one of the important state space reconstruction techniques. For a signal $x(n)$, we reconstruct a state space vector as:

$$x(n) = [x(n), x(n - \tau), \cdots, x(n - (m - 1)\tau)]^T \qquad \text{2-49}$$

where m is the embedding dimension and τ denotes the time lag. With N samples of $x(n)$, we can create $N - (m - 1)\tau$ state space vectors. Each state space vector can be considered as a point in an m-dimensional space, and the set of $N - (m - 1)\tau$ state space vectors traces out a trajectory in this space [50, 71].

2.2.1.5.1 Nonlinear interdependence

For each state space vector $x(i)$, we can measure the average squared Euclidean distance to all other state space vectors as:

$$R_i(X) = \frac{1}{N - (m - 1)\tau} \sum_{j \neq i} (x(i) - x(j))^T (x(i) - x(j)) \qquad \text{2-50}$$

Now we can identify the k other state space vectors that are closest, ie the k nearest neighbours, and denote the time indices of these neighbours by $r_{i,j}$, $j = 1, 2, \cdots, k$. Then for each state space vector $x(i)$, the average squared Euclidian distance to its k nearest neighbours is defined as:

$$R_i^{(k)}(X) = \frac{1}{k} \sum_j^k (x(i) - x(r_{i,j}))^T (x(i) - x(r_{i,j})) \qquad \text{2-51}$$

We can similarly define $R_i(Y)$ and $R_i^{(k)}(Y)$. In addition, we can identify the k state space vectors $y(j)$ that are closest to the state space vector $x(i)$, and denote the time indices of these

neighbours by $s_{i,j}$, $j = 1,2,\cdots,k$. We then measure the average squared Euclidean distance from $x(i)$ to the k state space vectors $x(s_{i,j})$, ie the time-partners of the nearest neighbours of the state space vectors $y(j)$. This gives the Y-conditioned average squared Euclidean distance defined as:

$$R_i^{(k)}(X|Y) = \frac{1}{k}\sum_{j=1}^{k}\left(x(i) - x(s_{i,j})\right)^T\left(x(i) - x(s_{i,j})\right)$$

2-52

The nonlinear interdependency $S^{(k)}$ can be defined in terms of these distances [6, 50, 60]:

$$S^{(k)}(X|Y) = \frac{1}{N-(m-1)\tau}\sum_{i=1+(m-1)\tau}^{N}\frac{R_i^{(k)}(X)}{R_i^{(k)}(X|Y)}$$

2-53

By definition, $R_i^{(k)}(X|Y) \geq R_i^{(k)}(X)$, thus $0 < S^{(k)}(X|Y) \leq 1$, ie the measure is normalised. Low values of $S^{(k)}(X|Y)$ represent independence between the two signals $x(n)$ and $y(n)$, while $S^{(k)}(X|Y) \to 1$ indicates the two signals are highly synchronised.

We can also define

$$H^{(k)}(X|Y) = \frac{1}{N-(m-1)\tau}\sum_{i=1+(m-1)\tau}^{N}\log\frac{R_i(X)}{R_i^{(k)}(X|Y)}$$

2-54

$$N^{(k)}(X|Y) = \frac{1}{N-(m-1)\tau}\sum_{i=1+(m-1)\tau}^{N}\frac{R_i(X) - R_i^{(k)}(X|Y)}{R_i(X)}$$

2-55

$H^{(k)}(X|Y)$ is not normalised, as $R^i(X|Y) \geq 0$ and $R_i^{(k)}(X|Y) \geq 0$, but we cannot conclude which is larger in general. Arnhold et al [50] note that it is very unlikely for $H^{(k)}(X|Y)$ to be negative. $N^{(k)}(X|Y)$ is a normalisation of $H^{(k)}(X|Y)$ [6]

2.2.1.5.2 **Omega complexity and s-estimator**

Omega complexity measures the dissimilarity of correlations in the trajectory of state space vectors. First we calculate the covariance matrix of the concatenated state space vectors of the two signals $x(n)$ and $y(n)$, ie $C = E[z^T(n)z(n)]$, where $z(n) = [x^T(n), y^T(n)]^T$. Then the normalised eigenvalues $\hat{\lambda}_i$ of the covariance matrix C are calculated

$$\hat{\lambda}_i = \frac{\lambda_i}{\sum_{i=1}^{2m} \lambda_i} = \lambda_i \bigg/ \sum_{i=1}^{2m} \lambda_i \qquad \text{2-56}$$

where λ_i are the eigenvalues of C. Then omega complexity Ω is defined as [72]:

$$\Omega = \exp\left(-\sum_{i=1}^{2m} \hat{\lambda}_i \log \hat{\lambda}_i \right) \qquad \text{2-57}$$

The S-estimator is a normalisation of Ω, defined as [51]:

$$S_{est} = 1 + \frac{1}{\log(2m)} \sum_{i=1}^{2m} \hat{\lambda}_i \log \hat{\lambda}_i \qquad \text{2-58}$$

When the signals are identical, the spectrum of eigenvalues is degenerate (all eigenvalues except one are equal to zero), giving the smallest value of $\Omega = 1$ and $S_{est} = 1$, corresponding to maximum synchrony. The largest value of $\Omega = 2m$ indicates a uniform distribution of the spectrum of eigenvalues, and corresponds to independent signals and $S_{est} = 0$.

2.2.2 **Effective connectivity measures (directional connectivity)**

Effective connectivity refers to the influence that one neural system has over another [4]. Influence of one time series on another was first proposed by Norbert Wiener who conceived the notion that if the prediction of one time series $x(t)$ could be improved by incorporating the knowledge of a second one $y(t)$, then the second series is said to have a causal influence on the first [73]. Later, in 1969, Granger used Wiener's idea to establish a mathematical formulation in the context of linear stochastic modelling of time series, so defining Granger

causality (GC) [74]. According to the Granger formulation, $x(t)$ is influenced by $y(t)$ if the variance of the autoregressive prediction error of $x(t)$ is reduced by the inclusion of past measurements of $y(t)$.

Granger causality is a measure based on multiple autoregressive models. An alternative approach that has the advantage of being model-free is based on information theory. Two such measures are transfer entropy (TE) [17, 75] and Kullback–Leibler (KL) divergence [76]. Transfer entropy quantifies the average information about x(t) obtained from the past of $y(t)$ that is not already contained in the past of $x(t)$ [77]. Transfer entropy can be viewed as conditional mutual information (CMI) [78] which could be interpreted as the diversity of state transitions in the destination minus associative noise between those state transitions and the state of the source [79, 80]

For three or more time series (the multivariate situation), one approach is reducing the situation to a set of bivariate situations by performing pair-wise analysis. This approach has some inherent limitations because bivariate measures may falsely detect (direct) causal connection between two time series when the influence is mediated by a third time series. For example, causal interaction between two time series may be erroneously detected by bivariate measures if they are both influenced by a third time series but with different delays [81, 82]. To address this problem, conditional Granger causality (CGC) has emerged as an extension of bivariate Granger causality for three time series [83]. Here, $y(t)$ influences $x(t)$ if the prediction error variance of $x(t)$ is reduced after including the past of y(t) in the model, when the past of the third time series $z(t)$ is included in both cases [84, 85].

TE also has been extended to include the conditioning effect of a third signal on the measurement of influence of the driving signal on the response signal, by including the third signal in the conditioning term of conditional mutual information. This is partial transfer

entropy (PTE) [78, 86, 87]. A natural extension of mutual information also accounts for the presence of a confounding signal. It measures the information shared between two time series that is not contained in third one, and is called partial mutual information (PMI) [19, 88].

Directed coherence (DC) and directed transfer function (DTF) also uses an MVAR model to describe the data, but viewed in the frequency domain. Both measure the relationship from one signal to the other as the normalised transfer function between the signals, but they use different normalisations) [15]. Partial directed coherence (PDC) is similar but is designed to only reflect direct relationships between signals [16, 56, 89]. Granger causality can also be reinterpreted in the frequency domain, yielding frequency-domain Granger causality (FGC) [90].

The MVAR model used in the original PDC approach only accounts for lagged effects among the time series and ignores instantaneous effects. Zero-lag interactions are likely to occur among simultaneously recorded signals. Therefore, DC and PDC derived from traditional MVAR modelling may produce ambiguous causal interaction. To identify the correct connectivity patterns in such situations, extended directed coherence (EDC) and extended partial directed coherence (EPDC), using an extension of the MVAR model that includes instantaneous effects, have been proposed [89]. "A disadvantage of the PDC is that it is not scale invariant" [91], so generalised partial directed coherence (GPDC) has been introduced to circumvent the numerical problem associated with time series scaling.

Granger causality is based on a linear frame work and is naturally inferred parametrically through autoregressive models of time series data, therefore it does not quantify high-order causality and is limited to detecting linear causality only [17]. A model-free Granger causality measure estimated using conditional copula has been introduced to consider nonlinear and high-order causality (QGC) [29].

Granger causality is based on a linear frame work and is naturally inferred parametrically through autoregressive models of time series data, therefore it does not quantify high-order causality and is limited to detecting linear causality only [85]. A model-free Granger causality measure estimated using conditional copula has been introduced to consider nonlinear and high-order causality (QGC) [92].

It is still a major concern that the ability of the above connectivity measures to estimate indirect interactions depends considerably on the ability to measure all related variables in a system. This is often impossible, because a system can be affected by both exogenous (unmeasured external noises) and latent variables (unmeasured underlying signals) [93].

To address the problem of exogenous inputs and latent variables, partial Granger causality (PGC) has been recently introduced, inspired by the definition of partial correlation in statistics. The variance of the common input is required to compute partial correlation and this variance can be accurately known when the common inputs are measurable, which is not the case for exogenous inputs or latent variables. PGC uses conditional variance to discount the effect of the latent and exogenous variable [94]. The multivariate Granger causality (MVGC) and spectral multivariate Granger causality (SMVGC) have also been recently proposed. These approaches to Granger causality are based on multiple equivalent representations of a vector autoregressive (VAR) model [95] in the time and frequency domains respectively

In contrast, directed phase-locking value (PLV) searches for a consistent phase relationship between two time series at a range of lags, choosing the largest [87].

2.2.2.1 Granger causality and extended measures

Granger causality is one of the most popular methods for measuring causal connectivity in neuronal time series [96-99].

According to the Granger causality formulation, an autoregressive model is fitted to each of the time series separately. This model is then compared with a bivariate autoregressive model, ie one where the past of both time series is included in the model. If the variance of the autoregressive prediction error of the first time series is statistically significantly decreased by the inclusion of past measurements from the second time series, then the second time series is said to have a causal influence on the first one.

Now we give the mathematical formulation of Granger causality and then proceed to define conditional, partial and multivariate Granger causality. Let $x(t)$ and $y(t)$ be two stationary time series, then they individually can be represented by autoregressive models

$$x(t) = \sum_{\ell=1}^{p} A_{11_\ell}\, x(t-\ell) + \eta_1(t) \qquad , var(\eta_{1t}) = \Sigma_1$$
$$y(t) = \sum_{\ell=1}^{p} A_{22_\ell}\, y(t-\ell) + \eta_2(t) \qquad , var(\eta_{2t}) = \Sigma_2$$

2-59

and jointly they can be represented by the following bivariate autoregressive model

$$x(t) = \sum_{\ell=1}^{P} A_{11_\ell}\, x(t-\ell) + A_{12_\ell} y(t-\ell) + e_x(t)$$
$$y(t) = \sum_{j=1}^{p} A_{21_\ell}\, x(t-\ell) + A_{22_\ell} y(t-\ell) + e_y(t)$$

2-60

where the noises $\eta_1(t), \eta_2(t), e_x(t)$ and $e_y(t)$ are individually zero mean and uncorrelated, ,

i.e. $\mathbb{E}\{\eta_i(t)\eta_i(t-\tau)\} = 0$, and $\mathbb{E}\{e_\alpha(t)e_\alpha(t-\tau)\} = 0$ for all $\tau \neq 0, i = 1,2$, and $\alpha = x,y$

Let $cov\left(e_x(t), e_y(t)\right) = \Sigma_{xy}$ then their noise covariance matrix can be presented as

$$\Sigma_{noise} = \begin{bmatrix} \Sigma_{xx} & \Sigma_{xy} \\ \Sigma_{yx} & \Sigma_{yy} \end{bmatrix}$$

2-61

The overall interdependence between two time series can be evaluated as:

$$F_{x,y} = ln \frac{\Sigma_1 \Sigma_2}{|\Sigma_{noise}|}$$

2-62

where $|.|$ denotes the determinant of the enclosed matrix. $F_{x,y}$ is non-zero if the two time series are dependent i.e. partial correlation between $x(t)$ and $y(t)$ (conditional on the past of those value) is zero. It is equal to the zero when two time series are independent [90]. $F_{X,Y}$ can be decomposed into three components

$$F_{x,y} = F_{y \to x} + F_{x \to y} + F_{x.y}$$

2-63

where $F_{y \to x}$ is the measure of linear causality from $x(t)$ to $y(t)$, given by

$$F_{y \to x} = ln \frac{\Sigma_1}{\Sigma_{xx}}$$

2-64

and $F_{x \to y}$ is the measure of linear causality from $x(t)$ to $y(t)$, given by

$$F_{x \to y} = ln \frac{\Sigma_2}{\Sigma_{yy}}$$

2-65

and $F_{x.y}$ is a measure of the instantaneous causality, given by

$$F_{x.y} = ln \frac{\Sigma_{xx}\Sigma_{yy}}{|\Sigma_{noise}|}$$

All measures are zero when the two time series are independent, and non-zero if and only if they are dependent.

2.2.2.1.1 Time domain conditional Granger causality

For three or more time series, we can reduce the problem to the bivariate scheme and perform pairwise analysis. But as discussed earlier, a pairwise analysis has some inherent limitations. The conditional Granger causality (CGC) is the one of the well-known extensions that directly

37

addresses these limitations [15, 83, 100]. CGC estimates the influence of one signal on another given knowledge of a third. Let $W(t) = [\omega_1(t), \omega_2(t), \ldots, \omega_n(t)]^T$ be a set of n stationary time series, where T indicates matrix transposition. Suppose that $W(t)$ has been decomposed into three non-overlapping sets of time series $x(t)$, $y(t)$ and $z(t)$ with dimensions k, l and m respectively, where $m + l + k = n$. The conditional Granger causality from $y(t)$ to $x(t)$ given $z(t)$ is defined as:

$$F_{y \to x|z} \qquad\qquad\qquad 2\text{-}66$$

$$= \ln \frac{var(x(t)|x(t-1), x(t-2), \cdots, z(t-1), z(t-2)\cdots)}{var(x(t)|x(t-1), x(t-2)\cdots, y(t-1)y(t-2), \cdots, z(t-1)z(t-2), \cdots)}$$

The above time domain definition can be achieved by combining two autoregressive models. First $x(t)$ and $z(t)$ are supposed to be related by the following bivariate model.

$$x(t) = \sum_{\ell=1}^{P} D_{11_\ell} x(t-\ell) + D_{13_\ell} z(t-\ell) + \Theta(t) \qquad\qquad 2\text{-}67$$

$$z(t) = \sum_{\ell=1}^{P} D_{31_\ell} x(t-\ell) + D_{33_\ell} z(t-\ell) + \Psi(t)$$

where the noises $\Theta(t)$ and $\Psi(t)$ are zero mean and uncorrelated over time.

Let $cov(\Theta(t), \Psi(t)) = \sum_{\Psi\Theta}$ then the noise covariance matrix for the bivariate model can be presented as

$$\sum_{noise(1)} = \begin{bmatrix} \sum_{\Theta\Theta} & \sum_{\Theta\Psi} \\ \sum_{\Psi\Theta} & \sum_{\Psi\Psi} \end{bmatrix} \qquad\qquad 2\text{-}68$$

The second autoregressive model is the following trivariate model involving $x(t), y(t)$ and $z(t)$

$$x(t) = \sum_{\ell=1}^{P} B_{11_\ell} x(t-\ell) + B_{12_\ell} y(t-\ell) + B_{13_\ell} z(t-\ell) + e_x(t)$$

$$y(t) = \sum_{\ell=1}^{P} B_{21_\ell} x(t-\ell) + B_{22_\ell} y(t-\ell) + B_{23_\ell} z(t-\ell) + e_y(t)$$

$$z(t) = \sum_{\ell=1}^{P} B_{31_\ell} x(t-\ell) + B_{32_\ell} y(t-\ell) + B_{33_\ell} z(t-\ell) + e_z(t)$$

where the noises $e_x(t)$, $e_y(t)$ and $e_z(t)$ are again supposed to be zero mean and uncorrelated over time.

Let $cov\big(e_x(t), e_y(t)\big) = \sum_{xy}$ then the covariance of all the noises is given by:

$$\Sigma_{noise(2)} = \begin{bmatrix} \Sigma_{xx} & \Sigma_{xy} & \Sigma_{xz} \\ \Sigma_{yx} & \Sigma_{yy} & \Sigma_{yz} \\ \Sigma_{zx} & \Sigma_{zy} & \Sigma_{zz} \end{bmatrix} \qquad \text{2-70}$$

The conditional Granger causality from $y(t)$ to $x(t)$ given $z(t)$ is defined as:

$$F_{y \to x|z} = \ln \frac{|\Sigma_{\theta\theta}|}{|\Sigma_{xx}|} \qquad \text{2-71}$$

If the inclusion of $y(t)$ results in improved prediction of $x(t)$ ($y(t)$ has a direct influence on $x(t)$), $|\Sigma_{\theta\theta}| > |\Sigma_{xx}|$ and $F_{y \to x|z} > 0$. In contrast if $x(t)$ and $y(t)$ are independent, $|\Sigma_{\theta\theta}| = |\Sigma_{xx}|$ and $F_{y \to x|z} = 0$ [101].

2.2.2.1.2 Conditional frequency domain Granger causality

The time-domain conditional Granger causality can be decomposed into its spectral domain. First, we normalise both bivariate and trivariate models in equation 2-68 and equation 2-70. Normalisation will remove the correlation between noises in bivariate and noises in trivariate models and ensure that the causality is the result of the interactions between the regression terms in trivariate model only.

For normalisation both equation of the bivariate model are pre-multiplied by the following transformation matrix

$$q = \begin{bmatrix} q_{11} & q_{12} \\ q_{21} & q_{22} \end{bmatrix} \qquad\qquad 2\text{-}72$$

where $q_{11} = I_m$, $q_{12} = 0$, $q_{21} = \sum_{\Psi\Theta}\sum_{\Psi\Psi}^{-1}$ and $q_{22} = I_k$

and both side of the trivariate model are pre-multiplied by

$$p_1 = \begin{bmatrix} p_{11} & p_{12} & p_{13} \\ p_{21} & p_{22} & p_{23} \\ p_{31} & p_{32} & p_{33} \end{bmatrix} \qquad\qquad 2\text{-}73$$

where $p_{11} = I_m, p_{12} = 0, p_{13} = 0, p_{21} = -\sum_{yx}\sum_{xx}^{-1}, p_{22} = I_n, p_{23} = 0, p_{31} = $

$(\sum_{yx}\sum_{xx}^{-1})(\sum_{zy} - \sum_{zx}\sum_{xx}^{-1}\sum_{xy})(\sum_{yy} - \sum_{yx}\sum_{xx}^{-1}\sum_{xy})^{-1} - \sum_{zx}\sum^{-1}{}_{xx}, p_{32} = -(\sum_{zy} - $

$\sum_{zx}\sum_{xx}^{-1}\sum_{xy})(\sum_{yy} - \sum_{yx}\sum_{xx}^{-1}\sum_{xy})^{-1}$ and $p_{33} = I_k$

The time domain conditional Granger causality can be expressed in the frequency domain as [84, 93, 100].

$$F_{y\to x|z}(f) = \ln\frac{|\Sigma_\Theta|}{|Q_{xx}(f)\Sigma_{xx}Q_{xx}^*(f)|} \qquad\qquad 2\text{-}74$$

where

$$Q(f) = \begin{bmatrix} Q_{xx}(f) & Q_{xy}(f) & Q_{xz}(f) \\ Q_{yx}(f) & Q_{yy}(f) & Q_{yz}(f) \\ Q_{zx}(f) & Q_{zy}(f) & Q_{zz}(f) \end{bmatrix}$$

$$= \begin{bmatrix} G_{xx}(f) & 0 & G_{xz}(f) \\ 0 & 1 & 0 \\ G_{zx}(f) & 0 & G_{zz}(f) \end{bmatrix}^{-1} \begin{bmatrix} H_{xx}(f) & H_{xy}(f) & H_{xz}(f) \\ H_{yx}(f) & H_{yy}(f) & H_{yz}(f) \\ H_{zx}(f) & H_{zy}(f) & H_{zz}(f) \end{bmatrix}$$

and $|\Sigma_\Theta| = Q_{xx}(f)\Sigma_{xx}Q_{xx}^*(f) + Q_{xy}(f)\Sigma_{yy}Q_{xy}^*(f) + Q_{xz}(f)\Sigma_{zz}Q_{xz}^*(f)$

The quantities in the above expression come from $G(f)$ and $H(f)$ which are the transfer function matrices for the normalised bivariate and trivariate models respectively, i.e. $G_{xx}(f) \overset{DFT}{\longleftrightarrow} B_{11l}$, $H_{xx}(f) \overset{DFT}{\longleftrightarrow} D_{11l}$ and similar.

2.2.2.1.3 Partial Granger causality

The ability of the conditional Granger causality to measure causal influence of one signal on another signal and deal with indirect interactions seriously depends on the all relevant variable in the system. Often it is impossible to measure all variables involved in the system due to the existence of the both exogenous and latent inputs. Thus, dealing with these unmeasured variables is the critical challenge when conditional Granger causality is applied to the signals in the real world. To confront this problem, the partial Granger causality has been proposed [94].

The partial Granger causality between $x(t)$ and $y(t)$ by removing all the effects of $z(t)$, can be evaluated by partitioning the noise covariance matrix $\Sigma_{noise(1)}$ (introduced in equation 2-10)

$$\Sigma_{noise(1)} = \begin{bmatrix} \Sigma_{\Theta\Theta} & \Sigma_{\Theta\Psi} \\ \Sigma_{\Psi\Theta} & \Sigma_{\Psi\Psi} \end{bmatrix} = \begin{bmatrix} \Sigma_{\Theta\Theta} & \Sigma_{\Theta\Psi} \\ \Sigma_{\Psi\Theta} & \Sigma_{\Psi\Psi} \end{bmatrix}$$

2-75

Hence the variance of Θ by eliminating the influence of Ψ can be defined as:

$$cov(\Theta,\Theta) - cov(\Theta,\Psi)cov(\Psi,\Psi)^{-1}cov(\Psi,\Theta) = \Sigma_{\Theta\Theta} - \Sigma_{\Theta\Psi}\Sigma_{\Psi\Psi}^{-1}\Sigma_{\Psi\Theta}$$

2-76

Similarly, we can partition $\Sigma_{noise(2)}$

$$\Sigma_{noise(2)} = \begin{bmatrix} \Sigma_{xx} & \Sigma_{xz} \\ \Sigma_{zx} & \Sigma_{zz} \end{bmatrix}$$

2-77

Similarly, the variance of the $e_x(t)$ by eliminating the influence the $e_z(t)$ is given by

$$cov(e_x(t),e_x(t)) - cov\big(e_x(t),e_z(t)\big)cov\big(e_z(t),e_z(t)\big)^{-1}cov\big(e_z(t),e_x(t)\big)$$
$$= \Sigma_{xx} - \Sigma_{xz}\Sigma_{zz}^{-1}\Sigma_{zx}$$

2-78

Hence the measure for partial Granger causality from $y(t)$ to $x(t)$ by eliminating the effect of $z(t)$ can be expressed as

$$F_{y \to x|z} = \ln\left(\frac{\Sigma_{\Theta\Theta} - \Sigma_{\Theta\Psi}\Sigma_{\Psi\Psi}^{-1}\Sigma_{\Psi\Theta}}{\Sigma_{xx} - \Sigma_{xz}\Sigma_{zz}^{-1}\Sigma_{zx}}\right)$$

2-79

2.2.2.1.4 Copula-based Granger causality

Let we have a set of time series $x_1(t), , ..., x_n(t)$. First the marginal distribution of each time series, $\tilde{F}_i$ are estimated. Next the observations are mapped to the Gaussian copula domain as $\tilde{f}_i(x_i(t)) = \tilde{\mu}_i + \tilde{\sigma}_i \Phi^{-1}\left(\tilde{F}_i(x_i(t))\right)$, where μ and σ are the mean and variance and $\Phi(\cdot)$ is the cdf of the unit Gaussian distribution. Finally, the Granger causality among the $\tilde{f}_i(x_i(t))$ is estimated [102].

Based on the copula method, the marginal properties of the data are separated from its dependency structure. But the interdependence between the mapped time series in the copula space are the same as the interdependence between the original time series [103]. Bahadori and liu in [102] showed that copula-based Granger causality is consistent in high dimensions, unlike Granger causality, and that it is able to efficiently capture non-linearity in the data.

2.2.2.1.5 Multivariate Granger causality

So far, we have considered pairwise Granger causality and its extensions (CGC and PGC), which consider at most three time series at a time. They can be applied to more time series, but this is done by repeated application to all sets of two or three time series as appropriate. In this section we define multivariate Granger causality, which analyses all signals simultaneously to determine direct and indirect connections involving more than three signals.

Let $x(t) = [x_1(t), x_2(t), ... x_n(t)]$ be an n-dimensional multivariate stochastic process. The influence of the time series $x_j(t)$ on $x_i(t)$ can be calculated as:

$$F_{x_j(t) \rightarrow x_i(t)} = \frac{\sum_{x_i(t)|x_1(t), \cdots x_{j-1}(t) x_{j+1}(t), \cdots x_n(t)}}{\sum_{x_i(t)|x_1(t) \cdots x_n(t)}} \qquad \text{2-80}$$

This is similar to conditional Granger causality, but we are conditioning on all other time series, not simply one time series.

2.2.2.1.6 **Multivariate frequency domain Granger causality**

The calculation of the multivariate Granger causality can also be performed in the spectral domain using a factorisation theorem that specifies that any given spectral density matrix $S(f)$ can be decomposed into a set of unique minimum-phase functions $\psi(f)$ [104, 105].

$$S(f) = \psi(f)\psi^H(f) \qquad \qquad 2\text{-}81$$

Using a Fourier-like analysis on the minimum-phase functions, we can calculate the noise covariance matrix $\sum$ and minimum phase- transfer function $H(f)$ as

$$\psi(f) = \sum_{k=0}^{\infty} R_k e^{ik2\pi f} \qquad \sum = R_0 R_0^T \qquad H(f) = \psi(f)R_0^{-1} \qquad \qquad 2\text{-}82$$

where T stands for matrix transposition.

As discussed in section 2.2.1.1.6 after fitting the MVAR model to the time series and Fourier transforming, the overall spectral density matrix can be calculated as

$$S(f) = H(f)\sum H^H(f)$$

where H denotes Hermitian transpose and $\sum$ is the covariance matrix of the noise vector.

The conditional Granger causality needs to compare this estimate of the noise covariance with noise covariance from a model that excludes the jth time series. We obtain this by taking the overall spectral density matrix $S(f)$ and removing the jth row and columns. The reduced spectral density matrix $\bar{S}(f)$ can now be factorised:

$$\bar{S}(f) = G(f)\bar{\sum}G^H(f) \qquad \qquad 2\text{-}83$$

where $G(f)$ is the transfer function matrix and $\bar{\sum}$ is the noise covariance matrix for the selected subsystem. To calculate the normalisation matrix Q(f), we need to extend the transfer function matrix G(f) by inserting zeros for the jth row and column, but with 1 at their intersection:

$$Q(f) = \begin{bmatrix} G_{(1...j-1)(1...j-1)}(f) & 0 & G_{(1...j-1)(1...j-1)}(f) \\ 0...0 & 1 & 0...0 \\ G_{(j+1...n)(1...j-1)}(f) & 0 & G_{(j+1...n)(j+1...n)}(f) \end{bmatrix}^{-1} H(f) \qquad 2\text{-}84$$

Finally, we can use equation 2-74 and calculate the conditional Granger causality from the jth time series to the ith time series as

$$F_{j \to i}(f) = \ln \frac{|\bar{\Sigma}_{ii}|}{|Q_{ii}(f)\Sigma_{ii}Q_{ii}^*(f)|} \qquad 2\text{-}85$$

2.2.2.2 Directional measures based on coherence

It is useful to define the inverse of the spectral density matrix and decompose it as

$$P(f) = S^{-1}(f) = \bar{A}^H(f)\Sigma^{-1}\bar{A}(f) \qquad 2\text{-}86$$

The ijth element of $S(f)$ and $P(f)$ can be represented as

$$S_{ij}(f) = h_i(f)\Sigma h_j^H, \qquad P_{ij}(f) = \bar{a}_i^H(f)\Sigma^{-1}\bar{a}_j(f) \qquad 2\text{-}87$$

where $h_m(f)$ and $\bar{a}_m$ are the mth rows of the transfer function matrix $H(f) = [h_1(f), \cdots h_n(f)]^T$ and coefficient matrix $\bar{A}(f) = [\bar{a}_1(f), \cdots \bar{a}_n(f)]^T$. Since the input white noises are uncorrelated even at lag zero, their covariance matrix $cov(e(t))$ reduces to diagonal form as

$$\Sigma = diag(\sigma_k{}^2)$$

and its inverse to diagonal matrix

$$\Sigma^{-1} = diag\left(\frac{1}{\sigma_k{}^2}\right)$$

where $\sigma_k{}^2$ is the variance of $e_k(t)$. $S_{ij}(f)$ and $P_{ij}(f)$ can be factorised into:

$$S_{ij}(f) = \sum_{m=1}^{n} \sigma_m{}^2 H_{im}(f) H_{jm}(f) \qquad 2\text{-}88$$

$$P_{ij}(f) = \sum_{m=1}^{n} \frac{1}{\sigma_m{}^2} \bar{A}^H{}_{im}(f) \bar{A}_{jm}(f) \qquad 2\text{-}89$$

2.2.2.2.1 Directed coherence (DC)

By substituting for $S_{ij}(f)$ and from equations 2-30 in the coherence equations defined in the section 2.2.1.1.6, the following directional coherence can be obtained

$$c_{ij}(f) = \frac{h_i(f) \sum h_j^H(f)}{\sqrt{h_i(f) \sum h_i^H(f)} \sqrt{h_j(f) \sum h_j^H(f)}} = \sum_{m=1}^{n} \frac{\sigma_m H_{im}(f)}{\sqrt{S_{ii}(f)}} \frac{\sigma_m H^H{}_{jm}(f)}{\sqrt{S_{jj}(f)}} \qquad \text{2-90}$$

$$= \sum_{m=1}^{n} \gamma_{im} \gamma_{jm}^*$$

The term γ_{ij} in the above equation measures the influence of x_j on x_i, the so-called directed coherence DC [56]

$$\gamma_{ij}(f) = \frac{\sigma_j H_{ij}(f)}{\sqrt{S_{ii}(f)}} \qquad \text{2-91}$$

where $S_{ii}(f) = \sum_{m=1}^{n} \sigma_m^2 |H_{im}(f)|^2$

DC can be normalised as $|\gamma_{ij}(f)|^2$, which gives 0 in the absence of any directed influence from x_j on x_i at the frequency f, and achieves 1 in the presence of maximum influence.

2.2.2.2.2 Directed transfer function (DTF)

DTF also uses the transfer function matrix $H(f)$, but normalises it in a simpler way [106]:

$$DTF_{ij} = \frac{H_{ij}(f)}{\sqrt{\sum_{m=1}^{n} |H_{im}(f)|^2}} \qquad \text{2-92}$$

DTF can be considered as a particular case of DC in which all input variances are 1 ($\sigma_1^2 = \sigma_2^2 = \cdots \sigma_n^2 = 1$).

2.2.2.2.3 Partial directed coherence (PDC) and generalised PDC (GPDC)

In the complex network where there are both direct and indirect pathways between two time series, both DC and DTF represent a balance of signal power that spreads from one time series to another via any of these pathways. In other words, a non-zero DC from time series x_j to x_i can be the result of either indirect or direct influence. To confront these issues, the measure partial coherence has been proposed.

Following section 2.2.2.2.1, we can substitute for $P_{ij}(f)$ from equation 2-31 into the expression for partial coherence in equation *2-10,* and write:

$$\Pi_{ij}(f) = \frac{\bar{a}_i^H(f)\Sigma^{-1}\bar{a}_j(f)}{\sqrt{\bar{a}_j^H(f)\Sigma^{-1}\bar{a}_j(f)}\sqrt{\bar{a}_i^H(f)\Sigma^{-1}\bar{a}_i(f)}} = \sum_{m=1}^{n} \frac{\frac{1}{\sigma_m}\bar{A}_{mj}(f)}{\sqrt{P_{jj}(f)}}\frac{\frac{1}{\sigma_m}\bar{A}_{mi}^H(f)}{\sqrt{P_{ii}(f)}} \qquad \textit{2-93}$$

$$= \sum_{m=1}^{n} \pi_{im}\pi_{jm}^H$$

The term π_{ij} in the above equation measures the influence of x_j on x_i, namely generalised partial directional coherency GPDC [107].

$$\pi_{ij} = \frac{\frac{1}{\sigma_m}\bar{A}_{ij}(f)}{\sqrt{P_{jj}(f)}} \qquad \textit{2-94}$$

where $\sqrt{P_{jj}(f)} = \sqrt{\sum_{m=1}^{n}\frac{1}{(\sigma_m)^2}\left|\bar{A}_{jm}(f)\right|^2}$

The original version of the equation () introduced in [56] did not include the input noise variance and was named PDC. The PDC is thus given by:

$$\pi_{ij}^{\omega} = \frac{\bar{A}_{ij}(f)}{\sqrt{\sum_{m=1}^{n}\left|\bar{A}_{mj}(f)\right|^2}} \qquad \textit{2-95}$$

2.2.2.2.4 Direct directed transfer function (DDTF)

To distinguish between direct causal connections between two signals and connections which are mediated by another signal, the directed directed transfer function (DDTF) was introduced [108]. It is defined by multiplying the directed transfer function by the partial coherence. The DDTF from signal j to signal i is defined as:

$$DDTF_{ij} = \pi_{ij}^{\omega}\, DTF_{ij} \qquad \textit{2-96}$$

2.2.2.2.5 Extended directed coherence (EDC) and extended partial directed coherence (EPDC)

The MVAR model introduced in equation $2\text{-}9$ use lagged versions of the time series in the regression model. In other word this model describes the effect of the past of one time series on another, but it does not account for instantaneous (not lagged) effects among time series.

Faes and Nollo proposed in [109] an alternative multivariate autoregressive model that includes instantaneous effects into the model of the time series.

Consider the following extended MVAR model with 0 lag inclusion

$$x(t) = \sum_{\ell=0}^{P} B(\ell)x(t-\ell) + u(t)$$

2-97

where $u(t) = [u_1(t), u_2(t), \cdots, u_m(t)]^T$ is a vector of zero-mean uncorrelated white noise processes with diagonal covariance matrix $\hat{\Sigma} = diag(\hat{\sigma}_k^2)$, and the diagonal of $B(0)$ is constrained to be zero.

We can rewrite equation 2-38 as

$$x(t) = B(0)x(t) + \sum_{\ell=1}^{P} B(\ell)x(t-\ell) + u(t)$$

To find the relationship between the above extended MVAR model and the classic MVAR model in equation (), the term $B(0)x(t)$ is moved to the left

$$x(t)[I - B(0)] = \sum_{\ell=1}^{P} B(\ell)x(t-\ell) + u(t)$$

Substituting for $x(t)$ in this equation with $x(t)$ from original MVAR models yields:

$$\sum_{j=1}^{P} A(\ell)x(t-\ell) + e(t)[I - B(0)] = \sum_{\ell=1}^{P} B(\ell)x(t-\ell) + u(t)$$

Therefore $B(\ell) = LA(\ell)$ and $u(t) = Le(t)$ where $L = [I - B(0)]^{-1}$ and $\Sigma = L\hat{\Sigma}L^T$

Hence the following algorithm can be used for forming the extended MVAR model to describe causal interactions among time series including instantaneous influence.

1. The noise covariance matrix Σ and $A(\ell)$ for the classic MVAR model are calculated.

2. The noise covariance matrix Σ is decomposed to yield the diagonal noise covariance matrix $\hat{\Sigma}$ and the lower triangular matrix L.

3. The instantaneous effects matrix $B(0)$ and coefficient matrices $B(\ell)$ can be calculated using above outlined relationships.

In the spectral domain we can represent the extended MVAR model by the Fourier transform of equation 2-38 as

$$X(f) = B(f)X(f) + U(f) \qquad\qquad 2\text{-}98$$

where $B(f)$ is the coefficient matrix in frequency domain

$$B(f) = B(0) + \sum_{\ell=1}^{P} B(\ell)e^{-i2\pi f \ell T}$$

The spectral matrix $S(f)$ and its inverse $P(f)$ of the extended MVAR model can be expressed as:

$$S(f) = G(f)\hat{\Sigma}G^{H}(f) \, , P(f) = \bar{B}^{H}(f)\hat{\Sigma}^{-1}\bar{B}(f) \qquad\qquad 2\text{-}99$$

where the transfer function $G(f) = [I - B(f)]^{-1}$.

Following the procedure described for GDC and GPDC, we can define the extended directional coherence (EDC) ξ_{ij} and extended partial directed coherence (EPDC) χ_{ij} from x_j to x_i as[110]:

$$\xi_{ij}(f) = \frac{\hat{\sigma}_j G_{ij}(f)}{\sqrt{\sum_{m=1}^{n} \hat{\sigma}_m^2 |G_{im}(f)|^2}} \qquad\qquad 2\text{-}100$$

$$\chi_{ij} = \frac{\frac{1}{\hat{\sigma}_j}\bar{B}_{ij}(f)}{\sqrt{\sum_{m=1}^{n} \frac{1}{(\hat{\sigma}_m)^2}|\bar{B}_{mj}(f)|^2}} \qquad\qquad 2\text{-}101$$

2.2.2.3 Information theoretic measures

In the following, we define information theoretic measures which allows to detect causal relationship between time series.

2.2.2.3.1 Transfer entropy

In section 2.2.1.4, we described information theoretic measures as the model-free measures for estimating functional interaction among time series. Mutual information is one of these measures which quantifies the amount of information that can be obtained about one time series by looking at another. However mutual information is a symmetric measure that describes shared information and not causal relationships. To obtain a causal measure within the information theoretic framework, transfer entropy (TE) has been proposed [111].

TE can be defined in terms of conditional mutual information [111-113], we can say that random variable X cause Y if the uncertainty about Y is decreased by the past knowledge of X.

The conditional mutual information $I(X;Y|Z)$ of the random variables X and Y given the variable Z is defined as [114]

$$I(X;Y|Z) = H(X|Z) + H(Y|Z) - H(X,Y|Z) \qquad \textit{2-102}$$

where $H(X|Z)$ is the conditional entropy of X given Z, as defined in section 2.2.1.4.

The transfer entropy from X to Y then corresponds to the conditional mutual information $I(Y_t; X_{t-1:t-\ell}|Y_{t-1:t-\ell})$, which quantifies the information about the current state of the response system, Y_t, obtained from the past of the driving system, $X_{t-1:t-\ell}$, that is not already contained in the past of the response system $Y_{t-1:t-\ell}$. Thus TE in terms of entropy is given by

$$TE_{X \to Y} = H(Y_t|Y_{t-1:t-\ell}) + H(X_{t-1:t-\ell}|Y_{t-1:t-\ell}) - H(Y_t, X_{t-1:t-\ell}|Y_{t-1:t-\ell}) \qquad \textit{2-103}$$

Since $H(X|Y) = H(X,Y) - H(Y)$, where $H(X,Y)$ denotes the joint entropy is outlined in section 2.2.1.4, the preceding expressions can be also written in the following form:

$$TE_{X \to Y} = H(Y_t, Y_{t-1:t-\ell}) - H(Y_{t-1:t-\ell}) + H(X_{t-1:t-\ell}, Y_{t-1:t-\ell}) \qquad \textit{2-104}$$
$$- H(Y_t, X_{t-1:t-\ell}, X_{t-1:t-\ell})$$

There are several algorithms for calculating TE, but many are prohibitively slow at calculating the required three-dimensional entropy. In this study, we used the binning method. The method is based on the discretisation of the time series into Q equiquantal bins, ie bins with equal counts and therefore different widths. Conditional mutual information can then be calculated by a simple box-counting algorithm based on equiqantal marginal bin [115]

2.2.2.3.2 Partial transfer entropy

In the previous sections, we described transfer entropy as a causality measure in terms of the entropy between two time series, ignoring all other time series. If two time series are a part of a bigger interacting system, e.g. three interacting time series X, Y and Z, then transfer entropy will estimate not only direct interactions between them, but also estimate indirect interactions including a third time series. To estimate only the information transferred directly between the two time series, we need to take into account the influence of the third time series. Partial transfer entropy (PTE) is the extension of TE designed for measuring the influence of X on Y conditioned on Z[116]. In other words, TE has been extended to include the effect of the past of Z on the current state of the response Y and the past of X. This can be done by including the past of Z to the condition term of the conditional mutual information [18, 116]:

$$PTE_{X \to Y|Z} = \text{I}\,(Y_t; X_{t-1:t-\ell}|Y_{t-1:t-\ell}, Z_{t-1:t-\ell}) \qquad \textit{2-105}$$

In terms of entropy, PTE is defined as

$$PTE_{X \to Y|Z} = H\,(X_{t-1:t-\ell}, Y_{t-1:t-\ell}, Z_{t-1:t-\ell}) \qquad \textit{2-106}$$
$$- H\,(Y_t, X_{t-1:t-\ell}, Y_{t-1:t-\ell}, Z_{t-1:t-\ell}) + H\,(Y_t, Y_{t-1:t-\ell}, Z_{t-1:t-\ell})$$
$$- H\,(Y_{t-1:t-\ell}, Z_{t-1:t-\ell})$$

2.2.2.3.3 **Partial mutual information**

As we described earlier mutual information measures information shared between two time series. The partial mutual information $I(X, Y|Z)$ represent the part of mutual information $I(X, Y)$ that is not also shared with a third signal Z.

2.2.2.3.4 **Symbolic transfer entropy (STE) and partial symbolic transfer entropy (PSTE)**

The symbolic transfer entropy (STE) and partial symbolic transfer entropy (PSTE) are defined similarly to TE and PTE, but the calculations use the ranks of the amplitudes rather than the amplitudes themselves [18, 117]. Using ranks rather than amplitudes can assist in fine-tuning parameters, as the distribution of the data is known in advance.

2.2.2.3.5 **Kullback-Leibler divergence**

As described in section 2.2.1.4.6, Kullback-Leibler divergence is an asymmetric measure in its original form, and so is a directional measure.

2.2.2.3.6 **Directional phase-locking value (dPLV)**

In section 2.2.1.3.1 we described mean phase coherence (or phase-locking value) as a measure that quantifies the (symmetrical) phase relationship between two time series. dPLV extends this to give directional information by delaying one signal, hence calculating mean phase coherence between $y(t)$ and a lagged version of time series $x(t - l)$. dPLV is determined by calculating these mean phase coherences for a range of lags and selecting then maximum value as the result. As only one signal is lagged, this introduces an asymmetry which allows access to the directional relationship between two signals.

$$\Delta\varphi(t) = n\varphi_x(t - l) - m\varphi_y(t) \qquad \textit{2-107}$$
$$R(l) = \langle e^{-i\Delta\varphi(t)} \rangle = \sqrt{\langle \cos(\Delta\varphi(t)) \rangle^2 + \langle \sin(\Delta\varphi(t)) \rangle^2}$$
$$dPLV = \max_{l=1,\ldots,L} R(l)$$

2.3 Significance analysis

2.3.1 Surrogate data

Surrogate data analysis was originally proposed to evaluate the existence of nonlinear dynamics [118]. Recently it has been used as an important way to provide a threshold for significance for connectivity measures [111, 119, 120]. Surrogate data are artificial data which mimic specific data properties of an original signal but randomise other properties of interest of the original signal.

The surrogates throughout this study are generated using iteratively refined amplitude adjusted Fourier transform (IAAFT) [121]. These surrogate data have the same Fourier amplitudes as the original data but with random phases, and also have the same distribution of time-domain amplitudes. Since the conventional power spectral density is the modulus squared amplitude of the Fourier transform, the original data and its surrogate generated by this technique have the same power spectral densities. Any underlying nonlinear interaction within the original data set is destroyed using phase randomisation. This type of surrogate, which maintains both the power spectrum and the amplitude distribution of the original data, is well suited to analyse the nonlinearity and complexity of signals [122, 123].

2.3.2 Methodology

The following steps were performed in order to identify when two signals have a statistically significant connection

1. IAAFT surrogate data was generated to give data with the same statistical properties as the original data but with the nonlinear dependencies between signals destroyed by the phase randomisation

2. The connectivity measures were computed for 100 surrogate realisations, and averaged over the 150 or 100 realisations of the original data.

3. This yielded 100 measurements of synchronisation on surrogate data, which we use as an estimate of the distribution of the measure in the absence of any synchronisation.

4. The fifth largest surrogate measurement was selected as the threshold to give a 5% significance level.

5. If the connectivity measure calculated on the original data exceeded this threshold, then it is regarded as statistically significant [87, 116, 118, 122].

Under this design, the false positive rate should be controlled at 5%. In order to check this, we ran the method under the null hypothesis for one of the simulated datasets (Hénon map) outlined in the following chapter when there is no coupling between time series. Results for 1000 iterations on five functional connectivity measures, one measure from each family, are recorded in Table 2-1. These results should be 0.05 +/- 0.007, using the binomial distribution for 1000 iterations. show that the false positive rate is always too small and less than or equal to the 0.05.

Table 2-1:   False positive rates for five functional connectivity measures under the null hypothesis that there is no connectivity. Due to the use of surrogates to identify significance, these rates should be controlled to be 5%. The simulation uses 1000 iterations, and hence using the binomial distribution the results should be 0.05 ± 0.007.

Measure	False positive rate
Correlation coefficient	0.056
Mutual information (histograms)	0.050
Phase synchronisation Hilbert	0.054
Omega Complexity	0.056
Event synchronisation	0.044

CHAPTER 3   FUNCTIONAL CONNECTIVITY MEASURES

In this section, we use simulated data, where we know the "truth", to compare different functional connectivity measures. Note that we are not optimizing any of the connectivity measures, we are using them as described in the literature review and using thresholds and other parameters as recommended by the proposers or users of the measures.

3.1 Uni-directionally coupled Hénon maps

Our first simulations to examine functional connectivity generate data from two coupled systems X and Y, a pair of unidirectionally coupled Hénon maps given by the following equations

$$X \begin{cases} x(k+1) = 1.4 - x^2(k) + bu(k) \\ u(k+1) = x(k) \end{cases}$$

$$Y \begin{cases} y(k+1) = 1.4 - \left[\mu\, x(k) + (1-\mu)y(k) \right]y(k) + dv(k) \\ v(k+1) = y(k) \end{cases}$$

These coupled equations for driver X and response Y are linked with the coupling strength μ, which varies from 0 to 1. Following the literature, we analyse three standard cases, commonly referred to as identical systems $(b = d = 0.3)$, and nonidentical systems $(b = 0.3, d = 0.1)$ and $(b = 0.1, d = 0.3)$ [13, 14, 124-129]. Throughout this thesis, we refer to these systems as IS, NS1 and NS2 respectively.

3.1.1 Variation of measures against coupling strength

We vary the strength of a relationship between signals by varying the coupling strength μ. For all cases we varied the coupling strength from $\mu = 0$ (no coupling) to $\mu = 1$ (complete coupling) in steps of 0.1 [13, 14, 124-129]. Simulations generated 10,000 data points but excised the first 1000 samples to avoid transient start up effects. The generation process was repeated 150 times with different random initial conditions, with the calculated synchronisation measures averaged over the 150 realisations

3.1.1.1 Identical systems

Figure 3-1 shows plots of $x(k)$ versus $y(k)$ for identical systems, for coupling strengths from 0 to 1. The plots show an increase in synchronisation as the coupling strength increases, but from $\mu = 0.7$ the system switches to perfect synchronisation, i.e. $x(k) = y(k)$ as the maximum sub-Lyapunov exponent goes negative [124]. This can be seen in the figure where the synchrony becomes increasingly apparent as the coupling strength approaches 0.7, and perfect synchrony is achieved for coupling strengths above 0.7.
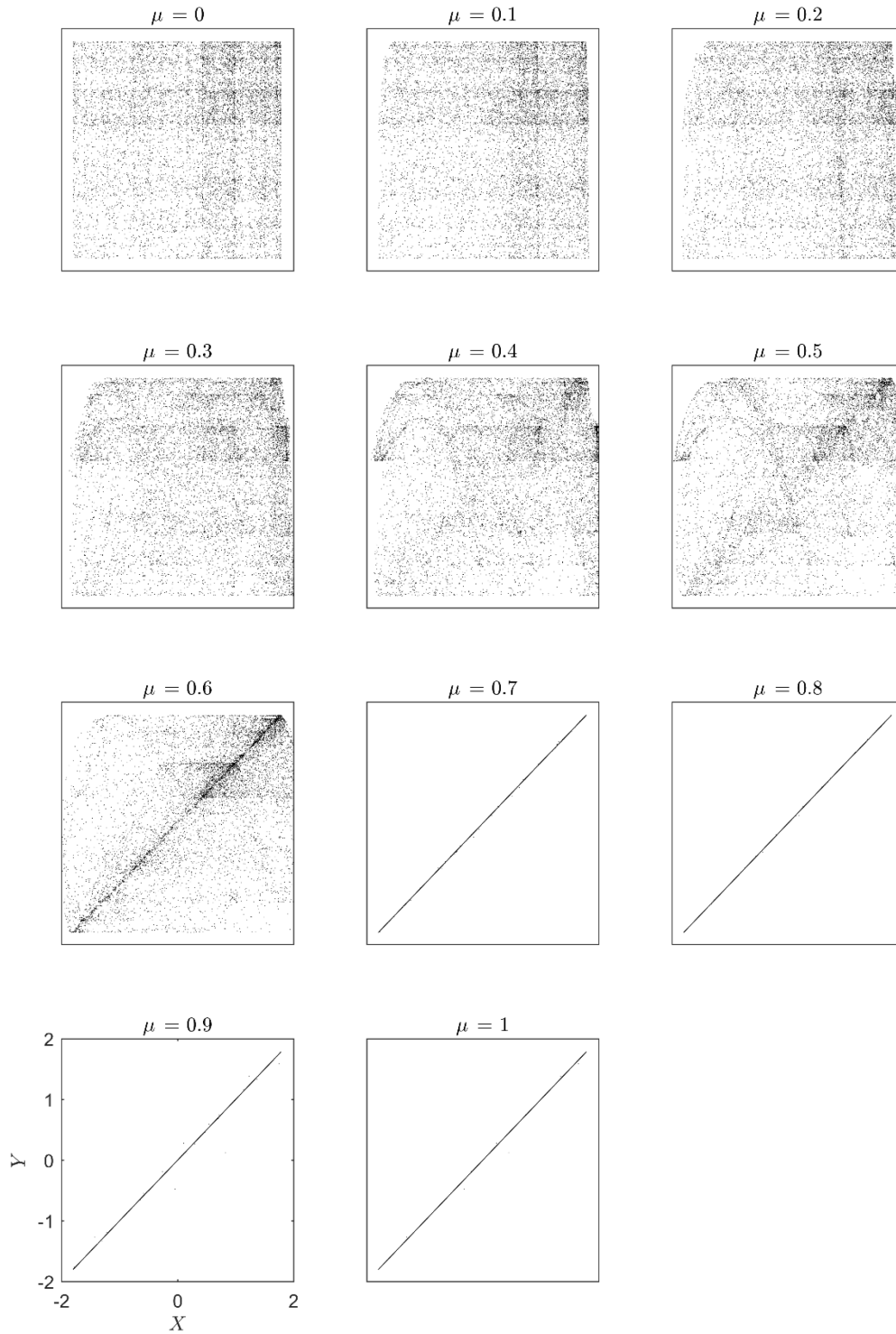
Figure 3-1:   Plots of x(k) vs y(k) for identical systems for coupling strengths μ from zero to one. Identical synchronisation between the systems takes place for sufficiently high levels of coupling, as indicated by the straight line at 45° for μ ≥ 0.7.

A plot of the largest sub-Lyapunov exponent calculated from the response system as a function of the coupling μ for identical systems is shown in Figure 3.1.2-2 (a). To examine identical synchronisation and understand its relation to sub-Lyapunov component, we also calculate the difference between two outputs of the response system $y(k)$ and $y'(k)$ that were driven with the same driver system output $x(k)$, but with different initial conditions for the response system. Figure 3-2 (b) shows a plot of this difference with the first 1000 data points deleted. If two responses are synchronised at a particular coupling strength, the difference should be zero. Figure 3-2 (a) and (b) indicate that the difference goes to zero when the largest sub-Lyapunov exponent becomes negative, i.e. at $0.47 \lesssim \mu \lesssim 0.52$ and $\mu \gtrsim 0.7$.

"This image has been removed due to copyright restrictions."

(a)

(b)
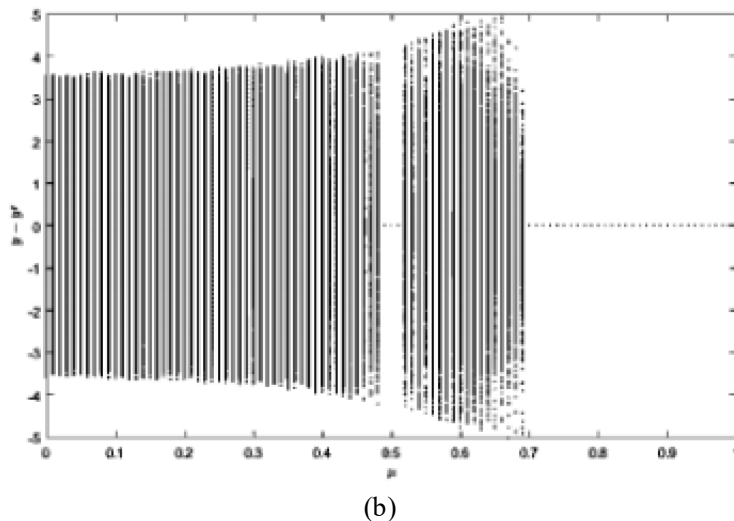
Figure 3-2: The largest sub-Lyapunov exponent for identical systems. (a) Plot of the largest sub-Lyapunov exponent as a function of coupling strength for identical systems [14] (b) Plot of the difference between two outputs of the response system, $y(k) - y'(k)$, calculated with the same driver system but different initial conditions in the response system, against increasing coupling strength.

3.1.1.2 Results for identical systems

Figure 3-3 shows the calculation of 29 synchronisation measures against increasing coupling strength between two identical Hénon maps. To discuss the results, it is convenient to split the figures into three regions. For low coupling strengths, the measures do not exceed the threshold for significance set by the surrogates, and so the shape of the curve is not important. After the measure, has detected a statistically significant level of synchronisation, all measures increase

with increasing coupling strength, except for the local hump in the region $0.47 \lesssim \mu \lesssim 0.52$ due to the largest sub-Lyapunov exponent being negative. The final region is $\mu \gtrsim 0.7$, where, as discussed earlier, identical synchronisation occurs [124]. In the final region all measures show the sharp increase at point $C \approx 0.7$ corresponds to the point when the identical synchronisation between the systems takes place and detect the synchronisation as expected.

Table 3-1 shows the lowest value of the coupling strength for which a measure detects significant synchrony. Four measures, viz partial coherence, mutual information (adaptive histograms), nonlinear interdependence (H^k) and nonlinear Interdependence (N^k), detect significant synchrony for $\mu \geq 0.1$, and so can be considered as robust measures for detecting weak coupling in this simulation. We also observe that correlation coefficient, coherence, mean phase coherence (wavelet), mutual information (kernels) detect synchronisation for $\mu \geq 0.2$, and correntropy coefficient, coh-entropy and nearest-neighbour mutual information detect synchronisation for $\mu \geq 0.3$, suggesting they are also measures that are sensitive to weak coupling. On the other hand, maximum likelihood mutual information, nonlinear interdependence (S^k), wave-entropy, event synchronisation, mutual information (time-frequency plane), Kullback-Leibler divergence (histogram), Rényi divergence, Jensen-Shannon divergence, Jensen-Rényi divergence, omega complexity and s-estimator first detect synchrony at $\mu = 0.5$, suggesting they are less able to detect weak levels of synchronisation.

Some measures give unsatisfactory results; Mean phase coherence (Hilbert), phase coherence value wrapped, conditional based phase synchrony and omega complexity detect synchrony when there is no coupling, suggesting that these measures are susceptible to finding synchrony when it is not present.

Note that the performance of linear measures is similar to the performance of nonlinear measures. More specifically, the three linear measures (partial coherence, correlation coefficient

and coherence) first detect synchronisation at a coupling strength of 0.1, 0.2 and 0.2 respectively. Hence, we conclude that linear measures are able to detect synchronisation in nonlinear systems, a point not acknowledged in the literature.

Figure 3-3: Functional connectivity measures for IS with no added measurement noise. Functional connectivity measures calculated from the original data (blue) and the threshold based on surrogate data (red) for IS with no added measurement noise, plotted against coupling strength.

Table 3-1:   The lowest value of coupling strength that detects significant synchrony for IS.   Good and unsatisfactory performance outcomes are highlighted by colouring the text blue and red respectively.

Measure	Lowest μ that achieves significant synchrony
Mean phase coherence (Hilbert)	0.0
Phase coherence value wrapped	0.0
Conditional probability based phase synchrony	0.0
Omega Complexity	0.0
Partial coherence	0.1
Mutual information (adaptive histograms)	0.1
Nonlinear Interdependence (H^k)	0.1
Nonlinear Interdependence (N^k)	0.1
Correlation coefficient	0.2
Coherence	0.2
Mean phase coherence (wavelet)	0.2
Mutual information (kernels)	0.2
Correntropy coefficient	0.3
Coh-entropy coefficient	0.3
Nearest-neighbour mutual information	0.3
Mean phase coherence (event)	0.4
Mutual information (histograms)	0.4
Wave-entropy	0.5
Event synchronisation	0.5
Mutual information (time-frequency plane)	0.5
Kullback Leibler divergence (histogram)	0.5
Rényi Divergence	0.5
Jensen-Shannon divergence	0.5
Jensen-Rényi divergence	0.5
S-estimator	0.5
Maximum likelihood mutual information	0.6
Nonlinear Interdependence (S^k)	0.6
Phase coherence value unwrapped	0.7

Correlation coefficient and related measures
Phase synchrony
Information-theoretic measures
Synchronisation based on state space
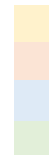
Unsatisfactory ————
Robust ————

3.1.1.3 Nonidentical systems type 1

Figure 3-4 shows plots of $x(k)$ versus $y(k)$ for NS1 ($b = 0.3, d = 0.1$), for coupling strengths from 0 to 1. The identical synchronisation situation (straight line at 45º) cannot be observed here. The absence of identical synchronisation is one of the main features of the nonidentical systems [130]. A plot of the largest sub-Lyapunov exponent calculated from the response system as a function of the coupling strength μ is shown in Figure 3.1.2-5. To explore the relationship between coupling strength and the maximum sub-Lyapunov exponent for this system, we again calculated the difference between two-time series drawn from the response system where both are driven with the same driving signal $x(k)$, but with different response system initial conditions. The difference is shown in Figure 3-5 (b). As mentioned earlier, if the response signals are synchronised at a value of the coupling strength, then the difference should be equal to zero. As Figure 3-5 (a) shows, the largest sub-Lyapunov exponent is negative in two distinct regions ($0.1 \lesssim \mu < 0.3$ and $\gtrsim 0.5$) ,corresponding to the response signals being synchronised and their difference equalling zero. We see the difference equalling zero is mostly true, but not always. This is explained by transients not disappearing yet. If 15000 samples are discarded then the "right" picture can be obtained. Here we present the plot which is generated using our simulations.
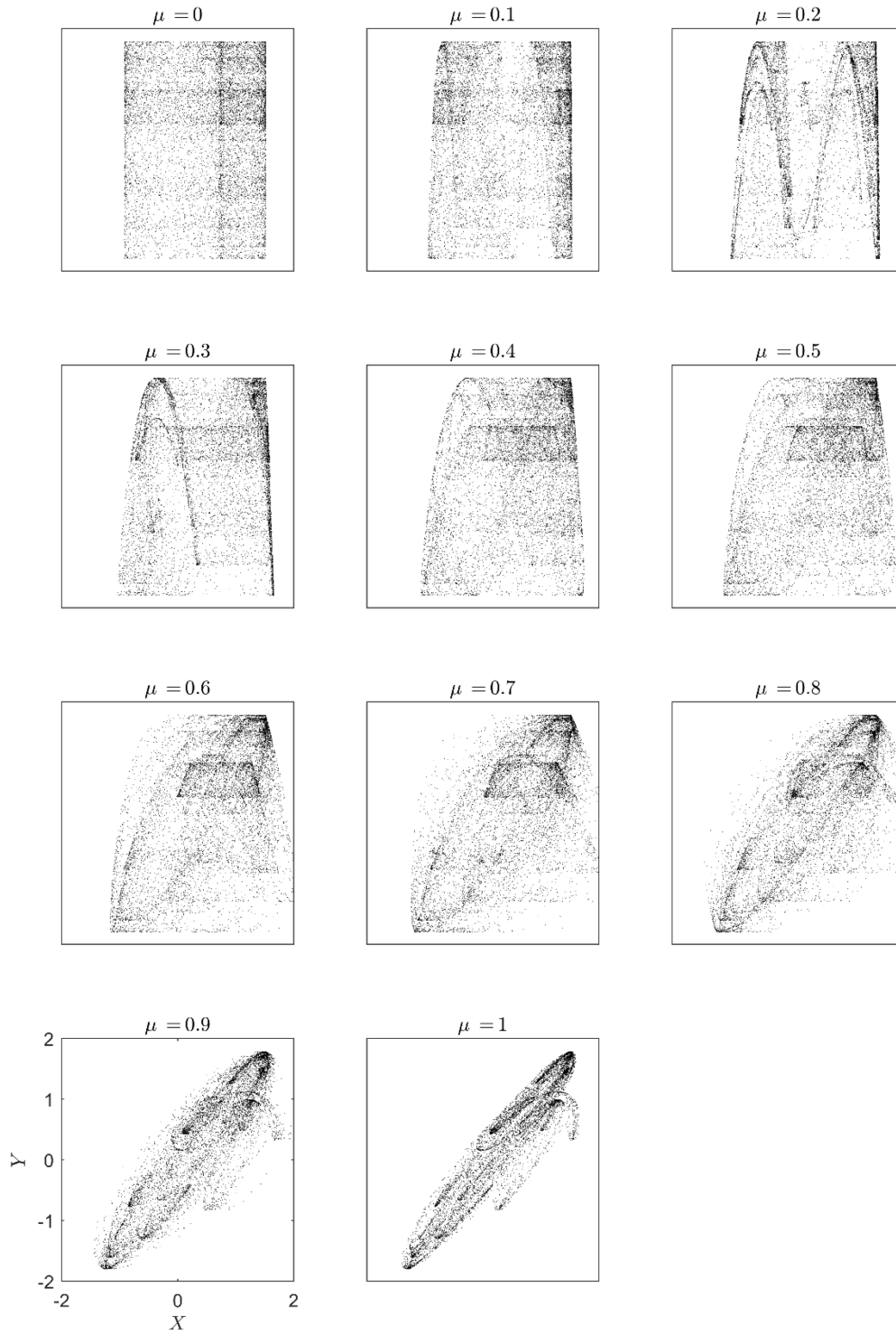
Figure 3-4:   Plot of X vs Y for NS1 for coupling strengths from 0 to 1 in separate plots. At no level of coupling strength is identical synchronisation achieved.

(a)

(b)
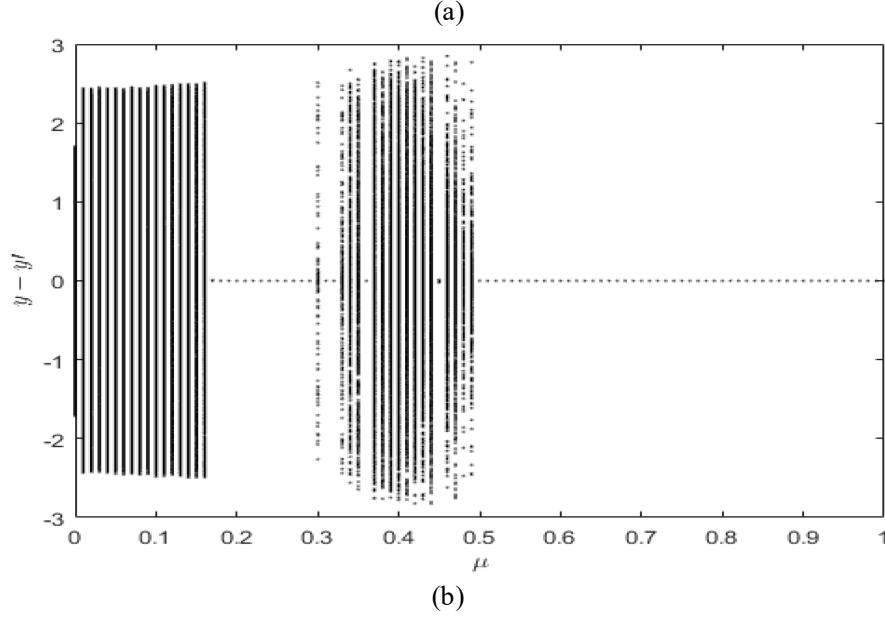
Figure 3-5: *Plot of largest sub-Lyapunov and difference between outputs for NS1 (a) Plot of the largest sub-Lyapunov exponent as a function of coupling strength for NS1 [14] (b) Plot of the difference between two outputs of the response system(y(k)-y'(k)) against increasing coupling strength.*

3.1.1.4 Results for nonidentical systems type 1

Figure 3-6 shows the calculation of 29 measures against increasing coupling strength μ for NS1. As there is synchrony, albeit weak, from $\mu = 0.1$ we would like to see a measure above its threshold from $\mu \geq 0.1$. Table 3-2 shows us when a measure first detects synchrony that is statistically significant. Correlation coefficient, coherence, partial coherence, mean phase coherence, phase coherence value unwrapped, mutual information (adaptive histograms), mutual information (kernels) first detect significant synchrony at $\mu = 0.1$, suggesting these measures are robust measures for detecting weak coupling. We also note that some measures, e.g. correlation and many others, show increasing synchrony as the coupling strength increases, but with a bump in the range $0.1 \lesssim \mu \lesssim 0.3$. While this visually conforms to the known dynamics of the system, this does not provide any statistically significant evidence in favor of any measure.

Some measures perform unsatisfactorily: wavelet-KL fails to detect synchrony at any coupling strength; wave-entropy and PCV unwrapped fail to detect synchrony at some coupling

strengths despite detecting it at lower coupling strengths; and Hilbert Phase, PCV wrapped and

lambda bar detect synchrony when there is none (coupling strength equals zero).
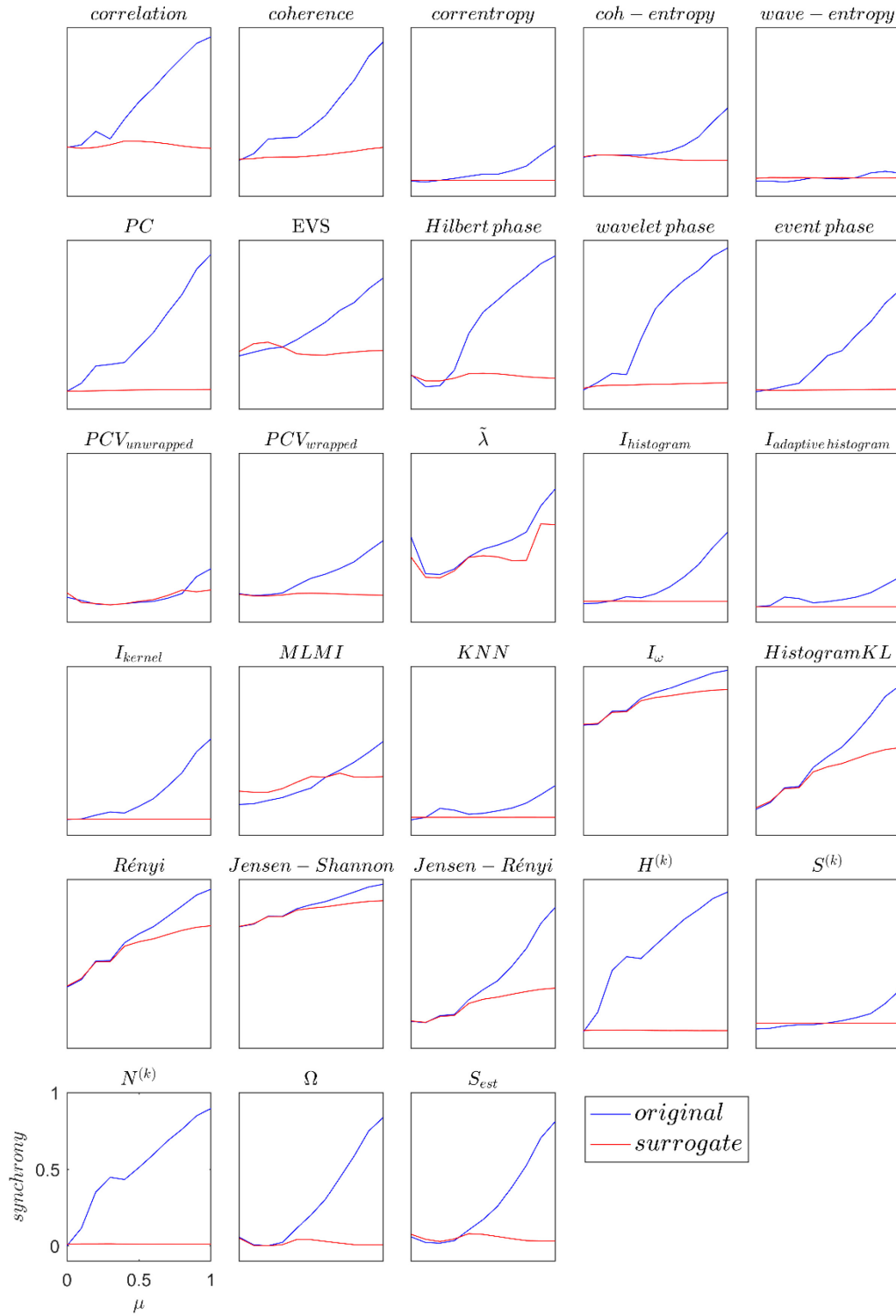
Figure 3-6:   Functional connectivity for NS1 with no added measurement noise. Functional connectivity measures calculated from the original data (blue) and the threshold based on surrogate data (red) for NS1 with no added measurement noise, plotted against coupling strength.

Table 3-2:   The lowest value of coupling strength that detects significant synchrony for NS1Good and unsatisfactory performance outcomes are highlighted by colouring the text blue and red respectively.

Measure	Lowest μ that achieves significant synchrony
Mean phase coherence (Hilbert)	0.0
Phase coherence value wrapped	0.0
Conditional probability based phase synchrony	0.0
Omega Complexity	0.0
Correlation coefficient	0.1
Coherence	0.1
Partial coherence	0.1
Mean phase coherence (wavelet)	0.1
Mean phase coherence (event)	0.1
Phase coherence value unwrapped	0.1
Mutual information (adaptive histograms)	0.1
Mutual information (kernels)	0.1
Nonlinear Interdependence (H^k)	0.1
Nonlinear Interdependence (N^k)	0.1
Coh-entropy coefficient	0.2
Mutual information (histograms)	0.2
Nearest-neighbour mutual information	0.2
Mutual information (time-frequency plane)	0.2
Kullback Leibler divergence (histogram)	0.2
Rényi Divergence	0.2
Jensen-Shannon divergence	0.2
Jensen- Rényi divergence	0.2
Correntropy coefficient	0.3
wave-entropy	0.4
Event synchronisation	0.4
S-estimator	0.4
Nonlinear Interdependence (S^k)	0.5
Maximum likelihood mutual information	0.7

Correlation coefficient and related measures
Phase synchrony
Information-theoretic measures
Synchronisation based on state space

Unsatisfactory
Robust

3.1.1.5 Nonidentical systems type 2

Figure 3-7 shows plots of $x(k)$ versus $y(k)$ for NS2, for coupling strengths from 0 to 1. Similar to the type 1 the identical synchronisation situation (straight line at 45º) cannot be observed here due to the absence of identical synchronisation. In Figure 3-9 we plot of $x(k)$ vs $y(k)$ for Hénon map for identical and both type of nonidentical systems at a coupling strength of $\mu = 1$. Observe that for the nonidentical systems the graph is less defined and spreads out, as shown in the magnified views. Note also that the nonidentical system type 2 shows more structure than type 1.

Figure 3-8 (a) shows a plot of the largest sub-Lyapunov exponent calculated from the response system as a function of coupling strength µ for the nonidentical system type 2. It also shows a plot of the difference between the outputs of the response system when the initial conditions of the driver system are the same, but the initial conditions of the response system are different. It can be seen that there are regions $(0.4 \lesssim \mu \lesssim 0.55$ and $\mu \gtrsim 0.6)$ where the response signals' difference is equal to zero while the sub-Lyapunov exponent is negative for $\mu \gtrsim 0.4$.
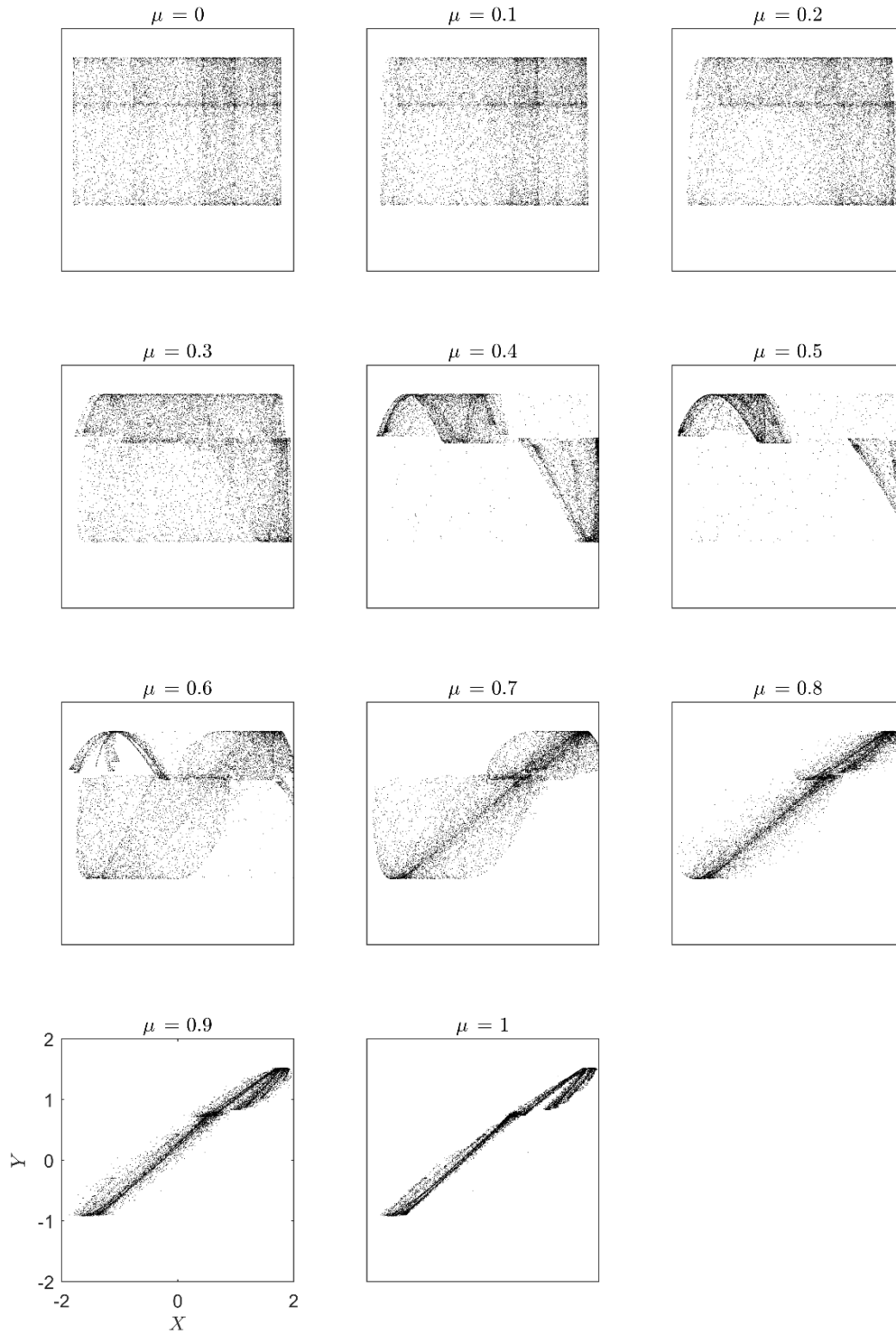
Figure 3-7:   Plot of X vs Y for NS2 for coupling strengths from 0 to 1 in separate plots. At no level of the coupling is identical synchronisation is achieved.

(a)
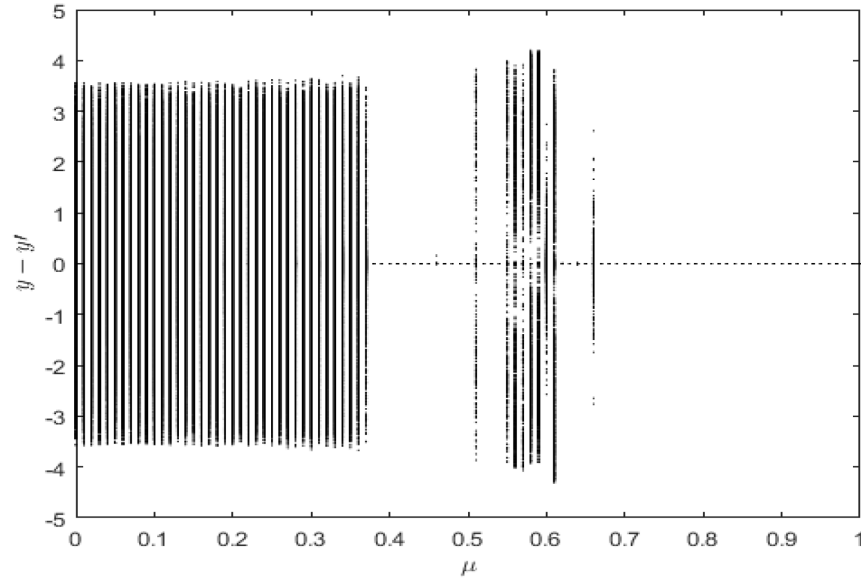
(b)

Figure 3-8: Plot of largest sub-Lyapunov and difference between outputs for NS2. (a) Plot of the largest sub-Lyapunov exponent as a function of coupling strength for NS2[10] (b) Plot of the difference between two outputs of the response system, $y(k) - y'(k)$ against increasing coupling strength.
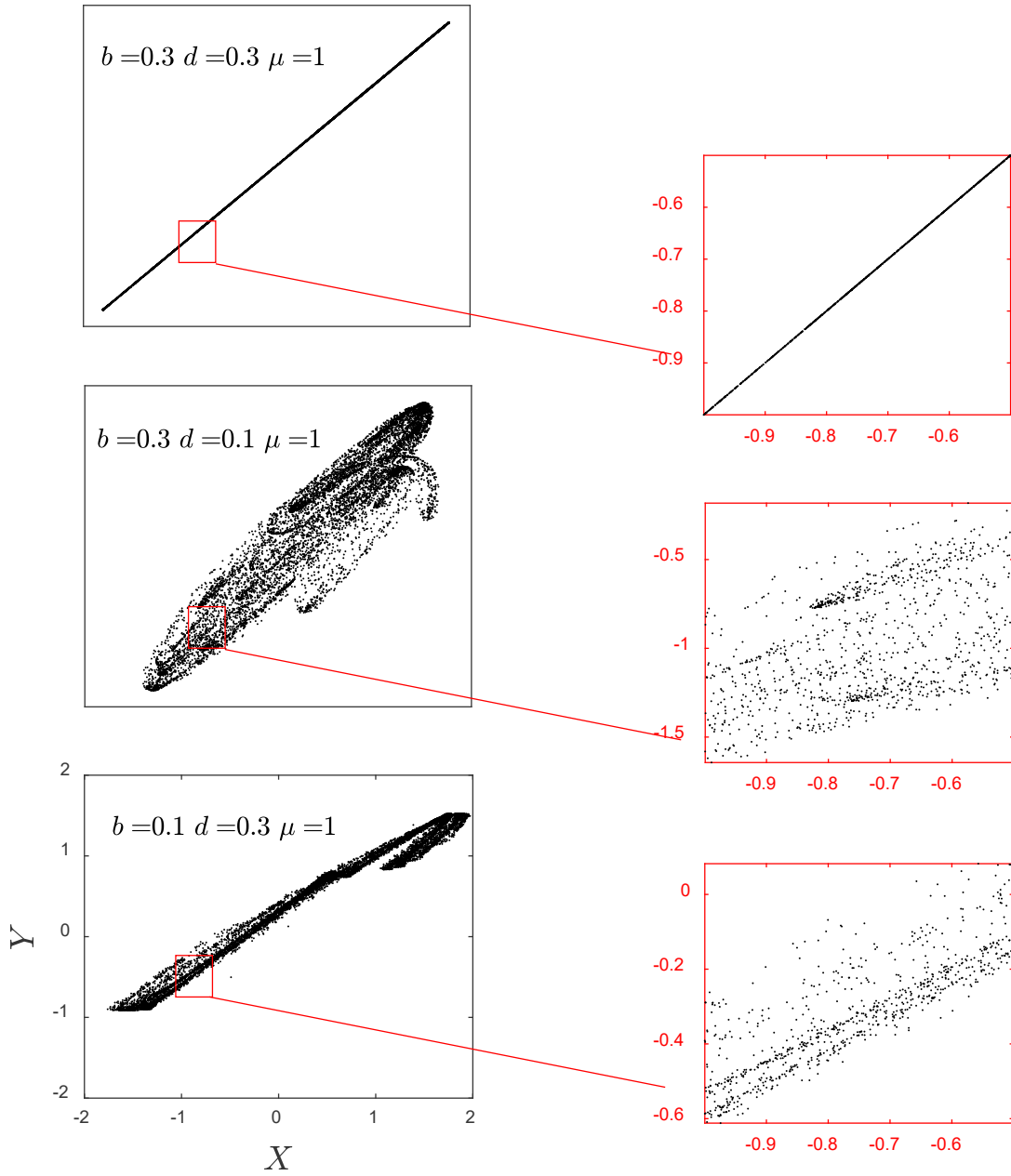
Figure 3-9: Plot of X vs Y for Hénon map for IS, NS1 and NS2 at a coupling strength of $\mu = 1$.

3.1.1.6 Results for nonidentical systems type 2

Figure 3-10 shows the estimates of synchronisation for each functional connectivity measure for the NS2 against coupling strength. Table 3-3 records the value of coupling strength for which statistically significant synchrony detection first occurs. We observe that coherence, partial coherence, mean phase coherence (wavelet), mean phase coherence (event) and mutual information adaptive histogram detect significant synchrony at lower levels of coupling

70

strength, suggesting these measures most able to detect weak synchrony in the NS2. Many of the measures visually show an increase in synchronisation with coupling strength, and a heightened synchronisation between $\mu = 0.4$ and $\mu = 0.6$. This negatively correlates with the shape of the maximum sub-Lyapunov exponent in this region (see in fig), as expected, but this does not provide statistically significant evidence in favour of any measure over another.

Some measures perform unsatisfactorily: mean phase coherence (Hilbert) and phase coherence value wrapped detected synchrony when there is none (coupling strength equals zero); Hilbert phase, wavelet phase, event phase, phase coherence value wrapped, and omega complexity failed to detect synchrony at some coupling strengths despite detecting it at lower coupling strengths; and phase coherence value unwrapped failed to detect synchronisation at the strongest coupling strengths, despite detecting it a some lower strengths.
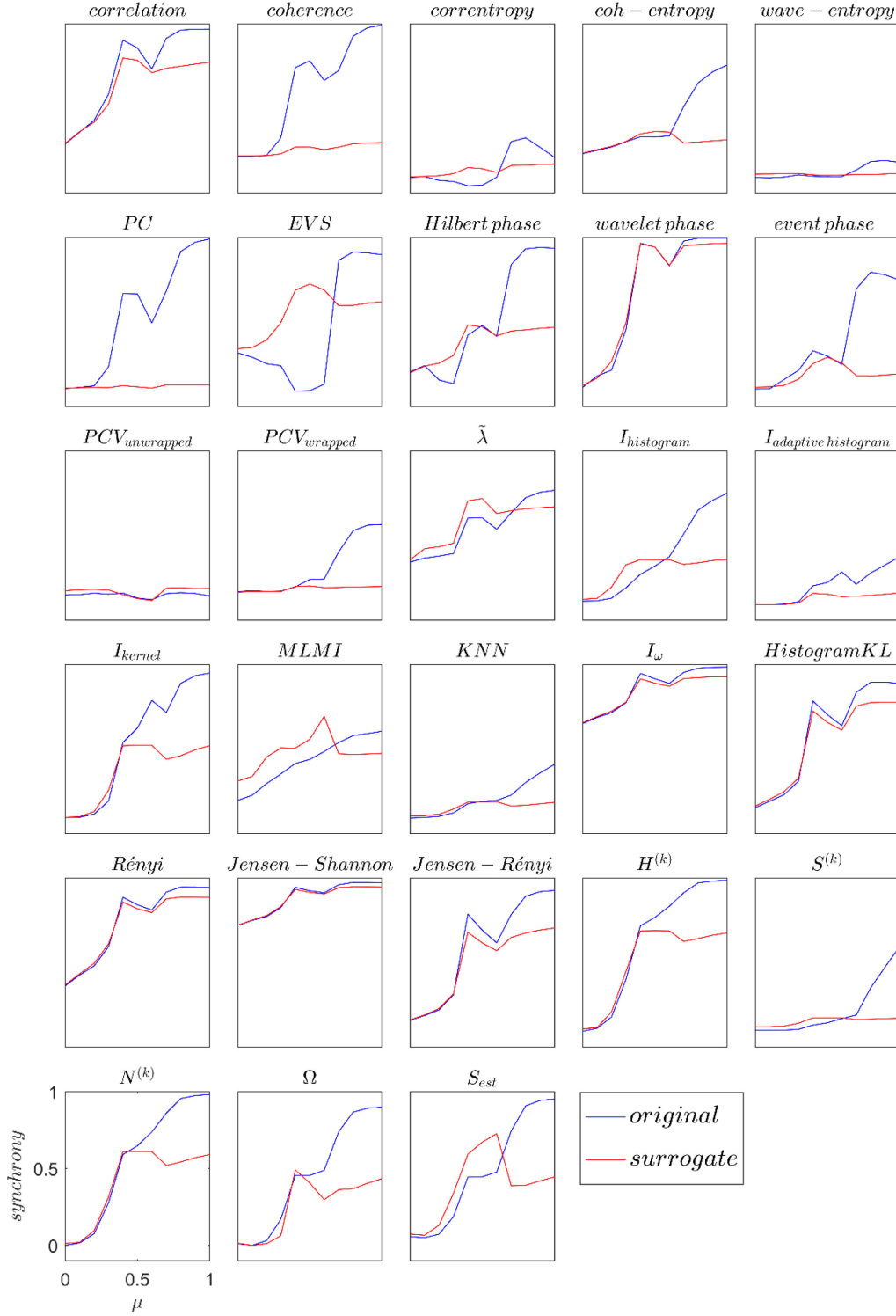
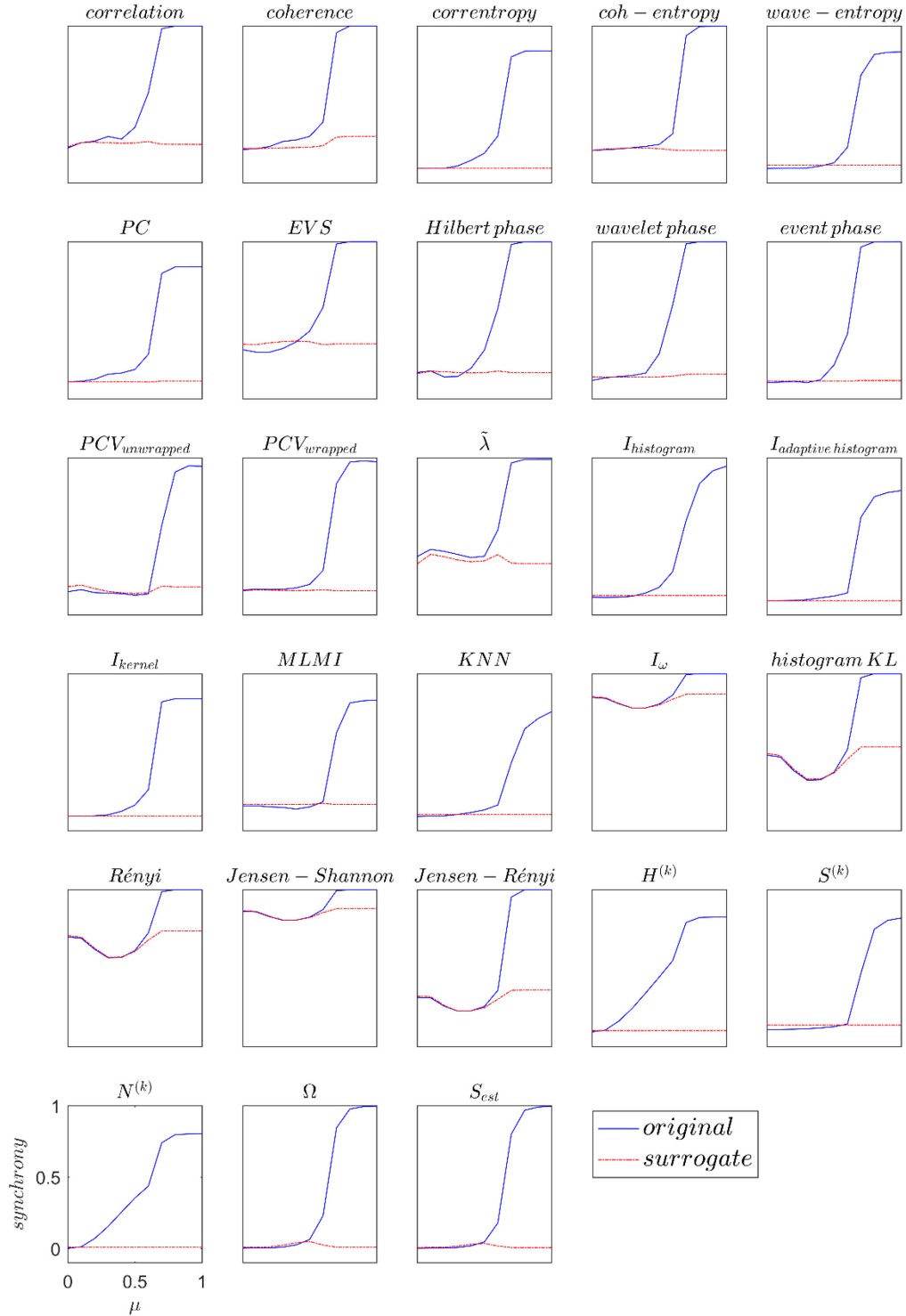*Figure 3-10: Functional connectivity measures for NS2. Functional connectivity measures calculated from the original data (blue line) and the threshold based on surrogate data (red line) for NS2 with no added measurement noise, plotted against coupling strength.*

Table 3-3:   The lowest value of coupling strength that detects significant synchrony for NS1. Good and unsatisfactory performance outcomes are highlighted by colouring the text blue and red respectively.

Measure	Lowest μ that achieves significant synchrony
Mean phase coherence (Hilbert)	0.0
Phase coherence value wrapped	0.0
Partial coherence	0.1
Mean phase coherence (wavelet)	0.1
Omega Complexity	0.1
Correlation coefficient	0.2
Coherence	0.2
Mean phase coherence (event)	0.2
Mutual information (adaptive histograms)	0.2
Phase coherence value unwrapped	0.4
Mutual information (kernels)	0.4
Mutual information (time-frequency plane)	0.4
Kullback Leibler divergence (histogram)	0.4
Rényi Divergence	0.4
Jensen-Shannon divergence	0.4
Jensen-Rényi divergence	0.4
Nonlinear Interdependence (H^k)	0.4
Nearest-neighbour mutual information	0.5
Nonlinear Interdependence (N^k)	0.5
Mutual information (histograms)	0.6
Correntropy coefficient	0.7
Coh-entropy coefficient	0.7
Event synchronisation	0.7
Maximum likelihood mutual information	0.7
Nonlinear Interdependence (S^k)	0.7
wave-entropy	0.7
S-estimator	0.7
Conditional probability based phase synchrony	0.8

Correlation coefficient and related measures
Phase synchrony
Information-theoretic measures
Synchronisation based on state space

Unsatisfactory ———
Robust ———

3.1.2 Detecting nonstationary relationship between signals

A nonstationary model changes the coupling strength μ with time. Here we follow the methodology of [127, 131-134], and switch the coupling strength of two coupled Hénon maps from $\mu = 0.0$ (no coupling) to $\mu = 0.9$ (tightly coupling) at $k = 50$ and back to $\mu = 0.0$ at $k = 150$. A sliding window of 50 samples was used to estimate the synchronisation measures. Simulations used 400 data samples after the first 10000 data are discarded.

Ideally, we expect the measures to begin to detect significant synchrony from $k = 50$ when the 0.9 coupling strength between systems X and Y is introduced. There are two factors that affect this expectation. Firstly, the window size means we expect a 100 samples rectangle due to the model convolved with a 50 samples rectangle due to the window. Secondly, there is a delay as the nonlinear system moves to the new coupling regime. We don't know how long this is, and it is likely asymmetric (as at 50 ms the highly coupled system drives to synchronise and at 150 ms the decoupled system drives to desynchronise, i.e. different systems). We can't easily assess this second factor, so we don't show an expectation, just the coupling (rectangle). In order to compare measures results we'd like value of the k when measures detect first significant synchrony (k_{min}) as close to 50 as possible, can't say what is "right", so smaller is better. We can argue that the value of the k when measures falling off back below the threshold (k_{max}) should be large, as smaller implies less sensitive to the persisting synchronisation. Hence best measure of goodness is a large difference between k_{max} and k_{min} (k_{diff}).

3.1.2.1 Results

Figure 3-11 shows the results for the 29 measures for IS and Table 3-4 shows the value of the time index k that first detects synchrony, the value of k that last detects synchrony, and the difference of these two. All measures can be seen to be sensitive to the time-dependent sudden change in the dynamics of the interacting systems. Two measures, correntropy coefficient and

coh-entropy, first detect synchrony at $k_{min} = 59$ and $k_{min} = 63$ respectively, which are closest to the ideal value. While most measures show a decrease in synchronisation from or slightly later than expected value $k = 150$, they do not fall below the threshold until considerably later. It is clear that there is a significant time required for the system to diverge from synchronisation and for the measure to reflect the absence of systemic synchronisation. Some measures perform unsatisfactorily, namely phase conditional entropy is not able to estimate significant synchrony for the time range $50 < k < 150$, and omega complexity detects significant synchrony for $k < 50$ and $k > 150$ where no synchrony exist. In addition, coh-entropy and correntropy coefficient show the largest difference between the time that a measure first detects significant synchrony and the time that it no longer detects significant synchrony (k_{diff}), recommending them as measures that are sensitive to nonstationary changes in synchronisation.
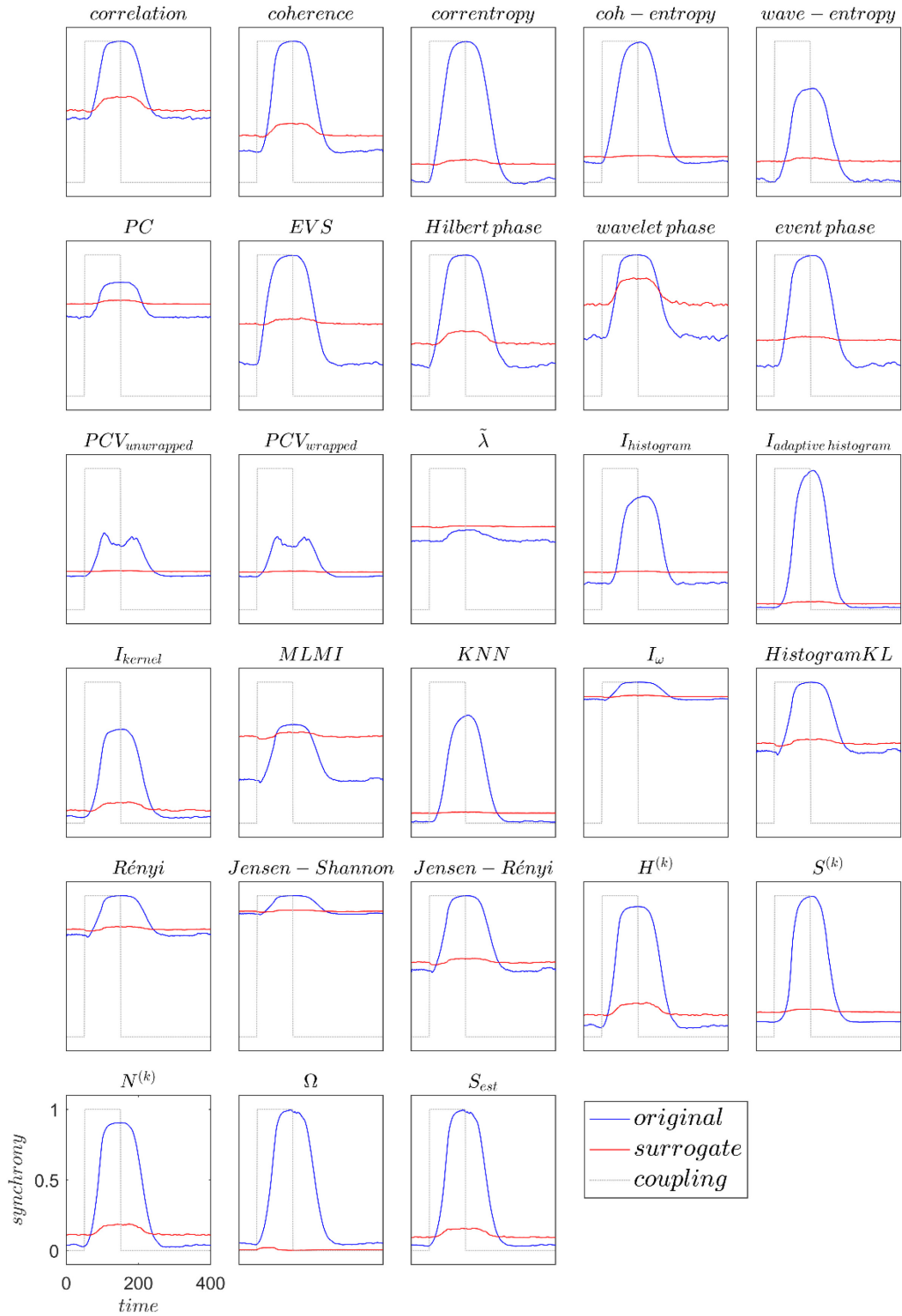
Figure 3-11: Synchrony measures against time for nonstationary IS with no added measurement noise. Result of synchronisation for original data (blue line); surrogate data (red line).

Table 3-4: *The values of (k_min), (k_max) and (k_diff) for nonstationary IS. The value of the time index k that first detects synchrony (k_min), the value of k that last detects synchrony (k_max), and the difference of these two (k_diff) for nonstationary IS with no added measurement noise. Good and unsatisfactory performance outcomes are highlighted by colouring the text blue and red respectively.*

Measure	k_{min}	k_{max}	k_{diff}
Correlation coefficient	72	235	163
Coherence	76	234	158
Correntropy coefficient	63	244	181
Coh-entropy coefficient	59	253	194
Wave-entropy	78	229	151
Partial coherence	88	211	123
Event synchronisation	70	215	145
Mean phase coherence (Hilbert)	68	234	166
Mean phase coherence (wavelet)	90	211	121
Mean phase coherence (event)	78	229	151
Phase coherence value unwrapped	68	243	175
Phase coherence value wrapped	66	243	177
Conditional probability based phase synchrony	NaN	NaN	NaN
Mutual information (histogram)	89	235	146
Mutual information (adaptive histogram)	71	247	176
Mutual information (kernel)	67	241	174
Maximum likelihood mutual information	2	400	398
Nearest-neighbour mutual information	74	237	163
Mutual information (time-frequency plane)	72	238	166
Kullback Leibler divergence (histogram)	72	243	171
Rényi Divergence	72	240	168
Jensen-Shannon divergence	72	243	171
Jensen-Rényi divergence	72	243	171
Nonlinear Interdependence (H^k)	66	239	173
Nonlinear Interdependence (S^k)	81	231	150
Nonlinear Interdependence (N^k)	67	239	172
Omega Complexity	1	400	399
S-estimator	67	243	176

Correlation coefficient and related measures
Phase synchrony
Information-theoretic measures
Synchronisation based on state space

Unsatisfactory ————
Robust ————

Simulations for the nonidentical systems were also run. Figure 3-12 shows the results for NS1.

Similar to the identical system, it is visually clear that all of the measures are able to detect the

sudden introduction of strong coupling. Table 3-5 shows the value of k when the

synchronisation measures are above the threshold level for the first time, when they fall below

the threshold level for the last time, and the difference between these two points which indicates the length of time detecting coupling. While none of the measures can first detect synchrony at the ideal value of $k = 50$, correntropy coefficient, coh-entropy, nonlinear interdependence H, nonlinear interdependence N, and S estimator all first detect synchrony close to the ideal time (indicated in table by the colour blue) as well as larger value of the k_{diff}. Some measures perform unsatisfactorily: wave entropy, conditional probability based phase synchrony and maximum likelihood mutual information detect no significant synchrony at all; and omega complexity detects significant synchrony at no coupling.
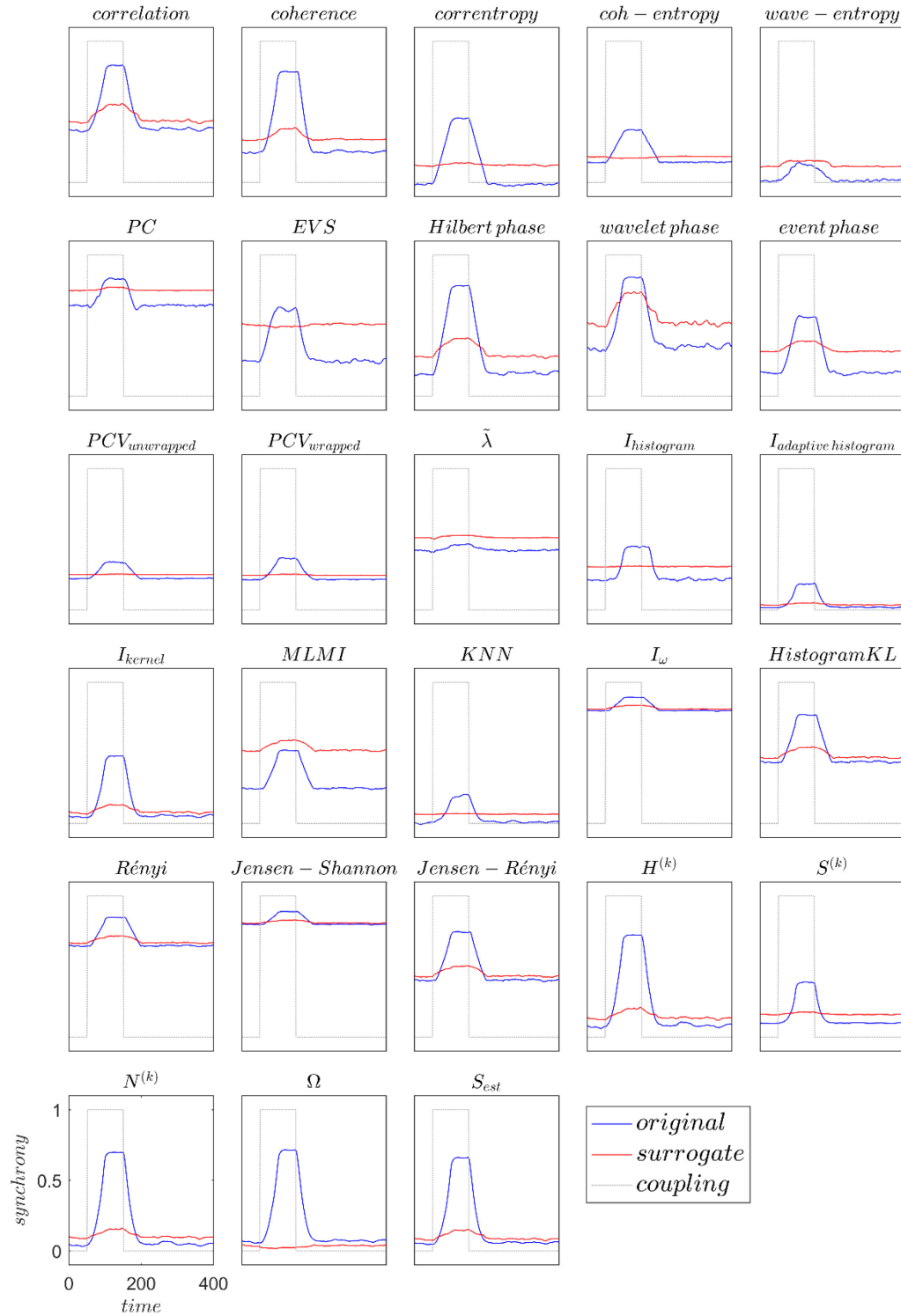
Figure 3-12: Synchrony measures against time for nonstationary NS1 with no added measurement noise. Result of synchronisation for original data (blue line); surrogate data (red line).

Table 3-5:   The values of (k_{min}), (k_{max}) and (k_{diff}) for nonstationary NS1. The value of the time index k that first detects synchrony (k_{min}), the value of k that last detects synchrony (k_{max}), and the difference of these two (k_{diff}) for nonstationary NS1 with no added measurement noise. Good and unsatisfactory performance outcomes are highlighted by colouring the text blue and red respectively.

Measure	k_{min}	k_{max}	k_{diff}
Correlation coefficient	75	179	104
Coherence	72	183	111
Correntropy coefficient	69	186	117
Coh-entropy coefficient	63	192	129
Wave-entropy	NaN	NaN	NaN
Partial coherence	91	166	75
Event synchronisation	78	162	84
Mean phase coherence (Hilbert)	72	182	110
Mean phase coherence (wavelet)	92	165	73
Mean phase coherence (event)	85	172	87
Phase coherence value unwrapped	72	184	112
Phase coherence value wrapped	72	182	110
Conditional probability based phase synchrony	NaN	NaN	NaN
Mutual information (histogram)	94	182	88
Mutual information (adaptive histogram)	76	178	102
Mutual information (kernels)	71	182	111
Maximum likelihood mutual information	NaN	NaN	NaN
Nearest-neighbour mutual information	85	171	86
Mutual information (time-frequency plane)	72	189	117
Kullback Leibler divergence (histogram)	72	189	117
Rényi Divergence	69	189	120
Jensen-Shannon divergence	69	190	121
Jensen-Rényi divergence	69	189	120
Nonlinear Interdependence (H^k)	68	185	117
Nonlinear Interdependence (S^k)	85	168	83
Nonlinear Interdependence (N^k)	68	185	117
Omega Complexity	1	400	399
S-estimator	68	184	116

Correlation coefficient and related measures
Phase synchrony
Information-theoretic measures
Synchronisation based on state space

Unsatisfactory ————
Robust ————

Figure 3-13 shows the results for NS2. It is still visually clear that all of the measures are able to detect the sudden introduction of strong coupling. Table 3-6 shows the value of k when the synchronisation measures are above the threshold level for the first time, when they fall below the threshold level for the last time, and the difference between these two points which

indicates the length of time that coupling has been detected. While none of the measures can first detect synchrony at the ideal value of $k = 50$, correntropy coefficient and mean phase coherence (Hilbert) are the closest, first detecting synchrony at $k_{min} = 59$ and $k_{min} = 63$ respectively. Additionally, these two measures also achieve the largest values of k_{diff}, suggesting that these measures are the best at identifying strong coupling with few samples of data. Coh-entropy, phase coherence value (wrapped), phase coherence value (unwrapped), nonlinear interdependence (S^k), omega complexity and S-estimator also perform well. The measure conditional probability-based phase synchrony performs unsatisfactorily: this measure detects no significant synchrony at all.
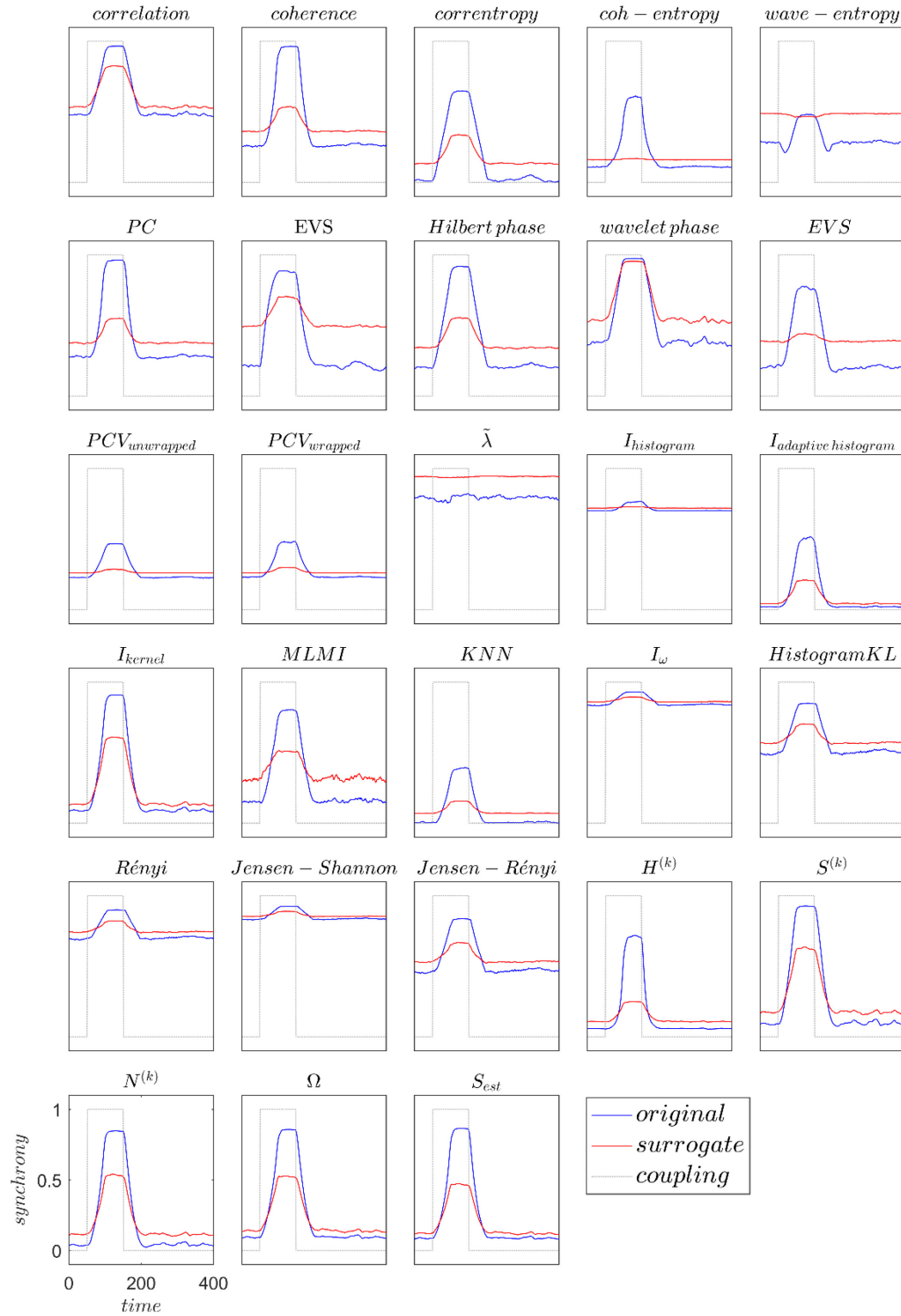
Figure 3-13: Synchrony measures against time for the nonstationary system NS2 with no added measurement noise, for the original data (black line) and surrogate data (red line).

Table 3-6:   The values of (k_{min}), (k_{max}) and (k_{diff}) for nonstationary NS2. The value of the time index k that first detects synchrony (k_{min}), the value of k that last detects synchrony (k_{max}), and the difference of these two (k_{diff}) for nonstationary NS2 with no added measurement noise. Good and unsatisfactory performance outcomes are highlighted by colouring the text blue and red respectively.

Measure	k_{min}	k_{max}	k_{diff}
Correlation coefficient	78	180	102
Coherence	79	182	103
Correntropy coefficient	66	191	125
Coh-entropy coefficient	70	184	114
Wave-entropy	108	153	45
Partial coherence	77	176	99
Event synchronisation	68	162	94
Mean phase coherence (Hilbert)	68	189	121
Mean phase coherence (wavelet)	94	161	67
Mean phase coherence (event)	79	178	99
Phase coherence value unwrapped	71	186	115
Phase coherence value wrapped	70	187	117
Conditional probability based phase synchrony	NaN	NaN	NaN
Mutual information (histograms)	89	170	81
Mutual information (adaptive histograms)	76	181	105
Mutual information (kernels)	74	186	112
Maximum likelihood mutual information	81	177	96
Nearest-neighbour mutual information	78	176	98
Mutual information (time-frequency plane)	77	186	109
Kullback Leibler divergence (histogram)	78	186	108
Rényi Divergence	78	186	108
Jensen-Shannon divergence	77	186	109
Jensen-Rényi divergence	76	186	110
Nonlinear Interdependence (H^k)	87	168	81
Nonlinear Interdependence (S^k)	72	186	114
Nonlinear Interdependence (N^k)	75	184	109
Omega Complexity	72	187	115
S-estimator	71	188	117

Correlation coefficient and related measures
Phase synchrony   Unsatisfactory ———
Information-theoretic measures   Robust ———
Synchronisation based on state space

3.1.3 Influence of noise

Real signals are contaminated by noise, so a valuable synchronisation measure should be robust

against noise. Here we consider only additive white Gaussian measurement noise, i.e. noise

added to the outputs after calculation via the Hénon map equations. The alternative, intrinsic noise, is added into the system hence perturbing the dynamics of the system. We are using simulated data to know a priori what the dynamics of the system are, hence we only consider measurement noise. White noise is added to the both driver X and response Y outputs. To test the performance of the measures at different noise levels, we set the signal-to-noise ratio (SNR) at 10 dB and 1 dB. Note that we have not recalculated the Hénon map data for different noise levels, it is identical in all cases.

3.1.3.1 Results for variation of measures against coupling

Figure 3-14 shows the performance of the synchronisation measures on the IS at 10 dB SNR. All measures still show the sharp increase in synchronisation at μ ≈ 0.7, and detect the synchronisation as expected in the final region.

Table 3-7 shows the lowest value of the coupling strength for which a measure detects significant synchrony. Measures mostly first detect significant synchrony at the same level of coupling as in the noise-free case. This suggests that when the low-level noise is added into the systems, the performance of the most measures is similar to the noise-free systems. Partial coherence, conditional entropy based phase synchrony and omega complexity first detect synchrony at $\mu = 0.1$, suggesting these measures are more robust in detecting weak coupling in this experimental situation. Mutual information (adaptive histograms), mutual information (kernels), nonlinear interdependence (H^k) and nonlinear interdependence (N^k) first detect statistical significant synchrony at a coupling strength one level greater than their noise-free

counterparts. Phase coherence value wrapped and mean phase synchrony (Hilbert) perform

unsatisfactorily, failing to detect synchrony at all coupling strengths.

Figure 3-14: Functional connectivity measures for IS at 10 dB SNR. Functional connectivity measures calculated from the original data (blue line) and the threshold based on surrogate data (red line) for IS at 10 dB SNR, plotted against coupling strength.

Table 3-7: The lowest value of coupling strength that detects synchrony for noisy IS at 10 dB SNR. Good and unsatisfactory performance outcomes are highlighted by colouring the text blue and red respectively.

Measure	Lowest μ that achieves significant synchrony
Mean phase coherence (Hilbert)	0.0
Phase coherence value wrapped	0.0
Partial coherence	0.1
Conditional probability based phase synchrony	0.1
Omega Complexity	0.1
Correlation coefficient	0.2
Coherence	0.2
Mean phase coherence (wavelet)	0.2
Mutual information (adaptive histogram)	0.2
Nonlinear Interdependence (H^k)	0.2
Nonlinear Interdependence (N^k)	0.2
Correntropy coefficient	0.3
Coh-entropy coefficient	0.3
Mutual information (kernels)	0.3
Mean phase coherence (event)	0.4
Mutual information (histograms)	0.4
Event synchronisation	0.5
Maximum likelihood mutual information	0.5
Mutual information (time-frequency plane)	0.5
Kullback Leibler divergence (histogram)	0.5
Rényi Divergence	0.5
Jensen-Shannon divergence	0.5
Jensen-Rényi divergence	0.5
Nonlinear Interdependence (S^k)	0.5
S-estimator	0.5
wave-entropy	0.6
Nearest-neighbour mutual information	0.6
Phase coherence value unwrapped	0.7

Correlation coefficient and related measures
Phase synchrony
Information-theoretic measures
Synchronisation based on state space

Unsatisfactory ———————
Robust ———————

Figure 3-15 shows the same experiment at a SNR of 1 dB. Note that the measures' curves at 1 dB substantially mimic those in Figure 3.1.4-1 (i.e. when noise-free), but with an overall degradation of the estimates due to the added noise. But the sudden increase at $\mu \approx 0.7$ is still observable for most measures. All measures except phase coherence value unwrapped detect synchronisation when the coupling is large. Table 3-8 shows the lowest value of the coupling

strength for which a measure detects synchrony. All measures fail to detect weak coupling at $\mu = 0.1$. The table suggest partial coherence, correlation coefficient, mean phase coherence (wavelet), nonlinear interdependence (H^k) and nonlinear interdependence (N^k) are more robust to noise than the other measures when the systems are contaminated with high level of the noise.

Figure 3-15: Functional connectivity measures for IS at 1 dB SNR. Functional connectivity measures calculated from the original data (blue line) and the threshold based on surrogate data (red line) for IS at 1 dB SNR, plotted against coupling strength.

Table 3-8:   The lowest value of coupling strength that detects significant synchrony for noisy IS at 1 dB SNR. Good and unsatisfactory performance outcomes are highlighted by colouring the text blue and red respectively.

Measure	Lowest μ that achieves significant synchrony
Phase coherence value wrapped	0.0
Omega Complexity	0.0
Partial coherence	0.2
Correlation coefficient	0.3
Mean phase coherence (wavelet)	0.3
Nonlinear Interdependence (H^k)	0.3
Nonlinear Interdependence (N^k)	0.3
Coherence	0.4
Correntropy coefficient	0.4
Coh-entropy coefficient	0.4
Mean phase coherence (Hilbert)	0.4
Mutual information (adaptive histogram)	0.4
Event synchronisation	0.5
Mean phase coherence (event)	0.5
Nonlinear Interdependence (S^k)	0.5
S-estimator	0.5
Conditional probability based phase synchrony	0.6
Mutual information (histograms)	0.6
Maximum likelihood mutual information	0.6
Mutual information (time-frequency plane)	0.6
Kullback Leibler divergence (histogram)	0.6
Rényi Divergence	0.6
Jensen-Shannon divergence	0.6
Jensen-Rényi divergence	0.6
wave-entropy	0.7
Mutual information (kernels)	0.7
Nearest-neighbour mutual information	0.7
Phase coherence value unwrapped	NaN

Correlation coefficient and related measures
Phase synchrony
Information-theoretic measures
Synchronisation based on state space
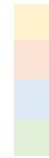
Unsatisfactory ———
Robust ———

Figure 3-16 shows the calculation of 29 measures against increasing coupling strength μ for NS1. Table 3-9 shows us when a measure first detects statistically significant synchrony. Correlation coefficient, coherence, partial coherence, mean phase coherence (wavelet), phase coherence value unwrapped, mutual information (adaptive histograms), and mutual information (adaptive histogram) first detect significant synchrony at $\mu = 0.1$, suggesting

these measures are robust measures for detecting weak coupling with noise. We also note that cross correlation, coherence, mutual information (time frequency plane), Kullback Leibler divergence (histogram), wavelet phase, Jensen-Rényi divergence, Jensen-Shannon divergence and Rényi divergence, show a bump in the range $0.1 \lesssim \mu \lesssim 0.3$. As mentioned earlier, while this visually conforms to the known dynamics of the system, this does not provide any statistically significant evidence in favor of any measure. Some measures perform unsatisfactorily: maximum likelihood mutual information fails to detect synchrony at any coupling strength; and mean phase coherence (Hilbert), phase coherence value unwrapped, phase coherence value wrapped and conditional probability based phase synchrony detect synchrony when there is none (coupling strength equals zero).

Figure 3-16: Functional connectivity measures for NS1 at 10 dB SNR. Functional connectivity measures calculated from the original data (blue line) and the threshold based on surrogate data (red line) for NS1 at 10 dB SNR, plotted against coupling strength.

Table 3-9:   The lowest value of coupling strength that detects significant synchrony for noisy NS1 at 10 dB SNR. Good and unsatisfactory performance outcomes are highlighted by colouring the text blue and red respectively.

Measure	Lowest μ that achieves significant synchrony
Mean phase coherence (Hilbert)	0.0
Phase coherence value unwrapped	0.0
Phase coherence value wrapped	0.0
Conditional probability based phase synchrony	0.0
Correlation coefficient	0.1
Coherence	0.1
Partial coherence	0.1
Mean phase coherence (wavelet)	0.1
Mutual information (adaptive histograms)	0.1
Correntropy coefficient	0.2
Coh-entropy coefficient	0.2
Mean phase coherence (event)	0.2
Mutual information (time-frequency plane)	0.2
Rényi Divergence	0.2
Jensen-Shannon divergence	0.2
Jensen-Rényi divergence	0.2
Event synchronisation	0.3
Mutual information (kernels)	0.3
Kullback Leibler divergence (histogram)	0.3
Mutual information (histograms)	0.4
Nonlinear Interdependence (S^k)	0.4
Nonlinear Interdependence (N^k)	0.4
Wave-entropy	0.5
Nonlinear Interdependence (H^k)	0.5
S-estimator	0.5
Omega Complexity	0.6
Nearest-neighbour mutual information	0.8
Maximum likelihood mutual information	NaN

Correlation coefficient and related measures
Phase synchrony
Information-theoretic measures   Unsatisfactory ———
Synchronisation based on state space   Robust   ———

Figure 3-17 shows the same experiment at a SNR of 1 dB for NS1. All correlation coefficient family measures and wavelet phase curves clearly show the bump in the region $0.1 \lesssim \mu \lesssim 0.3$ which is most likely due to the negativity of the maximum sub-Lyapunov exponent in this zone. All measures except maximum likelihood mutual information, conditional entropy based phase

synchrony and phase coherence value unwrapped detect synchrony for strong coupling. Table 3-10 records the lowest value of the coupling strength at which measures first detect synchrony. Correlation coefficient, partial coherence, mean phase coherence wavelet and omega complexity detect first statistical significant synchrony at $\mu = 0.1$, suggesting these measures are more robust than other measures at detecting weak coupling when the noise at a SNR of 1 dB is added to the NS1. The table also shows phase coherence value first detects synchrony at $\mu = 0.2$ and coh-entropy coefficient, event synchronisation, mutual information adaptive histogram, mutual information kernel, nonlinear interdependence (H^k) and nonlinear interdependence(N^k) first detect synchrony at $\mu = 0.3$, suggesting these measures also can be considered as sensitive measures for detecting weak coupling. Some measures performance is unsatisfactory; MLMI and phase synchrony unwrapped detect no synchrony at all and conditional based phase synchrony detects synchrony at $\mu = 0.7$ only.
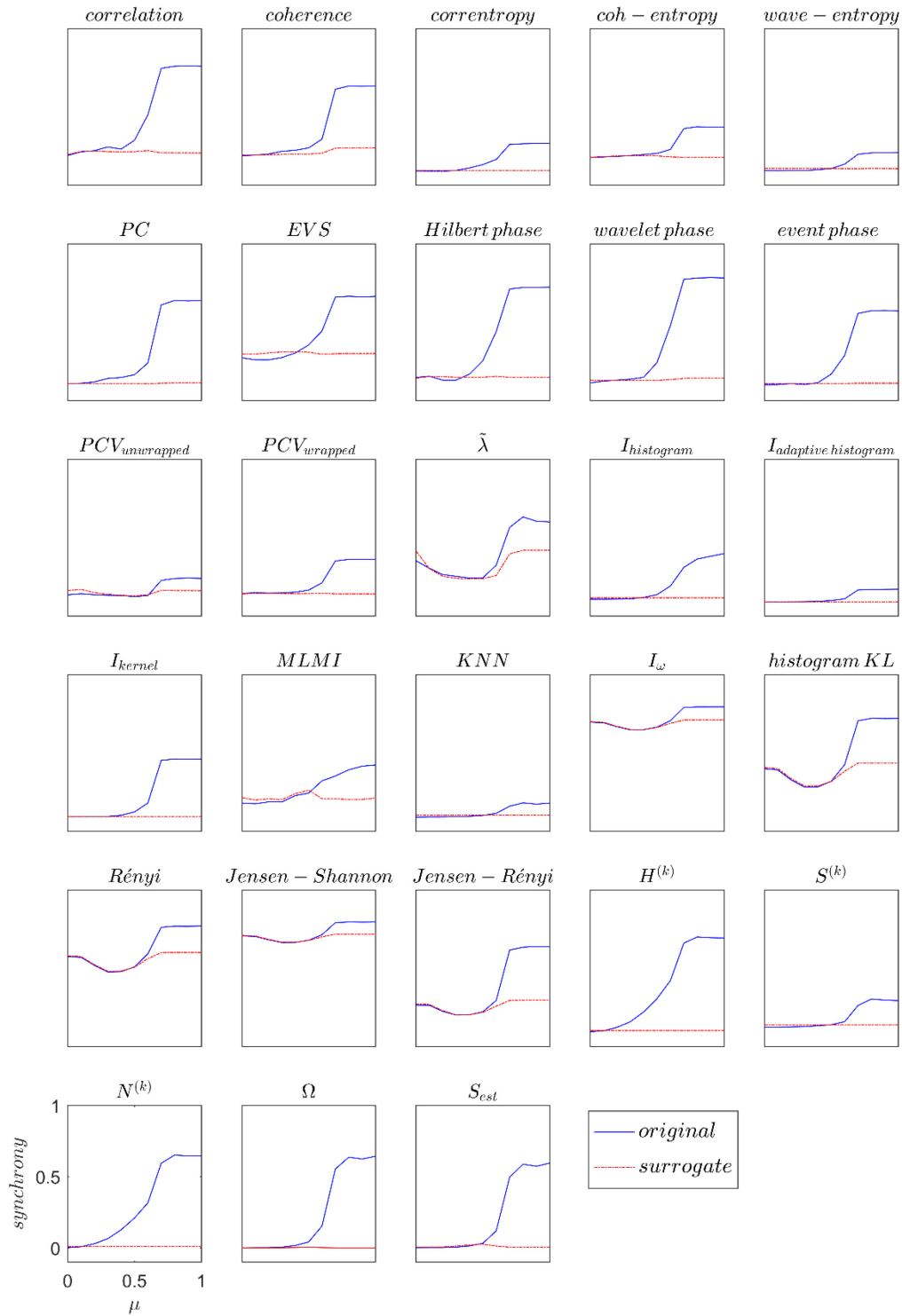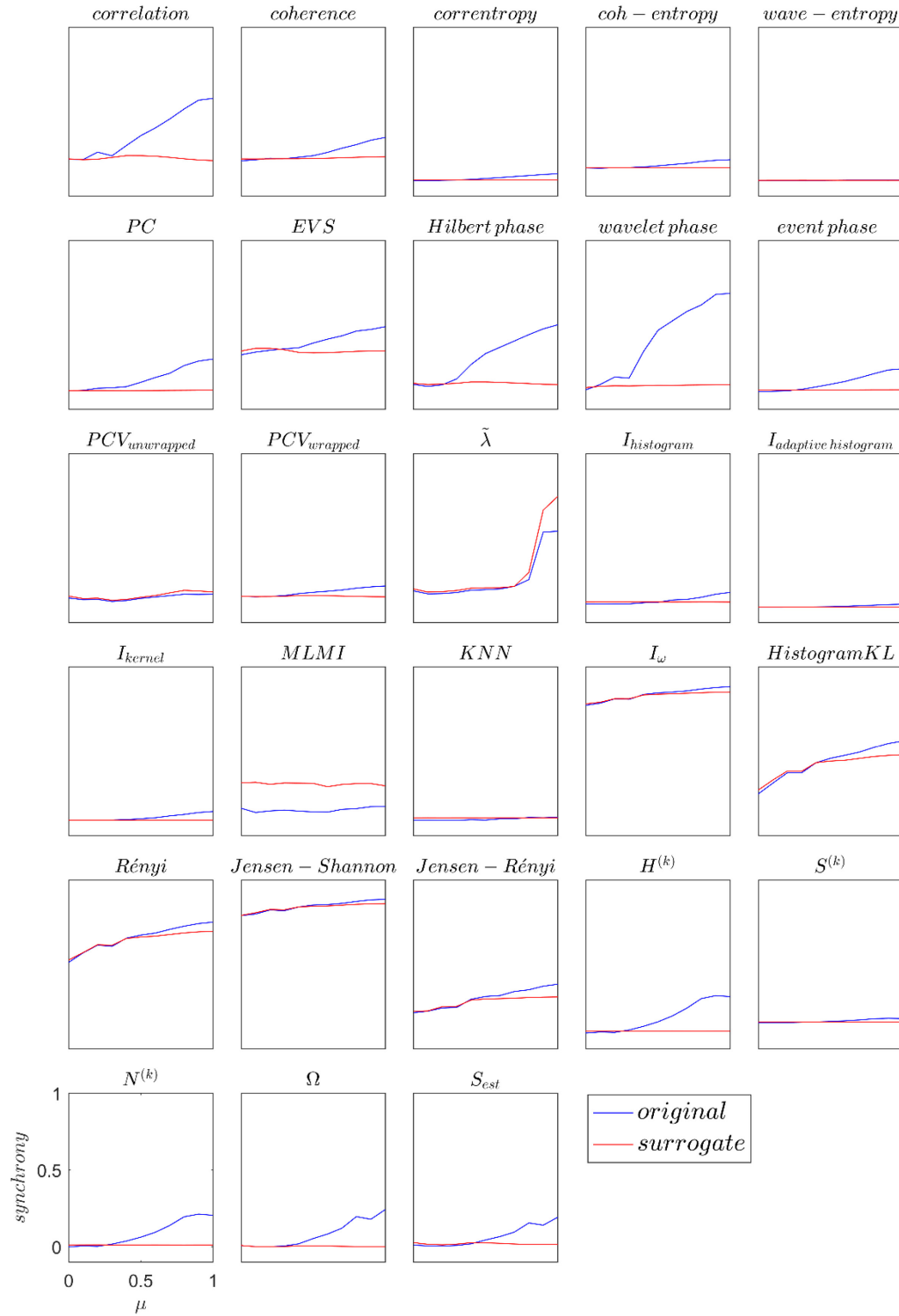
Figure 3-17: Functional connectivity measures for NS1 at 1 dB SNR. Functional connectivity measures calculated from the original data (blue line) and the threshold based on surrogate data (red line) for NS1 at 1 dB SNR, plotted against coupling strength.

Table 3-10: The lowest value of coupling strength that detects significant synchrony for noisy NS1 at 1 dB SNR. Good and unsatisfactory performance outcomes are highlighted by colouring the text blue and red respectively.

Measure	Lowest μ that achieves significant synchrony
Correlation coefficient	0.1
Partial coherence	0.1
Mean phase coherence (wavelet)	0.1
Omega Complexity	0.1
Coherence	0.2
Phase coherence value wrapped	0.2
Coh-entropy coefficient	0.3
Event synchronisation	0.3
Mean phase coherence (Hilbert)	0.3
Mean phase coherence (event)	0.3
Mutual information (adaptive histogram)	0.3
Mutual information (kernels)	0.3
Nonlinear Interdependence (H^k)	0.3
Nonlinear Interdependence (N^k)	0.3
Correntropy coefficient	0.4
Mutual information (time-frequency plane)	0.4
Rényi Divergence	0.4
Jensen-Rényi divergence	0.4
Nonlinear Interdependence (S^k)	0.4
Kullback Leibler divergence (histogram)	0.5
Jensen-Shannon divergence	0.5
S-estimator	0.5
wave-entropy	0.6
Mutual information (histogram)	0.6
Conditional probability based phase synchrony	at 0.7 only
Nearest-neighbour mutual information	0.8
Phase coherence value unwrapped	NaN
Maximum likelihood mutual information	NaN

Correlation coefficient and related measures
Phase synchrony
Information-theoretic measures
Synchronisation based on state space

Unsatisfactory ───────
Robust ───────

Figure 3-18 shows the calculation of 29 measures against increasing coupling strength μ at a SNR of 10 dB for NS2. Table 3-11 shows us when a measure first detects statistically significant synchrony. Mean phase coherence (wavelet) first detects significant synchrony at $\mu = 0.1$, and then correlation coefficient, partial coherence, mean phase coherence, mean phase coherence (event) and mutual information (adaptive histogram) first detect significant

synchrony at $\mu = 0.2$, suggesting these measures are robust measures for detecting weak coupling in low amplitude noise. Many of the measures still visually show a heightened synchronisation between $\mu = 0.4$ and $\mu = 0.6$. As outlined earlier this negatively correlates with the shape of the maximum sub-Lyapunov exponent in this region, but this does not provide statistically significant evidence in favour of any measure over another. Some measures perform unsatisfactorily: wave entropy fails to detect synchrony at any coupling strength; and mean phase coherence (Hilbert), phase coherence value unwrapped, phase coherence value wrapped and conditional-probability-based phase synchrony detect synchrony when there is none (coupling strength equals zero).
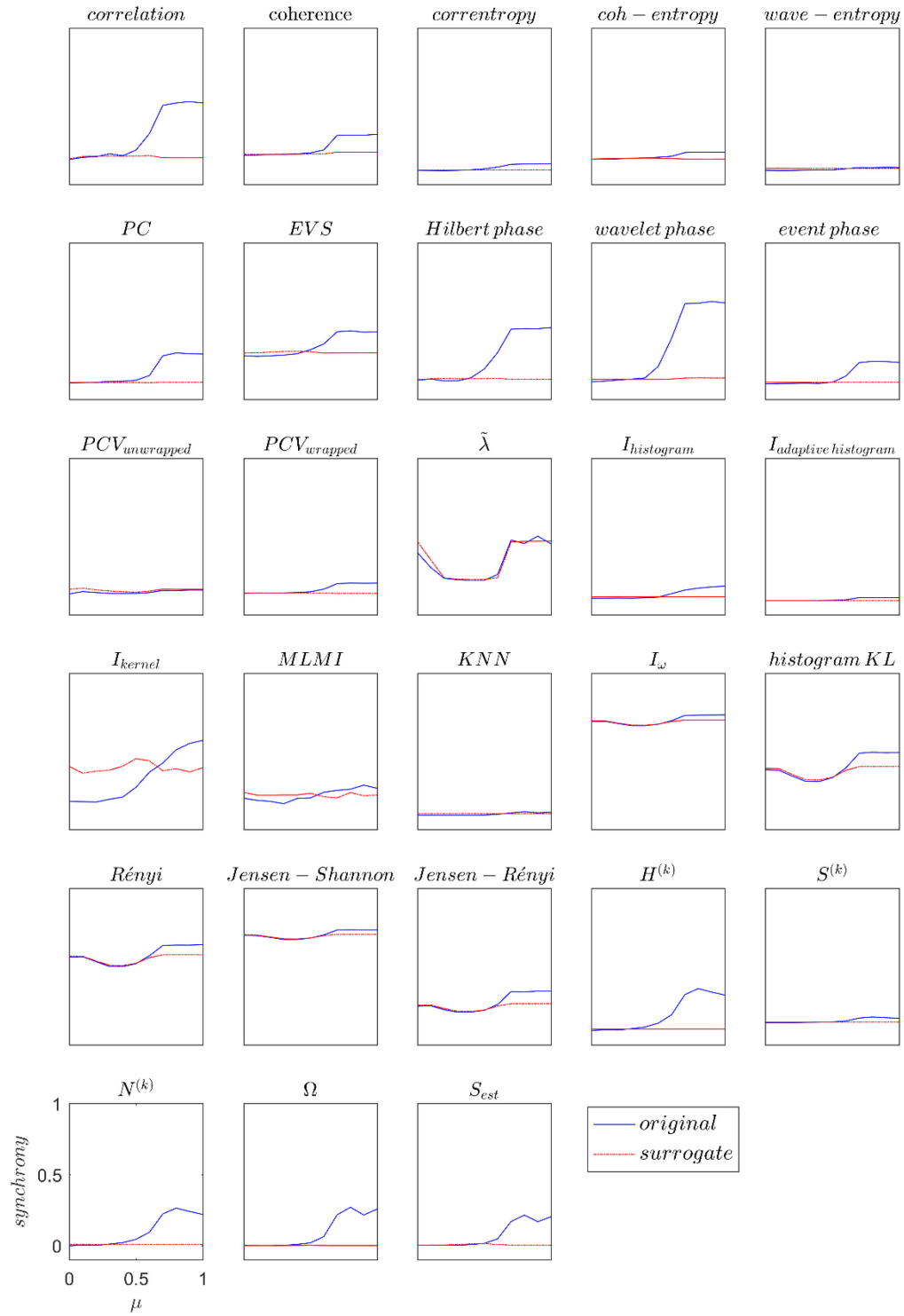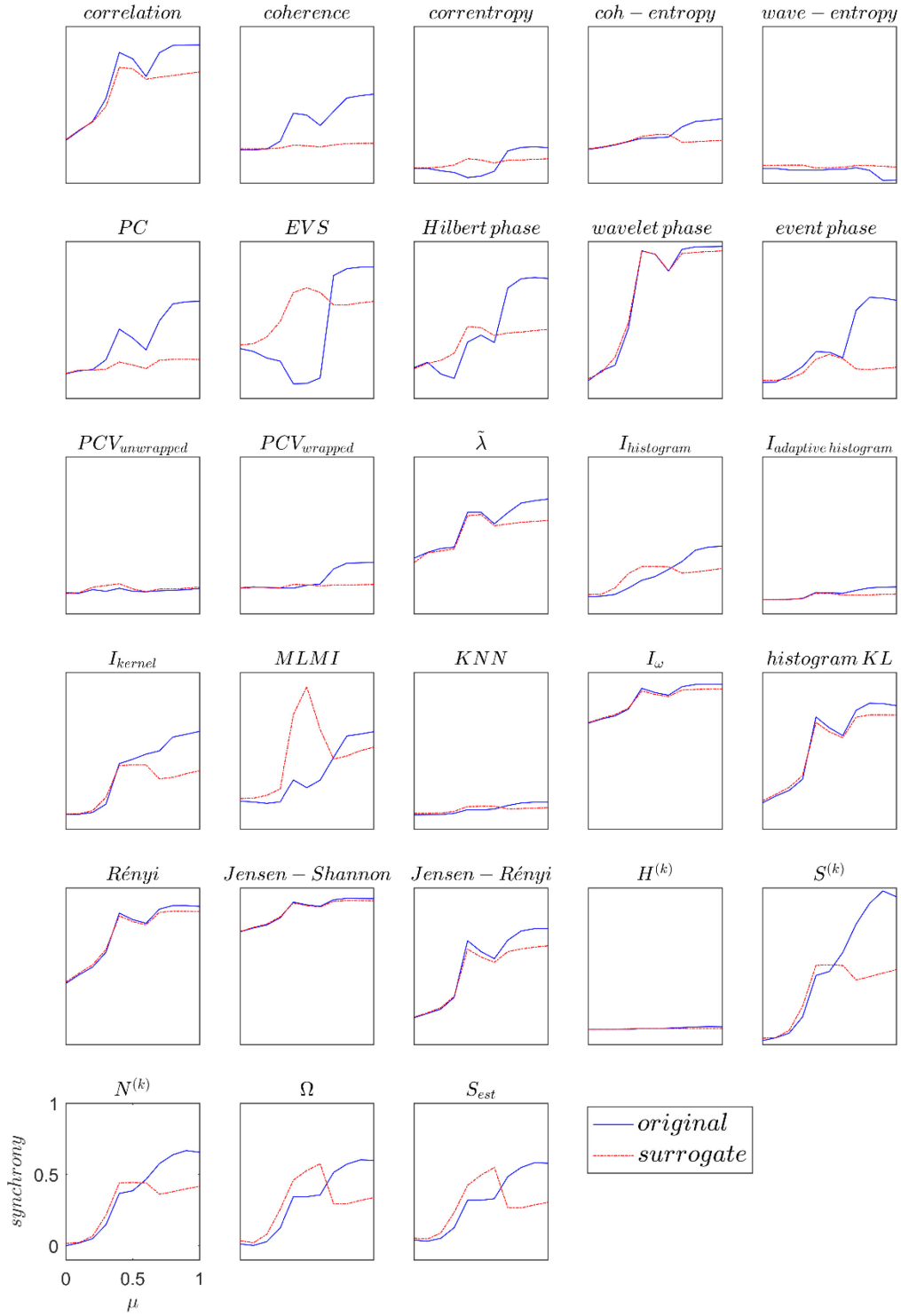
Figure 3-18: Functional connectivity measures for NS2 at 10 dB SNR. Functional connectivity measures calculated from the original data (blue line) and the threshold based on surrogate data (red line) for NS2 at 10 dB SNR, plotted against coupling strength.

Table 3-11: The lowest value of coupling strength that detects significant synchrony for noisy NS2 at 10 dB SNR. Good and unsatisfactory performance outcomes are highlighted by colouring the text blue and red respectively.

Measure	Lowest μ that achieves significant synchrony
Mean phase coherence (Hilbert)	0.0
Phase coherence value unwrapped	0.0
Phase coherence value wrapped	0.0
Conditional probability based phase synchrony	0.0
Mean phase coherence (wavelet)	0.1
Correlation coefficient	0.2
Partial coherence	0.2
Mean phase coherence (event)	0.2
Mutual information (adaptive histograms)	0.2
Coherence	0.3
Mutual information (kernels)	0.4
Mutual information (time-frequency plane)	0.4
Kullback-Leibler divergence (histogram)	0.4
Rényi Divergence	0.4
Jensen-Shannon divergence	0.4
Jensen-Rényi divergence	0.4
Nonlinear Interdependence (H)	0.6
Nonlinear Interdependence (S)	0.6
Nonlinear Interdependence (N)	0.6
Correntropy coefficient	0.7
Coh-entropy coefficient	0.7
Event synchronisation	0.7
Mutual information (histograms)	0.7
Maximum likelihood mutual information	0.7
Nearest-neighbour mutual information	0.7
Omega Complexity	0.7
S-estimator	0.7
wave-entropy	NaN

Correlation coefficient and related measures
Phase synchrony
Information-theoretic measures
Synchronisation based on state space

Unsatisfactory ———
Robust ———

Figure 3-19 shows the calculation of 29 measures against increasing coupling strength μ at a SNR of 1 dB for NS2. Table 3-12 shows us when a measure first detects statistically significant synchrony. Correlation coefficient and partial coherence first detect significant synchrony at $\mu = 0.3$, suggesting these measures are robust measures for detecting weak coupling.

Correlation coefficient and many of the measures still visually show a heightened synchronisation between $\mu = 0.4$ and $\mu = 0.6$, as expected. Some measures perform unsatisfactorily: Wave entropy and phase coherence value unwrapped fails to detect synchrony at any coupling strength; Hilbert phase, mean phase coherence (event) and PCV wrapped fail to detect synchrony at some coupling strengths despite detecting it at lower coupling strengths; nearest-neighbour mutual information, mutual information (time-frequency plane) and Kullback Leibler divergence fail to detect synchrony at large coupling, $\mu > 0.9$; and conditional based phase synchrony detect synchrony when there is none (coupling strength equals zero).
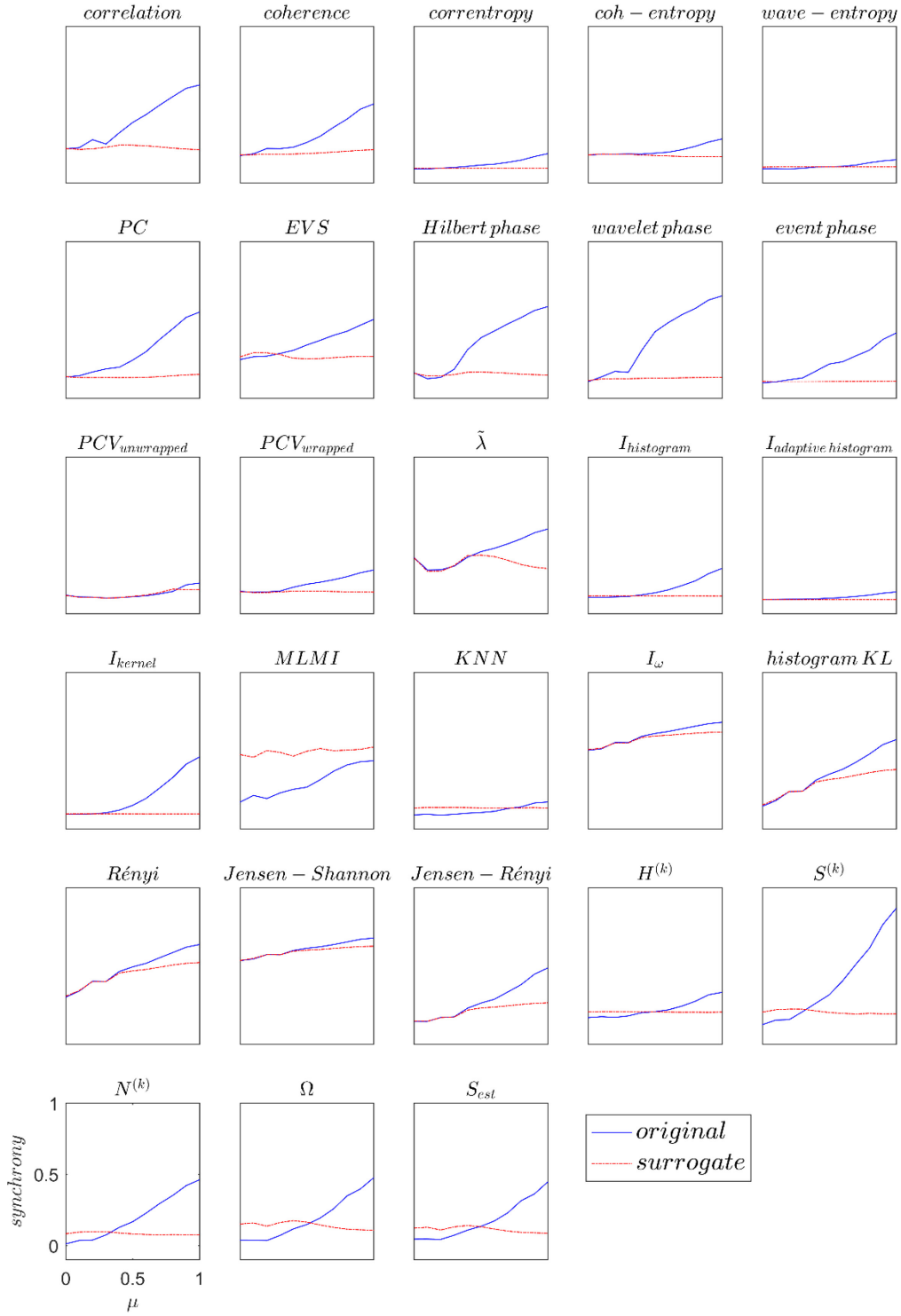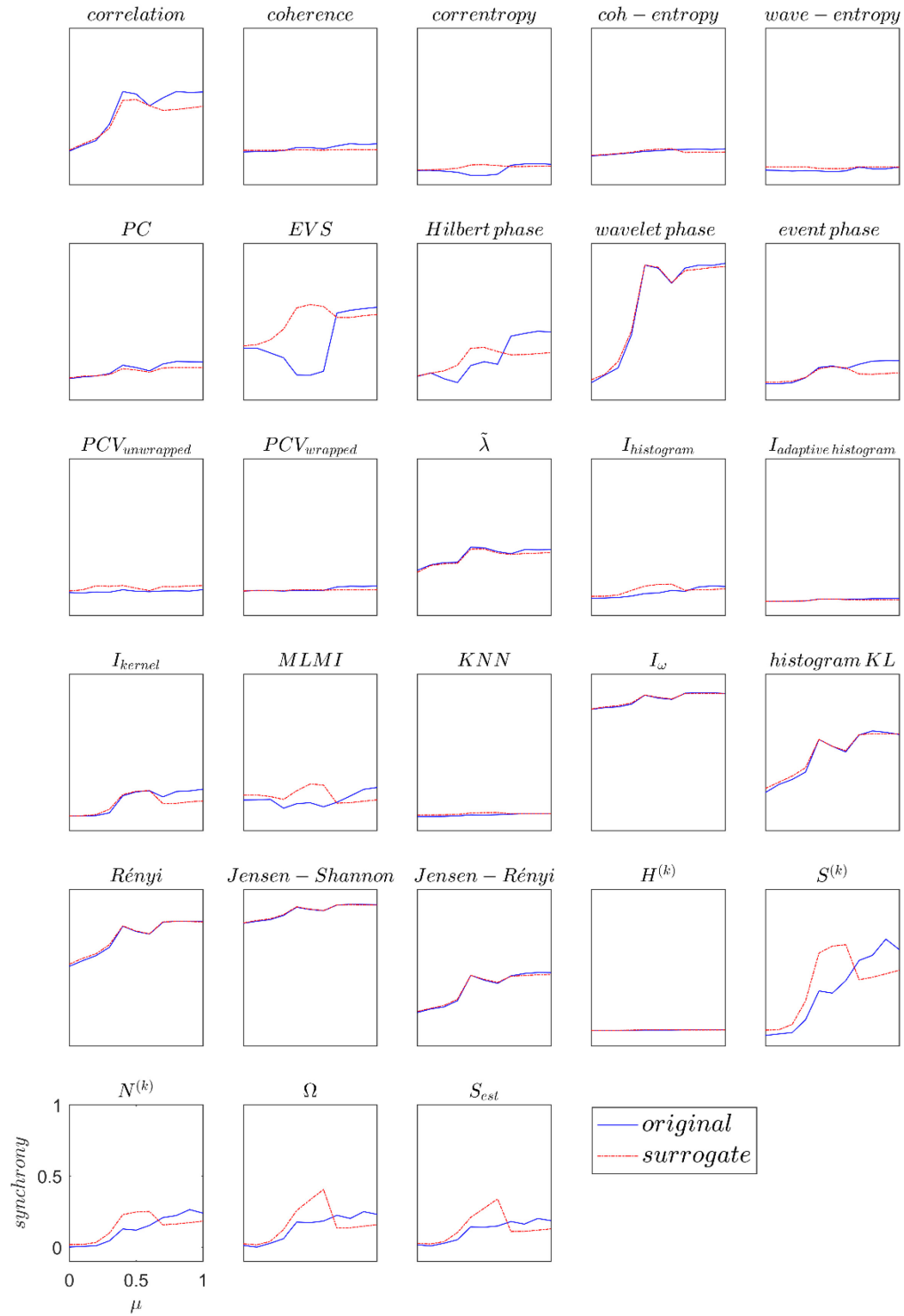
Figure 3-19: Functional connectivity measures for NS2 at 1 dB SNR. Functional connectivity measures calculated from the original data (blue line) and the threshold based on surrogate data (red line) for NS2 at 1 dB SNR, plotted against coupling strength.

Table 3-12: The lowest value of coupling strength that detects significant synchrony for noisy NS2 at 1 dB SNR. Good and unsatisfactory performance outcomes are highlighted by colouring the text blue and red respectively.

Measure	Lowest μ that achieves significant synchrony
Conditional probability based phase synchrony	0.0
Mean phase coherence (Hilbert)	0.1
Phase coherence value wrapped	0.1
Correlation coefficient	0.3
Partial coherence	0.3
Coherence	0.4
Mean phase coherence (event)	0.4
Mutual information (adaptive histograms)	0.4
Jensen-Rényi divergence	0.4
Kullback Leibler divergence (histogram)	0.5
Correntropy coefficient	0.7
Coh-entropy coefficient	0.7
Event synchronisation	0.7
Mean phase coherence (wavelet)	0.7
Mutual information (kernels)	0.7
Maximum likelihood mutual information	0.7
Mutual information (time-frequency plane)	0.7
Nonlinear Interdependence (H)	0.7
Nonlinear Interdependence (S)	0.7
Nonlinear Interdependence (N)	0.7
Omega Complexity	0.7
S-estimator	0.7
Mutual information (histograms)	0.8
Nearest-neighbour mutual information	0.8
Rényi Divergence	0.8
Jensen-Shannon divergence	0.8
wave-entropy	NaN
Phase coherence value unwrapped	NaN

Correlation coefficient and related measures
Phase synchrony
Information-theoretic measures
Synchronisation based on state space

Unsatisfactory ————
Robust ————

Figure 3-20 shows the lowest value of coupling strength that detects synchrony for three SNRs, and for each of IS, NS1 and NS2 as well as the ideal result. We can observe that partial coherence is the closest to the ideal result, so partial coherence can be considered as the most robust measure for detecting weak coupling in both noise free and noisy systems. Note that coherence and correlation also perform very well some measures show little change with

increasing noise, such as event synchronisation, S-estimator, and nonlinear interdependency (S). Although their performance is not as good as other measures, perhaps they would be a good choice when the noise levels are very high.

Figure 3-20: The lowest value of coupling strength that detects synchrony against SNR (noise-free, SNR of 10 dB, and SNR of 1 dB) for IS (blue diamond), NS1 (black triangle), NS2 (red square), and the ideal result (black asterisk).

3.1.3.2 Results for nonstationary systems

Figure 3-21 shows the results when the noise at 10 dB SNR is added to the IS with nonstationary coupling explored in section 3.3.1. All measures still show the increase and decrease due to the sudden changes in the dynamics of interacting systems, caused by change in the coupling strength. Table 3-13 shows the value of the time index k that first detects synchrony, the value of k that last detects synchrony, and the difference of these two. Coh-entropy first detects synchrony at $k_{min} = 64$, which is closest to the ideal value. This measure also shows the large difference between the time that a measure first detects synchrony and the time that it no longer detects synchrony (k_{diff}), suggesting this measure is most robust to low levels of noise. In addition, correntropy coefficient, mutual information kernel, nonlinear interdependence (H), nonlinear interdependence and S estimator also achieve a value of k_{min} close to the ideal value and a large k_{diff}, suggesting they can be also considered as good measures in low levels of noise. Some measures perform unsatisfactorily; maximum likelihood mutual information, and conditional probability based phase synchrony are not able to detect synchrony at all, and omega complexity detects synchrony at all-time points.

Figure 3-21: Synchrony measures applied to noisy IS with nonstationary coupling at 10 dB SNR. Result of synchronisation for original data (blue line); surrogate data (red line).

Table 3-13: The values of (k_{min}), (k_{max}) and (k_{diff}) for nonstationary IS at 10 dB SNR. The value of the time index k that first detects synchrony (k_{min}), the value of k that last detects synchrony (k_{max}), and the difference of these two (k_{diff}) for noisy IS with nonstationary coupling at 10 dB SNR. Good and unsatisfactory performance outcomes are highlighted by colouring the text blue and red respectively

Measure	k_{min}	k_{max}	k_{diff}
Correlation coefficient	75	226	151
Coherence	77	224	147
Correntropy coefficient	67	230	163
Coh-entropy coefficient	64	232	168
Wave-entropy	94	206	112
Partial coherence	100	192	92
Event synchronisation	75	205	130
Mean phase coherence (Hilbert)	70	227	157
Mean phase coherence (wavelet)	92	202	110
Mean phase coherence (event)	86	216	130
Phase coherence value unwrapped	75	223	148
Phase coherence value wrapped	72	228	156
Conditional probability based phase synchrony	NaN	NaN	NaN
Mutual information (histograms)	93	226	133
Mutual information (adaptive histogram)	74	225	151
Mutual information (kernels)	69	237	168
Maximum likelihood mutual information	NaN	NaN	NaN
Nearest-neighbour mutual information	87	211	124
Mutual information (time-frequency plane)	79	229	150
Kullback Leibler divergence (histogram)	79	228	149
Rényi Divergence	77	228	151
Jensen-Shannon divergence	79	228	149
Jensen-Rényi divergence	74	230	156
Nonlinear Interdependence (H)	69	230	161
Nonlinear Interdependence (S)	80	221	141
Nonlinear Interdependence (N)	70	230	160
Omega Complexity	1	400	399
S-estimator	69	232	163

.

Correlation coefficient and related measures
Phase synchrony
Information-theoretic measures
Synchronisation based on state space

Unsatisfactory ———
Robust ———

Figure 3-22 shows the same experiment at a SNR of 1 dB. Measures mostly show the expected increase and decrease, due to the sudden changes in the coupling strength altering the dynamics of interacting systems, but fewer measures are able to get a value above threshold. Table 3-14 records the values of k_{min}, k_{max} and k_{diff}. Nonlinear Interdependence (H), nonlinear Interdependence (S), nonlinear Interdependence (N) and S-estimator and mutual information

(kernel) first detect synchrony at the closer level of the coupling to the ideal value. Note that the k_{diff} also is large for these measures. Thus, we can consider these measures as the best measures for detecting weak coupling in IS contaminated with large noise. Some measures perform unsatisfactorily. Wave entropy, partial coherence, mean phase coherence, conditional based phase synchrony, mutual information histogram, maximum likelihood mutual information and nearest neighbour mutual information fail to detect synchrony at all. Rényi divergence and event synchronisation only detect synchrony at a single time point. Omega complexity detects synchrony at all-time points.

Figure 3-22: Synchrony measures applied to noisy IS with nonstationary coupling at 1 dB SNR. Result of synchronisation for original data (black line); surrogate data (red line).

Table 3-14: The values of (k_{min}), (k_{max}) and (k_{diff}) for nonstationary IS at 1 dB SNR. The value of the time index k that first detects synchrony (k_{min}), the value of k that last detects synchrony (k_{max}), and the difference of these two (k_{diff}) for noisy IS with nonstationary coupling at 1 dB SNR. Good and unsatisfactory performance outcomes are highlighted by colouring the text blue and red respectively.

Measure	k_{min}	k_{max}	k_{diff}
Correlation coefficient	86	209	123
Coherence	88	207	119
Correntropy coefficient	87	203	116
Coh-entropy coefficient	86	207	121
Wave-entropy	NaN	NaN	NaN
Partial coherence	NaN	NaN	NaN
Event synchronisation	162	162	0
Mean phase coherence (Hilbert)	85	205	120
Mean phase coherence (wavelet)	105	186	81
Mean phase coherence (event)	NaN	NaN	NaN
Phase coherence value unwrapped	121	174	53
Phase coherence value wrapped	92	204	112
Conditional probability based phase synchrony	NaN	NaN	NaN
Mutual information (histograms)	NaN	NaN	NaN
Mutual information (adaptive histogram)	93	203	110
Mutual information (kernels)	78	224	146
Maximum likelihood mutual information	NaN	NaN	NaN
Nearest-neighbour mutual information	NaN	NaN	NaN
Mutual information (time-frequency plane)	152	174	22
Kullback Leibler divergence (histogram)	128	170	42
Rényi divergence	108	108	0
Jensen-Shannon divergence	124	189	65
Jensen-Rényi divergence	118	167	49
Nonlinear Interdependence (H)	82	219	137
Nonlinear Interdependence (S)	84	219	135
Nonlinear Interdependence (N)	82	219	137
Omega Complexity	1	400	399
S-estimator	78	221	143

Correlation coefficient and related measures
Phase synchrony
Information-theoretic measures
Synchronisation based on state space

Unsatisfactory ————
Robust ————

Figure 3-23 shows the results of synchrony measures applied to IS with nonstationary coupling for three SNRs. Ideally, we would like to see a measure detect synchrony as early as possible, and continue to detect it for as long as possible. Hence one measure of performance is the length of time that a measure detects synchrony. Additionally, a good measure would reliably

detect synchrony through this period, not have inconsistent detection. We would also like a measure to have low noise on its estimate.

Overall, we can see that only 12 measures perform satisfactorily, with details collected in Table 3-15. In particular, we measured the length of time from first detection of synchrony to last, for each of the three SNRs, we qualitatively assessed the amount of noise on the estimates, and whether the detection of synchrony was consistent over the period of high connectivity.

Coh-entropy generally detects the synchrony earlier than other measures, though its performance at high noise is not as good. S-estimator is generally very good in all situations, though its estimates of synchrony become quite noisy as the measurement noise increases. Mutual information (kernel) has clean estimates and reliably detects synchrony at all noise levels, but does not detect the changes as quickly as some other measures. Correntropy coefficient, mean phase coherence (Hilbert), phase coherence (unwrapped), nonlinear interdependence (H), nonlinear interdependence (S), nonlinear interdependence (N) also detect synchrony at all SNRs, and perform better than other measures in some limited way. Correlation, coherence and mutual information (adaptive histogram) also detect synchrony at all SNRs.
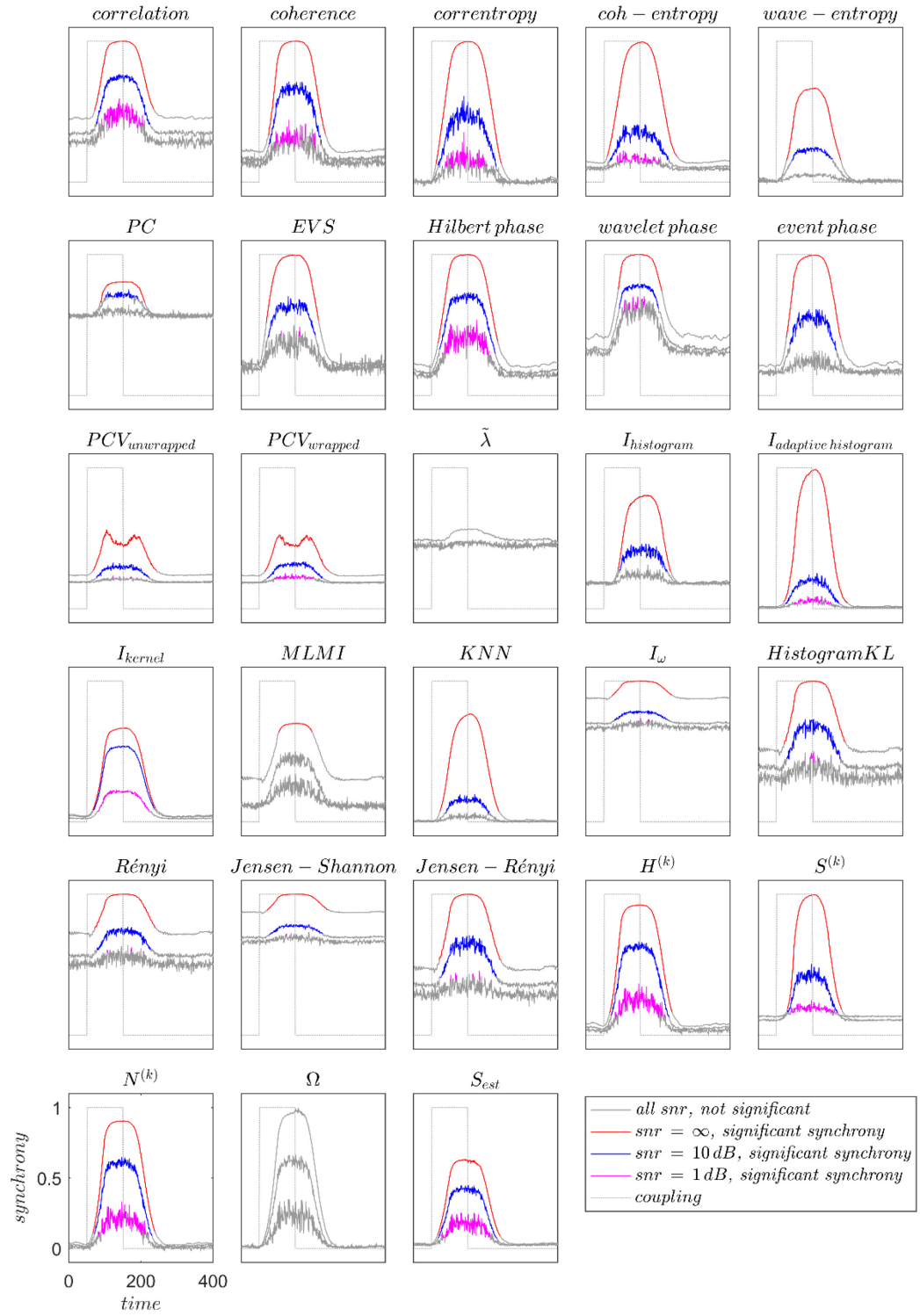
Figure 3-23: *Synchrony measures against time for nonstationary IS. Non-significant results are shown in grey for all SNRs, significant results for SNR = ∞ dB are in red, for SNR = 10 dB are in blue, and for SNR = 1 dB are in magenta.*

Table 3-15: List the connectivity measures that perform satisfactorily for IS data. On IS data, we list the connectivity measures that perform satisfactorily, the length of time that synchrony is detected for no noise, 10 dB SNR, and 1 dB SNR, plus a qualitative assessment of the amount of noise on the estimates, and whether a measure consistently detects synchrony during the high-connectivity period. Good performance outcomes are highlighted by colouring the text blue.

Measure	k_{diff}			Noise	Consistency
	∞	10	1		
Correlation coefficient	104	66	65	High	Good
Coherence	111	69	69	High	Poor
Correntropy coefficient	117	70	71	High	Poor
Coh-entropy coefficient	129	77	77	Medium	Poor
Mean phase coherence (Hilbert)	110	87	87	High	Good
Phase coherence value wrapped	110	56	56	Low	Good
Mutual information (adaptive histogram)	102	45	45	Low	Good
Mutual information (kernels)	111	109	86	Low	Excellent
Nonlinear Interdependence (H^k)	117	75	75	High	Good
Nonlinear Interdependence (S^k)	83	68	68	Low	Good
Nonlinear Interdependence (N^k)	117	75	75	High	Good
S-estimator	116	94	94	High	Good

Figure 3-24 shows the results when measurement noise at 10 dB SNR is added to the NS1 with nonstationary coupling. Measures mostly still show the increase and decrease due to the sudden changes in the dynamics of the interacting systems, caused by the changes in coupling strength. Table 3-16 shows the value of the time index k that first detects synchrony, the value of k that last detects synchrony, and the difference of these two. Overall only 12 measure perform satisfactory. Mutual information (kernel) and S-estimator first detect synchrony closest to the ideal value. These measures also show the largest time difference k_{diff}, suggesting these measures are most sensitive to NS1 in low levels of noise. In addition, correntropy coefficient, coh-entropy, nonlinear interdependence (N^k), and nonlinear interdependence (H_k) perform well. Some measures perform unsatisfactorily: wave entropy, event synchronisation, phase coherence value unwrapped, conditional probability-based phase synchrony, mutual information (histograms), maximum likelihood mutual information, nearest-neighbour mutual information (time-frequency plane), Rényi divergence, Jensen-Shannon divergence, Jensen-Rényi divergence, and omega complexity are not able to detect synchrony at all. Mean phase

coherence (wavelet) and Kullback-Leibler divergence (histogram) detected significant synchrony at only 1 and 2 time points respectively.
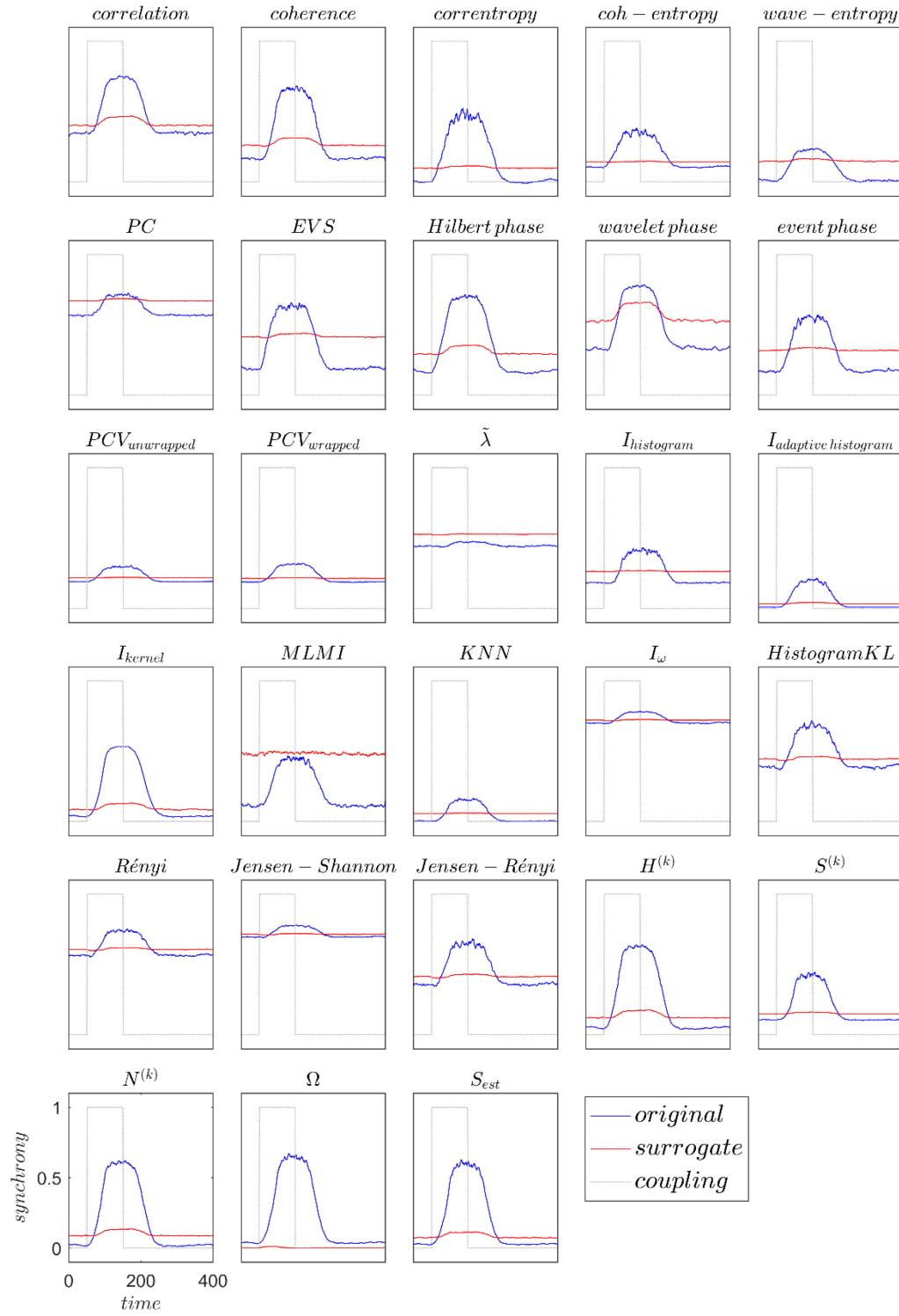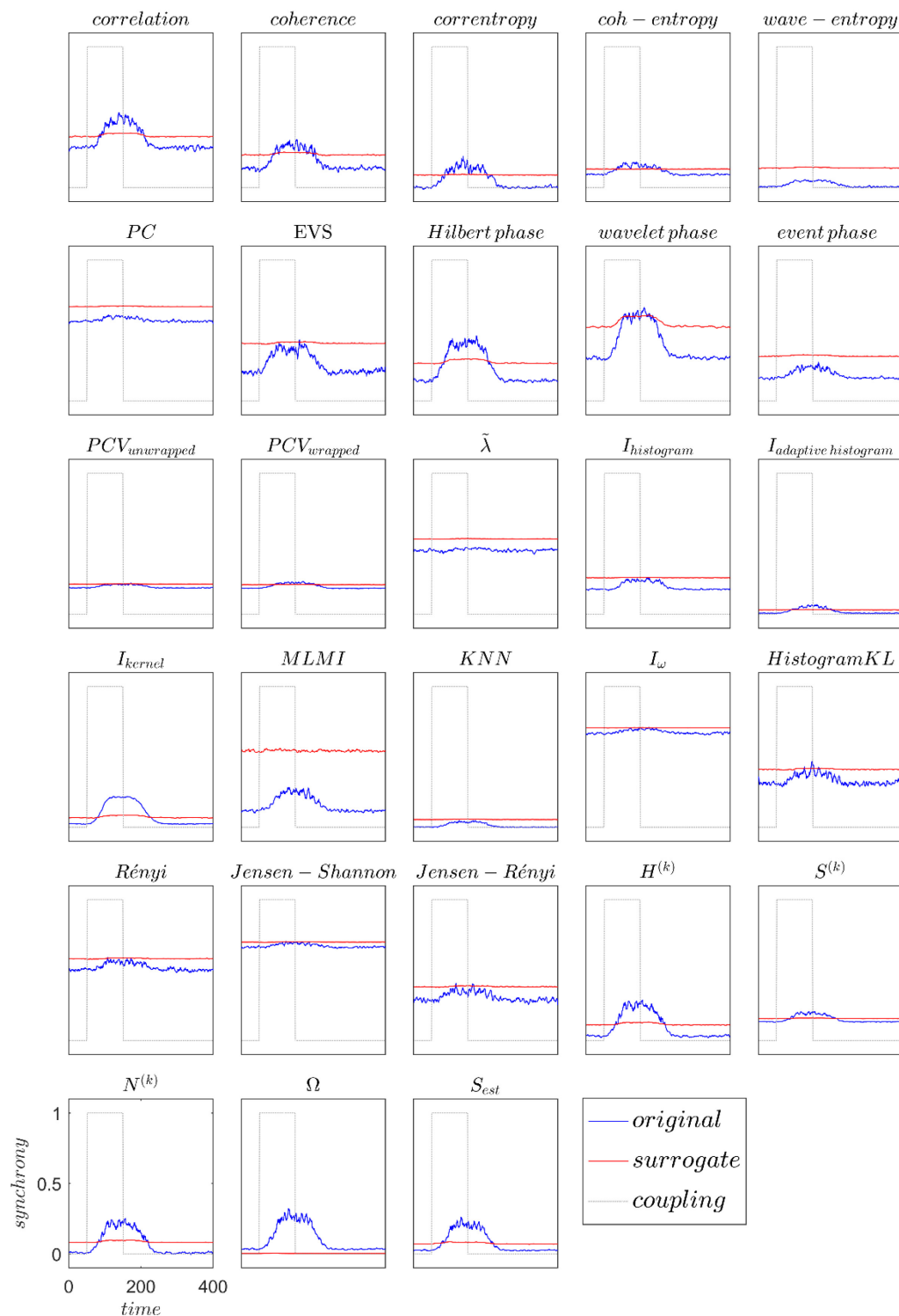

Figure 3-24: Synchrony measures applied to noisy NS1 with nonstationary coupling at 10 dB SNR. Result of synchronisation for original data (blue line); surrogate data (red line).

Table 3-16: The values of (k_{min}), (k_{max}) and (k_{diff}) for nonstationary NS1 at 10 dB SNR. The value of the time index k that first detects synchrony (k_{min}), the value of k that last detects synchrony (k_{max}), and the difference of these two (k_{diff}) for NS1 with nonstationary coupling at 10 dB SNR. Good and unsatisfactory performance outcomes are highlighted by colouring the text blue and red respectively.

Measure	k_{min}	k_{max}	k_{diff}
Correlation coefficient	99	165	66
Coherence	88	157	69
Correntropy coefficient	89	159	70
Coh-entropy coefficient	89	166	77
Wave-entropy	NaN	NaN	NaN
Partial coherence	74	172	98
Event synchronisation	NaN	NaN	NaN
Mean phase coherence (Hilbert)	88	175	87
Mean phase coherence (wavelet)	144	144	0
Mean phase coherence (event)	NaN	NaN	NaN
Phase coherence value unwrapped	NaN	NaN	NaN
Phase coherence value wrapped	98	154	56
Conditional probability based phase synchrony	NaN	NaN	NaN
Mutual information (histograms)	NaN	NaN	NaN
Mutual information (adaptive histograms)	114	159	45
Mutual information (kernels)	73	182	109
Maximum likelihood mutual information	NaN	NaN	NaN
Nearest-neighbour mutual information	NaN	NaN	NaN
Mutual information (time-frequency plane)	NaN	NaN	NaN
Kullback Leibler divergence (histogram)	148	150	2
Rényi Divergence	NaN	NaN	NaN
Jensen-Shannon divergence	NaN	NaN	NaN
Jensen-Rényi divergence	NaN	NaN	NaN
Nonlinear Interdependence (H^k)	91	166	75
Nonlinear Interdependence (S^k)	91	159	68
Nonlinear Interdependence (N^k)	91	166	75
Omega Complexity	NaN	NaN	NaN
S-estimator	78	172	94

Correlation coefficient and related measures
Phase synchrony
Information-theoretic measures
Synchronisation based on state space

Unsatisfactory ————
Robust ————

Figure 3-25 shows the results when noise at 1 dB SNR is added to the NS1 with nonstationary coupling. Most measures show an increase and decrease in value corresponding to the changes in coupling strength, though for many measures the increase and decrease are small. However, fewer than half of the measures reliably exceed the threshold during the high coupling. Table

3-17 records the values of k_{min}, k_{max} and k_{diff}. None of the measures first detect synchrony at the time close to the ideal value, nor is k_{diff} appropriately large for any of the measures. Cross correlation, coherence, correntropy coefficient, coh-entropy coefficient, mean coherence Hilbert, mutual information kernel, nonlinear interdependence(H^k), nonlinear interdependence (S^k), nonlinear interdependence (N^k) and S-estimator are the measures which are able to detect synchrony corresponding to the coupling zone, which suggests these measures are suitable for analysing the nonstationary NS1 contaminated with a high level of noise.

Figure 3-25: Synchrony measures applied to noisy NS1 with nonstationary coupling at 1 dB SNR. Result of synchronisation for original data (blue line); surrogate data (red line).

Table 3-17: The values of (k_{min}), (k_{max}) and (k_{diff}) for nonstationary NS1 at 1 dB SNR. The value of the time index k that first detects synchrony (k_{min}), the value of k that last detects synchrony (k_{max}), and the difference of these two (k_{diff}) for noisy NS1 with nonstationary coupling at 1 dB SNR. Good and unsatisfactory performance outcomes are highlighted by colouring the text blue and red respectively.

Measure	k_{min}	k_{max}	k_{diff}
Correlation coefficient	99	164	65
Coherence	88	157	69
Correntropy coefficient	88	159	71
Coh-entropy coefficient	89	166	77
Wave-entropy	NaN	NaN	NaN
Partial coherence	NaN	NaN	NaN
Event synchronisation	NaN	NaN	NaN
Mean phase coherence (Hilbert)	88	175	87
Mean phase coherence (wavelet)	143	144	1
Mean phase coherence (event)	NaN	NaN	NaN
Phase coherence value unwrapped	NaN	NaN	NaN
Phase coherence value wrapped	98	154	56
Conditional probability based phase synchrony	NaN	NaN	NaN
Mutual information (histograms)	NaN	NaN	NaN
Mutual information (adaptive histograms)	114	159	45
Mutual information (kernels)	85	171	86
Maximum likelihood mutual information	NaN	NaN	NaN
Nearest-neighbour mutual information	NaN	NaN	NaN
Mutual information (time-frequency plane)	NaN	NaN	NaN
Kullback Leibler divergence (histogram)	148	150	2
Rényi Divergence	NaN	NaN	NaN
Jensen-Shannon divergence	NaN	NaN	NaN
Jensen-Rényi divergence	NaN	NaN	NaN
Nonlinear Interdependence (H^k)	91	166	75
Nonlinear Interdependence (S^k)	91	159	68
Nonlinear Interdependence (N^k)	91	166	75
Omega Complexity	1	400	399
S-estimator	78	172	94

Correlation coefficient and related measures
Phase synchrony
Information-theoretic measures
Synchronisation based on state space

Unsatisfactory ———
Robust ———

Figure 3-26 shows the results of synchrony measures applied to NS1 with nonstationary coupling for three SNRs. Again, we seek low noise estimates that give early and continued detection of synchrony, and so use the same indicators of performance as use for the IS system, detailed in Table 3-18.

Overall we can see that only 12 measures perform satisfactorily. S-estimator and mutual information (kernel) perform the best of all the measures, with S-estimator generally detecting synchrony for longer while mutual information (kernel) has less noise on its estimates of synchrony. Mean phase coherence (Hilbert), phase coherence (unwrapped), mutual information (adaptive histogram), nonlinear interdependence (H^k), nonlinear interdependence (S^k), nonlinear interdependence (N^k) also detect synchrony at all SNRs, and perform better than other measures in some limited way. Correlation, coherence, correntropy coefficient and coh-entropy also detect synchrony at all SNRs.
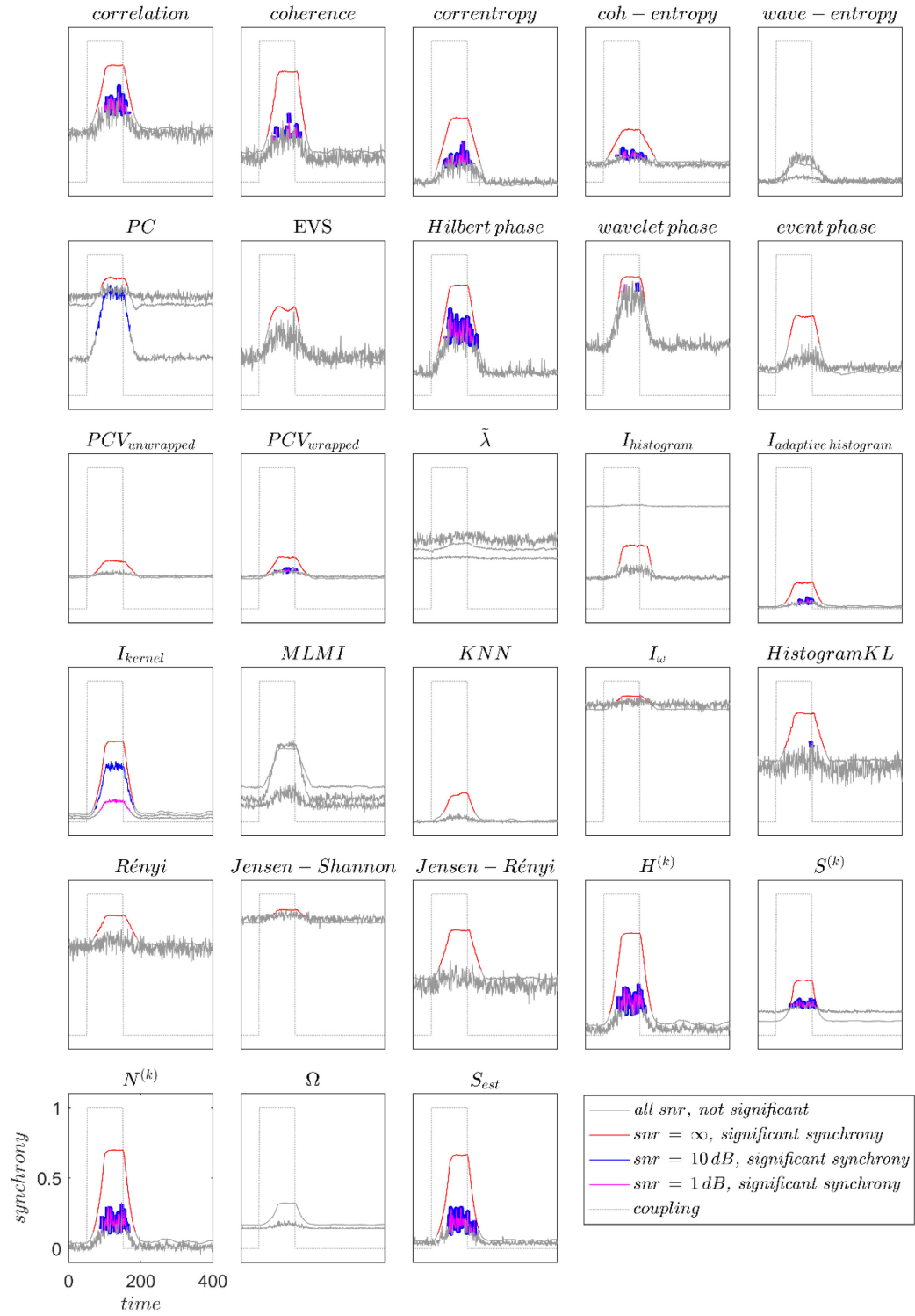
Figure 3-26: Synchrony measures against time for nonstationary NS1. Non-significant results are shown in grey for all SNRs, significant results for $SNR = \infty$ dB are in red, for $SNR = 10$ dB are in blue, and for $SNR = 1$ dB are in magenta.

119

Table 3-18: List the connectivity measures that perform satisfactorily for NS1 data. On NS1 data, we list the connectivity measures that perform satisfactorily, the length of time that synchrony is detected for no noise, 10 dB SNR, and 1 dB SNR, plus a qualitative assessment of the amount of noise on the estimates, and whether a measure consistently detects synchrony during the high-connectivity period. Good performance outcomes are highlighted by colouring the text blue.

Measure	k_{diff}			Noise	Consistency
	∞	10	1		
Correlation coefficient	104	66	65	High	Good
Coherence	111	69	69	High	Poor
Correntropy coefficient	117	70	71	High	Poor
Coh-entropy coefficient	129	77	77	Medium	Poor
Mean phase coherence (Hilbert)	110	87	87	High	Good
Phase coherence value wrapped	110	56	56	Low	Good
Mutual information (adaptive histogram)	102	45	45	Low	Good
Mutual information (kernels)	111	109	86	Low	Excellent
Nonlinear Interdependence (H)	117	75	75	High	Good
Nonlinear Interdependence (S)	83	68	68	Low	Good
Nonlinear Interdependence (N)	117	75	75	High	Good
S-estimator	116	94	94	High	Good

Figure 3-27 shows the results when measurement noise at 10 dB SNR is added to the NS2 with nonstationary coupling. All measures except wave entropy and conditional probability-based phase synchrony still show the increase and decrease due to the sudden changes in the dynamics of interacting systems, caused by change in the coupling strength. Table 3-19 shows the value of the time index k that first detects synchrony, the value of k that last detects synchrony, and the difference of these two. Correntropy coefficient and mean phase coherence (Hilbert) first detects synchrony at $k_{min} = 71$ and $k_{min} = 72$ which are closest to the ideal value. These measures also show the largest time difference k_{diff}, suggesting these measures are most robust to low levels of noise for the NS2. In addition, mutual information kernel, nonlinear interdependence (N^k), nonlinear interdependence (H^k) and phase coherence value wrapped also perform well and they can be also considered as good measures in low levels of noise. Some measures perform unsatisfactorily; wave entropy, conditional probability-based phase synchrony and mutual information (Histogram) are not able to detect synchrony at all.
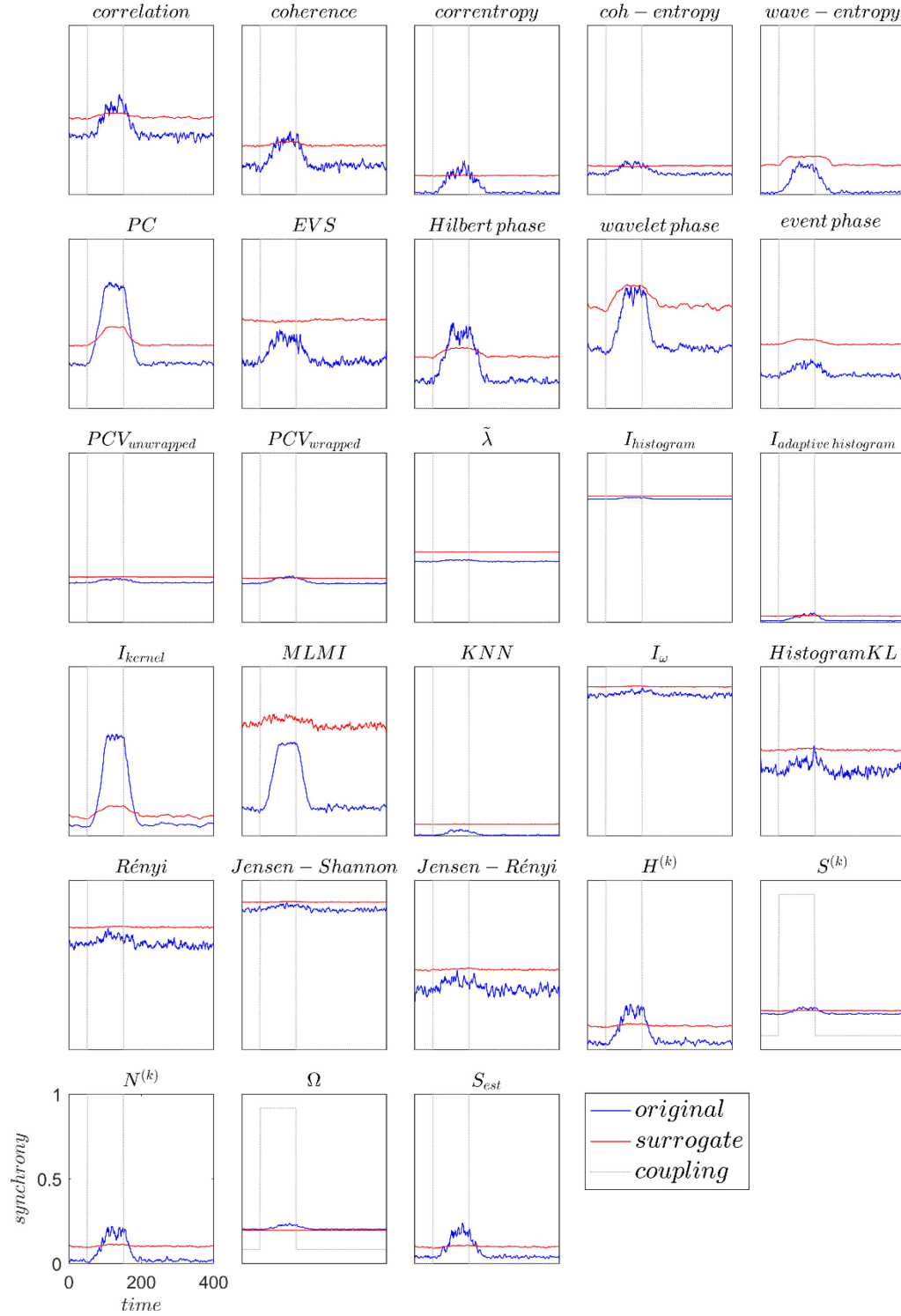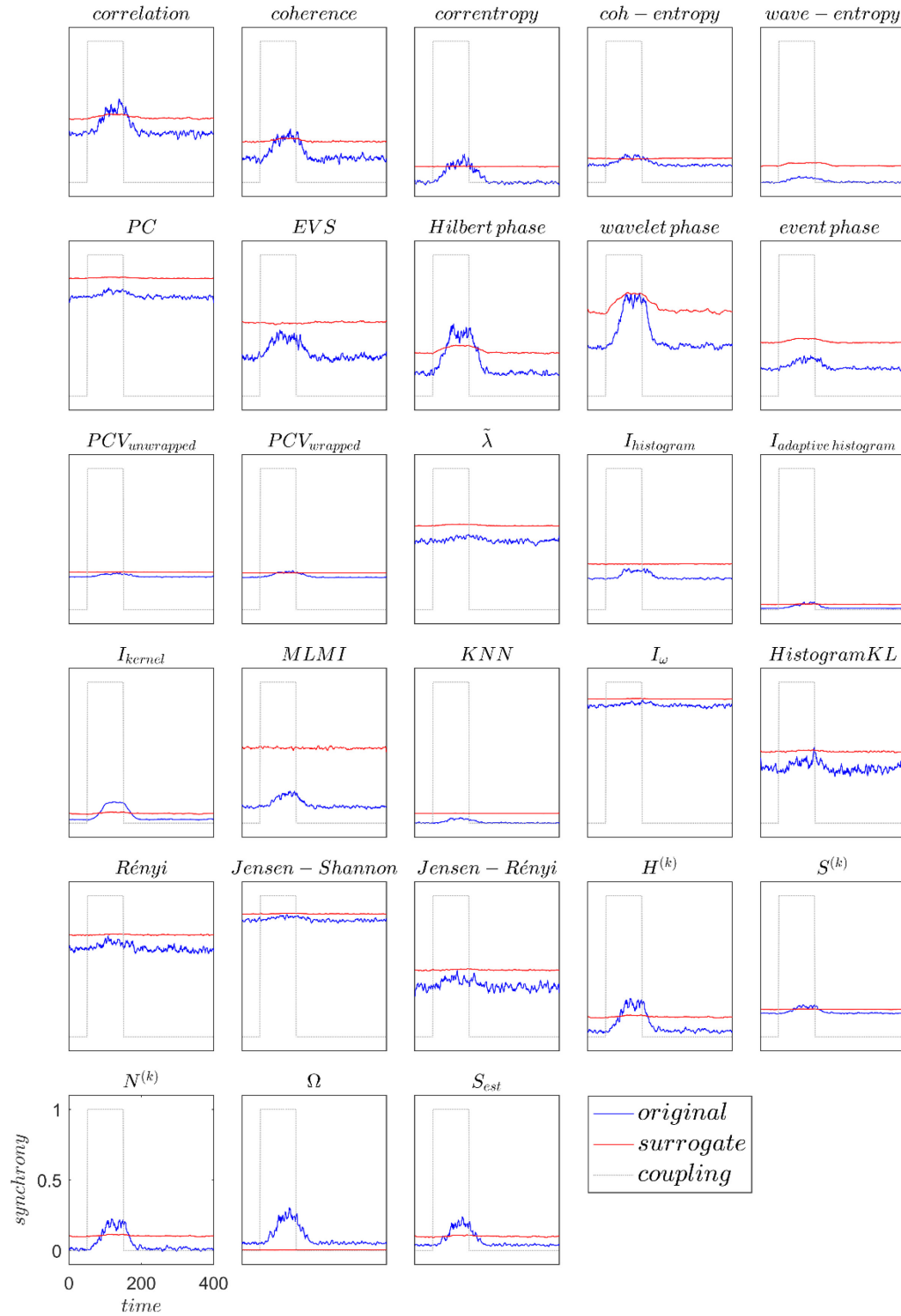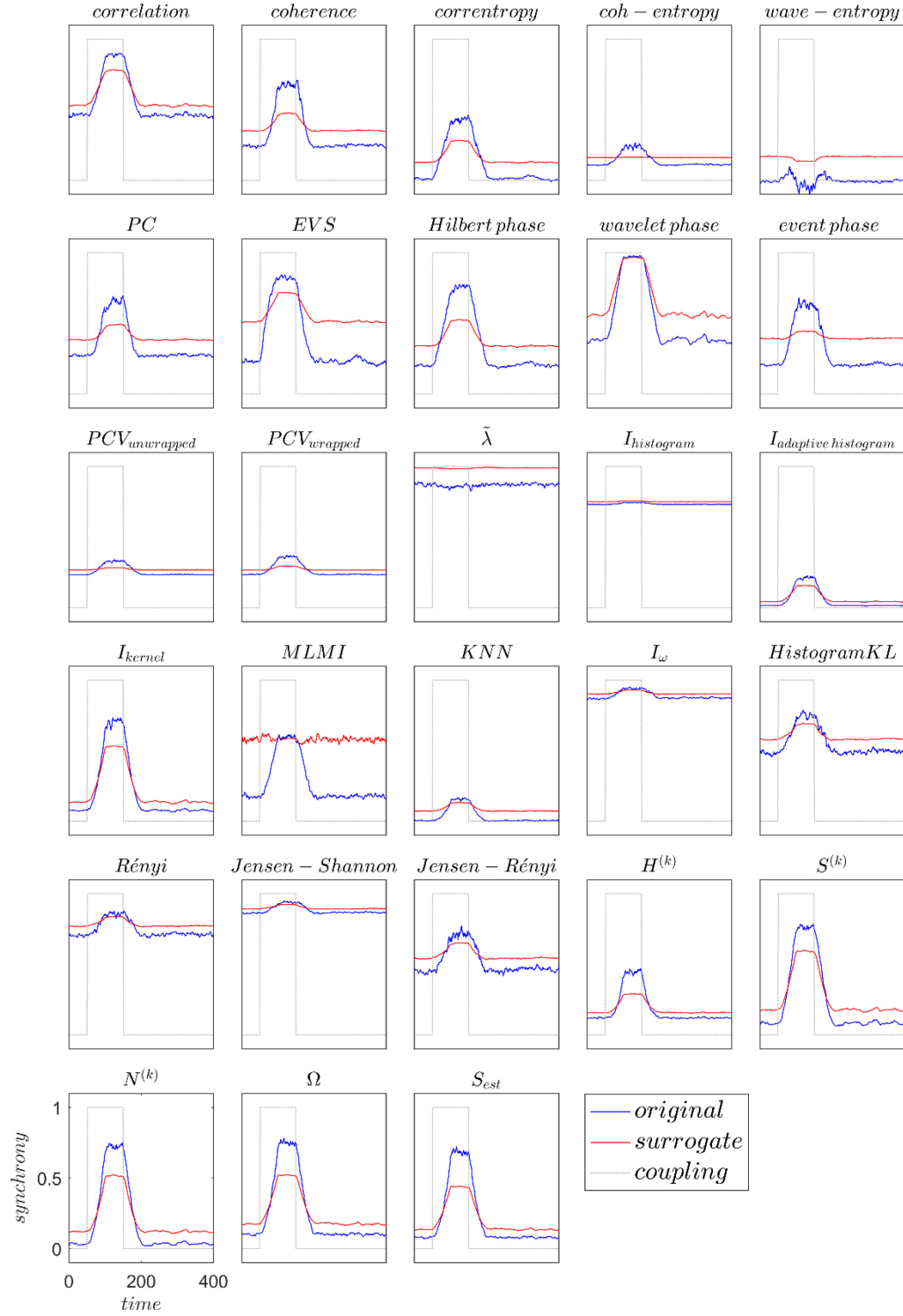
Figure 3-27: Synchrony measures applied to noisy NS2 with nonstationary coupling at 10 dB SNR. Result of synchronisation for original data (blue line); surrogate data (red line).

Table 3-19:   The values of (k_{min}), (k_{max}) and (k_{diff}) for nonstationary NS2 at 10 dB SNR. The value of the time index k that first detects synchrony (k_{min}), the value of k that last detects synchrony (k_{max}), and the difference of these two (k_{diff}) for noisy NS2 with nonstationary coupling at 10 dB SNR. Good and unsatisfactory performance outcomes are highlighted by colouring the text blue and red respectively.

Measure	k_{min}	k_{max}	k_{diff}
Correlation coefficient	86	173	87
Coherence	84	174	90
Correntropy coefficient	71	186	115
Coh-entropy coefficient	81	176	95
Wave-entropy	NaN	NaN	NaN
Partial coherence	84	171	87
Event synchronisation	73	158	85
Mean phase coherence (Hilbert)	72	186	114
Mean phase coherence (wavelet)	99	157	58
Mean phase coherence (event)	85	175	90
Phase coherence value unwrapped	81	176	95
Phase coherence value wrapped	78	179	101
Conditional probability based phase synchrony	NaN	NaN	NaN
Mutual information (histograms)	NaN	NaN	NaN
Mutual information (adaptive histograms)	86	173	87
Mutual information (kernels)	81	180	99
Maximum likelihood mutual information	101	157	56
Nearest-neighbor mutual information	99	162	63
Mutual information (time-frequency plane)	88	182	94
Kullback Leibler divergence (histogram)	91	182	91
Rényi Divergence	89	178	89
Jensen-Shannon divergence	98	179	81
Jensen-Rényi divergence	89	178	89
Nonlinear Interdependence (H^k)	84	173	89
Nonlinear Interdependence (S^k)	77	184	107
Nonlinear Interdependence (N^k)	80	183	103
Omega Complexity	81	177	96
S-estimator	81	179	98

Correlation coefficient and related measures
Phase synchrony
Information-theoretic measures
Synchronisation based on state space

Unsatisfactory ———————
Robust ———————

Figure 3-28 shows the results of the same experiment when measurement noise at 1 dB SNR is added to NS2. The measures mostly still show the increase and decrease due to the sudden changes in the dynamics of interacting systems but with an overall degradation of the estimates

due to the extra noise. Only 10 measures are able to detect synchrony, i.e. exceed the threshold, corresponding to the coupling zone ($50 < k < 150$). These measures fluctuate around the threshold, inconsistently detecting synchrony. These 10 measures are more robust to a high level of measurement noise for NS2 than the other 18 measures. Table 3-20 shows the values of the time indices k_{min} and k_{max}, and their difference k_{diff}. Two more column were added to this table to capture the inconsistent detection of synchrony. One column counts the number of times that the measure detects statistically significant synchrony N_{sig}. The percentage rate of detections in the range of detections $R_{sig} = N_{sig} / (k_{max} - k_{min}) * 100$ was also calculated and recorded in the last column. Clearly, mean phase coherence (Hilbert) outperforms all other measures with the largest count $N_{sig} = 61$ and rate $R_{sig} = 42\%$, meaning this measure is most robust to high levels of noise for NS2. Omega complexity and s estimator also perform well, suggesting they may be also considered as good measures in high levels of noise in NS2. 18 measures performed unsatisfactorily; they are not able to detect synchrony in this data at all.
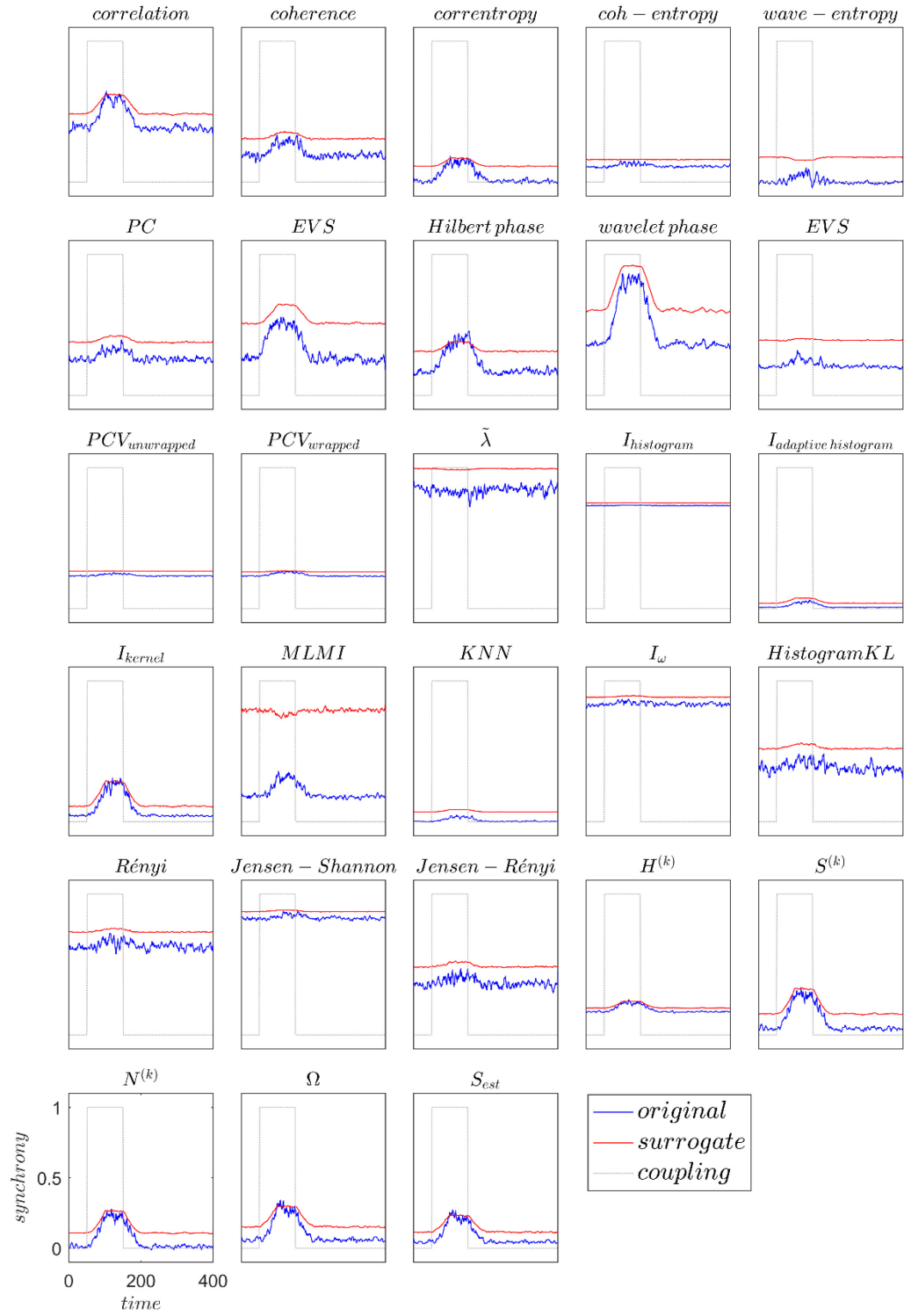
Figure 3-28: Synchrony measures applied to noisy NS2 with nonstationary coupling at 1 dB SNR. Result of synchronisation for original data (blue line); surrogate data (red line).

Table 3-20: The values of (k_{min}), (k_{max}), (k_{diff}), N_{sig} and R_{sig} for nonstationary NS2 at 1dB SNR. The value of the time index k that first detects synchrony (k_{min}), the value of k that last detects synchrony (k_{max}), the difference of these two (k_{diff}), the number of times that the measure detects statistically significant synchrony N_{sig}, the percentage rate of detections in the range of detections $R_{sig} = N_{sig}/ (k_{max} - k_{min}) * 100$ for noisy NS2 with nonstationary coupling at 1 dB SNR. Good and unsatisfactory performance outcomes are highlighted by colouring the text blue and red respectively.

Measure	k_{min}	k_{max}	k_{diff}	R_{sig}	N_{sig}
Correlation coefficient	102	144	42	21	9
Coherence	NaN	NaN	NaN	0	0
Correntropy coefficient	102	157	55	9	5
Coh-entropy coefficient	NaN	NaN	NaN	0	0
Wave-entropy	NaN	NaN	NaN	0	0
Partial coherence	NaN	NaN	NaN	0	0
Event synchronisation	NaN	NaN	NaN	0	0
Mean phase coherence (Hilbert)	97	165	68	61	42
Mean phase coherence (wavelet)	NaN	NaN	NaN	0	0
Mean phase coherence (event)	NaN	NaN	NaN	0	0
Phase coherence value unwrapped	NaN	NaN	NaN	0	0
Phase coherence value wrapped	137	137	0		1
Conditional probability based phase synchrony	NaN	NaN	NaN	0	0
Mutual information (histograms)	NaN	NaN	NaN	0	0
Mutual information (adaptive histograms)	NaN	NaN	NaN	0	0
Mutual information (kernels)	111	145	34	26	9
Maximum likelihood mutual information	NaN	NaN	NaN	0	0
Nearest-neighbour mutual information	NaN	NaN	NaN	0	0
Mutual information (time-frequency plane)	NaN	NaN	NaN	0	0
Kullback Leibler divergence (histogram)	NaN	NaN	NaN	0	0
Rényi Divergence	NaN	NaN	NaN	0	0
Jensen-Shannon divergence	NaN	NaN	NaN	0	0
Jensen-Rényi divergence	NaN	NaN	NaN	0	0
Nonlinear Interdependence (H^k)	93	120	27	18	5
Nonlinear Interdependence (S^k)	93	118	25	8	2
Nonlinear Interdependence (N^k)	93	118	25	8	2
Omega Complexity	100	149	49	30	15
S-estimator	100	149	49	32	16

Correlation coefficient and related measures
Phase synchrony
Information-theoretic measures
Synchronisation based on state space

Unsatisfactory ———
Robust ———

Figure 3-29 shows the results of synchrony measures applied to NS2 with nonstationary coupling for three SNRs. Again, we seek low noise estimates that give early and continued detection of synchrony, and so use the same indicators of performance use previously, here detailed in Table 3-21.

Here, no measure can satisfactorily detect synchrony at 1 dB, though 8 measures can inconsistently detect it. Correntropy coefficient, mean phase coherence (Hilbert) and nonlinear interdependence (S) detect synchrony sooner and longer at the higher SNRs, with nonlinear interdependence (N) and S-estimator also doing well. Correlation, mutual information (kernel) and nonlinear interdependence (H) also detected synchrony at 1 dB, but were not outstanding at higher SNRs.
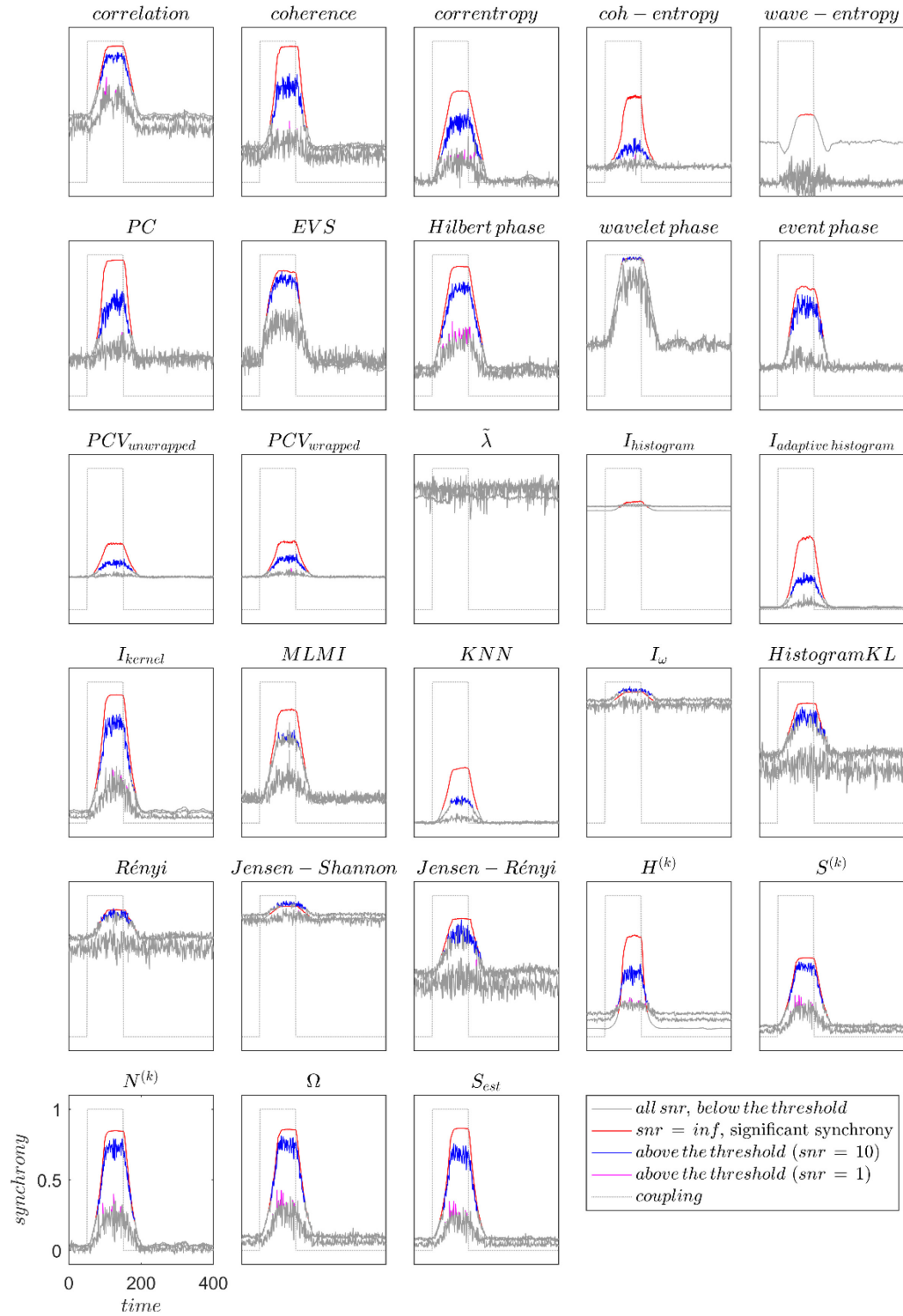
Figure 3-29: Synchrony measures against time for nonstationary NS2. Non-significant results are shown in grey for all SNRs, significant results for SNR = ∞ dB are in red, for SNR = 10 dB are in blue, and for SNR = 1 dB are in magenta.

Table 3-21: List the connectivity measures that perform satisfactorily for NS2 data. On NS2 data, we list the connectivity measures that perform satisfactorily, the length of time that synchrony is detected for no noise, 10 dB SNR, and 1 dB SNR, plus a qualitative assessment of the amount of noise on the estimates, and whether a measure consistently detects synchrony during the high-connectivity period. Good performance outcomes are highlighted by colouring the text blue.

Measure	k_{diff}			Noise	Consistency
	∞	10	1		
Correlation coefficient	102	87	*42*	High	Poor
Correntropy coefficient	125	115	*55*	High	Poor
Mean phase coherence (Hilbert)	121	114	*68*	High	Poor
Mutual information (kernels)	112	99	*34*	High	Poor
Nonlinear Interdependence (H)	81	89	*27*	High	Poor
Nonlinear Interdependence (S)	114	107	*25*	High	Poor
Nonlinear Interdependence (N)	109	103	*25*	High	Poor
S-estimator	117	98	*49*	High	Poor

3.1.4 Simulated EEG

150 realisations of 2 channels of simulated EEG were generated, representing responses to repeated trials. Each trial ran from −1 s to +2 s, sampled at 1 kHz, with the simulated EEG being pink noise (ie its power spectrum is approximately proportional to $1/f$). An alpha burst (a Hamming windowed 10.7 Hz sinusoid with added pink noise at 0 dB) ran from 300 ms to 700 ms with random timing jitter spread uniformly from −5 ms to +5 ms. The data were analysed for alpha synchrony using a sliding window of 300 ms, after pre-processing with a bandpass filter with corner frequencies of 5 Hz and 15 Hz. One realisation of one channel of simulated EEG signal, alpha burst and their superposition is shown in Figure 3-30.
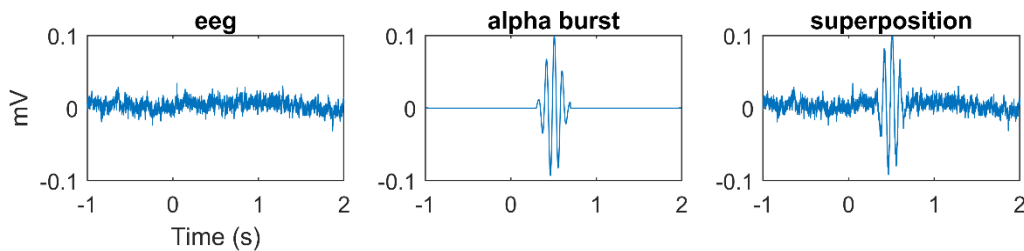
Figure 3-30: Simulated eeg (left), alpha burst (middle) and superposition (right).

3.1.4.1 Results

Figure 3.1.5-1 shows the results of applying the connectivity measures to the simulated EEG. The alpha burst envelope is shown in grey, the connectivity measure in blue, and the threshold from the surrogates in red. Ideally, ignoring the smearing effect of the pre-processing alpha filter, a measure could first detect the alpha burst at 300 ms, as the burst data first enters the sliding window, and last detect the burst at 1 s, as the last of the burst exits the sliding window. Nine measures showed good performance, with coherence, correntropy coefficient, mutual information (kernel), nearest-neighbour mutual information, nonlinear interdependence (S), nonlinear interdependence (N) and S-estimator slightly outperforming mutual information (histogram) and mutual information (adaptive histogram). Details of their performance are provided in Table 3.1.5-1. Two measures fail to detect synchrony: mean phase coherence (wavelet) and conditional probability based phase synchrony. Two other measures also produce very noisy estimates: wave-entropy and maximum likelihood mutual information.
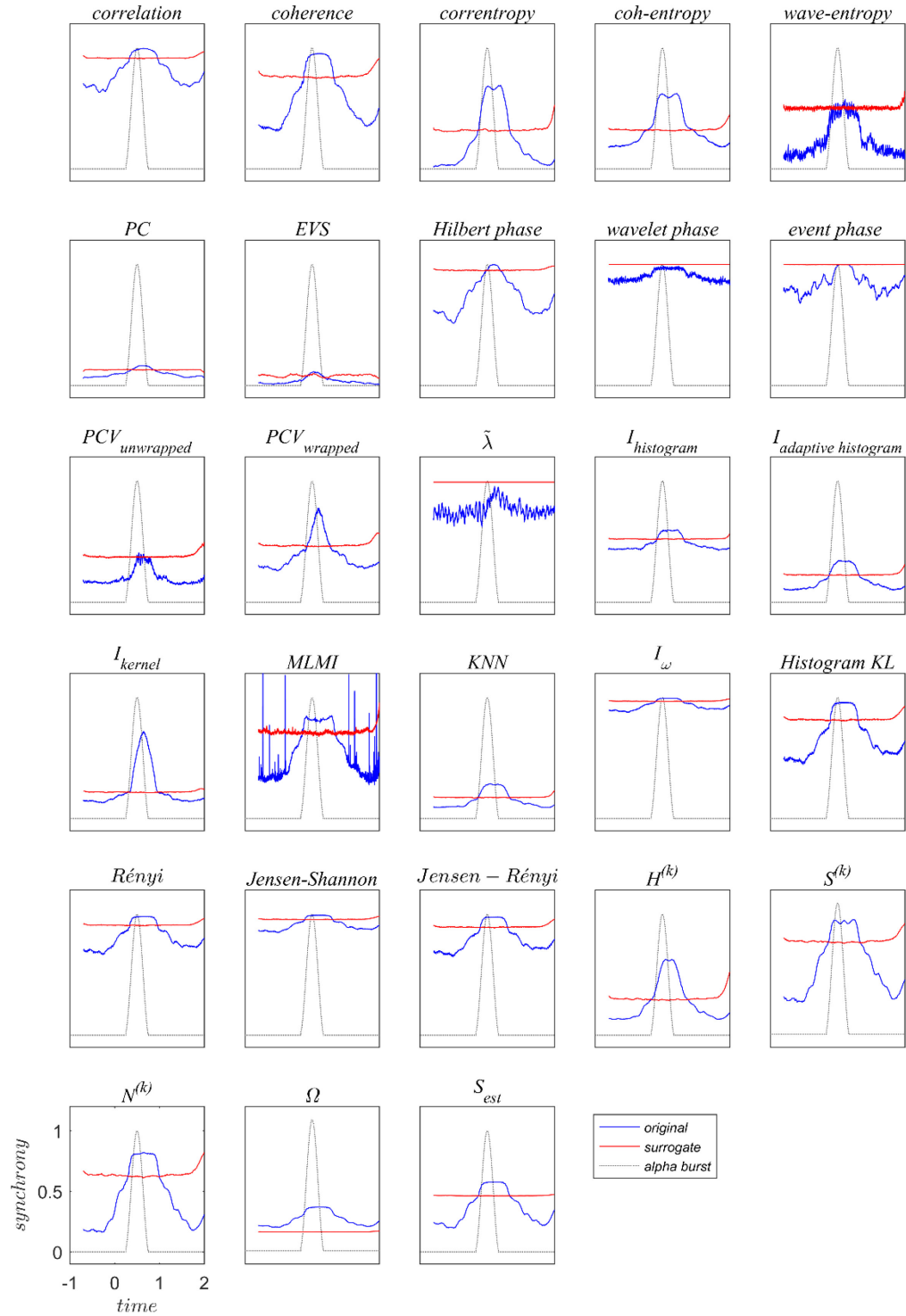
Figure 3-31: Connectivity measures against time for a simulated two-channel EEG. Connectivity measures (blue) and threshold for significance based on surrogates (red) against time for a simulated two-channel EEG system. The data contains an alpha burst who envelope is shown in grey. The connectivity measures use a 300 ms sliding window, with the result time-locked to the last sample used in the window.

Table 3-22: The values of t_{min}, t_{max} and t_{diff} for simulated EEG data. The time that synchrony is first detected (t_{min}), the time that it is last detected (t_{max}), and the period for which it is detected (t_{diff}) for simulated EEG data. Good performance outcomes are highlighted by colouring the text blue.

Measure	t_{min} (s)	t_{max} (s)	t_{diff} (s)
Correlation coefficient	0.331	0.959	0.628
Coherence	0.314	0.989	0.675
Correntropy coefficient	0.305	1.000	0.695
Coh-entropy coefficient	0.153	1.196	1.043
Wave-entropy	0.366	0.902	0.536
Partial coherence	0.385	0.888	0.503
Event synchronisation	0.409	0.792	0.383
Mean phase coherence (Hilbert)	0.478	0.793	0.315
Mean phase coherence (wavelet)	NaN	NaN	NaN
Mean phase coherence (event)	0.540	0.744	0.204
Phase coherence value unwrapped	0.493	0.658	0.165
Phase coherence value wrapped	0.387	0.904	0.517
Conditional probability based phase synchrony	NaN	NaN	NaN
Mutual information (histogram)	0.375	0.975	0.600
Mutual information (adaptive histogram)	0.313	0.980	0.667
Mutual information (kernels)	0.300	0.970	0.670
Maximum likelihood mutual information	-0.601	1.935	2.536
Nearest-neighbour mutual information	0.308	0.997	0.689
Mutual information (time-frequency plane)	0.349	0.939	0.590
Kullback Leibler divergence (histogram)	0.341	0.957	0.616
Rényi Divergence	0.342	0.956	0.614
Jensen-Shannon divergence	0.341	0.957	0.616
Jensen-Rényi divergence	0.344	0.953	0.609
Nonlinear Interdependence (H^k)	0.249	1.068	0.819
Nonlinear Interdependence (S^k)	0.300	1.002	0.702
Nonlinear Interdependence (N^k)	0.302	0.999	0.697
Omega Complexity	NaN	NaN	NaN
S-estimator	0.301	0.997	0.696

Correlation coefficient and related measures
Phase synchrony
Information-theoretic measures
Synchronisation based on state space

Unsatisfactory --------
Robust --------

Table 3-23: The time (seconds) required to estimate each measure for three sizes of data: few data ($N_{samples}$ = 30) and few channels ($N_{channels}$ = 2), many data ($N_{samples}$ = 9000) and few channels ($N_{channels}$ = 2), and few data ($N_{samples}$ = 30) and many channels ($N_{channels}$ = 128).

Measure	Time (s)		
	$N_{samples}$ = 30 $N_{channels}$ = 2	$N_{samples}$ = 9000 $N_{channels=}$ 2	$N_{samples}$ = 30 $N_{channels=}$ 128
Correlation coefficient	0.002	0.010	0.909
Coherence	0.020	0.035	66.424
Correntropy coefficient	0.003	0.327	24.626
Coh-entropy coefficient	0.008	0.015	1.665
Wave-entropy	0.011	0.856	7.666
Partial coherence	0.188	0.192	538.753
Event synchronisation	0.003	0.013	1.665
Mean phase coherence (Hilbert)	0.002	0.016	1.260
Mean phase coherence (wavelet)	0.002	0.009	1.453
Mean phase coherence (event)	0.002	0.005	0.508
Phase coherence value unwrapped	0.003	0.138	1.724
Phase coherence value wrapped	0.003	0.138	2.058
Conditional probability based phase synchrony	0.003	0.071	2.255
Mutual information (histogram)	0.007	0.381	80.770
Mutual information (adaptive histogram)	0.008	0.534	33.953
Mutual information (kernels)	0.010	5.255	2223.419
Maximum likelihood mutual information	0.307	38.203	15.786
Nearest-neighbour mutual information	0.011	194.222	12.678
Mutual information (time-frequency plane)	0.010	0.324	23.576
Kullback Leibler divergence (histogram)	0.012	0.099	11.646
Rényi Divergence	0.008	0.060	11.873
Jensen-Shannon divergence	0.008	0.059	12.512
Jensen-Rényi divergence	0.009	0.064	2.058
Nonlinear Interdependence (H)	0.005	173.386	17.276
Nonlinear Interdependence (S)	0.005	173.386	17.276
Nonlinear Interdependence (N)	0.005	173.386	17.276
Omega Complexity	0.008	0.073	1.200
S estimator	0.008	0.073	1.200

3.2 Discussion and conclusion

We compared 28 functional connectivity measures from five families using three different simulated data sets to identify suitable measures for detecting true connections between nonstationary, nonlinear and noisy signals similar to EEG. Our study differs from *prima facie* similar studies in one or more ways:

- Real (EEG) data does not have known connections, making comparisons between measures complex;

- Comparisons of only a few measures are of limited value;

- Comparisons of non-directional and directional measures have conceptual difficulties ;

- Without a statistical basis, direct comparison of measures is inappropriate;

- Use of measures as features into classifiers does not require hard decisions.

With these differences noted, we compare our conclusions with published papers that admit useful comparison.

Xu et al. [135] takes a simplistic view that linear measures, e.g. cross correlation and coherence, can only detect linear relationships between time series. They concluded that correntropy coefficient performed better than cross correlation on two unidirectionally coupled Hénon maps, but only provided results for correntropy coefficient to support their claim. A more recent study [7] compared seven connectivity measures, including cross correlation and nonlinear measures, using simulated EEG signals and found that cross correlation is one of the most reliable measures for detecting direct links between signals. Ansari-Asl et al. [136] compared eleven functional connectivity measures including linear and nonlinear measures, and also found that cross correlation performs well in all situations. They concluded that it is reasonable to apply cross correlation as "a first attempt to characterize the functional coupling in studied systems in absence of *a priori* information about its nature". The results in this thesis support the view that cross correlation is a reliable estimator of nonlinear connectivity.

Lachaux et al. [137] asserts that phase synchronization should be preferred to coherence on theoretical grounds, namely the lack of a stationarity assumption and the relative importance of phase over amplitude in identifying synchrony. In contrast, [59] found that phase synchronization was not superior to coherence in human sleep EEG. Sakkalis et al. [138] assessed two linear and three nonlinear synchronisation measures in inter-ictal EEG in humans

with epilepsy, concluding both linear and nonlinear measures were effective. In particular, coherence was best at identifying synchronisation at low frequencies, and nonlinear measures were better at higher frequencies. The review in [139] similarly concludes that both linear and nonlinear measures are valuable. Hence we have chosen to test all measures on all datasets and let the results speak. We found for the tests with stationary and nonlinear data, where data are plenty, coherence and correlation performed the best, and that these measures also generally perform well on non-stationary data. These results are consistent with the findings in [7, 136]. Dauwels et al. [6] is an important paper that applies many functional and effective connectivity measures to the EEG of patients with mild cognitive impairment (MCI) that later developed into Alzheimer's disease. However there are several difficulties with comparing our results to this paper. In the Introduction, we argued that it was not appropriate to compare directed and nondirected measures. More importantly, the main purpose in [6] is to classify MCI (against controls), with a secondary aim of comparing measures. Finally, when using real EEG there is a presumption that the changes in functional connectivity are known. With MCI and Alzheimer's disease, [6, 140] claim known reductions in connectivity, but [10] suggests some increases are also present. Given these caveats, we note that [6] states that using multiple measures drawn from a variety of families is advised, consistent with our findings. They also found several measures yielded significant results: cross correlation, coherence, correntropy coefficient, wave-entropy, nonlinear interdependence (N^k), nonlinear interdependence (H^k), nonlinear interdependence (S^k), S-estimator and mean phase coherence. Our results also suggest that all these measures, except wave entropy, performed well in most situations.

Kreuz et al. [140] compared two methods for calculating phase synchronisation, based on the Hilbert or wavelet transforms. Their results show that for broad-band systems like the Hénon

system, Hilbert phase based synchronization measure is superior. In this thesis, we also found that mean phase coherence (Hilbert) is the best among all phase synchronisation measures.

Quiroga et al. [10] applied nonlinear interdependence (H^k) and (S^k) to both identical and non-identical Hénon map systems to learn driver-response relationships from synchronisation patterns. They found that nonlinear interdependence (H^k) is more robust than nonlinear interdependence (S^k), consistent with our findings.

In summary, it is not always straightforward to compare the results in this thesis with previous studies due to significant differences in methodology. However, the conclusions as to which measures are better than others are broadly in agreement with our conclusions. Additionally, our results do provide a much more comprehensive comparison of many measures.

No measure consistently performs better than other measures. For the tests with stationary data, where data are plenty, coherence and correlation perform the best. Six measures consistently performed well on non-stationary and noisy datasets: correntropy coefficient, mean-phase coherence (Hilbert), mutual information (kernel), nonlinear interdependence (S^k), nonlinear interdependence (N^k) and S-estimator.

The choice of measure clearly depends on several factors: noise level, stationarity of data, number of channels, number of samples and available time. Figure 3-32 shows a flow chart, synthesizing all results and conclusions in this paper, to assist in the choice of which measures are best in any particular situation, with examples of possible application areas. If these factors are not known or poorly known, selecting on the basis of "worst case" would be recommended. This thesis has not considered the significant issue of incorrectly detecting synchrony that is not truly present, and hence the results are most applicable to situations where few EEG channels have been recorded.

For situations such as using EEG in a brain-computer interface, where it is not possible to repeat measurements to reduce noise and decisions must be made in real-time, measures that are effective in high noise and fast to calculate are required. Our results would recommend correlation coefficient and S-estimator, preferring correlation coefficient if weak coupling is expected, and preferring S-estimator if the noise is particularly strong. If we are calculating event-related activity, then it is likely we will have many repetitions reducing the noise. If there is no particular limit on calculation time and we are interested in estimating the strength of synchrony accurately, then mutual information (kernel) would be a good choice.
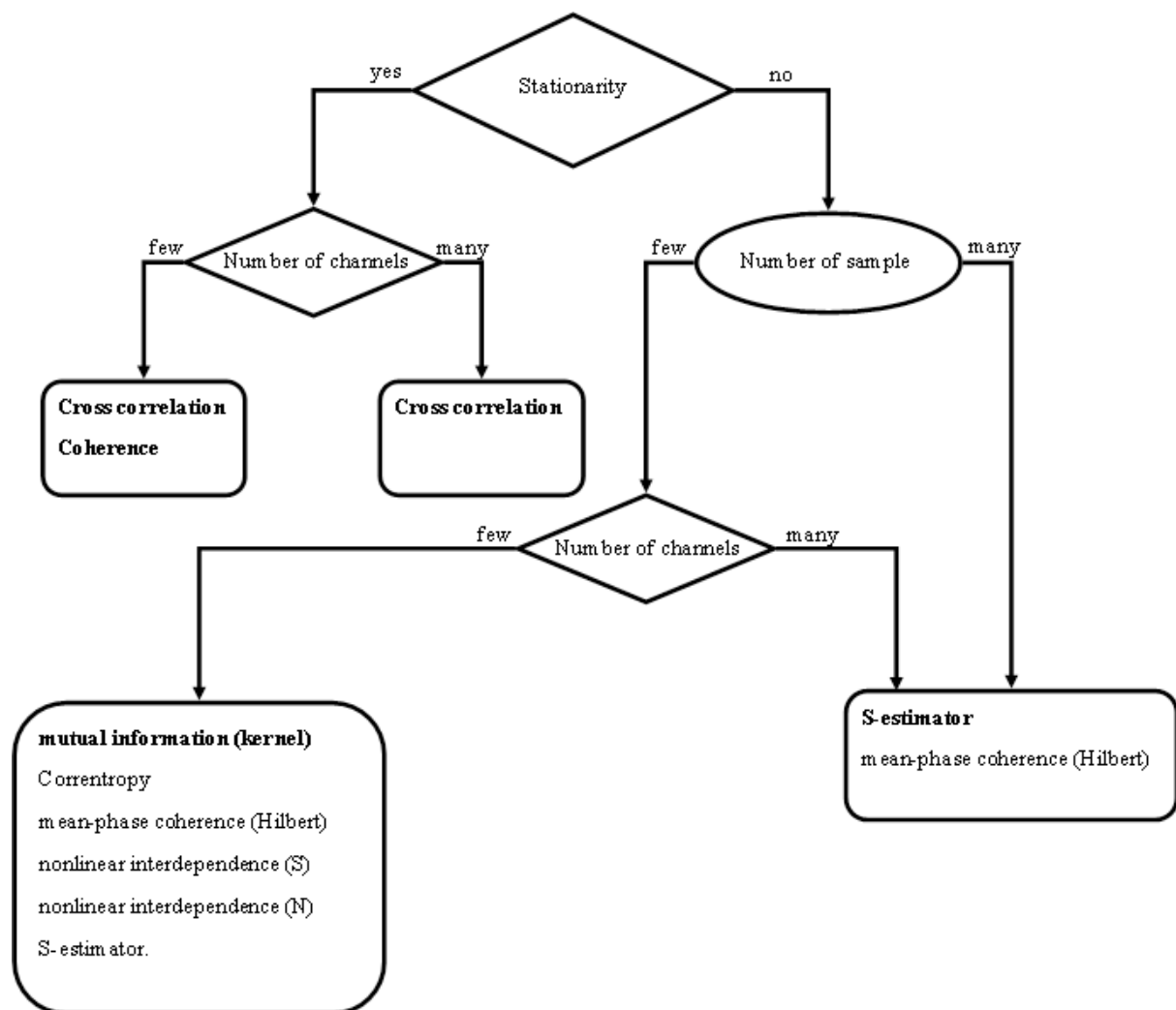
Figure 3-32: *Flow chart to assist in choosing an appropriate measure for functional connectivity analysis.*

CHAPTER 4   EFFECTIVE CONNECTIVITY MEASURES

This chapter is based on the published conference paper *(2014 IEEE EMBS Conference on Biomedical Engineering and Sciences, © 2014 IEEE. In reference to IEEE copyrighted material which is used with permission in this thesis, the IEEE does not endorse any of Flinders University's products or services. Internal or personal use of this material is permitted. If interested in reprinting/republishing IEEE copyrighted material for advertising or promotional purposes or for creating new collective works for resale or redistribution, please go to http://www.ieee.org/publications_standards/publications/rights/rights_link.html to learn how to obtain a License from RightsLink),* and paper published in the journal Computers in Biology and Medicine (https://doi.org/10.1016/j.compbiomed.2019.103329)   Details can be seen in Appendix A-2

In this section we applied all effective connectivity measures defined in section 2.2.2 to linear and nonlinear synthetic data sets where we know the true relationship between the signals. First we used a well-understood nonlinear system (three coupled Hénon maps), then a seventh-order MVAR model with and without exogenous inputs, and finally we applied all measures to simulated EEG.

The ability of measures to identify a direct causal connection was evaluated. Simulations were repeated 100 times with different random initial conditions and for each simulation 100 surrogate data were generated using the surrogate method described in section 2.3. We estimate the causality measure from the original time series and for each surrogate time series.   A direct causal connection was identified if the mean of connectivity values from the original data is greater than the mean of the surrogates using a two-sample t-test at the 0.05 significance level. Results were evaluated by measuring the percentage of directed causal connections that were correctly identified (true positive rate) and the percentage of directed pairs that do not have a direct causal link that are identified incorrectly as a causal link (false positive rate). The false

positive rate includes indirect causal connections, such as when one signal influences another only indirectly through a third signal.

4.1 System 1 (three coupled Hénon maps)

The first simulation generated data from the system consists of three coupled Hénon maps with nonlinear couplings, $X_1 \rightarrow X_2 \rightarrow X_3$, defined by the following equations:

$$
\begin{aligned}
x_1(k+1) &= 1.4 + 0.3\,x_1(k-1) - x_1^2(k) \\
x_2(k+1) &= 1.4 + 0.3x_2(k-1) - [\mu\,x_1(k) + (1-\mu)x_2(k)]x_2(k) \\
x_3(k+1) &= 1.4 + 0.3x_3(k-1) - [\mu x_2(k) + (1-\mu)x_3(k)]x_3(k)
\end{aligned}
\qquad 4\text{-}1
$$

Simulations used 2048 data points with fixed coupling strength μ, with the coupling strength varying across simulations from $\mu = 0$ (no coupling) to $\mu = 0.5$ (strong coupling). Most measures have parameters that need to be selected, and that this can have a significant influence on their performance. Hence to optimise performance on system 1 and following the literature [141], we set parameters as follows:

- For model-based measures, we set the model order P = 2.

- For frequency measures, we used the normalised range [0.4, 0.5] where the spectra of the signals show peaks.

- For measures that require a range of lags, e.g. PTE, we used the range 1 to 5 and the maximum value of the measure among the results was selected.

4.2 Results for system 1

Results for system 1 for connectivity measures versus coupling strength μ are shown in Figure 4.1.2-1, where the blue line shows the estimated connectivity strength and the red line shows the threshold for significance. When significance is achieved, the area between the two lines is filled in blue. The best result would show connectivity (filled blue area) only in the top central and central right squares. As can be seen from this figure, seven measures perform well in that

the separation between the measure and its threshold increases with coupling strength: transfer entropy, partial Granger causality, conditional Granger causality, Copula-Granger causality, multivariate Granger causality, spectral multivariate Granger causality and partial transfer entropy. These measures are able to detect all casual connections (true positives) but they also detect some connections that do not exist (false positives). Therefore we calculated the false positive rates (FPR), true positive rates (TPR), false negative rate (FNR) and true negative rate (TNR) for a deeper understanding, and the results are shown in Figure 4.1.2-2. The measures in Figure 4.1.2-2 have been sorted by informedness. Informedness or bookmaker informedness (BM) is equal to the true positive rate minus the false positive rate. Its value ranges from -1 to 1, where a value of 1 indicates that there we have 100% true positive rate and 0% false positive rate, i.e. the measure is perfect. The partial transfer entropy and transfer entropy outperform other measures, achieving 100% and 80% detection of causal connections respectively, and 0% incorrect detection of an absence of a causal connection. Both measures obtain large positive values only for the two correct direct causal links, and this holds even for few data points and low coupling strengths μ. Extended Granger causality, Copula-based Granger causality, multivariate Granger causality in time and frequency domain, conditional Granger causality and partial Granger causality were able to detect all of the causal connections, but also incorrectly identified some absences of connections as connections. Extended directed coherence extended partial directed coherence and directed phase looking value performed little better than chance. Frequency domain conditional Granger causality, generalised partial directed coherence, partial directed coherence, directed transfer function, partial mutual information, generalised partial directed coherence and directed coherence displayed poor

performance, incorrectly identifying more than 50% of the absences of connections as causal connections.
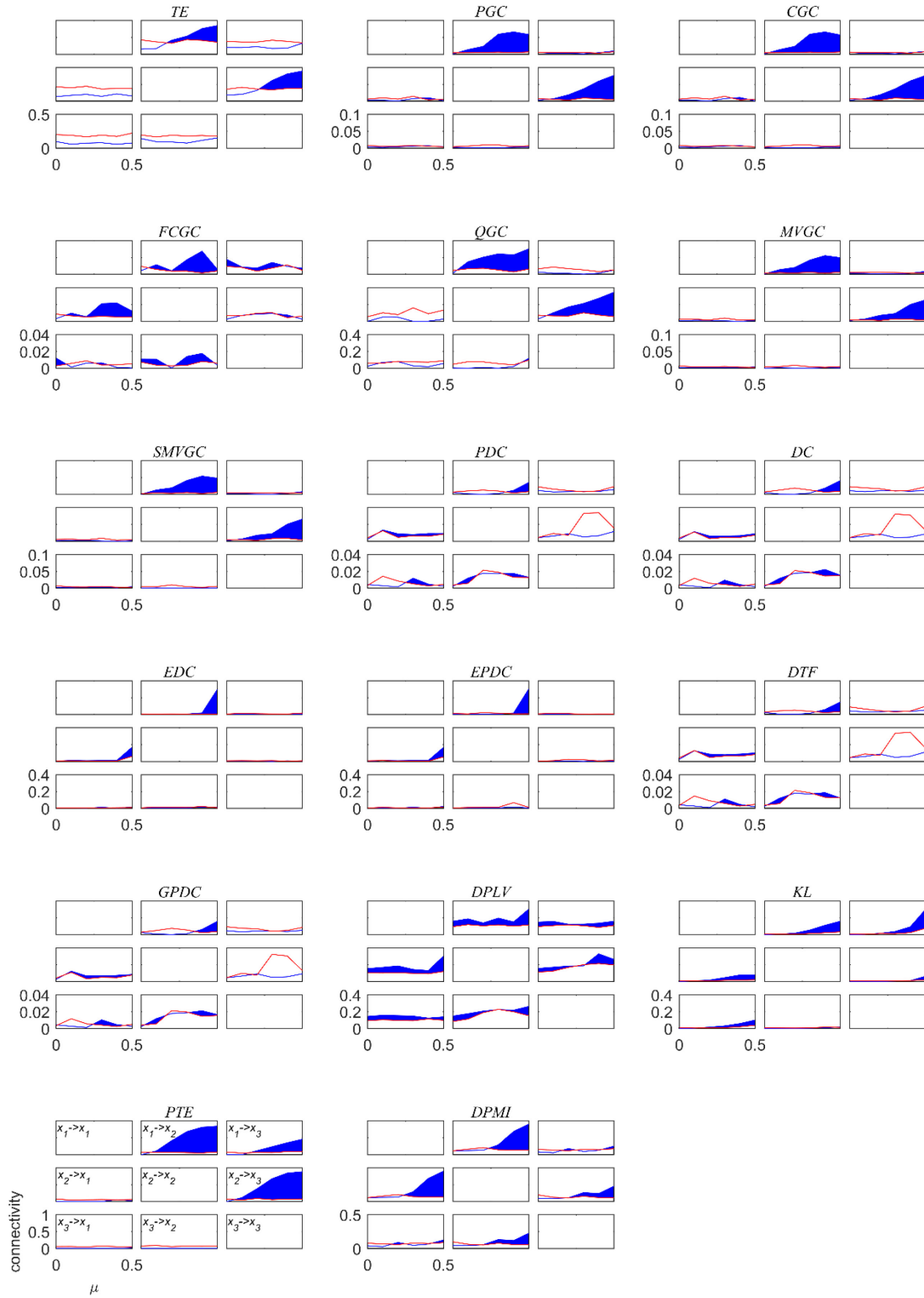
Figure 4-1: Estimated connectivity measures versus coupling strength. Estimated connectivity strength (blue line) and threshold for significance (red line) for 18 connectivity measures versus coupling strength μ. When significance is achieved, the area between the two lines is filled in blue. The best result would show connectivity (filled blue area) only in the top central and central right squares.
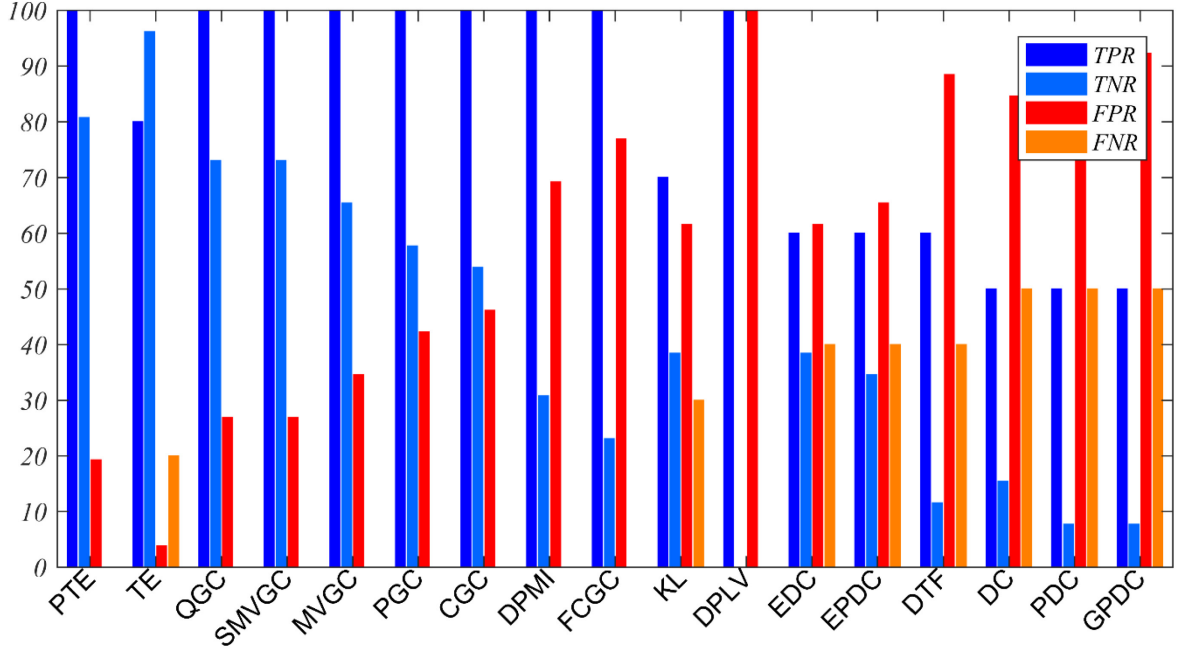
Figure 4-2: TPR, TNR, FPR and FNR for system 1. The percentage of directed causal connections that were correctly identified (true positive rate, dark blue bars), the percentage of directed pairs that do not have a causal link that were correctly identified (true negative rate, light blue bars), the percentage of directed pairs that do not have a causal link that are identified incorrectly as a causal link (false positive rate, red bars), and the percentage of directed causal connections that are identified incorrectly as directed pairs that do not have a causal link (false negative rate, orange bars) for each effective connectivity measure analysing data from system 1. ©2014 IEEE

4.3 System 2 (MVAR model)

The second simulation is an MVAR model, inspired by the model used in [142], represented by the following set of linear difference equations with 7 nodes and exogenous sources S_1 and S_2.

$$
\begin{aligned}
x_1(k) &= 0.95\sqrt{2}\,x_1(k-1) - 0.9025\,x_1(k-2) + e_1(k) + S_1(k) \\
x_2(k) &= 0.5x_1(k-1) + e_2(k) \\
x_3(k) &= -0.4x_1(k-3) + e_3(k) \\
x_4(k) &= -0.5x_1(k-1) + 0.25\sqrt{2}\,x_4(k-1) + 0.25\sqrt{2}\,x_5(k-1) + e_4(k) \qquad \textit{4-2} \\
x_5(k) &= -0.25\sqrt{2}\,x_4(k-1) + 0.25\sqrt{2}\,x_5(k-1) + e_5(k) \\
x_6(k) &= 0.95\sqrt{2}\,x_6(k-1) - 0.9025\,x_6(k-2) + e_6(k) + S_2(k) \\
x_7(k) &= -0.1x_6(k-2) + e_7(k)
\end{aligned}
$$
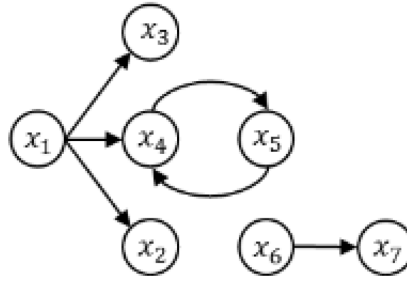
Figure 4-3:   The unweighted directed graph summarising the connections between signals in the MVAR model defined in equation(s) 4.2. $x_1 - x_7$ denote the output signals of the model, and S1 and S2 denote the exogenous inputs (EEG signals). ©2014 IEEE

System 2A sets the exogenous inputs S_1 and S_2 to zero, whereas system 2B uses pre-processed EEG as the inputs. The EEG applied in the simulation was recorded at four locations (CP1, CP2, FC1, FC2) from a separate study during an eyes-closed resting or baseline task. The scalp recordings were pre-processed by filtering in the gamma frequency band (bandpass filter, 35 to 100 Hz), and 50001 data points (25 seconds sampled at 2 kHz) were used. All 12 different combinations of selecting S_1 and S_2 from these four channels were used in simulations. The averaged measure over the 12 realisations of different EEG pairs was used for analysis.

For model-based measures, the model order was optimised with multichannel Akaike information criterion (AIC) and set to $p = 3$ for the system 2A and set to $p = 5$ for the system 2B. For measures that optimise over a range of lags, the maximum lag was set by analogy to the optimised model order p. Frequency-based connectivity measures were calculated over the range of normalised frequencies [0, 0.4], consistent with other publications and also where the spectra of the signals are high.

4.4   Results for system 2

For systems 2A and 2B, connectivity matrices are shown in Figures 4.1.4-1 (a) and (b) respectively. The true/false positive/negative rates (expressed as percentages) for systems 2A and 2B are displayed in Figure 4.1.6-2 (a) and (b) respectively. For both systems 2A and 2B, partial Granger causality, conditional Granger causality, and generalised partial coherence

obtained the best results of all measures, with an 100% true positive rate and less than 8% false positive rate. Multivariate Granger causality, Copula-based Granger causality, partial directed coherence and directed coherence detected all causal connections correctly, but with larger false positive rates. The performance of directed transfer function has improved from its system 1 performance; however transfer entropy and partial transfer entropy showed worse performance. Unsatisfactory results were obtained in both system 2A and 2B for extended directed coherence, conditional frequency domain Granger causality, extended partial directed coherence, Kullback-Leibler divergence, and for multivariate frequency domain Granger causality in system 2A. Kullback-Leibler divergence and multivariate frequency domain Granger causality could not identify any of the six direct causal effects for system 2A.

(a)
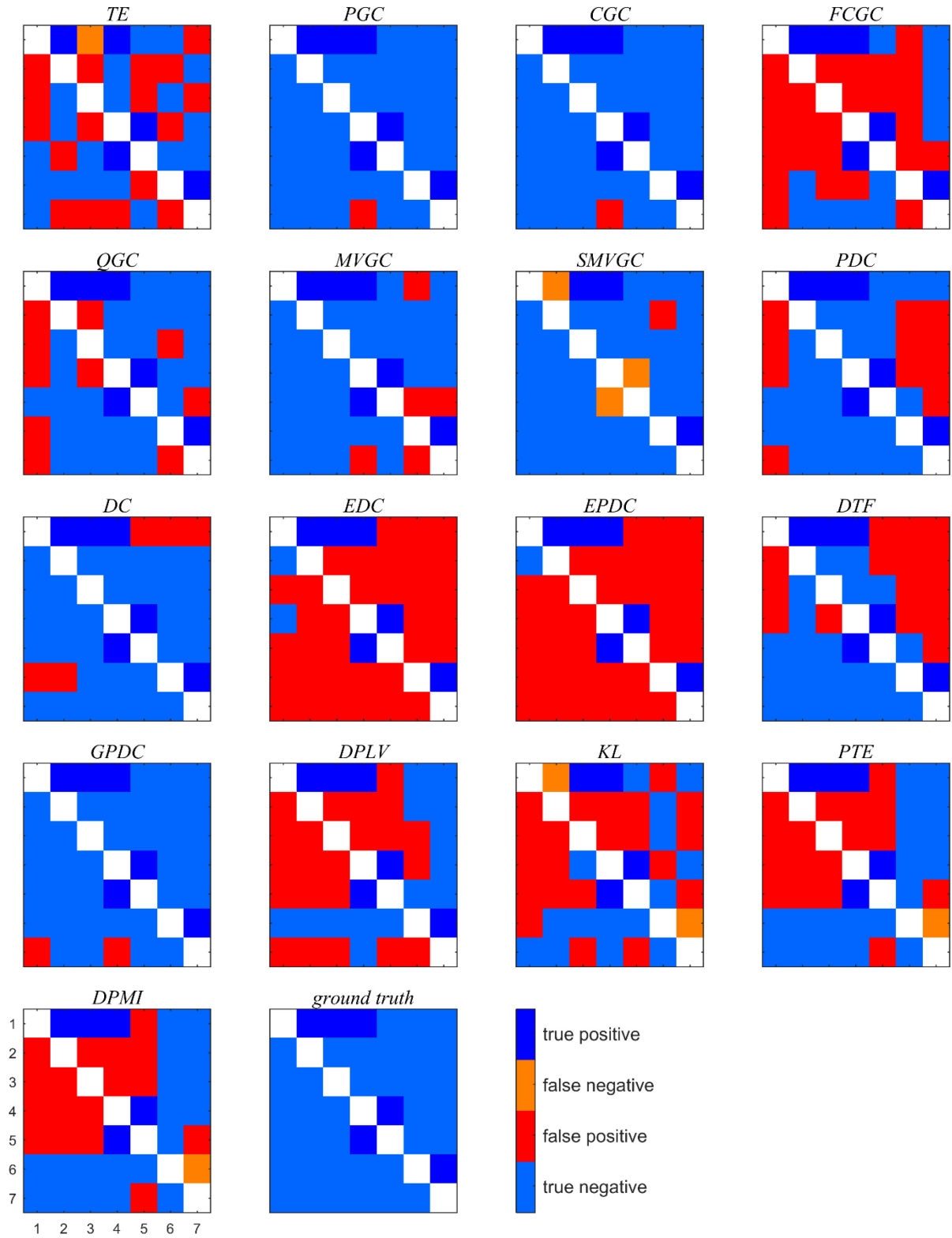
Figure 4-4: Connection matrices for system 2A in (a) and for system 2B in (b). Ground truth shows the true connectivity structure in the systems. Numbers on the *x* and *y* axes of the lower left connection matrix denote channel numbers, e.g. the cell at the first row and second column of each matrix indicates the connectivity result from channel one to channel two.
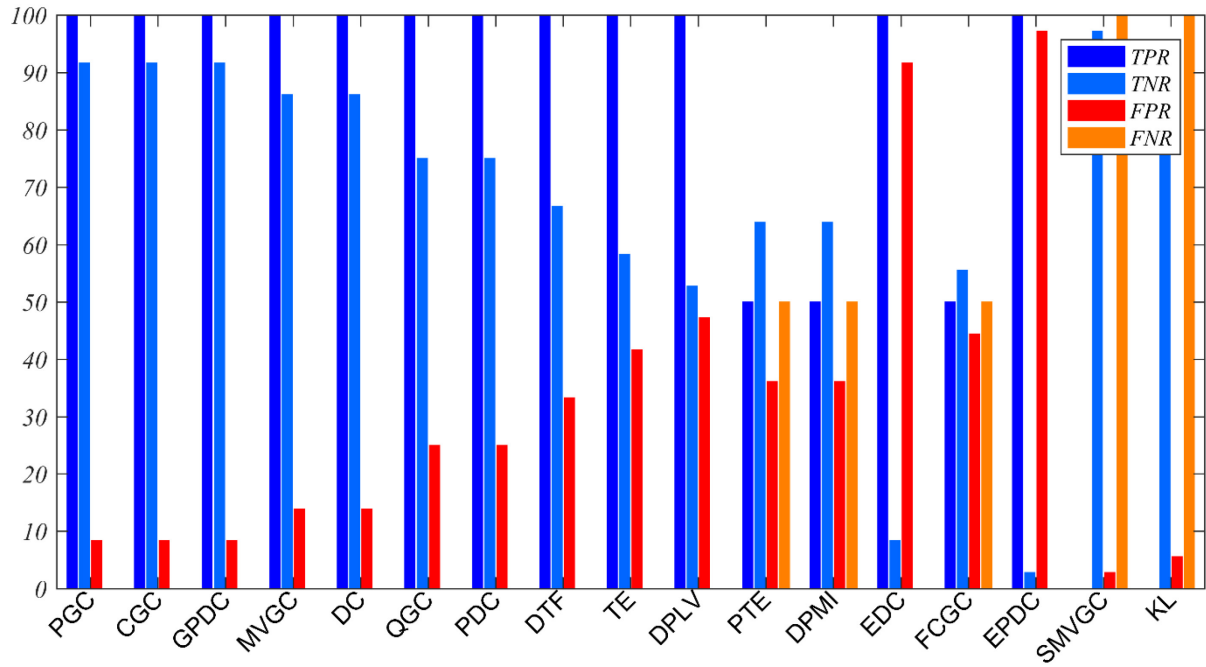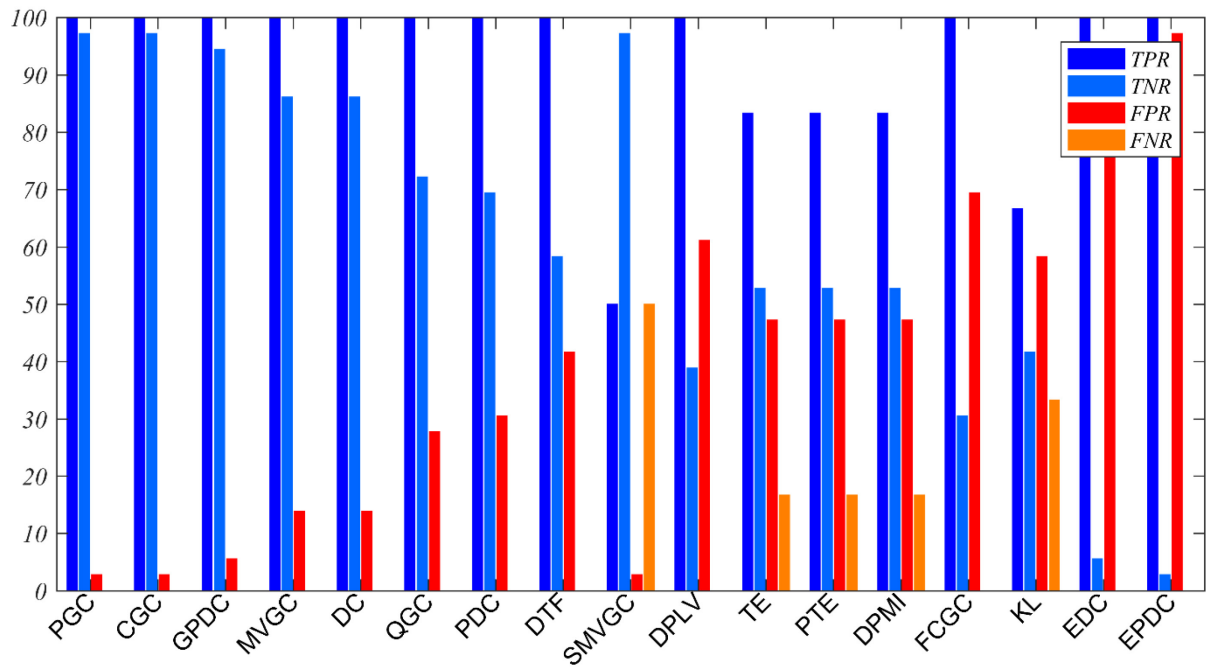
Figure 4-5: TPR, TNR, FPR and FNR for system 2A and system 2B. The percentage of directed causal connections that were correctly identified (true positive rate, dark blue bars), the percentage of directed pairs that do not have a causal link that were correctly identified (true negative rate, light blue bars), the percentage of directed pairs that do not have a causal link that are identified incorrectly as a causal link (false positive rate, red bars), and the percentage of directed causal connections that are identified incorrectly as directed pairs that do not have a causal link (false negative rate, orange bars) for each effective connectivity measure analysing data from system 2A in (a) and for system 2B in (b). Measures are sorted by informedness. ©2014 IEEE

4.5   System 3

3 channels of simulated EEG were generated, representing responses to repeated trials. Each trial ran from −0.5 s to +1.0 s, and contained a noisy alpha burst with added pink noise at 0 dB. The alpha burst (a Hamming windowed 10 Hz sinusoid) ran from 300 ms to 700 ms with random timing jitter spread uniformly from −5 ms to +5 ms and an additional fixed delay of 20 ms in second channel and 40 ms in the third channel. The amplitudes of second and third channels were set to 0.5 and 0.2 times the amplitude of the first channel respectively. The three simulated EEG signals from one trial are shown in Figure 4-6.
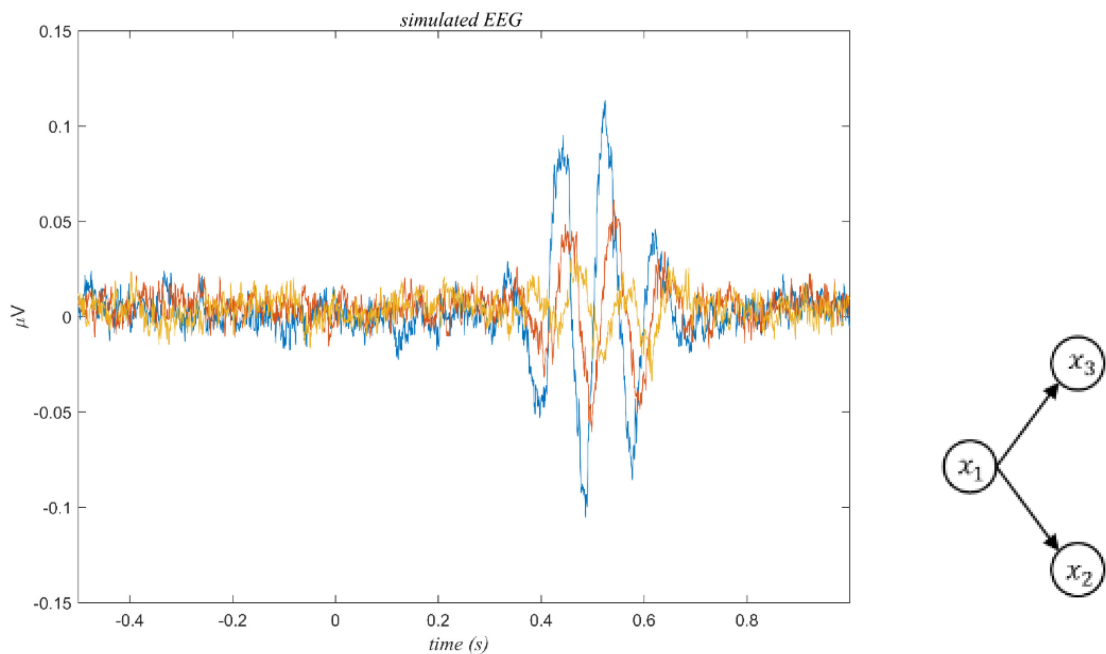
Figure 4-6:   Three channels of simulated EEG and the unweighted directed graph(left). (a) 3 channels of simulated EEG from one trial. The unweighted directed graph of the directional connectivity structure for system 3, $x_1 - x_3$ denote the output signals of the model(right). ©2014 IEEE

The data of system 3 were analysed for alpha connectivity using a sliding window of width 300 ms, sliding 50 ms between analyses. Frequency-based connectivity measures were estimated for the range of the alpha band (8 - 13 Hz). We averaged the measures over windows containing the alpha bursts (from 300 to 740 ms) where we expect measures to detect the direct causal

connections $x_1 \rightarrow x_2$ and $x_1 \rightarrow x_3$. We also analysed the system over the time frame [0, 300ms] where there is no causal connection between any pair of signals.

4.6 Results for system 3

The results from system 3 for both time ranges are displayed in Figure 4.1.6-1 and Figure 4.1.6-2. Many measures correctly detect no connections for the time range from 0 to 300 ms as expected, namely transfer entropy, partial Granger causality, conditional Granger causality, Copula-based Granger causality, multivariate Granger causality, multivariate frequency domain Granger causality, partial transfer entropy and partial mutual information. During the alpha burst, directed coherence and directed transfer function correctly found all connections and no others, Copula-based Granger causality and extended directed coherence correctly found all connections but incorrectly identified a third connection, and partial directed coherence and generalised partial directed coherence found one of the two connections correctly.

(a)

149

(b)
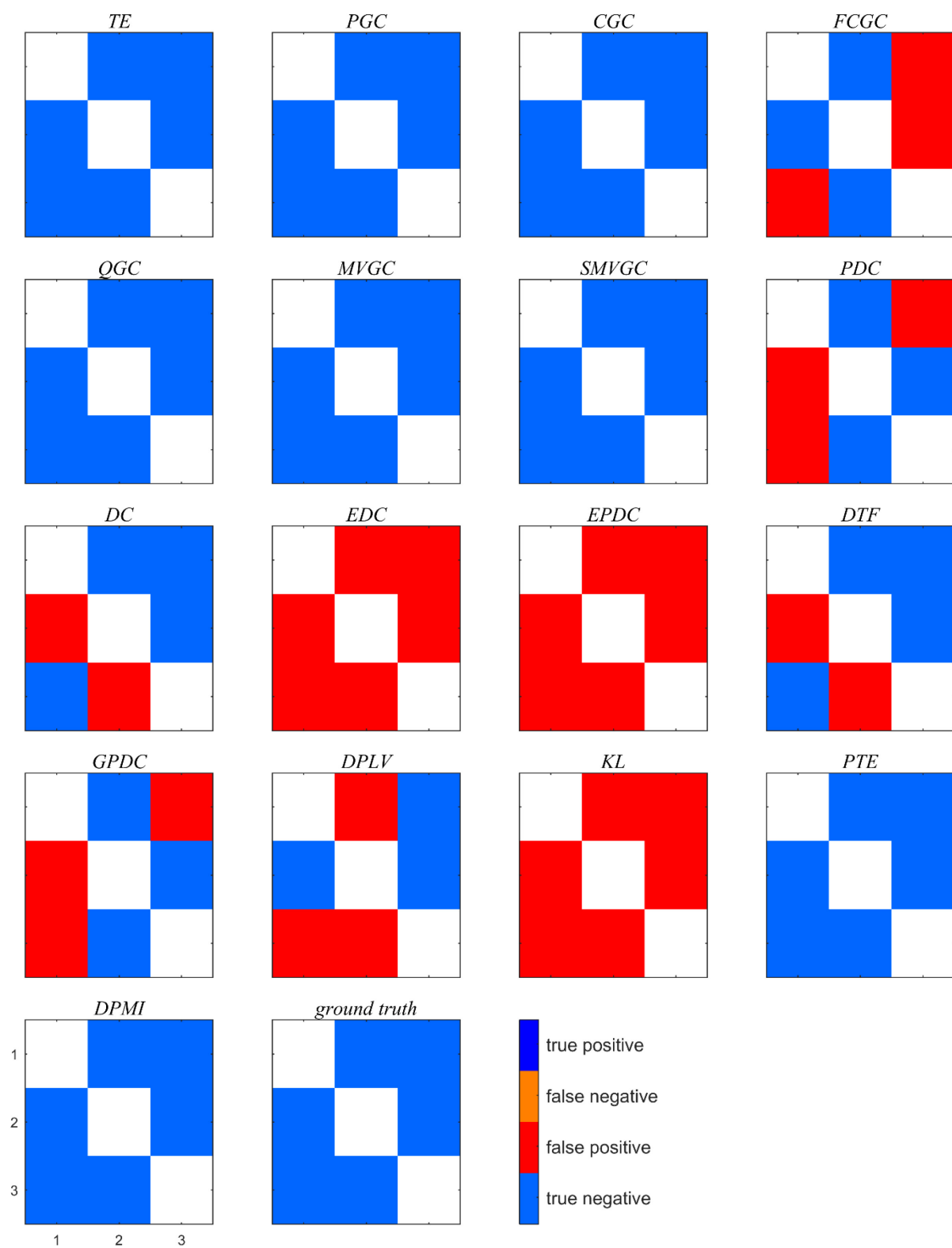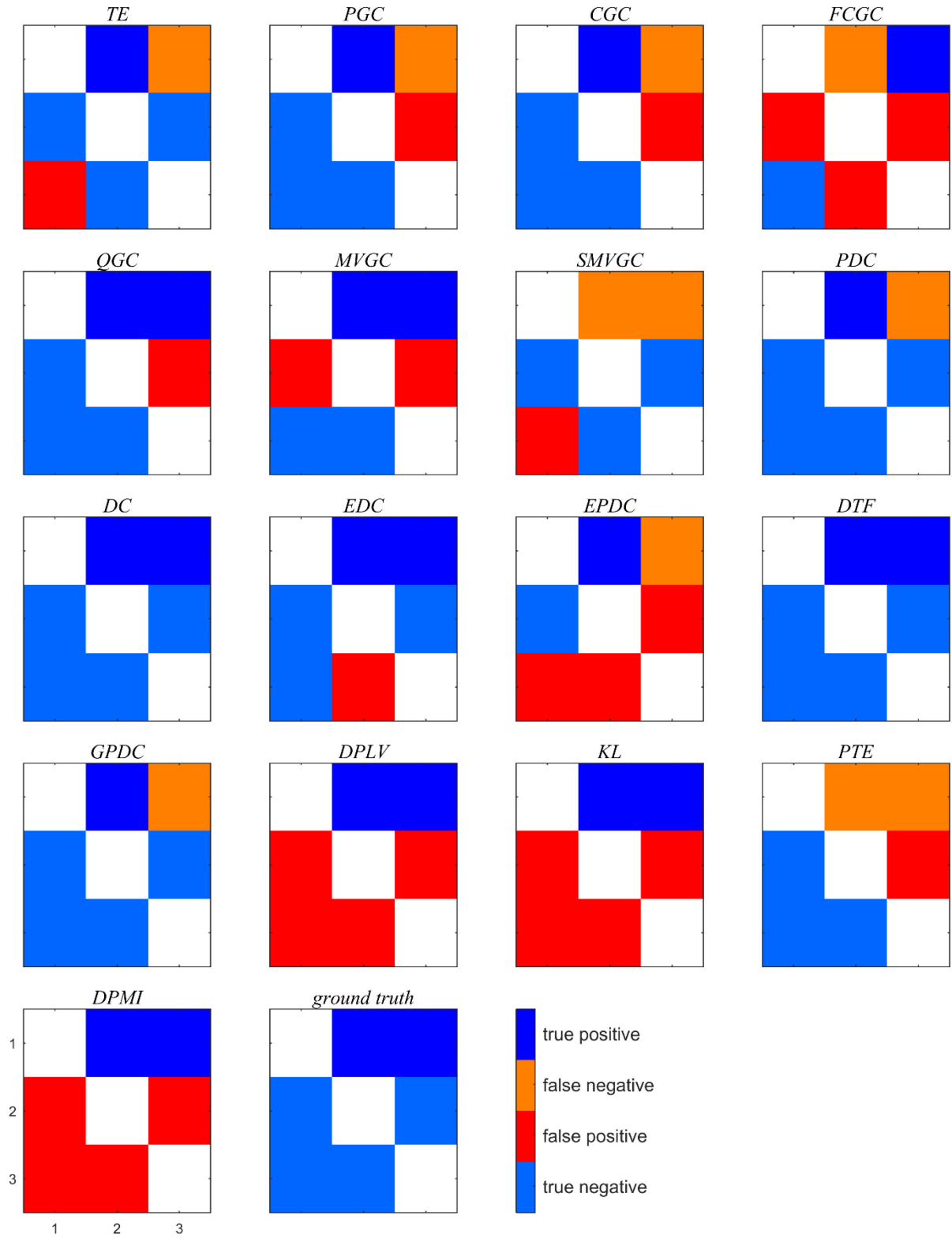
Figure 4-7: Connection matrices for system 3 over the time ranges (a) 0 to 300 ms, where no causal connections exist, and (b) 300 to 740 ms, where direct causal connections do exist. Ground truth shows the true connectivity structure in the systems. Numbers on the x and y axes of the lower left connection matrix denote channel numbers, e.g. the cell at the first row and second column of each matrix indicates the connectivity result from channel one to channel two.
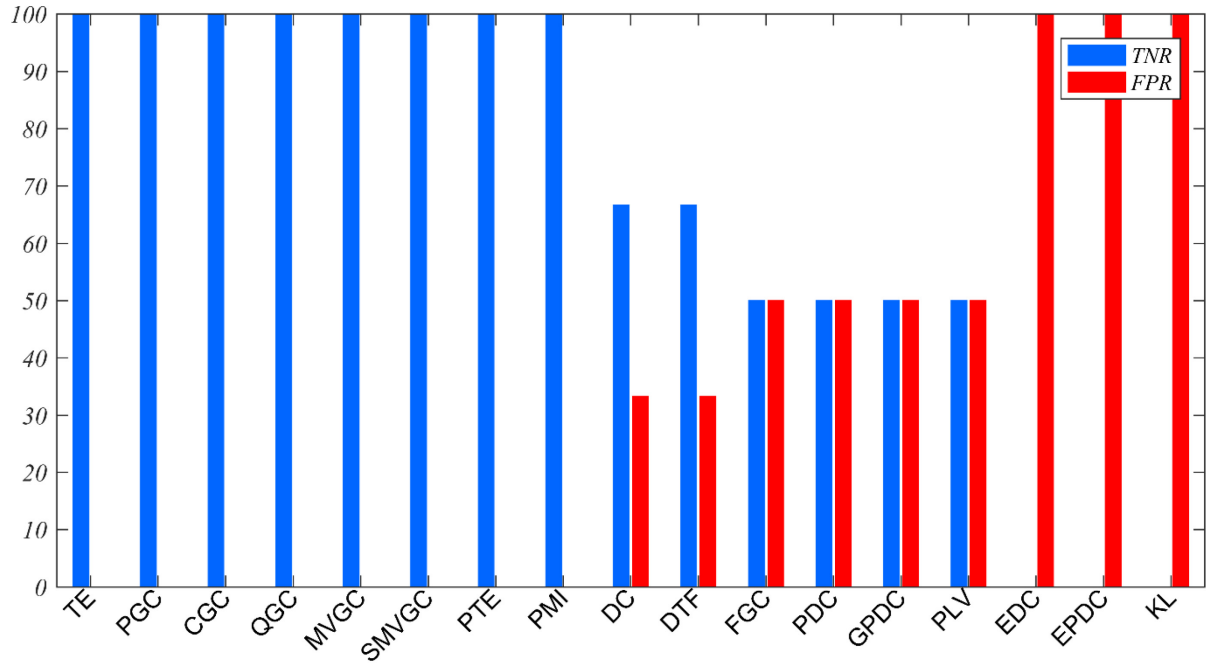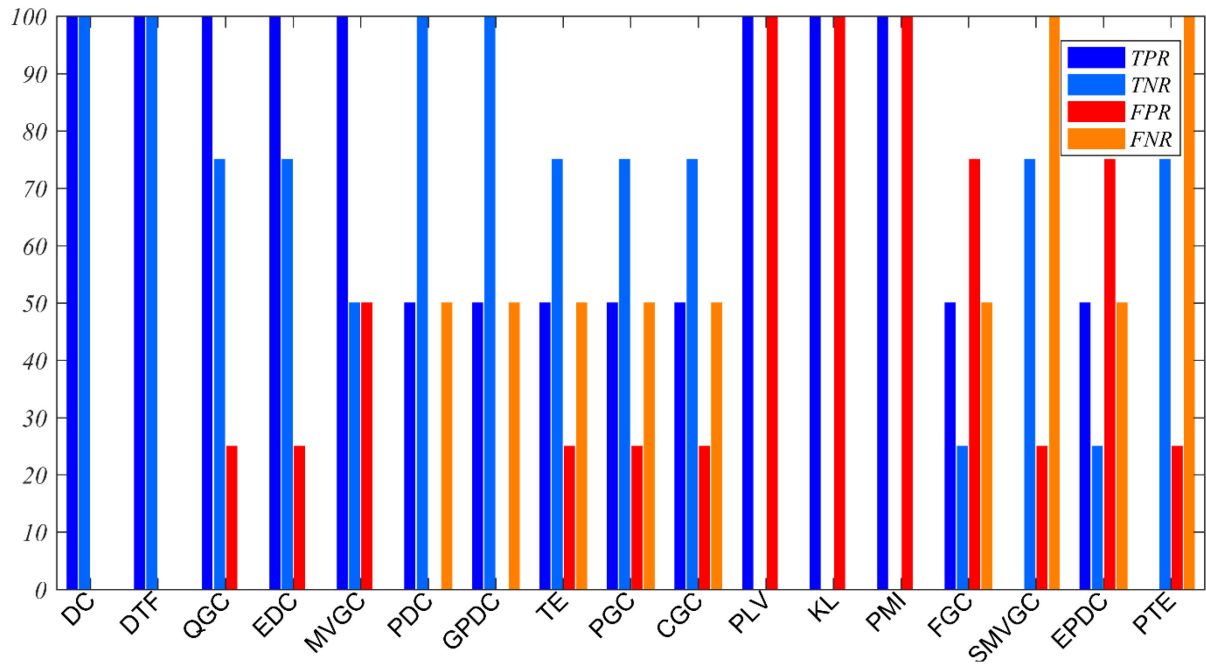
Figure 4-8: TPR, TNR, FPR and FNR for system 3. The percentage of directed causal connections that were correctly identified (true positive rate, dark blue bars), the percentage of directed pairs that do not have a causal link that were correctly identified (true negative rate, light blue bars), the percentage of directed pairs that do not have a causal link that are identified incorrectly as a causal link (false positive rate, red bars), and the percentage of directed causal connections that are identified incorrectly as directed pairs that do not have a causal link (false negative rate, orange bars) for each effective connectivity measure analysing data from system 3, calculated over the time ranges (a) 0 to 300ms, where no causal connections exist, and (b) 300 to 740 ms, where direct causal connections do exist. All measures are sorted by informedness. ©2014 IEEE

151

4.7 Execution time

It is important to note that different measures require different calculations that take different amounts of time. In particular, partial and conditional measures would reasonably be expected to require longer execution times. Table 4.1.7-1 lists the execution times for the 18 effective connectivity measures under three conditions: few data and few channels, many data and few channels, and many data and many channels. Computations for this table were performed in Matlab R2017b using 128 channels of real EEG on a Windows 10 PC with 16 GB of RAM and an i7-7700 CPU running at 3.6 GHz. It is preferable, in general, for a measure to scale slowly with the number of samples and the number of channels, though in some situations this may not be necessary. Transfer entropy is the fastest measure, followed by frequency-domain Granger causality, multivariate Granger causality, conditional Granger causality and Kullback-Leibler divergence, all of which scale less well with the number of channels. Execution time increases significantly for partial transfer entropy and partial mutual information for with both the number of channels and the number of data. Partial Granger causality and frequency domain multivariate Granger causality scale poorly with the number of channels, and Copula Granger causality scales poorly with the number of data.

Table 4-1: *The time (seconds) required to estimate each measure for three sizes of data: few data ($N_{samples}$ = 300) and few channels ($N_{channels}$ = 3), many data ($N_{samples}$ = 50001) and few channels ($N_{channels}$ = 3), and few data ($N_{samples}$ = 300) and many channels ($N_{channels}$ = 60).*

Measure	Time (s)		
	$N_{samples} = 300$ $N_{channels} = 3$	$N_{samples} = 50001$ $N_{channels} = 3$	$N_{samples} = 300$ $N_{channels} = 60$ model order =max lag =5
PGC	0.024	0.447	771.783
FGC	0.031	0.031	10.918
DC	0.188	0.404	19.406
DTF	0.188	0.404	19.406
PDC	0.188	0.404	19.406
EPDC	0.188	0.404	19.406
EDC	0.188	0.404	19.406
GPDC	0.188	0.404	19.406
QGC	0.041	14.367	3.974
MVGC	0.025	0.029	21.562
TE	0.013	0.017	0.960
PMI	0.104	13.828	2864
PTI	0.103	9.322	2718
CGC	0.010	0.100	6.114
SMVGC	0.030	0.039	390.264
KL	0.046	0.066	6.133

4.8 Discussion and conclusion

Previous studies of effective connectivity measures have concentrated on a few measures. Some studies focused on model-based measures, while some studies have considered information theoretic measures or phase locking value or compared effective and functional connectivity measures. There is no thorough comparison of many effective connectivity measures from different families on simulated data. We include in this thesis most of the known effective connectivity measures from different families: namely model-based measures, information theoretic measures, and directional phase locking value. Because of these differences, it is not straightforward to compare our results with those studies. We comment on related papers that allow useful comparison.

Wu et al. [143] compared six multivariate causality measures, three of which are included in our study (multivariate Granger causality, directed transfer function, and partial directed coherence). When tested on simulated MVAR data, their conclusion was that Granger causality outperformed the two other measures, consistent with our finding. Additionally, both [143] and this study found Granger causality outperformed all other measures from the directed coherence family.

Papana et al. [141] assessed the performance of six directed causality measures: conditional Granger causality, partial Granger causality, partial directed coherence, partial transfer entropy, partial symbolic transfer entropy and partial mutual information on mixed embedding. All these measures were included in our studies except partial mutual information, as its execution time is prohibitively large. The datasets used were four linear MVAR models, including one with latent and exogenous inputs, and three nonlinear models (including one nearly identical to the Hénon map system studied in this thesis). They found that conditional Granger causality, partial Granger causality and partial directed coherence performed better than other measures for the linear systems, with partial Granger causality best when latent and exogenous inputs were present. The non-directional measure partial mutual information on mixed embedding outperformed all others for the nonlinear systems. Similarly, our studies showed that Copula Granger causality, multivariate Granger causality, partial Granger causality and conditional Granger causality performed best overall for MVAR systems, whereas transfer entropy should be preferred for nonlinear systems. Consistent with [141], Granger causality measures perform best for linear models, and an information theoretic measure performs best for nonlinear models.

Guo et al. [94] introduced partial Granger causality and tested partial Granger causality and conditional Granger causality with data from an MVAR model with exogenous and latent inputs. Their results demonstrated that partial Granger causality can reliably detect effective

connections between signals in the presence of exogenous inputs, whereas conditional Granger causality frequently fails. In contrast, our results show little difference between partial Granger causality and conditional Granger causality, though the largest difference does occur with System 2B, which is an MVAR model with exogenous inputs.

Papana et al. [144] compared two effective connectivity measures, the nonlinear measure partial transfer entropy and the linear measure partial directed coherence, on one linear MVAR model and two nonlinear models (again, one being a similar Hénon map model). Their results showed that for the linear model, partial transfer entropy and partial directed coherence performed equally well, whereas for the nonlinear models partial transfer entropy performed better than partial directed coherence. A similar study [7] compared six connectivity measures: three functional connectivity measures (cross correlation, coherence and phase synchronisation index) and three directional measures (transfer entropy, directed transfer function and partial directed coherence). They used simulated data generated from an MVAR model with two exogenous inputs (similar to the system 2B studied in this thesis). They concluded that directed transfer function and partial directed coherence performed better than other measures. With one exception, these results are consistent with our findings, and consistent with the view that the best linear measures outperform the best nonlinear measures on linear data, but the best nonlinear measures outperform the best linear measures on data drawn from nonlinear models. The exception here is that [144] found that linear and nonlinear measures performed equally on linear data. This may be due to their use of a small three-node MVAR model with strong coupling, making the task of identifying connections relatively easy. Faes et al. [109] introduced two extensions of directed coherence, namely extended directed coherence and extended partial directed coherence. They claim that traditional directed coherence and partial directed coherence may produce misleading connectivity patterns when there are instantaneous links between signals. Their results show better performance using the extended measures. Our

results for System 1 are consistent: where there are instantaneous links between signals, the extended measures outperform the original measures. However, we found that for all other systems, where there are no instantaneous links, the extended measures performance is less that the original measures. Given no other studies on the extended measures, we do not recommend their use unless the system under consideration is known to have instantaneous links.

Smit et al. [145] compared two effective connectivity measures, transfer entropy and directed transfer function, in high density resting state EEG data in eyes open and eyes closed tasks. They found that the differences between the eyes closed and eyes open condition identified by transfer entropy better matched the expectations from the literature than the differences found by DTF. Our results also found that transfer entropy outperformed DTF, and particularly when the data were not drawn from an MVAR model.

In summary, we considered 18 of the best-known connectivity measures and studied their performance for different sets of simulated time series (S1: non-linear coupled Hénon maps, S2a and S2b: MVAR model without and with exogenous inputs, and S3: simulated EEG). Table 4.1.7-1 shows the TPR, TNR, FPR and FNR for all measures and all systems, and an overall measure of performance. Optimum rates are coloured green, fading to white at performance equal to chance, strengthening to red as performance approaches all decisions incorrect. Copula Granger causality, multivariate Granger causality, partial Granger causality and conditional Granger causality performed best overall, with good performance in almost every situation. Partial Granger causality was therefore the best of the "partial" measures (partial Granger causality, partial directed coherence, partial transfer entropy), consistent with the findings in [141].

Partial transfer entropy and transfer entropy performed very well when the data were not generated from an MVAR system, but did not give as good results when the data were drawn from an MVAR model. Directed coherence and directed transfer function performed poorly on system 1, where the data are not drawn from an MVAR system and do not have energy concentrated in a specific frequency range. For system 2, when the data are MVAR, and system 3, where the data are focussed in a specific frequency band, they performed well. The worst performance was obtained by extended directed coherence and extended partial directed coherence, where almost all pairs of signals are deemed to have a connection. The addition of exogenous EEG inputs did not have any significant effect on the TPR of any connectivity measure except transfer entropy, whose performance degraded. However, several measures showed decreases in TNR, indicating that the presence of exogenous inputs results in an increase in the identification of false connections.

Our results suggest that there is not one measure that is consistently superior to all other measures, and that performance is critically dependent on the genesis of the data under analysis.

Overall, the measure with the best performance in a variety of situations and a low computational cost is conditional Granger causality. Partial Granger causality and multivariate Granger causality can also be used as reliable measures, but their computational cost rises rapidly with the number of channels. Similarly, Copula Granger causality can also be used reliably, but its computational cost rises rapidly with the number of data. This may not be an issue if the data under analysis is epoched to handle non-stationarity.

For EEG data, where the genesis of the data is unknowable, we recommend that using more than one measure is wise. Including a measure from each family, such as copula Granger causality or conditional Granger causality from the Granger causality family, along with

transfer entropy as an information theoretic measure, and directed coherence from the coherence family, would be an appropriate choice.

Table 4-2:   TPR, TNR, FPR and FNR for all measures and all systems, and an overall measure of performance. Optimum rates are coloured green, fading to white at performance equal to chance, strengthening to red as performance approaches all decisions incorrect.

overall	measure	TPR					TNR					FPR					FNR				
		S1	S2A	S2B	S3n	S3	S1	S2A	S2B	S3n	S3	S1	S2A	S2B	S3n	S3	S1	S2A	S2B	S3n	S3
55	TE	80	100	83		50	96	58	53	100	75	4	42	47	0	25	20	0	17		50
71	PGC	100	100	100		50	58	92	97	100	75	42	8	3	0	25	0	0	0		50
70	CGC	100	100	100		50	54	92	94	100	75	46	8	6	0	25	0	0	0		50
8	FCGC	100	50	100		50	23	56	31	50	25	77	44	69	50	75	0	50	0		50
77	QGC	100	100	100		100	73	75	72	100	75	27	25	28	0	25	0	0	0		0
75	MVGC	100	100	100		100	65	86	86	100	50	35	14	14	0	50	0	0	0		0
32	SMVGC	100	0	50		0	73	97	97	100	75	27	3	3	0	25	0	100	50		100
34	PDC	50	100	100		50	8	75	69	50	100	92	25	31	50	0	50	0	0		50
57	DC	50	100	100		100	15	86	86	67	100	85	14	14	33	0	50	0	0		0
8	EDC	60	100	100		100	39	8	6	0	75	62	92	94	100	25	40	0	0		0
-17	EPDC	60	100	100		50	35	3	3	0	25	65	97	97	100	75	40	0	0		50
47	DTF	60	100	100		100	12	67	58	67	100	89	33	42	33	0	40	0	0		0
43	GPDC	50	100	100		50	8	92	94	50	100	92	8	6	50	0	50	0	0		50
20	DPLV	100	100	100		100	0	53	39	50	0	100	47	61	50	100	0	0	0		0
-9	KL	70	0	67		100	39	94	42	0	0	62	6	58	100	100	30	100	33		0
35	PTE	100	50	83		0	81	64	53	100	75	19	36	47	0	25	0	50	17		100
29	DPMI	100	50	83		100	31	64	53	100	0	69	36	47	0	100	0	50	17		0

S1   : System 1

S2A   : System 2A

S2B   : System 2B over

S3n   : System 3 over the time frame (0 to 300)

S3   : System 3 over the time frame (300 to 740)

all correct

chance

all incorrect

CHAPTER 5   EXPLORING THE FREE PARAMETERS OF EFFECTIVE CONNECTIVITY MEASURES

So far, we have compared measures by applying them to noisy, nonstationary and nonlinear data set to find suitable measures for EEG. For some measures, we need to select a model order, and for some others we need to select a maximum lag. Therefore optimising these parameter for estimating connectivity is an important and essential task There are several methods that have been suggested for model order selection, such as Akaike information criterion (AIC) [146] and Bayesian information criterion (BIC) [147]. These criteria were original proposed for and studied on linear models, and their generalisation to any nonlinear model is not necessarily appropriate. Another approach to confront the problem of the model order selection is to use measures whose estimates of connectivity vary little with changes in model order. Such measures can be used with less concern about the process for selecting parameter values. In this chapter, therefore, we aim to identify which measures are stable, ie are not significantly affected by the choice of model order (p) or maximum lag (L_{max}). We study this question for short and medium data lengths (N).

5.1 Simulation studies

For simulation data, we again used the nonlinear system (three coupled Hénon maps), the seven-dimensional second-order MVAR model with and without exogenous inputs, and simulated EEG, as described in sections 4.1.1, 4.1.3, and 4.1.5. We varied L_{max} and p from 1 to 10 for signals with lengths of $N = 512$ and $N = 2048$. Here we selected the value of 10 for the maximum model order or maximum lag, as a compromise between execution time limitations and the power of the model to describe real EEG. A maximum order of 10 is large in comparison to many previous studies, but is possibly too small for some situations such as applying linear measures to nonlinear systems. Some constraints on calculation required the number of samples to be a multiple of 3, and some initial samples were discarded as transients resulting in small variations from the original 512 and 2048 samples. The ability of 15 effective connectivity measures to identify direct causal connections was evaluated. Simulations were repeated 100 times with different random initial conditions. Results were evaluated by measuring the TPR, FPR, FNR and TNR, and the derived measure of informedness (BM).

We are looking for:

1. the least variation, so choice of parameter is not really important; and
2. the highest informedness.

Four measures were excluded from this study. Kullback-Leibler divergence does not use lags or model order and so cannot be included. Similarly, directional phase locking value requires a maximisation over lags, and so cannot be included. Extended directed coherence and extended partial directed coherence performed unsatisfactorily in the most situations in Chapter 4, and were excluded for efficiency. Two measures were included. Given the strong performance of transfer entropy, two variants (symbolic transfer entropy and symbolic partial transfer entropy) were included to see if they could outperform transfer entropy.

160

5.1.1 Results for system 1

The results for system 1 for informedness (BM), true positive rate (TPR), and false positive rate (FPR) versus maximum lag L_{max} or model order p are shown in Figure 5-1 (a) for signal length $N = 512$ and (b) for signal length $N = 2048$. The informedness values as percentages are shown in Table 5-1.Transfer entropy and extended transfer entropy measures (symbolic transfer entropy, partial transfer entropy, and symbolic partial transfer entropy) had the lowest variation of informedness among all measures for both signal lengths. Generally, measures based on transfer entropy outperformed those based on Granger causality. The remaining measures, ie based on coherence or mutual information, performed worse than chance. Transfer entropy and symbolic transfer entropy showed the highest informedness among all measures, both achieving 92.3% BM for maximum lag $L_{max} = 4$ for signal length $N = 2048$, and 80% BM for maximum lag $L_{max} = 1$ for signal length $N = 512$. However, for short data lengths and at a maximum lag of one, partial transfer entropy and Copula Granger causality outperformed the overall best measures by at least 5

(a)

161
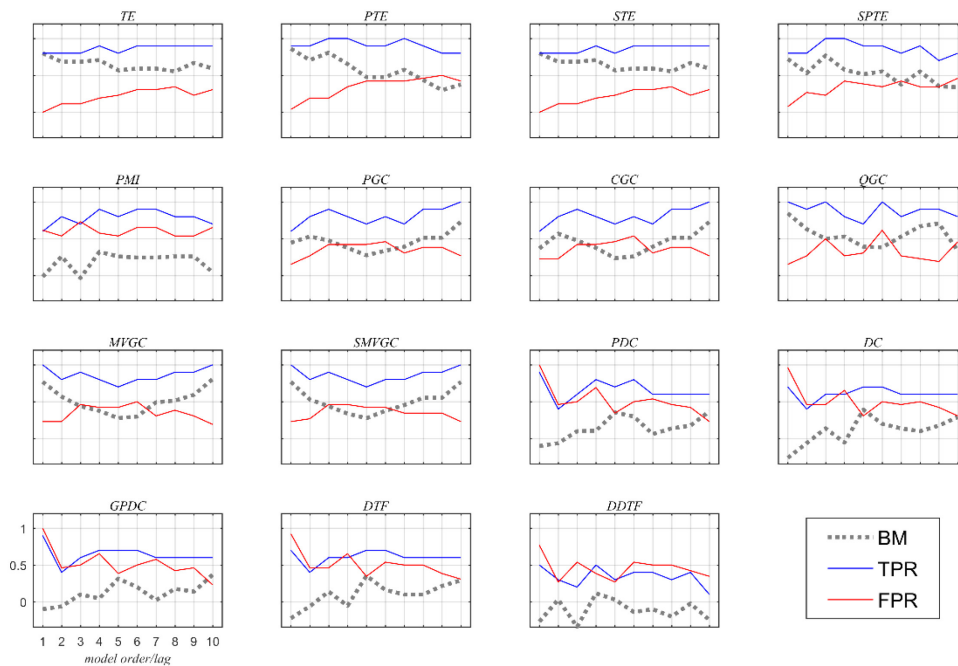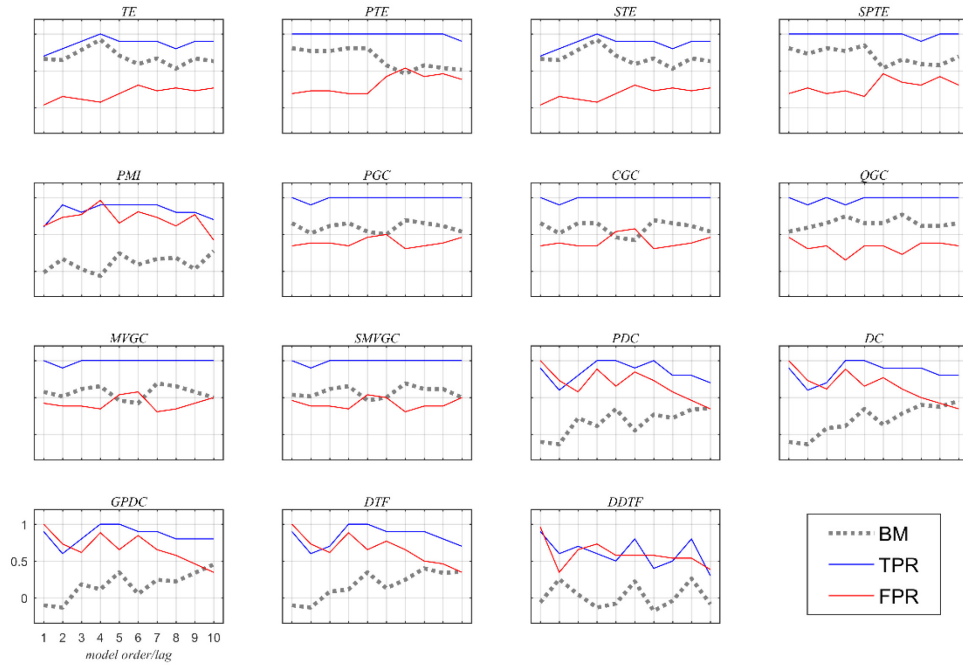
(b)

Figure 5-1: Results of system 1 for informedness (BM), true positive rate (TPR) and false positive rate (FPR), versus value of lag L for TE, STE, PTE, SPTE, PMI, QGC, CGC, MVGC and SMVGC and P for DC, PDC, GPDC, DTF and DDTF (a) for signal length N=512 and (b) for signal length N=2048. ©2018 IEEE.

Overall		66.2	66.2	61.7	61.55	60.1	54.1	53.9	53	51.55	15.7	15.15	14.9	14.75	14.1	4.65
	p/L	TE	STE	PTE	SPTE	QGC	MVGC	SMVGC	PGC	CGC	PDC	DC	PMI	GPDC	DTF	DDTF
N=512	1	80	80	86	72	85	77	77	45	37	-10	-26	-2	-10	-22	-27
	2	68	68	71	53	63	57	53	53	57	-6	-6	26	-6	-6	3
	3	68	68	81	77	50	44	44	48	48	10	14	-3	10	14	-34
	4	71	71	65	58	53	38	34	38	38	11	-5	32	5	-5	12
	5	57	57	48	52	39	28	28	28	24	35	39	26	32	35	3
	6	59	59	48	55	38	30	38	34	26	30	20	25	20	16	-14
	7	59	59	58	38	53	49	45	39	39	6	14	25	2	10	-10
	8	55	55	44	55	67	52	55	52	52	14	10	26	18	10	-20
	9	67	67	30	35	71	59	55	52	52	18	18	26	14	22	-2
	10	59	59	38	34	34	81	77	73	73	37	29	5	37	29	-25
N=2048	1	66	66	81	81	54	58	54	65	65	-10	-10	-2	-10	-10	-6
	2	65	65	77	73	59	52	52	52	52	-13	-13	17	-13	-13	25
	3	78	78	77	81	65	62	62	62	65	22	8	3	18	8	5
	4	92	92	81	77	75	65	65	65	65	12	12	-6	12	12	-13
	5	71	71	81	85	65	46	46	54	46	35	35	25	35	35	-8
	6	59	59	58	54	65	42	50	50	42	5	13	9	5	13	22
	7	67	67	46	65	77	69	69	69	69	27	28	17	25	25	-18
	8	53	53	58	59	62	65	62	65	65	22	40	18	22	40	-4
	9	67	67	54	58	62	58	62	62	62	34	38	3	34	34	26
	10	63	63	52	69	65	50	50	54	54	35	45	28	45	35	-8

all correct

chance

all incorrect

.

5.1.2 Results for system 2

For the second simulation system, frequency-based connectivity measures were calculated over the range of frequencies (0, 0.4), consistent with the literature and also where the spectra of the signals were high. For system 2A, the value of the informedness (BM), true positive rate (TPR) and false positive rate (FPR) versus maximum lag (L_{max}) are displayed in Figure 5-2 (a) for signal length $N = 512$ and (b) for signal length $N = 2048$. The informedness as percentages are shown in Table 5-2. The measures showing the least variation overall were generalised partial directed coherence, frequency domain multivariate Granger causality, partial Granger

causality, conditional Granger causality, directed coherence, Copula Granger causality. Generalised partial directed coherence achieved the highest informedness among all measures for both signal lengths, achieving 100% at maximum lag $L_{max} = 5$ for $N = 512$ and at $L_{max} = 6$ for $N = 2046$. Extended Granger causality measures except frequency domain multivariate Granger causality, and directed coherence also achieved high informedness scores. In general, measures who rely on a signal model that is autoregressive, ie Granger causality or directed coherence, performed better on system 2 than on system 1. Similarly, measures without an autoregressive model, ie information theoretic measures, performed worse on system 2 than on system 1, but still satisfactorily.
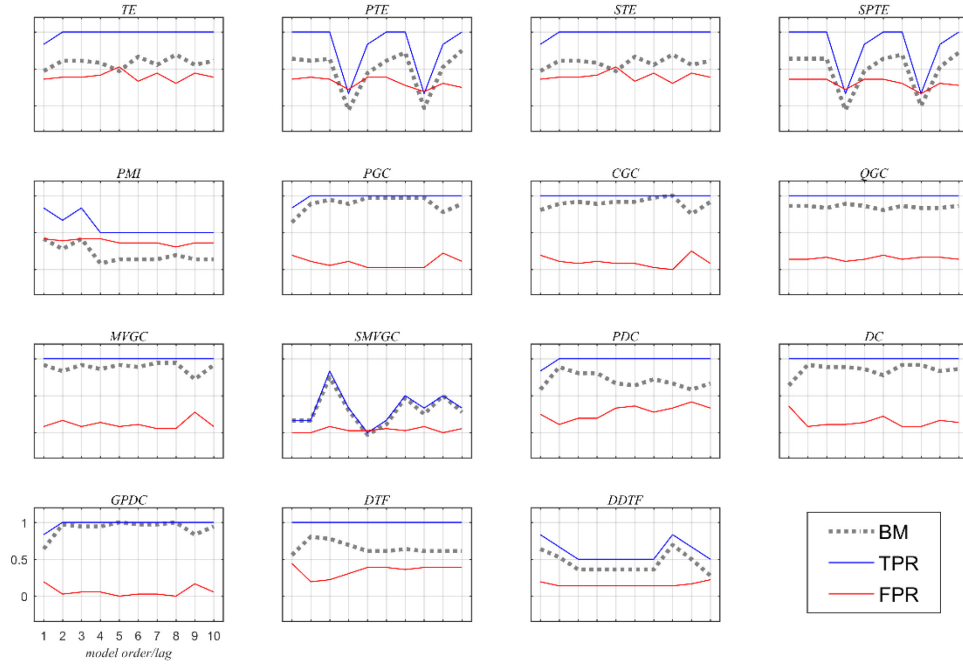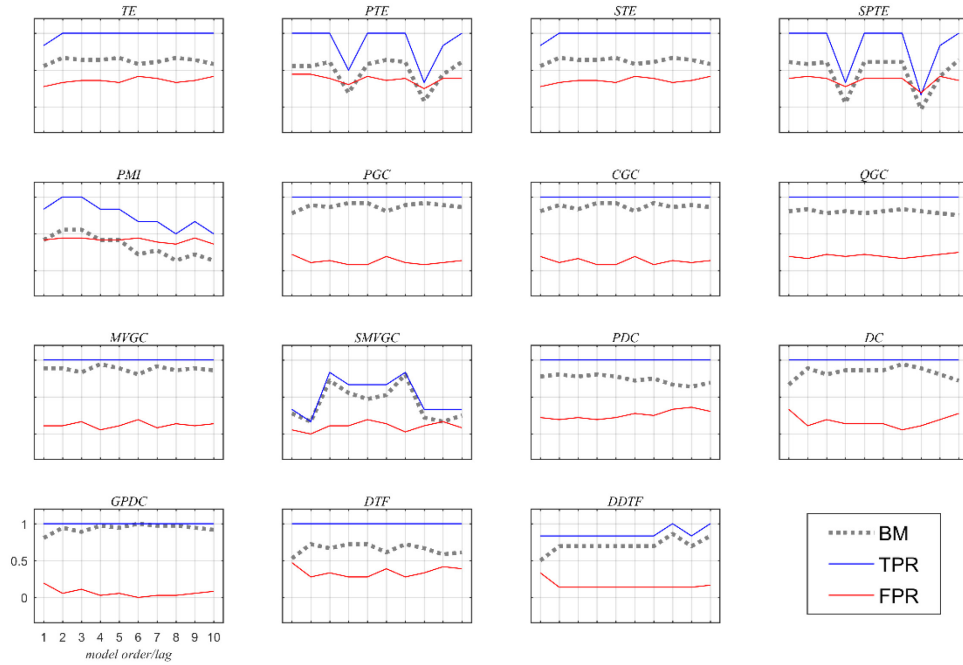
Figure 5-2: Results of system 2A for informedness (BM), true positive rate (TPR) and false positive rate (FPR), versus value of lag L for TE, STE, PTE, SPTE, PMI, QGC, CGC, MVGC and SMVGC and P for DC, PDC, GPDC, DTF and DDTF (a) for signal length N = 512 and (b) for signal length N = 2048. © 2018 IEEE.

165

Table 5-2: Table of informedness (BM) versus value of lag L for system 2A. Table of informedness (BM), versus value of lag L and an overall measure of performance for TE, STE, PTE, SPTE, PMI, QGC, CGC, MVGC and SMVGC and P for DC, PDC, GPDC, DTF and DDTF for signal length N=512 and signal length N=2048 for system 2A. Optimum rates are coloured green, fading to white at performance equal to chance, strengthening to red as performance approaches all decisions incorrect.

Overall		92.75	88.5	88.25	88.2	84.1	82.4	72.35	65.4	60.45	60.45	57.3	48.65	48.15	35.8	27.35
	p/L	GPDC	CGC	PGC	MVGC	DC	QGC	PDC	DTF	TE	STE	DDTF	PTE	SPTE	SMVGC	PMI
N=512	1	64	81	64	92	64	86	58	56	47	47	64	64	64	17	42
	2	97	89	89	83	92	86	89	81	61	61	53	61	64	17	28
	3	94	92	94	92	89	83	81	78	61	61	36	64	64	75	42
	4	94	89	89	86	89	89	81	69	58	58	36	-6	-6	31	8
	5	100	92	97	92	86	86	67	61	47	47	36	44	47	-3	14
	6	97	92	97	89	78	81	64	61	67	67	36	61	64	11	14
	7	97	97	97	94	92	86	72	64	56	56	36	72	69	47	14
	8	100	100	97	94	92	83	67	61	69	69	69	-3	0	25	19
	9	83	75	78	72	83	83	58	61	56	56	50	53	53	50	14
	10	94	92	89	92	86	86	67	61	61	61	28	75	72	28	14
N=2048	1	81	81	78	89	67	81	78	53	56	56	50	56	61	28	42
	2	94	89	89	89	89	83	81	72	67	67	69	56	58	17	56
	3	89	83	86	83	81	78	78	67	64	64	69	61	61	72	56
	4	97	92	92	94	86	81	81	72	64	64	69	19	6	56	42
	5	94	92	92	89	86	78	78	72	67	67	69	58	61	47	42
	6	100	81	81	81	86	81	72	61	58	58	69	64	61	53	22
	7	97	92	89	92	94	83	75	72	61	61	69	61	61	81	28
	8	97	86	92	86	89	81	67	67	67	67	86	8	-3	22	14
	9	94	89	89	89	81	78	64	58	64	64	69	44	42	17	22
	10	92	86	86	86	72	75	69	61	58	58	83	61	64	25	14

.

all correct

chance

all incorrect
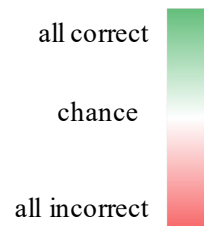
The values of BM, TPR and FPR for system 2B is displayed in Figure 5-3. The informedness percentages are shown in Table 5-3. The ranking of measures in system 2B is substantially the same as in system 2A, but with lower informedness scores overall. The variation of informedness has increased, and some measures show low variation at one data length and high variation at the other. The only measure that consistently has low variation is Copula Granger causality.
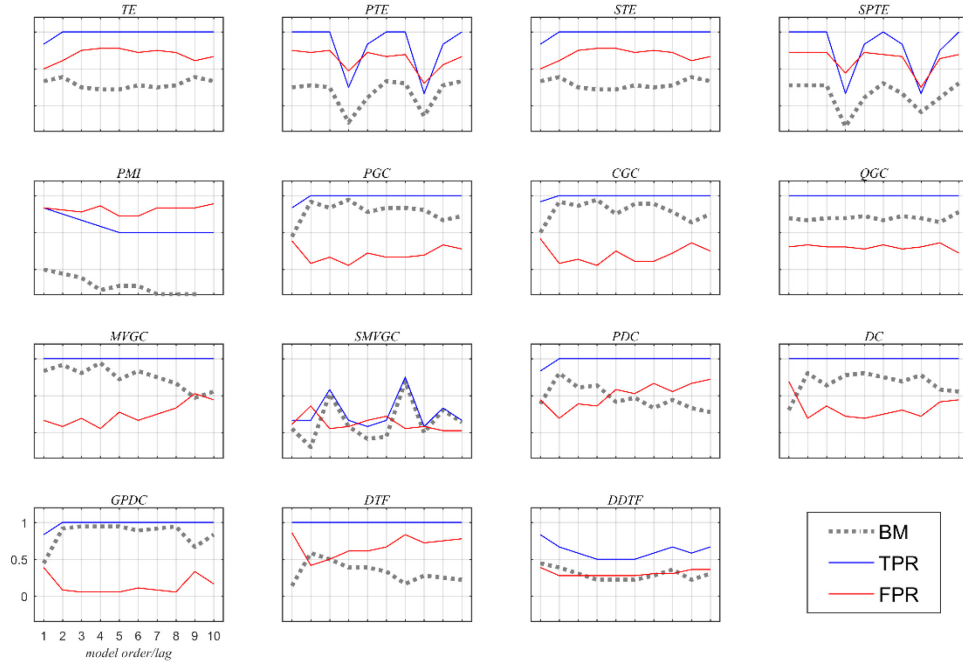
(a)
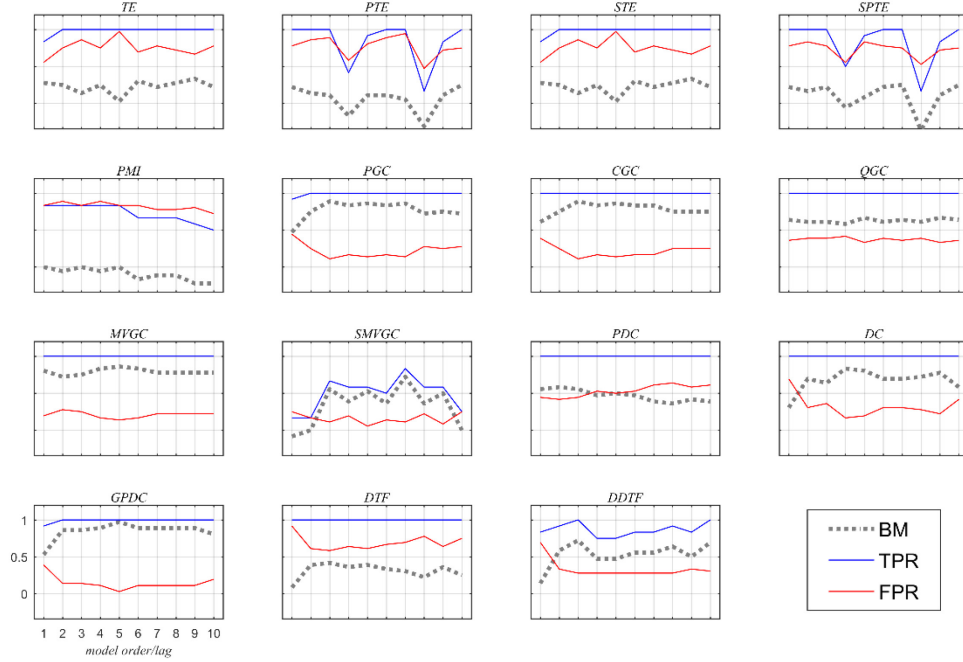
(b)

Figure 5-3: Results of system 2B for informedness (BM), true positive rate (TPR) and false positive rate (FPR), versus value of lag L for TE, STE, PTE, SPTE, PMI, QGC, CGC, MVGC and SMVGC and P for DC, PDC, GPDC, DTF and DDTF (a) for signal length N=506 and (b) for signal length N=2046. ©2018 IEEE.

Table 5-3: Table of informedness (BM) versus value of lag L for system 2B. Table of informedness (BM), versus value of lag L and an overall measure of performance for TE, STE, PTE, SPTE, PMI, QGC, CGC, MVGC and SMVGC and P for DC, PDC, GPDC, DTF and DDTF for signal length N=512 and signal length N=2048 for system 2B. Optimum rates are coloured green, fading to white at performance equal to chance, strengthening to red as performance approaches all decisions incorrect.

| Overall	84.55	77.1	78.85	77.25	67.25	66.2	41.5	47.1	24.1	31.8	26.25	26.25	12.95	12.05	16.1
	p/L	GPDC	MVGC	CGC	PGC	DC	QGC	DDTF	PDC	SMVGC	DTF	TE	STE	SPTE	PTE	PMI
N=512	1	44	83	50	44	31	69	44	39	6	14	33	33	28	25	0
	2	92	92	92	92	81	67	39	81	-19	58	39	39	28	28	-6
	3	94	81	86	83	64	69	31	61	53	50	25	25	28	25	-11
	4	94	94	94	94	78	69	22	64	8	39	22	22	-28	-22	-28
	5	94	72	75	78	81	72	22	42	-8	39	22	22	11	11	-22
	6	89	83	89	83	75	67	22	47	-6	33	28	28	31	33	-22
	7	92	75	89	83	69	72	28	33	69	17	25	25	17	31	-33
	8	94	67	78	81	78	69	36	44	0	28	28	28	-8	-14	-33
	9	67	47	64	67	58	64	22	33	31	25	39	39	11	28	-33
	10	83	56	75	72	56	78	31	28	14	22	33	33	31	33	-39
N=2048	1	53	81	61	47	31	64	14	56	-8	8	28	28	22	22	0
	2	86	72	75	75	69	61	58	58	0	39	25	25	17	14	-6
	3	86	75	89	89	64	61	72	56	56	42	14	14	22	11	0
	4	89	83	83	83	83	58	47	47	39	36	25	25	-6	-17	-6
	5	97	86	86	86	81	67	47	50	53	39	3	3	8	11	0
	6	89	83	83	83	69	61	56	47	36	33	31	31	22	11	-17
	7	89	78	83	86	69	64	56	39	72	31	22	22	25	6	-11
	8	89	78	75	72	72	61	64	36	36	22	28	28	-36	-31	-11
	9	89	78	75	75	78	67	50	42	50	36	33	33	11	11	-22
	10	81	78	75	72	58	64	69	39	0	25	22	22	25	25	-22

.

all correct

chance

all incorrect

5.1.3 Results for system 3

The data for system 3 were analysed for alpha connectivity using a window of 300 ms that was repeatedly slid 50 ms between calculations. Frequency-based connectivity measures were estimated in the range of the alpha band (8–13 Hz). We averaged the measures over windows containing the alpha bursts (from 300 to 740 ms), where we expected measures to detect the direct causal connections $x_1 \rightarrow x_2$ and $x_1 \rightarrow x_3$. We also analysed the system over the time

frame 0–300 ms, where there was no causal connection between any pair of signals. Data were resampled to achieve data lengths of $N = 512$ and $N = 2048$ for the full epoch of 1.5 s. With no causal link, there are no true positives or false negatives, therefore the informedness has no meaning. Hence we can only measure performance with the false positive rate (or, equivalently, the true negative rate), which is ideally zero.

The results from system 3 for the time range 0 to 300 ms (ie no causal links) are displayed in Figure 5-4 for both signal lengths. The false positive rates, as percentages, are shown in Table 5-4. The measures showing the least variation overall were frequency-based multivariate Granger causality and transfer entropy, with Cupola Granger causality, conditional Granger causality, and multivariate Granger causality also showing minimal variation.

Transfer entropy achieved the lowest false positive rate among all measures. This measure correctly detected no connection for most values of lag, and incorrectly identified only one link for a few values of lag. Cupola Granger causality and partial Granger causality also achieved low false positive rates. For the longer data length, Cupola Granger causality, partial Granger causality, partial transfer entropy and multivariate Granger causality, conditional Granger causality and frequency domain Granger causality correctly detected no connection for all value of the lags. Information theoretic measures and measure based on Granger causality perform better when the number of samples increased. Partial mutual information performed well for the longer data length, while its performance was not satisfactory for the shorter data length. In general, measures based on directed coherence did not perform well, though their performance improved as the model order increased.
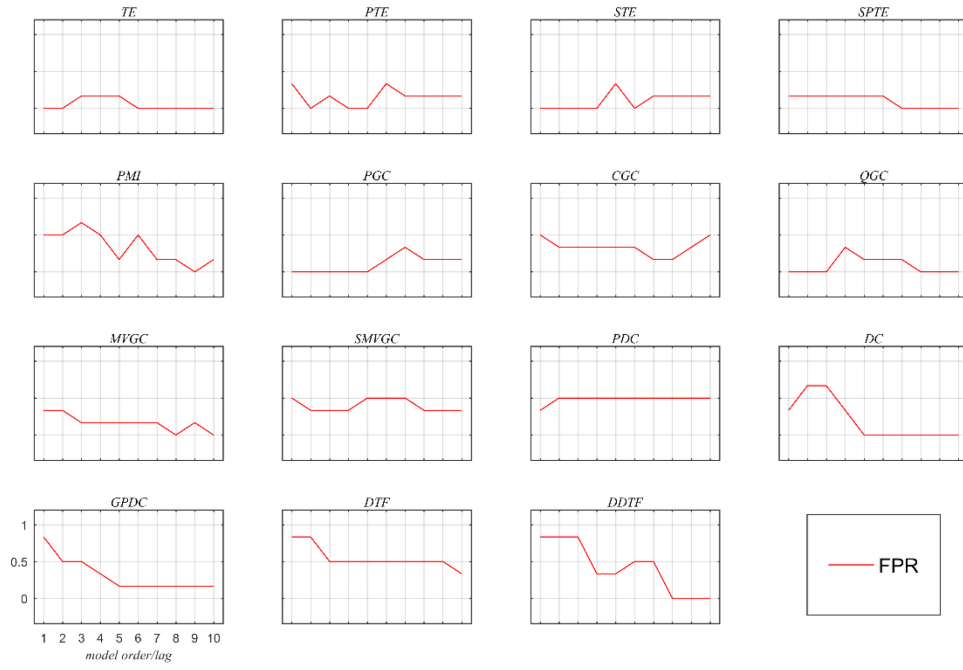
(a)
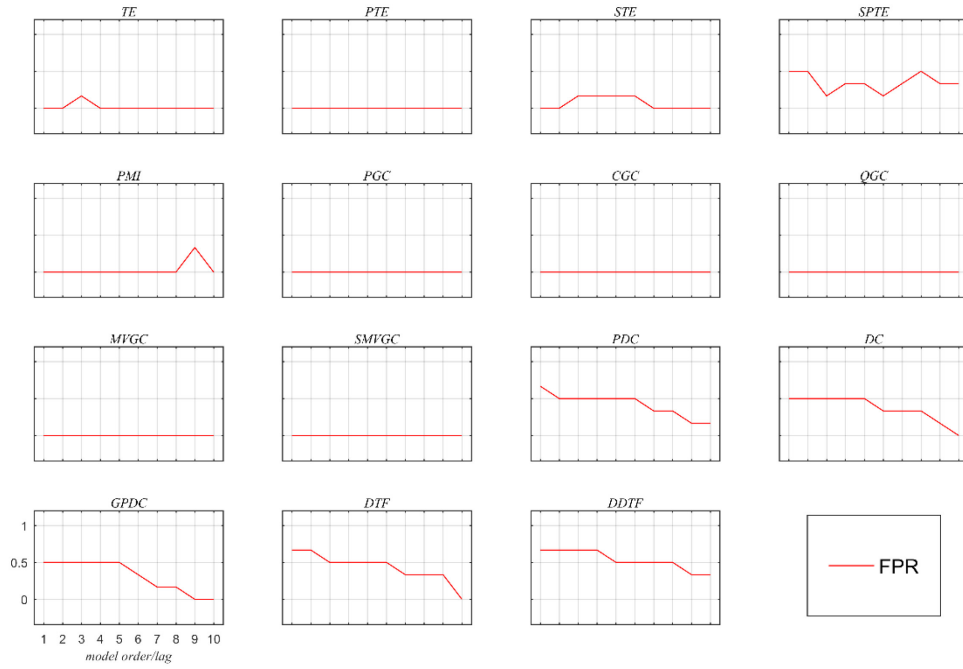
(b)

Figure 5-4:   Results of system 3 for false positive rate (FPR) versus value of lag L for TE, STE, PTE, SPTE, PMI, QGC, CGC, MVGC and SMVGC and P for DC, PDC, GPDC, DTF and DDTF, calculated over the time range 0 to 300ms, where no causal connections exist (a) for signal length N=506 and (b) for signal length N=2046. ©2018 IEEE.

Table 5-4:   Table of informedness (BM) versus value of lag L for system 3 over the time range from 0 to 300ms. Table of informedness (BM), versus value of lag L and an overall measure of performance for TE, STE, PTE, SPTE, PMI, QGC, CGC, MVGC and SMVGC and P for DC, PDC, GPDC, DTF and DDTF for signal length N=512 and signal length N=2048 for system 3 calculated over the time range from 0 to 300ms, where no causal connections exist. Optimum rates are coloured green, fading to white at performance equal to chance, strengthening to red as performance approaches all decisions incorrect.

|	Overall	3.4	4.2	5.05	7.55	8.4	8.45	16.6	18.4	19.9	22.55	28.3	31.75	45	47.45	49.1
	p/L	TE	QGC	PGC	PTE	MVGC	STE	CGC	PMI	SMVGC	DC	SPTE	GPDC	DDTF	PDC	DTF
N=512	1	0	0	0	33	33	0	50	50	50	17	33	83	33	83	83
	2	0	0	0	0	33	0	33	50	33	17	67	50	50	83	83
	3	17	0	0	17	17	0	33	67	33	17	67	50	50	83	50
	4	17	33	0	0	17	0	33	50	33	17	33	33	50	33	50
	5	17	17	0	0	17	33	33	17	50	17	0	17	50	33	50
	6	0	17	17	33	17	0	33	50	50	17	0	17	50	50	50
	7	0	17	33	17	17	17	17	17	50	0	0	17	50	50	50
	8	0	0	17	17	0	17	17	17	33	0	0	17	50	0	50
	9	0	0	17	17	17	17	33	0	33	0	0	17	50	0	50
	10	0	0	17	17	0	17	50	17	33	0	0	17	50	0	33
N=2048	1	0	0	0	0	0	0	0	0	0	50	50	50	67	67	67
	2	0	0	0	0	0	0	0	0	0	50	50	50	50	67	67
	3	17	0	0	0	0	17	0	0	0	17	50	50	50	67	50
	4	0	0	0	0	0	17	0	0	0	33	50	50	50	67	50
	5	0	0	0	0	0	17	0	0	0	33	50	50	50	50	50
	6	0	0	0	0	0	17	0	0	0	17	33	33	50	50	50
	7	0	0	0	0	0	0	0	0	0	33	33	17	33	50	33
	8	0	0	0	0	0	0	0	0	0	50	33	17	33	50	33
	9	0	0	0	0	0	0	0	33	0	33	17	0	17	33	33
	10	0	0	0	0	0	0	0	0	0	33	0	0	17	33	0

all correct

chance

all incorrect

.

The results from system 3 for the time range 300 to 740 ms (ie causal links are present) are displayed in Figure 5.1.3-2 for both signal lengths. The measures showing the least variation overall were Copula Granger causality, transfer entropy, symbolic transfer entropy, symbolic partial transfer entropy, partial transfer entropy and multivariate Granger causality.

Copula Granger causality and transfer entropy achieved the highest informedness among all measures. Copula Granger achieved 100% informedness at lags $L_{max} = 4$ and 9 for $N = 2048$. Transfer entropy achieved 100% informedness at $L_{max} = 2$ and 9. Symbolic transfer

entropy, multivariate Granger causality, partial Granger causality and partial transfer entropy also achieved high informedness scores. All measures from the directed coherence family, plus partial mutual information, performed poorly.

(a)

(b)
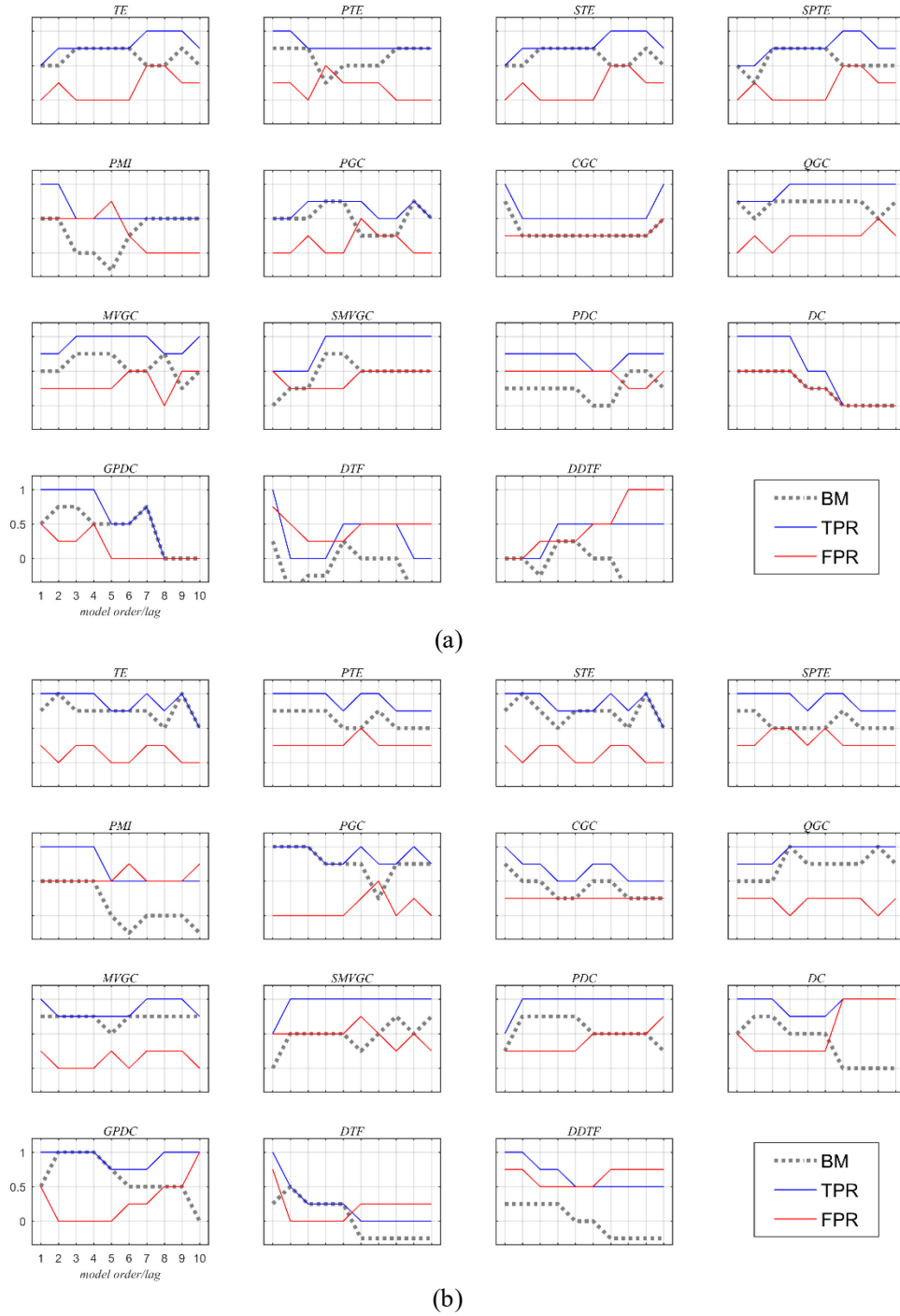
Figure 5-5:   Results of system 3 for False positive rate (FPR) versus value of lag L for TE, STE, PTE, SPTE, PMI, QGC, CGC, MVGC and SMVGC and P for DC, PDC, GPDC, DTF and DDTF for system 3, calculated over the time range from 300 ms to 750 ms, where direct causal connections do exist (a) for signal length N=50 and (b) for signal length N=2046. © 2018 IEEE.
Detecting synchrony in EEG: A comparative study of functional connectivity measures

Table 5-5:   Table of informedness (BM) versus value of lag L for system 3 over the time range from 300 to 740ms. Table of informedness (BM), versus value of lag L and an overall measure of performance for TE, STE, PTE, SPTE, PMI, QGC, CGC, MVGC and SMVGC and P for DC, PDC, GPDC, DTF and DDTF for signal length N=512 and signal length N=2048 for system 3 calculated over the time range from 300 to 740 ms, where causal connections do exist. Optimum rates are coloured green, fading to white at performance equal to chance, strengthening to red as performance approaches all decisions incorrect.

Overall		71.25	68.75	67.5	65	63.75	62.5	57.5	52.5	46.25	40	36.25	30	22.5	6.25	6.25
	p/L	QGC	TE	STE	MVGC	PGC	PTE	SPTE	GPDC	SMVGC	PDC	CGC	DC	PMI	DTF	DDTF
N=512	1	75	50	50	50	50	75	50	50	0	25	75	50	50	0	25
	2	50	50	50	50	50	75	25	75	25	25	25	50	50	0	-50
	3	75	75	75	75	50	75	75	75	25	25	25	50	0	-25	-25
	4	75	75	75	75	75	25	75	50	75	25	25	50	0	25	-25
	5	75	75	75	75	75	50	75	50	75	25	25	25	-25	25	25
	6	75	75	75	50	25	50	75	50	50	0	25	25	25	0	0
	7	75	50	50	50	25	50	50	75	50	0	25	0	50	0	0
	8	75	50	50	75	25	75	50	0	50	50	25	0	50	-50	0
	9	50	75	75	25	75	75	50	0	50	50	25	0	50	-50	-50
	10	75	50	50	50	50	75	50	0	50	25	50	0	50	-50	-50
N=2048	1	50	75	75	75	100	75	75	50	0	25	75	50	50	25	25
	2	50	100	100	75	100	75	75	100	50	75	50	75	50	25	50
	3	50	75	75	75	100	75	50	100	50	75	50	75	50	25	25
	4	100	75	50	75	75	75	50	100	50	75	25	50	50	25	25
	5	75	75	75	50	75	50	50	75	50	75	25	50	0	0	25
	6	75	75	75	75	75	50	50	50	25	50	50	50	-25	0	-25
	7	75	75	75	75	25	75	75	50	50	50	50	0	0	-25	-25
	8	75	50	50	75	75	50	50	50	75	50	25	0	0	-25	-25
	9	100	100	100	75	75	50	50	50	50	50	25	0	0	-25	-25
	10	75	50	50	75	75	50	50	0	75	25	25	0	-25	-25	-25

.

all correct

chance

all incorrect

5.2   Discussion and conclusion

In this chapter, we have looked at the variation of BM across multiple data sets for all effective connectivity measures. Table 5-6 summarises these results, showing the BM and interquartile range (IQR) for all measures and all systems. Optimum values of BM are coloured green, fading to white at performance equal to chance, strengthening to red as performance approaches all decisions incorrect. For IQR, the desired low variation of connectivity measures

with their parameters (L_{max} or p) and data length is coloured green, fading to white and then strengthening to red as the variation increases. The measures that show the smallest IQR, or lowest variation of BM with parameter, are Copula Granger causality and transfer entropy.

Wu et al. [143] compared six multivariate causality measures, three of which are included in our study (multivariate Granger causality, directed transfer function, and partial directed coherence). Simulated MVAR data was analysed using measures with model orders of 4, 8, 12 and 16. Their results showed that the accuracy (proportion of correct decisions) of partial directed coherence decreased as the model order was increased, which is consistent with our results when the data were generated from an MVAR model.

This study also found that multivariate Granger causality is insensitive to changes in model order (lag). This agrees with our results when the data are drawn from an MVAR model without exogenous inputs, as well as an MVAR model with exogenous inputs where data length is medium. But our results show that when the data are generated from an MVAR model with exogenous inputs and the data length is short, multivariate Granger causality performs better for smaller values of the model order.

Wang et al. [8] compared measures including members of the cross correlation family, measures based on coherence, information theoretic measures, and Granger causality and its extended measures. Unlike this thesis, [8] used simulated fMRI data and simulated NIRS data, ie their interest does not include EEG. Additionally, performance was measured from receiver operator characteristics, and not from surrogate-derived thresholds. One of their findings showed that transfer entropy was quite robust against variation of maximum lag. Despite significant differences in the studies, this result is consistent with our finding in this chapter that transfer entropy is one of the most robust measures.

In summary, this chapter concludes that the optimum maximum lag or maximum model order depends on the data set at hand. For EEG, we don't know the optimum values, and estimating them can be difficult and time-consuming. Measures that give consistent estimates of connectivity across a wide range of parameter values are attractive, as estimating these parameters becomes less critical to performance. Transfer entropy and Copula Granger causality are good choices, as they show low variation in connectivity estimates with variation of these parameter.

Table 5-6: Table of informedness (overall BM) ; the value of the BM for the value of the lags from 1 to 10 for TE, STE PTE, SPTE, QGC, MVGC and SMVGC was calculated and then averaged. The value of the BM for the value of the model order p from 1 to 10 for the DC, PDC, GPDC, DTF, DDTF and PMI was calculated and then averaged. The similar procedure has been down to evaluate IQR. Optimum rates of BM are coloured green, fading to white at performance equal to chance, strengthening to red as performance approaches all decisions incorrect. For the IQR, the low variation of the connectivity measures against variation of the parameters (L/P) and data length are coloured green and strengthening to red for the higher variation.

measures	overall BM across L/p					IQR							
	S1	S2A	S2B	S3n	S3	S1	S2A	S2B	S3n	S3	overall	overall IQR	overall BM
TE	66.2	60.45	26.25	3.4	68.75	10.5	8.5	10	0	25	164.25	10.8	43.65
STE	66.2	60.45	26.25	8.45	67.5	10.5	8.5	10	17	25	140.95	14.2	42.39
PTE	61.7	48.65	12.05	7.55	62.5	31	18.5	18	17	25	67.85	21.9	35.47
SPTE	61.55	48.15	12.95	28.3	57.5	21.5	19.5	17	50	25	18.85	26.6	30.37
QGC	60.1	88.5	66.2	4.2	71.25	13	5	6.5	0	12.5	244.85	7.4	56.37
MVGC	64.1	88.2	77.1	8.4	65	18.5	6	9.5	17	25	210	15.2	57.2
SMVGC	53.9	35.8	24.1	19.9	46.25	16.5	34.5	51.5	33	12.5	-7.85	29.6	28.03
PGC	53	88.25	77.25	5.05	63.75	17	7	12.5	8.5	25	207.2	14	55.44
CGC	51.55	88.5	78.85	16.6	36.25	24.5	7.5	12.5	13	25	156.05	16.5	47.71
PDC	15.7	72.35	47.1	47.45	40	26.5	12.5	17	34	50	-12.3	28	25.54
DC	15.15	84.1	67.25	22.25	30	30.5	8	17	16	25	77.75	19.3	34.85
GPDC	14.75	92.75	84.55	31.75	52.5	23	4	8.5	33	25	119.3	18.7	42.56
DTF	14.1	65.4	31.8	49.1	-6.25	25	33	15.5	8.5	50	-76.05	26.4	11.19
DDTF	-4.95	57.3	41.5	45	-6.25	30	8.5	31	8.5	50	-85.4	25.6	8.52
PMI	14.9	27.35	-16.1	18.4	22.25	20	28	19	41.5	50	-128.5	31.7	6

CHAPTER 6   CONCLUSION

6.1 Thesis achievements

Fundamentally, this thesis has achieved a large study that is a fair comparison of many measures. In particular, there are five approaches used in this thesis that expand on previous studies.

6.1.1 Simulated data

Some publications use real EEG for the comparison of measures [6]. The difficulty with using EEG is that we don't know when a measure is giving the "right" answer. We claim that there is merit in comparing measures on simulated data where the true connections are known, rather than on real EEG data where our understanding is imperfect. Hence we use datasets that in some sense mimic EEG, but where we know when a measure is giving the "right" answer.

6.1.2 Effective vs functional

There are several publications that compare many measures that include both functional measures and effective measures, e.g. [6-8]. We argue that there are significant difficulties with comparing directed and nondirected measures. For example, we can generate data from a simulated system with directed connections, and compare the detected connections from a directed measure to the truth. But for a non-directed measure, we have only a single connection between two signals, so we either compare to both the directed connections or to the combination of them. In the first case, the non-directed measure can never detect the truth unless the connection is bidirectional, and in the second case the non-directed measure has half the comparisons of the directed measure. Hence neither comparison is clearly fair, and so in this thesis we compare non-directed (ie functional) measures and directional (ie effective) measures separately.

6.1.3 Linear vs nonlinear

In addition, the literature generally takes a simplistic view that linear measures won't perform well on nonlinear datasets, but provides little evidence supporting this. It is also difficult to usefully characterise the strength of the "linear component" in a nonlinear dataset, as a linear measure may not be totally insensitive to the "nonlinear component", and different measures may be differentially sensitive. Hence we have chosen to test all measures on all datasets and let the results speak. We have demonstrated that linear synchronisation measures are able to detect nonlinear relationships, and in some situations they can estimate nonlinear relationships more reliably than nonlinear synchronisation measures.

6.1.4 Large, multiple-family comparisons

Previous studies have mostly focused on a few measures [3, 9-14]. Many of the comparative studies of connectivity measures have focused on bivariate tests e.g. [15], while some studies have considered the effectiveness of only model-based measures, e.g. [2, 16] or information theoretic measures, e.g. [17-19]. Hence we claim that there are no thorough comparisons of many measures on simulated data, and completing this comparison is an achievement of this thesis.

6.1.5 Significance analysis

One of the most significant issue in comparing connectivity measures is that different measures do not calculate values on the same scale. A higher value of connectivity in one measure may indicate no connection between two signals, whereas a lower value in a different measure may indicate a connection between the signals. Because they are not measuring on the same scale, significant variation in the raw values can be seen across measures. Hence to reliably compare different measures we need a statistical approach to identify when a connectivity value is significantly different from its background level.

177

To test the statistical significance of a connectivity value and determine whether connectivity is detected, we generate surrogate data to give data with the same statistical properties as the simulated data but without the dependencies between signals. A collection of surrogate data can be analysed with the connectivity measure to obtain a distribution of connectivity values corresponding to signals without connectivity, and a threshold determined from the surrogate ensemble. If the connectivity measure calculated on the original data exceeds this threshold, then it is regarded as statistically significant. There is a computational cost associated with this approach, but it removes the arbitrariness of selecting a threshold.

While the use of surrogates is not new, the literature only has studies using surrogates with a very limited number of measures. Hence the use of surrogates to reliably manage the variation in raw values from many measures in this study is new.

6.2 Further work

6.2.1 Partial functional connectivity

With functional connectivity, we are looking for a synchronous relationship between pairs of signals. If we have three signals, and signals 1 and 2 are connected, and signals 2 and 3 are connected, then it is reasonable to expect there will also be a relationship between signals 1 and 3. Hence simple functional connectivity measures should find connections between all pairs of the three signals. A similar argument holds for a system where signal 1 drives both signals 2 and 3.

There are more complex functional connectivity measures that take into account the involvement of a third signal. These partial measures can in principle differentiate between direct connections between signals from indirect connection. So in the first example above, a partial measure can identify that the relationship between signals 1 and 3 is completely explained by the intermediate signal 2.

There are publications that claim partial measures perform better than non-partial measures where the system is complex with many interconnected signals e.g. many EEG channels, or where there are exogenous inputs and/or latent variables. But there is a question as to whether it is fair to compare non-partialized functional connectivity measures with partialized measures. It is reasonable for a non-partial measure to detect indirect connections as being present, whereas it is not reasonable for a partial measure to do so. Hence in this thesis we have only considered non-partial functional measures. It is an open question as to how to fairly compare partial and non-partial function measures.

6.2.2 A comparison of surrogate algorithms

A variety of algorithms have been proposed to generate surrogate data. We used an algorithm that is well suited for testing for nonlinearity and is recommended in the literature [122, 123]. It is possible another algorithm is better, and a careful comparison of the performance of different algorithms would be a useful study. It is possible that the conclusion will depend on the choice of connectivity measure or measures used in the comparison.

6.2.3 Data segmentation

In chapters 4 and 5 we calculated connectivity measures on the whole data sample. This can cause difficulties with nonstationary data, as the results cannot capture the nonstationarity, and with sets with many data, as execution time may become prohibitive. However reducing the size of the data sample can also cause difficulties. If the window size is too small, the detection of connectivity may fail due to insufficient power. Additionally, a small window size will give many windows to analyse, and that may cause issues with storage and/or execution time. A study exploring window size to identify the minimum window size that allows good estimates of connectivity would be valuable. Combining this information with knowledge of the sampling rate of the data and its level of nonstationarity would allow an appropriate choice of data segmentation.

6.2.4 Speeding up slow measures

Many of the measures have a significant execution time, especially measures that require phase space reconstruction or use k-nearest neighbour algorithms. Finding fast implementations of these measures would be of benefit. In particular, an online or iterative implementation of phase space reconstruction that updates when a new sample or block of samples arrives could be valuable.

6.2.5 Directionalising functional measures

In this literature, there are examples of functional (non-directional) measures that have been modified to provide directional information as well. This is typically done by selecting the maximum functional connectivity between two signals over a range of positive lags for an effective connectivity measurement in one direction, and over a range of negative lags for an effective connectivity measurement in the other direction. However, not all functional measures have been directionalised, so there is scope to consider additional directionalised measures, or alternative ways to directionalise measures.

6.2.6 Partialising functional measures

As discussed earlier, there are advantages in using partial measures that allow indirect connections to be differentiated from direct connections. A full comparison of the current partial measures is needed. Additionally, it may be possible to design new partial measures. For example, partial cross correlation is an extension of cross correlation that uses the correlations between all signals to discount indirect connections. Similarly, partial mutual information extends mutual information, and partial coherence extends coherence. Exploring these and other ways to partialise other functional measures may yield functional measures with better performance.

6.2.7 Simulated EEG

In this thesis we used simulated EEG generated using pink noise to capture the spectral characteristic of EEG. Since real EEG is more complex than this, we think still there is scope to test other techniques for simulating EEG. Two possibilities proposed in the literature are brain electrical source analysis (BESA) [148] and neural mass models (NMMs) [149].

Extending the complexity of simulated EEG models would also be a further step to allow the findings of this thesis to be confidently applied to real EEG. Another appropriate step would be to rigorously test the measures on real EEG in situations where other experimental work has provided strong evidence for connectivity, such as in dementia [6].

6.3 Summary of main findings

No measure consistently performs better than other measures. The choice of best measure clearly depends on several factors. This thesis has provided evidence to support a variety of choices depending on noise level, stationarity of data, number of channels, number of samples and available time.

For functional connectivity measures:

- Correlation coefficient and S-estimator work well in almost every situation
  - preferring correlation coefficient if weak coupling is expected
  - preferring S-estimator if the noise is particularly strong or the data are nonstationary;
- If the SNR is poor and calculation time unimportant, then mutual information (kernel) is the best choice.

For effective connectivity measures:

- The optimum maximum lag or maximum model order depends on the data set at hand. For EEG, we don't know the optimum values, and estimating them can be difficult. In such cases, measures that show low variation in connectivity estimates with variation in these parameters are good choices. Most Granger causality measures, but especially Copula Granger causality, and transfer entropy are therefore good choices.

- Overall, the measure with the best performance in a variety of situations and with a low computational cost is conditional Granger causality;

- Partial Granger causality and multivariate Granger causality are also good measures, but their computational cost rises rapidly with the number of channels;

- Copula Granger causality can also be used reliably, but its computational cost rises rapidly with the number of data;

- Model-specific measures, such as in the coherence and Granger causality families, performed better on data generated from a matching model, and worse on data not generated from a matching model;

- Frequency domain measures performed better on narrowband data;

- Where data is broadband and from an unknown/unidentified system, model-free measures such as transfer entropy and partial transfer entropy may perform better;

- For real data of unknown origin, we recommend using more than one measure from more than one family.

EEG signals are nonlinear, noisy and nonstationary, and we do not have a reliable model for their generation. Therefore we recommend using multiple measures from more than one family. For functional connectivity, we recommend cross correlation, S-estimator, and mutual information (kernel). For effective connectivity, we recommend Copula Granger causality, transfer entropy and directed coherence. However, if computation time is an issue, then mutual

information (kernel) will be impractical and should be omitted, and conditional Granger causality should be used instead of Copula Granger causality.

References

[1]   C. W. J. Granger, "Testing for causality: A personal viewpoint," *Journal of Economic Dynamics and Control,* vol. 2, pp. 329-352, // 1980.

[2]   B. Schelter, M. Winterhalder, M. Eichler, M. Peifer, B. Hellwig, B. Guschlbauer*, et al.*, "Testing for directed influences among neural signals using partial directed coherence," *Journal of neuroscience methods,* vol. 152, pp. 210-219, 2006.

[3]   J.-W. Xu, H. Bakardjian, A. Cichocki, and J. C. Principe, "A new nonlinear similarity measure for multichannel signals," *Neural Networks,* vol. 21, pp. 222-231, 2008.

[4]   H. G. Schuster, *Reviews of Nonlinear Dynamics and Complexity*: Wiley, 2010.

[5]   B. P. Rogers, V. L. Morgan, A. T. Newton, and J. C. Gore, "Assessing functional connectivity in the human brain by fMRI," *Magnetic resonance imaging,* vol. 25, pp. 1347-1357, 2007.

[6]   J. Dauwels, F. Vialatte, T. Musha, and A. Cichocki, "A comparative study of synchrony measures for the early diagnosis of Alzheimer's disease based on EEG," *NeuroImage,* vol. 49, pp. 668-693, 2010.

[7]   M. J. Silfverhuth, H. Hintsala, J. Kortelainen, and T. Seppänen, "Experimental comparison of connectivity measures with simulated EEG signals," *Medical & biological engineering & computing,* vol. 50, pp. 683-688, 2012.

[8]   H. E. Wang, C. G. Bénar, P. P. Quilichini, K. J. Friston, V. K. Jirsa, and C. Bernard, "A systematic framework for functional connectivity measures," *Frontiers in neuroscience,* vol. 8, p. 405, 2014.

[9]   J. Bhattacharya, E. Pereda, and H. Petsche, "Effective detection of coupling in short and noisy bivariate data," *Systems, Man, and Cybernetics, Part B: Cybernetics, IEEE Transactions on,* vol. 33, pp. 85-95, 2003.

[10]   R. Q. Quiroga, J. Arnhold, and P. Grassberger, "Learning driver-response relationships from synchronization patterns," *Physical Review E,* vol. 61, p. 5142, 2000.

[11]   R. Q. Quiroga, A. Kraskov, T. Kreuz, and P. Grassberger, "Reply to "Comment on 'Performance of different synchronization measures in real data: A case study on electroencephalographic signals'"," *Physical Review E,* vol. 67, p. 063902, 2003.

[12]   A. Gunduz and J. C. Principe, "Correntropy as a novel measure for nonlinearity tests," *Signal Processing,* vol. 89, pp. 14-23, 1// 2009.

[13]   M. C. Romano, M. Thiel, J. Kurths, and C. Grebogi, "Estimation of the direction of the coupling by conditional probabilities of recurrence," *Physical Review E,* vol. 76, p. 036211, 2007.

[14]   S. J. Schiff, P. So, T. Chang, R. E. Burke, and T. Sauer, "Detecting dynamical interdependence and generalized synchrony through mutual prediction in a neural ensemble," *Physical Review E,* vol. 54, p. 6708, 1996.

[15]   M. Kamiński, M. Ding, W. A. Truccolo, and S. L. Bressler, "Evaluating causal relations in neural systems: Granger causality, directed transfer function and statistical assessment of significance," *Biological cybernetics,* vol. 85, pp. 145-157, 2001.

[16]   L. Astolfi, F. Cincotti, D. Mattia, M. G. Marciani, L. A. Baccala, F. D. V. Fallani, *et al.*, "Assessing cortical functional connectivity by partial directed coherence: simulations and application to real data," *Biomedical Engineering, IEEE Transactions on,* vol. 53, pp. 1802-1812, 2006.

[17]   T. Schreiber, "Measuring Information Transfer," *Physical Review Letters,* vol. 85, pp. 461-464, 07/10/ 2000.

[18]   D. Kugiumtzis, "Partial transfer entropy on rank vectors," *arXiv preprint arXiv:1303.6454,* 2013.

[19]   S. Frenzel and B. Pompe, "Partial Mutual Information for Coupling Analysis of Multivariate Time Series," *Physical Review Letters,* vol. 99, p. 204101, 11/14/ 2007.

[20]   Y. Li, J. Huang, H. Zhou, and N. Zhong, "Human Emotion Recognition with Electroencephalographic Multidimensional Features by Hybrid Deep Neural Networks," *Applied Sciences,* vol. 7, p. 1060, 2017.

[21]   R. Oostenveld, P. Fries, E. Maris, and J.-M. Schoffelen, "FieldTrip: open source software for advanced analysis of MEG, EEG, and invasive electrophysiological data," *Computational intelligence and neuroscience,* vol. 2011, p. 1, 2011.

[22]   H. Bakhshayesh, "Synchronization in brain," Electronic Engineering (Honours), Faculty of Science & Engineering, Flinders University, South Australia, 2012.

[23]   E. Niedermeyer, W. Froescher, and R. Fisher, "Epileptic seizure disorders," *Journal of neurology,* vol. 232, pp. 1-12, 1985.

[24]   E. W. Lang, A. M. Tomé, I. R. Keck, J. Górriz-Sáez, and C. G. Puntonet, "Brain connectivity analysis: a short survey," *Computational intelligence and neuroscience,* vol. 2012, p. 8, 2012.

[25]   K. Friston, C. Frith, P. Liddle, and R. Frackowiak, "Functional connectivity: the principal-component analysis of large (PET) data sets," *Journal of Cerebral Blood Flow & Metabolism,* vol. 13, pp. 5-14, 1993.

[26]   A. Aertsen and H. Preissl, "Dynamics of activity and connectivity in physiological neuronal networks," in *Nonlinear dynamics and neuronal networks*, ed: VHC-Verlaag, 1991.

[27]   O. Sporns. (2007, 4 Feb, 2014). *Brain connectivity*. Available: http://www.scholarpedia.org/article/Brain_connectivity

[28]   A. Pikovsky, M. Rosenblum, and J. Kurths, *Synchronization: a universal concept in nonlinear sciences* vol. 12: Cambridge university press, 2003.

[29] M. Rosenblum, A. Pikovsky, and J. Kurths, "Phase synchronization in noisy and chaotic oscillators," in *Stochastic Dynamics*. vol. 484, L. Schimansky-Geier and T. Pöschel, Eds., ed: Springer Berlin Heidelberg, 1997, pp. 232-244.

[30] P. L. Nunez and R. Srinivasan, *Electric fields of the brain: the neurophysics of EEG*: Oxford university press, 2006.

[31] C. S. Herrmann, M. Grigutsch, and N. A. Busch, "EEG Oscillations and Wavelet Analysis," *Event-related potentials: A methods handbook,* p. 229, 2005.

[32] C. Torrence and G. P. Compo, "A practical guide to wavelet analysis," *Bulletin of the American Meteorological society,* vol. 79, pp. 61-78, 1998.

[33] R. Q. Quiroga, T. Kreuz, and P. Grassberger, "Event synchronization: a simple and fast method to measure synchronicity and time delay patterns," *Physical review E,* vol. 66, p. 041904, 2002.

[34] A. Thungtong, "Synchronization, Variability, and Nonlinearity Analysis: Applications to Physiological Time Series," Case Western Reserve University, 2013.

[35] D. Gabor, *Theory of communication*: Institution of Electrical Engineering, 1946.

[36] J.-P. Lachaux, E. Rodriguez, J. Martinerie, and F. J. Varela, "Measuring phase synchrony in brain signals," *Human brain mapping,* vol. 8, pp. 194-208, 1999.

[37] Z. Ziqiang and S. Puthusserypady, "Analysis of schizophrenic EEG synchrony using empirical mode decomposition," in *Digital Signal Processing, 2007 15th International Conference on*, 2007, pp. 131-134.

[38] P. Tass, M. Rosenblum, J. Weule, J. Kurths, A. Pikovsky, J. Volkmann*, et al.*, "Detection of n: m phase locking from noisy data: application to magnetoencephalography," *Physical review letters,* vol. 81, p. 3291, 1998.

[39] J. Wang, X. Liao, and Z. Yi, *Advances in Neural Networks - ISNN 2005: Second International Symposium on Neural Networks, Chongqing, China, May 30 - June 1, 2005, Proceedings*: Springer, 2005.

[40] C. Krier, D. François, V. Wertz, and M. Verleysen, "Feature scoring by mutual information for classification of mass spectra," *Applied Artificial Intelligence,* vol. 10, pp. 557-564, 2006.

[41] S. Aviyente, "Information theoretic measures for quantifying the integration of neural activity," in *Information Theory and Applications Workshop, 2007*, 2007, pp. 20-26.

[42] J. T. Lizier, "Measuring the dynamics of information processing on a local scale in time and space," in *Directed Information Measures in Neuroscience*, ed: Springer, 2014, pp. 161-193.

[43] L. Batina, B. Gierlichs, E. Prouff, M. Rivain, F.-X. Standaert, and N. Veyrat-Charvillon, "Mutual information analysis: a comprehensive study," *Journal of Cryptology,* vol. 24, pp. 269-291, 2011.

[44] T. Suzuki, M. Sugiyama, J. Sese, and T. Kanamori, "Approximating mutual information by maximum likelihood density ratio estimation," in *New challenges for feature selection in data mining and knowledge discovery*, 2008, pp. 5-20.

[45] A. Kraskov, H. Stögbauer, and P. Grassberger, "Estimating mutual information," *Physical review E,* vol. 69, p. 066138, 2004.

[46] S. Aviyente, "A measure of mutual information on the time-frequency plane," in *Acoustics, Speech, and Signal Processing, 2005. Proceedings.(ICASSP'05). IEEE International Conference on*, 2005, pp. iv/481-iv/484 Vol. 4.

[47] M. S. Khalid, M. U. Ilyas, K. Mahmoo, M. S. Sarfaraz, and M. B. Malik, "Kullback-Leiber divergence measure in correlation of gray-scale objects," in *Proc. 2nd IntŠl conf. on innovations in Information Technology (IIT05)*, 2005.

[48] S. Kullback and R. A. Leibler, *The Annals of Mathematical Statistics,* vol. 22 pp. 79–86, 1951.

[49] M. Liuni, A. Röbel, M. Romito, and X. Rodet, "Rényi information measures for spectral change detection," in *Acoustics, Speech and Signal Processing (ICASSP), 2011 IEEE International Conference on*, 2011, pp. 3824-3827.

[50] J. Arnhold, P. Grassberger, K. Lehnertz, and C. E. Elger, "A robust method for detecting interdependences: application to intracranially recorded EEG," *Physica D: Nonlinear Phenomena,* vol. 134, pp. 419-430, 12/10/ 1999.

[51] C. Carmeli, M. G. Knyazeva, G. M. Innocenti, and O. De Feo, "Assessment of EEG synchronization based on state-space analysis," *NeuroImage,* vol. 25, pp. 339-354, 4/1/ 2005.

[52] R. Q. Quiroga, "Bivariable and Multivariable Analysis of EEG Signals."

[53] F. L. da Silva, "EEG analysis: theory and practice," *Electroencephalography: Basic Principles, Clinical Applications and Related Fields, 4th edition,* pp. 1135-1163, 1998.

[54] J. Shawe-Taylor and N. Cristianini, *Kernel methods for pattern analysis*: Cambridge university press, 2004.

[55] B. W. Silverman, *Density estimation for statistics and data analysis* vol. 26: CRC press, 1986.

[56] L. A. Baccalá and K. Sameshima, "Partial directed coherence: a new concept in neural structure determination," *Biological cybernetics,* vol. 84, pp. 463-474, 2001.

[57] M. Kaminski and H. Liang, "Causal influence: advances in neurosignal analysis," *Critical Reviews™ in Biomedical Engineering,* vol. 33, 2005.

[58] M. Le Van Quyen, J. Foucher, J.-P. Lachaux, E. Rodriguez, A. Lutz, J. Martinerie*, et al.*, "Comparison of Hilbert transform and wavelet methods for the analysis of neuronal synchrony," *Journal of neuroscience methods,* vol. 111, pp. 83-98, 2001.

[59] K. Mezeiová and M. Paluš, "Comparison of coherence and phase synchronization of the human sleep electroencephalogram," *Clinical Neurophysiology,* vol. 123, pp. 1821-1830, 2012.

[60] R. Q. Quiroga, A. Kraskov, T. Kreuz, and P. Grassberger, "Performance of different synchronization measures in real data: a case study on electroencephalographic signals," *Physical Review E,* vol. 65, p. 041903, 2002.

[61] F. Mormann, K. Lehnertz, P. David, and C. E. Elger, "Mean phase coherence as a measure for phase synchronization and its application to the EEG of epilepsy patients," *Physica D: Nonlinear Phenomena,* vol. 144, pp. 358-369, 2000.

[62] M. Rosenblum, A. Pikovsky, J. Kurths, C. Schäfer, and P. A. Tass, "Phase synchronization: from theory to data analysis," *Handbook of biological physics,* vol. 4, pp. 93-94, 2001.

[63] R. K. Otnes and L. Enochson, *Digital time series analysis*: John Wiley & Sons, Inc., 1972.

[64] A. F. McDaid, D. Greene, and N. Hurley, "Normalized mutual information to evaluate overlapping community finding algorithms," *arXiv preprint arXiv:1110.2515,* 2011.

[65] L. Ana and A. K. Jain, "Robust data clustering," in *Computer Vision and Pattern Recognition, 2003. Proceedings. 2003 IEEE Computer Society Conference on*, 2003, pp. II-II.

[66] D. Freedman and P. Diaconis, "On the histogram as a density estimator: L 2 theory," *Zeitschrift für Wahrscheinlichkeitstheorie und verwandte Gebiete,* vol. 57, pp. 453-476, 1981.

[67] G. A. Darbellay and I. Vajda, "Estimation of the information by an adaptive partitioning of the observation space," *IEEE Transactions on Information Theory,* vol. 45, pp. 1315-1321, 1999.

[68] S. Gao, G. Ver Steeg, and A. Galstyan, "Efficient Estimation of Mutual Information for Strongly Dependent Variables," in *AISTATS*, 2015.

[69] D. Johnson and S. Sinanovic, "Symmetrizing the kullback-leibler distance," 2001.

[70] K.-S. Song, "Rényi information, loglikelihood and an intrinsic distribution measure," *Journal of Statistical Planning and Inference,* vol. 93, pp. 51-69, 2001.

[71] K. Kyamakya and A. Bouchachia, *Intelligence for nonlinear dynamics and synchronisation*: Atlantis Press, 2010.

[72] N. Saito, T. Kuginuki, T. Yagyu, T. Kinoshita, T. Koenig, R. D. Pascual-Marqui, *et al.*, "Global, Regional, and Local Measures of Complexity of Multichannel Electroencephalography in Acute, Neuroleptic-Naive, First-Break Schizophrenics," *Biological Psychiatry,* vol. 43, pp. 794-802, 6/1/ 1998.

[73] Winner, "The theory of prediction," in *Modern Mathematics for Engineers*, E. Beckenbach, Ed., ed New york: McGraw, 1956.

[74]   C. W. J. Granger, "Investigating Causal Relations by Econometric Models and Cross-spectral Methods," *Econometrica,* vol. 37, pp. 424-438, 1969.

[75]   H. Marko, "The Bidirectional Communication Theory--A Generalization of Information Theory," *Communications, IEEE Transactions on,* vol. 21, pp. 1345-1351, 1973.

[76]   S. L, *Population (French Edition),* vol. 17, pp. 377-378, 1962.

[77]   J. T. Lizier, M. Prokopenko, and A. Y. Zomaya, "Local information transfer as a spatiotemporal filter for complex systems," *Physical Review E,* vol. 77, p. 026110, 02/15/ 2008.

[78]   D. Kugiumtzis, "Partial transfer entropy on rank vectors," *The European Physical Journal Special Topics,* vol. 222, pp. 401-420, 2013/06/01 2013.

[79]   R. Solé and S. Valverde, "Information Theory of Complex Networks: On Evolution and Architectural Constraints," in *Complex Networks*. vol. 650, E. Ben-Naim, H. Frauenfelder, and Z. Toroczkai, Eds., ed: Springer Berlin Heidelberg, 2004, pp. 189-207.

[80]   M. Prokopenko, F. Boschetti, and A. J. Ryan, "An information-theoretic primer on complexity, self-organization, and emergence," *Complex.,* vol. 15, pp. 11-28, 2009.

[81]   K. J. Blinowska, R. Kuś, and M. Kamiński, "Granger causality and information flow in multivariate processes," *Physical Review E,* vol. 70, p. 050902, 11/22/ 2004.

[82]   M. Eichler, "Graphical modelling of multivariate time series," *Probability Theory and Related Fields,* vol. 153, pp. 233-268, 2012/06/01 2012.

[83]   J. F. Geweke, "Measures of conditional linear dependence and feedback between time series," *Journal of the American Statistical Association,* vol. 79, pp. 907-915, 1984.

[84]   Y. Chen, S. L. Bressler, and M. Ding, "Frequency decomposition of conditional Granger causality and application to multivariate neural field potential data," *Journal of Neuroscience Methods,* vol. 150, pp. 228-237, 1/30/ 2006.

[85]   M. Ding, Y. Chen, and S. L. Bressler, "Granger Causality: Basic Theory and Application to Neuroscience," in *Handbook of Time Series Analysis*, ed: Wiley-VCH Verlag GmbH & Co. KGaA, 2006, pp. 437-460.

[86]   P. G. Larsson, A. Papana, and D. Kugiumtzis, "Detection of direct causal effects and application to epileptic electroencephalogram analysis," *International Journal of Bifurcation and Chaos,* vol. 22, p. 1250222, 2012.

[87]   V. A. Vakorin, B. Mišić, O. Krakovska, G. Bezgin, and A. R. McIntosh, "Confounding Effects of Phase Delays on Causality Estimation," *PLoS ONE,* vol. 8, p. e53588, 2013.

[88]   I. Luna, S. Soares, and R. Ballini, "Partial mutual information criterion for modelling time series via neural networks," in *Proc. of the 11th Information Processing and Management of Uncertainty International Conference*, 2006, pp. 2012-2019.

[89]   L. Faes and G. Nollo, "Multivariate frequency domain analysis of causal interactions in physiological time series," *Biomedical Engineering, Trends in Electronics, Communications and Software,* pp. 403-428, 2011.

[90]   J. Geweke, "Measurement of linear dependence and feedback between multiple time series," *Journal of the American Statistical Association,* vol. 77, pp. 304-313, 1982.

[91]   L. Wang and H. Garnier, *System Identification, Environmental Modelling, and Control System Design*: Springer, 2011.

[92]   M. Hu and H. Liang, "A copula approach to assessing Granger causality," *NeuroImage,* vol. 100, pp. 125-134, 10/15/ 2014.

[93]   S. Guo, C. Ladroue, and J. Feng, "Granger Causality: Theory and Applications," in *Frontiers in Computational and Systems Biology*. vol. 15, J. Feng, W. Fu, and F. Sun, Eds., ed: Springer London, 2010, pp. 83-111.

[94]   S. Guo, A. K. Seth, K. M. Kendrick, C. Zhou, and J. Feng, "Partial Granger causality— Eliminating exogenous inputs and latent variables," *Journal of Neuroscience Methods,* vol. 172, pp. 79-93, 7/15/ 2008.

[95]   L. Barnett and A. K. Seth, "The MVGC multivariate Granger causality toolbox: A new approach to Granger-causal inference," *Journal of Neuroscience Methods,* vol. 223, pp. 50-68, 2/15/ 2014.

[96]   L. Baccala, K. Sameshima, G. Ballester, A. Do Valle, and C. Timo-Iaria, "Studying the interaction between brain structures via directed coherence and Granger causality," *Applied Signal Processing,* vol. 5, p. 40, 1998.

[97]   B. Gourévitch, R. Le Bouquin-Jeannes, and G. Faucon, "Linear and nonlinear causality between signals: methods, examples and neurophysiological applications," *Biological cybernetics,* vol. 95, pp. 349-369, 2006.

[98]   C. W. Granger, "Investigating causal relations by econometric models and cross-spectral methods," *Econometrica: Journal of the Econometric Society,* pp. 424-438, 1969.

[99]   C. W. Granger, "Testing for causality: a personal viewpoint," *Journal of Economic Dynamics and control,* vol. 2, pp. 329-352, 1980.

[100] S. Malekpour and W. A. Sethares, "Conditional Granger causality and partitioned Granger causality: differences and similarities," *Biological cybernetics,* vol. 109, pp. 627-637, 2015.

[101] B. Schelter, M. Winterhalder, and J. Timmer, *Handbook of time series analysis: recent theoretical developments and applications*: John Wiley & Sons, 2006.

[102] M. T. Bahadori and Y. Liu, "An examination of practical granger causality inference," in *Proceedings of the 2013 SIAM International Conference on data Mining*, 2013, pp. 467-475.

[103] T. V. Guy, M. Kárný, and D. H. Wolpert, *Decision Making: Uncertainty, Imperfection, Deliberation and Scalability*: Springer International Publishing, 2015.

[104] G. M. Jenkins and D. G. Watts, *Spectral analysis and its applications*: Holden-Day, 1969.

[105] G. T. Wilson, "The factorization of matricial spectral densities," *SIAM Journal on Applied Mathematics,* vol. 23, pp. 420-426, 1972.

[106] M. Kaminski and K. J. Blinowska, "A new method of the description of the information flow in the brain structures," *Biological cybernetics,* vol. 65, pp. 203-210, 1991.

[107] L. A. Baccalá, K. Sameshima, and D. Takahashi, "Generalized partial directed coherence," in *Digital Signal Processing, 2007 15th International Conference on*, 2007, pp. 163-166.

[108] A. Korzeniewska, M. Mańczak, M. Kamiński, K. J. Blinowska, and S. Kasicki, "Determination of information flow direction among brain structures by a modified directed transfer function (dDTF) method," *Journal of neuroscience methods,* vol. 125, pp. 195-207, 2003.

[109] L. Faes and G. Nollo, "Multivariate frequency domain analysis of causal interactions in physiological time series," in *Biomedical Engineering, Trends in Electronics, Communications and Software*, ed: InTech, 2011.

[110] L. Faes and G. Nollo, "Extended causal modeling to assess Partial Directed Coherence in multiple time series with significant instantaneous interactions," *Biological cybernetics,* vol. 103, pp. 387-400, 2010.

[111] R. Vicente, M. Wibral, M. Lindner, and G. Pipa, "Transfer entropy—a model-free measure of effective connectivity for the neurosciences," *Journal of computational neuroscience,* vol. 30, pp. 45-67, 2011.

[112] P.-O. Amblard and O. J. Michel, "On directed information theory and Granger causality graphs," *Journal of computational neuroscience,* vol. 30, pp. 7-16, 2011.

[113] K. Hlaváčková-Schindler, M. Paluš, M. Vejmelka, and J. Bhattacharya, "Causality detection based on information-theoretic approaches in time series analysis," *Physics Reports,* vol. 441, pp. 1-46, 2007.

[114] M. Vejmelka and M. Paluš, "Inferring the directionality of coupling with conditional mutual information," *Physical Review E,* vol. 77, p. 026214, 2008.

[115] M. Paluš, V. Albrecht, and I. Dvořák, "Information theoretic test for nonlinearity in time series," *Physics Letters A,* vol. 175, pp. 203-209, 1993.

[116] A. Papana, D. Kugiumtzis, and C. Kyrtsou, "A nonparametric causality test: Detection of direct causal effects in multivariate systems using corrected partial transfer entropy," in *Topics in Nonparametric Statistics*, ed: Springer, 2014, pp. 197-206.

[117] M. Staniek and K. Lehnertz, "Symbolic transfer entropy," *Physical Review Letters,* vol. 100, p. 158101, 2008.

[118] J. Theiler, S. Eubank, A. Longtin, B. Galdrikian, and J. Doyne Farmer, "Testing for nonlinearity in time series: the method of surrogate data," *Physica D: Nonlinear Phenomena,* vol. 58, pp. 77-94, 1992.

[119] L. Astolfi, F. Cincotti, D. Mattia, M. G. Marciani, L. A. Baccala, F. D. V. Fallani, *et al.*, "Assessing cortical functional connectivity by partial directed coherence: simulations and application to real data," *IEEE Transactions on Biomedical Engineering,* vol. 53, pp. 1802-1812, 2006.

[120] F. Jacobacci, M. Sapir, S. Collavini, S. Kochen, and A. Blenkmann, "Assessing effective connectivity in epileptogenic networks. A model-based simulation approach," in *Journal of Physics: Conference Series,* 2013, p. 012037.

[121] T. Schreiber and A. Schmitz, "Improved surrogate data for nonlinearity tests," *Physical Review Letters,* vol. 77, p. 635, 1996.

[122] A. Porta, S. Guzzetti, R. Furlan, T. Gnecchi-Ruscone, N. Montano, and A. Malliani, "Complexity and nonlinearity in short-term heart period variability: comparison of methods based on local nonlinear prediction," *IEEE Transactions on Biomedical Engineering,* vol. 54, pp. 94-106, 2007.

[123] R. Benitez, E. Alvarez-Lacalle, B. Echebarria, P. Gomis, M. Vallverdu, and P. Caminal, "Characterization of the nonlinear content of the heart rate dynamics during myocardial ischemia," *Medical Engineering and Physics,* vol. 31, pp. 660-667, 2009.

[124] R. Q. Quiroga, J. Arnhold, and P. Grassberger, "Learning driver-response relationships from synchronization patterns," *Physical Review E,* vol. 61, pp. 5142-5148, May 2000.

[125] J. Xu, "Nonlinear signal processing based on reproducing kernel Hilbert space," University of Florida, 2007.

[126] H. Wen, "A review of the Hénon map and its physical interpretations," *School of Physics Georgia Institute of Technology, Atlanta, GA,* pp. 30332-0430.

[127] M. A. Kramer, E. Edwards, M. Soltani, M. S. Berger, R. T. Knight, and A. J. Szeri, "Synchronization measures of bursting data: application to the electrocorticogram of an auditory event-related experiment," *Physical Review E,* vol. 70, p. 011914, 2004.

[128] B. M. Krishna, P. Indic, U. Nair, and R. Pratap, "Quantifying chaotic synchronization using error evolution," *Communications in Nonlinear Science and Numerical Simulation,* vol. 14, pp. 3682-3692, 2009.

[129] L. Junge and U. Parlitz, "Synchronization using dynamic coupling," *Physical Review E,* vol. 64, p. 055204, 2001.

[130] S. J. Schiff, P. So, T. Chang, R. E. Burke, and T. Sauer, "Detecting dynamical interdependence and generalized synchrony through mutual prediction in a neural ensemble," *Physical Review E,* vol. 54, pp. 6708-6724, 12/01/ 1996.

[131] J. Bhattacharya, E. Pereda, and H. Petsche, "Effective detection of coupling in short and noisy bivariate data," *IEEE Trans Syst Man Cybern B Cybern,* vol. 33, pp. 85-95, Feb 2003.

[132] J. W. Xu, H. Bakardjian, A. Cichocki, and J. C. Principe, "A new nonlinear similarity measure for multichannel biological signals," *2007 IEEE International Joint Conference on Neural Networks, Vols 1-6,* pp. 2046-2051, 2007.

[133] M. Kramer, E. Edwards, M. Soltani, R. Knight, M. Berger, and A. Szeri, "Measures of linear and nonlinear interdependence of electrocortigram time series from evoked-response potential experiments," in *Engineering in Medicine and Biology Society, 2004. IEMBS'04. 26th Annual International Conference of the IEEE*, 2004, pp. 558-561.

[134] C. Stam and B. Van Dijk, "Synchronization likelihood: an unbiased measure of generalized synchronization in multivariate data sets," *Physica D: Nonlinear Phenomena,* vol. 163, pp. 236-251, 2002.

[135] J.-W. Xu, H. Bakardjian, A. Cichocki, and J. C. Principe, "A new nonlinear similarity measure for multichannel signals," *Neural Networks,* vol. 21, pp. 222-231, 3// 2008.

[136] K. Ansari-Asl, L. Senhadji, J.-J. Bellanger, and F. Wendling, "Quantitative evaluation of linear and nonlinear methods characterizing interdependencies between brain signals," *Physical Review E,* vol. 74, p. 031916, 2006.

[137] J. P. Lachaux, E. Rodriguez, J. Martinerie, and F. J. Varela, "Measuring phase synchrony in brain signals," *Human brain mapping,* vol. 8, pp. 194-208, 1999.

[138] V. Sakkalis, C. D. Giurc, P. Xanthopoulos, M. E. Zervakis, V. Tsiaras, Y. Yang*, et al.*, "Assessment of linear and nonlinear synchronization measures for analyzing EEG in a mild epileptic paradigm," *IEEE Transactions on Information Technology in Biomedicine,* vol. 13, pp. 433-441, 2009.

[139] V. Sakkalis and M. Zervakis, "Linear and nonlinear synchronization analysis and visualization during altered states of consciousness," in *Recent advances in biomedical engineering*, ed: InTech, 2009.

[140] T. Kreuz, F. Mormann, R. G. Andrzejak, A. Kraskov, K. Lehnertz, and P. Grassberger, "Measuring synchronization in coupled model systems: A comparison of different approaches," *Physica D: Nonlinear Phenomena,* vol. 225, pp. 29-42, 2007.

[141] A. Papana, C. Kyrtsou, D. Kugiumtzis, and C. Diks, "Simulation Study of Direct Causality Measures in Multivariate Time Series," *Entropy,* vol. 15, pp. 2635-2661, 2013.

[142] L. A. Baccalá and K. Sameshima, "Overcoming the limitations of correlation analysis for many simultaneously processed neural structures," *Progress in brain research,* vol. 130, pp. 33-47, 2001.

[143] M.-H. Wu, R. E. Frye, and G. Zouridakis, "A comparison of multivariate causality based measures of effective connectivity," *Computers in biology and medicine,* vol. 41, pp. 1132-1141, 2011.

[144] A. Papana, D. Kugiumtzis, and P. G. Larsson, "Detection of direct causal effects and application to epileptic electroencephalogram analysis," *International Journal of Bifurcation and Chaos,* vol. 22, p. 1250222, 2012.

[145] D. J. Smit, C. J. Stam, D. Posthuma, D. I. Boomsma, and E. J. De Geus, "Heritability of "small-world" networks in the brain: A graph theoretical analysis of resting-state EEG functional connectivity," *Human brain mapping,* vol. 29, pp. 1368-1378, 2008.

[146] H. Akaike, "Information theory and an eztension oof the maximum likefood principle," in *Second International Symposium on Information Theory, 1973*, 1973, pp. 267-281.

[147] G. Schwarz, "Estimating the dimension of a model," *The annals of statistics,* vol. 6, pp. 461-464, 1978.

[148] W. Miltner, C. Braun, R. Johnson Jr, G. Simpson, and D. Ruchkin, "A test of brain electrical source analysis (BESA): A simulation study," *Electroencephalography and clinical neurophysiology,* vol. 91, pp. 295-310, 1994.

[149] S. Ponten, A. Daffertshofer, A. Hillebrand, and C. J. Stam, "The relationship between structural and functional connectivity: graph theoretical analysis of an EEG neural mass model," *Neuroimage,* vol. 52, pp. 985-994, 2010.

[150] H. Bakhshayesh, S. P. Fitzgibbon, and K. J. Pope, "Detection of coupling with linear and nonlinear synchronization measures for EEG," in *Biomedical Engineering (MECBME), 2014 Middle East Conference on*, 2014, pp. 240-243.

[151] H. Bakhshayesh, S. P. Fitzgibbon, and K. J. Pope, "A comparative study of the detection of direct causal influence with bivariate and multivariate measures for EEG," in *Biomedical Engineering and Sciences (IECBES), 2014 IEEE Conference on*, 2014, pp. 719-723.

[152] H. Bakhshayesh, T. S. Grummett, A. S. Janani, S. P. Fitzgibbon, and K. J. Pope, "Towards Detecting Connectivity in EEG: A Comparative Study of Parameters of Effective Connectivity Measures on Simulated Data," in *2018 IEEE-EMBS Conference on Biomedical Engineering and Sciences (IECBES)*, 2018, pp. 297-301.

[153] H. Bakhshayesh, S. P. Fitzgibbon, A. S. Janani, T. S. Grummett, and K. J. Pope, "Detecting synchrony in EEG: A comparative study of functional connectivity measures," *Computers in biology and medicine,* vol. 105, pp. 1-15, 2019.

APPENDIX A   PUBLISHED AND SUBMITTED PAPERS

This appendix contains three accepted papers, and one submitted. Content from all papers is similar to content in the Introduction, Literature Review and Conclusion of this thesis.

A-1 First paper

This published conference paper (IEE 2014 Middle East Conference on Biomedical Engineering) is related to Chapter 3 of this thesis. In this paper we only compared 6 functional connectivity measures, whereas in chapter three we extended our comparison to 28 measures, including the addition of measures from the Granger causality and state space families and the event synchrony measure. In this paper we did not use surrogate analysis to provide a threshold for significance for connectivity measures, instead we simply compared raw connectivity values. Therefore, the content of this paper can be found in chapter three, but the chapter is a substantial extension and improvement on the paper.

This article [150] removed due to copyright restrictions.

A-2 Second paper

Chapter 4 is based on this published conference paper (2014 IEEE EMBS Conference on Biomedical Engineering and Sciences). The methods and results are the same, however the presentation of the results has been expanded in chapter 4 to include more graphs and tables to give a more detailed representation. The discussion and conclusion have also been expanded.

This article[151] removed due to copyright restrictions

A-3 Third paper

This published paper (2018 IEEE EMBS Conference on Biomedical Engineering and Sciences) is almost identical to Chapter 5. Chapter 5 also contains some additional tables that enhance the presentation of the results, and the discussion and conclusion is expanded.

This article [152] removed due to copyright restrictions.

A-4 Fourth paper

This article [153] removed due to copyright restriction.